

University of Alberta

**Carbon–Carbon Bond Formation and Unexpected Carbon–Hydrogen Bond
Activation at Adjacent Metal Centres**

by

Tiffany Jayne MacDougall

A thesis submitted to the Faculty of Graduate Studies and Research
in partial fulfillment of the requirements for the degree of

Doctor of Philosophy

Department of Chemistry

©Tiffany Jayne MacDougall

Spring 2012

Edmonton, Alberta

Permission is hereby granted to the University of Alberta Libraries to reproduce single copies of this thesis and to lend or sell such copies for private, scholarly or scientific research purposes only. Where the thesis is converted to, or otherwise made available in digital form, the University of Alberta will advise potential users of the thesis of these terms.

The author reserves all other publication and other rights in association with the copyright in the thesis and, except as herein before provided, neither the thesis nor any substantial portion thereof may be printed or otherwise reproduced in any material form whatsoever without the author's prior written permission.

Abstract

The formation of carbon–carbon (C–C) bonds is central to the transformation of small, readily available hydrocarbons into value-added products with useful chemical and physical properties. An important industrial process involving C–C bond formation is the Fischer-Tropsch (FT) process which converts carbon monoxide and hydrogen into a range of useful hydrocarbons. Although this heterogeneous process is not well understood, the importance of surface-bound, bridging methylene groups in this process is recognized.

This dissertation seeks to gain a further understanding of the chemistry of bridging methylene groups. Chapter 2 of this thesis explores the formation of C–C bonds by a methylene-bridged Ir/Ru system through the coupling of methylene groups with cumulene substrates. Although C–C bond formation is observed in these complexes, we also observe unexpected multiple C–H bond activations, including the unusual activation of geminal C–H bonds in olefins. In Chapter 3, we report the C–H activation of cumulenes, conjugated dienes, and monoolefins, by the tetracarbonyl Ir/Ru complex and a mechanism is presented for these activations.

The original goal of C–C bond formation is revisited in Chapters 4 and 5 as we report the reactivity of the methylene-bridged Ir/Os complex with unsaturated substrates towards hydrocarbyl-bridged complexes. This metal combination appears to be a better model for FT chemistry, owing to the strong metal–carbon bonds. The reactivity of the tetracarbonyl Ir/Os complex is also

reported with unsaturated substrates (Chapter 5), as a comparison to the Ir/Ru analogue.

The reactivity of the Ir/M (M = Ru, Os) systems are compared to the analogous Rh/M (M = Ru, Os) systems, describing the effects of changing the group 8 metal, the group 9 metal, or both. Throughout this thesis, we attempt to elucidate the roles of the adjacent metals in C–C bond formation and C–H bond activation.

Acknowledgements

Although a PhD thesis only has one author, many people leave their mark on its pages in many different ways. There are many people who have helped me grow as a person and as a scientist. First and foremost, I would like to thank my PhD supervisor, Dr. Martin Cowie, for all he has taught me and all of the help he has given me over the course of my degree. As a teacher, Marty is second to none; he demands high quality work and dedication, and in return gives nothing but truth, knowledge, and respect. Although oftentimes excessive with red pens and yellow pages, his patience, attention to detail, and possible sheer pleasure in dissecting my work, has helped me to become a better writer and ambassador for science.

Over the course of this degree, my lab mates have acted as a surrogate family. When I first joined the Cowie lab, Rahul Samant took me under his wing in the lab and it was because of his mentoring that I was able to get my project off of the ground, and I thank him for all of his help. I also want to thank Kyle Wells, Lindsay Hounjet (my fellow Saskatchewanian), Matt Zamora, Mike Slaney, and MD Hosnay Mobarok for the hours of chemistry talk and discussions, practice talks, grill sessions, and of course, the much needed lunch and/or after work pints. Having X-ray crystallographers Bob McDonald and Mike Ferguson conveniently located right across the hall was such a blessing, and although I am sure they were tired of my too small, twinned, and often sea urchin-like crystals, they never once scoffed at my thousands of questions and from them I have learned so much. If it wasn't for the NMR lab, specifically Mark Miskolzie, this project would not have been possible; his help in designing and interpreting NMR has allowed me to make sense of what I many would refer to as 'dogs breakfast'. I would also like to thank the Analytical Services and Mass Spectrometry labs at the University of Alberta for all of their time and effort.

Beyond the lab, I would like to thank all of my friends and family for their unwavering support through a long university career. I would like to thank my

parents for always having my back and constantly pushing me to be all that I could be. To my mom – you have always been the person whom I strive to take after. You are patient, kind, strong, resilient, and nothing short of extraordinary, and whenever I get knocked down, for what feels like the millionth time, you always pull me back up. To my husband – your love and support has been unwavering, and your patience has been unbelievable. You have been by my side since the beginning, and I am excited to move on to bigger and better things together.

I have met wonderful people over the course of my career at the University of Alberta and they have often turned some pretty horrible days into renewed motivation. Mike Slaney, you have seen me at my best, but more than that, you've had to see me and deal with me at my worst, which can be a challenge. We've both had our mo-ments, but I was glad that we could always laugh about them and regroup over a quick trip for coffee. Matt Zamora, although we didn't realize how good of friends we were until our last year together, you have left me with so much inspiration to be a better person and to work my butt off to achieve anything that I want. Our Friday nachos and happy hour pints literally saved my life the last few months and you will be missed. Nicole Beckers, I want to thank you for years of listening to me vent, in person or via email. It was nice to not always have to talk chemistry and be reminded that there is life outside of work. Although I do not have enough room to speak about everyone individually I would also like to acknowledge the following friends and family: Bob McDonald, Mike Ferguson, Ryan Lewis, Anne Slaney, Justin Beckers, Crystal Zorn, Barry Craigie, Landon Craigie, Amanda Ulmer, Andrea Walker, Brandon Ulmer, Randi Walker, Courtney MacDougall, Mare MacDougall, Pete MacDougall, Doug Ulmer, Wendy Brooks, Kim and Diane MacDougall, and Fay and Glen Wright. Without your unwavering support, I definitely would not have made it this far, and will cherish you always.

Hillary (a.k.a Tiffany)

Table of Contents

Chapter 1: Introduction and Background Information	1
1.1 Carbon–Carbon Bond Formation	1
1.1.1 Olefin Hydroformylation and Methanol Carbonylation.....	2
1.1.2 Olefin Polymerization	5
1.1.3 Cross Coupling Reactions	6
1.1.4 Olefin Metathesis and Metal Alkylidenes	8
1.1.5 Fischer-Tropsch (FT) Chemistry.....	10
1.2 Heterogeneous vs. Homogeneous Catalysts	16
1.3 Surface Models and Multinuclear Complexes	17
1.3.1 Polynuclear Complexes.....	17
1.3.2 Bimetallic Complexes and Metal-Metal Cooperativity.....	18
1.3.3 Homogeneous Organometallic Complexes as Models for FT Chain-Growth.....	20
1.3.4 Methylene-Bridged Bimetallic Complexes	23
1.3.5 Carbon–Carbon Coupling Using Methylene-Bridged Complexes.	24
1.4 Goals of This Thesis	28
1.5 References	30
Chapter 2: Facile Carbon–Carbon Bond Formation and Multiple Carbon–Hydrogen Bond Activations Promoted by Methylene- Bridged Iridium/Ruthenium Complexes	40
2.1 Introduction	40
2.2 Results, Compound Characterization, and Discussion	41

2.2.1	Carbon–Carbon Bond Formation	41
2.2.1.1	Alkyl Cumulenes.....	41
2.2.1.2	1,1-Difluoroallene	49
2.2.1.3	Allene	53
2.2.2	Multiple Carbon–Hydrogen Bond Activations	54
2.3	Conclusions	62
2.4	Experimental Section	64
2.4.1	General Comments	64
2.4.2	Preparation of Compounds.....	65
2.4.3	X-Ray Structure Determinations	74
2.4.3.1	General	74
2.4.3.2	Special Refinement Conditions.....	75
2.5	References	78
Chapter 3: Geminal Carbon–Hydrogen Bond Activation in Cumulenes Promoted by Adjacent Iridium/Ruthenium Centres		83
3.1	Introduction	83
3.2	Results and Compound Characterization	86
3.2.1	Activation of Propadiene and 1,2-Butadiene	86
3.2.2	Activation of 1,1-Dimethylallene.....	89
3.2.3	Reaction with 1,1-Difluoroallene	93
3.2.4	C–H Bond Activation in Monoolefins	95
3.2.5	Mechanistic Insights into the Geminal Activation of Olefinic C–H Bonds.....	100
3.3	Discussion and Conclusions	103

3.4	Experimental Section	106
3.4.1	General Comments	106
3.4.2	Preparation of Compounds	107
3.4.3	X-Ray Structure Determinations	117
3.4.3.1	General	117
3.4.3.2	Special Refinement Conditions	118
3.5	References	120

Chapter 4: Alkyne/Methylene Coupling at Adjacent Iridium/Osmium Centres: Facile Carbon–Carbon and Carbon–Oxygen Bond Formation 124

4.1	Introduction	124
4.2	Results and Compound Characterization	125
4.2.1	Methylene-Bridged Precursor	125
4.2.2	C ₃ -Bridged Species from [IrOs(CO) _x (μ-CH ₂)(dppm) ₂][CF ₃ SO ₃] (x = 3 or 4)	129
4.2.3	C ₂ -Bridged Species	142
4.3	Discussion	145
4.4	Conclusions	150
4.5	Experimental Section	151
4.5.1	General Comments	151
4.5.2	Preparation of Compounds	151
4.5.3	X-Ray Structure Determinations	161
4.5.3.1	General	161
4.5.3.2	Special Refinement Conditions	162

4.6	References	163
Chapter 5: Reactions of Iridium/Osmium Complexes with Cumulenes: A Comparative Study		
		166
5.1	Introduction	166
5.2	Results and Compound Characterization	167
5.2.1	Reactivity of $[\text{IrOs}(\text{CO})_3(\mu\text{-CH}_2)(\text{dppm})_2]^+$ with Cumulenes	167
5.2.1.1	Allene	167
5.2.1.2	Methylallene	172
5.2.1.3	1,1-Dimethylallene	174
5.2.2	Reactivity of $[\text{IrOs}(\text{CO})_4(\text{dppm})_2]^+$ with Cumulenes	176
5.2.2.1	Allene and Methylallene	177
5.2.2.2	1,1-Dimethylallene	179
5.2.2.3	1,1-Difluoroallene	181
5.3	Discussion	183
5.3.1	Reactivity of $[\text{IrOs}(\text{CO})_3(\mu\text{-CH}_2)(\text{dppm})_2]^+$ with Cumulenes	184
5.3.2	Reactivity of $[\text{IrOs}(\text{CO})_4(\text{dppm})_2]^+$ with Cumulenes	188
5.4	Conclusions	189
5.5	Experimental Section	190
5.5.1	General Comments	190
5.5.2	Preparation of Compounds	191
5.5.3	X-Ray Structure Determinations	198
5.5.3.1	General	198
5.5.3.2	Special Refinement Conditions	198

5.6	References	199
Chapter 6:	Conclusions and Final Remarks	203
6.1	Foundations for Thesis Goals	203
6.2	Ir/Ru Complexes	204
6.3	Ir/Os Complexes	206
6.4	Roles of Adjacent Metals	208
6.5	Future Work and Closing Remarks	209
6.6	References	211
Appendix I:	Attempted C–H Bond Activation of Monoolefins with [IrOs(CO)₄(dppm)₂]⁺	214
Appendix II:	Drying Agents/Indicators for Solvents	221
Appendix III:	Crystallographic Experimental Details	222
AIII.1	Crystallographic Details for Chapter 2 Compounds ...	222
AIII.2	Crystallographic Details for Chapter 3 Compounds ...	224
AIII.3	Crystallographic Details for Chapter 4 Compounds ...	226
AIII.4	Crystallographic Details for Chapter 5 Compounds ...	228
AIII.5	Crystallographic Details for Appendix I	230
Appendix IV:	Crystallographic Data	231

Appendix V: Coauthor Contributions	233
AV.1 Chapters 1 and 6	233
AV.2 Chapter 2	233
AV.3 Chapter 3	233
AV.4 Chapter 4	234
AV.5 Chapter 5	234

List of Tables

Chapter 1

Table 1-1.	World Reserves of “Carbon” Relative to Oil	11
-------------------	--	----

Chapter 2

Table 2-1.	Selected Bond Lengths and Angles for Both Disordered Forms of 4	45
Table 2-2.	Selected Bond Lengths and Angles for Both Disordered Forms of 5	47
Table 2-3.	Selected Bond Lengths and Angles for Both Disordered Forms of 8-CF₃SO₃	57
Table 2-4.	Selected Bond Lengths and Angles for 10	60
Table 2-5.	Spectroscopic Data for the Compounds	66

Chapter 3

Table 3-1.	Selected Bond Lengths and Angles for 14-CF₃SO₃	88
Table 3-2.	Selected Bond Lengths and Angles for 16-CF₃SO₃	91
Table 3-3.	Selected Bond Lengths and Angles for 21-CF₃SO₃	99
Table 3-4.	Spectroscopic Data for the Compounds	108

Chapter 4

Table 4-1.	Selected Bond Lengths and Angles for 28	128
Table 4-2.	Selected Bond Lengths and Angles for 32	134
Table 4-3.	Selected Bond Lengths and Angles for 33	139
Table 4-4.	Selected Bond Lengths and Angles for 37	144

Table 4-5.	Spectroscopic Data for the Compounds.....	152
-------------------	---	-----

Chapter 5

Table 5-1.	Selected Bond Lengths and Angles for 41/41a-CF₃SO₃	172
-------------------	---	-----

Table 5-2.	Selected Bond Lengths and Angles for 44	179
-------------------	--	-----

Table 5-3.	Selected Bond Lengths and Angles for 47	183
-------------------	--	-----

Table 5-4.	Spectroscopic Data for the Compounds.....	192
-------------------	---	-----

Appendix I

Table I-1.	Selected Bond Lengths and Angles for 48	217
-------------------	--	-----

Appendix III

Table III.1-1	Crystallographic Details for 4·Et₂O and 5·Et₂O	222
----------------------	--	-----

Table III.1-2	Crystallographic Details for 8-CF₃SO₃·1.5CH₂Cl₂ and 10·2CH₂Cl₂	223
----------------------	--	-----

Table III.2-1	Crystallographic Details for 14-CF₃SO₃·0.5CH₂Cl₂·Et₂O and 16-CF₃SO₃·3.5THF	224
----------------------	---	-----

Table III.2-2	Crystallographic Details for 21-CF₃SO₃·0.5CH₂Cl₂	225
----------------------	---	-----

Table III.3-1	Crystallographic Details for 28·3.5CH₃CN and 35·1.5CH₂Cl₂	226
----------------------	---	-----

Table III.3-2	Crystallographic Details for 33-BF₄ and 37-BF₄·2CH₂Cl₂	227
----------------------	--	-----

Table III.4-1	Crystallographic Details for 41·2CH₂Cl₂ and 44·0.5Et₂O ..	228
----------------------	--	-----

Table III.4-2	Crystallographic Details for 47·CH₂Cl₂	229
----------------------	---	-----

Table III.5-1	Crystallographic Details for 48·1.5CH₂Cl₂	230
----------------------	--	-----

Appendix IV

Table IV.1	Chapter 2 Crystallographic Reference Numbers	231
Table IV.2	Chapter 3 Crystallographic Reference Numbers	231
Table IV.3	Chapter 4 Crystallographic Reference Numbers	232
Table IV.4	Chapter 5 Crystallographic Reference Numbers	232
Table IV.5	Appendix I Crystallographic Reference Numbers	232

List of Charts

Chapter 1

- Chart 1-1.** Olefin metathesis catalysts.....9
- Chart 1-2.** Stanley's bimetallic hydroformylation catalyst 18
- Chart 1-3.** Bimetallic group 8/9 dppe-bridged complexes.....29

Chapter 3

- Chart 3-1.** Geminal activation of olefins by a bimetallic complex 84

Chapter 4

- Chart 4-1.** Valence-bond formulations for **28** 129
- Chart 4-2.** Structural comparison of **28** with $[\text{MM}'(\text{CO})_4(\mu\text{-CH}_2)(\text{dppe})_2]^+$
($\text{MM}' = \text{RhRu, RhOs, IrRu}$) 146

List of Figures

Chapter 1

Figure 1-1. Anderson-Schulz-Flory Statistics in FT Chemistry	14
---	----

Chapter 2

Figure 2-1. $^{31}\text{P}\{\text{H}\}$ NMR spectrum of 2 in CD_2Cl_2	43
Figure 2-2. Perspective view of the complex cation of 4	44
Figure 2-3. Perspective view of the complex cation of 5	46
Figure 2-4. $^{31}\text{P}\{\text{H}\}$ NMR spectra of a mixture of 6 and 7 at 24 h and 60 h in CD_2Cl_2	51
Figure 2-5. ^{19}F NMR spectrum of 7 in CD_2Cl_2	52
Figure 2-6. $^{31}\text{P}\{\text{H}\}$ NMR spectrum of compounds 8 and 9 in CD_2Cl_2	55
Figure 2-7. Perspective view of the complex cation of 8-CF₃SO₃	56
Figure 2-8. Perspective view of the complex cation of 10	59
Figure 2-9. Alternate view of the complex cation 10	60
Figure 2-10. View of the disorder in the complex cation of 4	75
Figure 2-11. View of the disorder in the complex cation of 5	76
Figure 2-12. View of the disorder in the complex cation of 8	77

Chapter 3

Figure 3-1. Perspective view of the complex cation of 14-CF₃SO₃	88
Figure 3-2. Perspective views of the complex cation of 16-CF₃SO₃	90
Figure 3-3. $^{31}\text{P}\{\text{H}\}$ NMR spectrum of a mixture of compounds 18 and 13 in CD_2Cl_2 at $-20\text{ }^\circ\text{C}$	96

Figure 3-4. Perspective view of the complex cation of **21-CF₃SO₃**98

Figure 3-5. View of the disorder in the complex cation of **16-CF₃SO₃** 119

Chapter 4

Figure 4-1. ³¹P{¹H} NMR spectrum of **28** in CD₂Cl₂..... 126

Figure 4-2. Perspective views of the complex cation of **28** 127

Figure 4-3. ³¹P{¹H} NMR spectrum of **30** and **31** in CD₂Cl₂..... 130

Figure 4-4. Selected regions of the ¹⁹F NMR spectrum of **32** in CD₂Cl₂ 132

Figure 4-5. Perspective views of the complex cation of **32** 133

Figure 4-6. ¹H NMR spectrum of **33** in CD₂Cl₂ 135

Figure 4-7. Perspective view of the complex cation of **33**..... 137

Figure 4-8. Alternate view of the complex cation of **33** 138

Figure 4-9. Selected regions of the ¹H and ¹H{³¹P} spectra for the two CH₂ groups of **34** in CD₂Cl₂..... 141

Figure 4-10. Perspective view of the complex cation of **37**..... 143

Chapter 5

Figure 5-1. ³¹P{¹H} NMR spectrum of **41/41a** in CD₂Cl₂..... 169

Figure 5-2. Perspective views of the complex cation of **41/41a-CF₃SO₃** ... 170

Figure 5-3. ³¹P{¹H} NMR spectrum of **43** in CD₂Cl₂..... 175

Figure 5-4. Perspective views of the complex cation of **44** 178

Figure 5-5. Perspective view of the complex cation of **47**..... 182

Appendix I

Figure I-1. $^{31}\text{P}\{^1\text{H}\}$ NMR spectrum of **48** in CD_2Cl_2215

Figure I-2. Perspective views of the complex cation of **48**216

List of Schemes

Chapter 1

Scheme 1-1. Mechanism of cobalt catalyzed hydroformylation	3
Scheme 1-2. Mechanism of palladium catalyzed cross coupling	8
Scheme 1-3. Mechanism of olefin metathesis	9
Scheme 1-4. Fischer-Tropsch methylene polymerization mechanism	11
Scheme 1-5. Brady and Pettit proposal for FT chain growth	13
Scheme 1-6. Dry proposal for FT chain growth	15
Scheme 1-7. Support for Dry proposal using $\text{Fe}_2(\text{CO})_8(\mu\text{-CH}_2)$	15
Scheme 1-8. Metal-metal cooperativity in C–F Bond Activation (I)	19
Scheme 1-9. Metal-metal cooperativity in C–F Bond Activation (II).....	20
Scheme 1-10. Reduction of $\mu\text{-CO}$ to $\mu\text{-CH}_2$	20
Scheme 1-11. Decomposition of $[\text{Cp}^*\text{Rh}(\mu\text{-CH}_2)(\text{Me})]_2$	21
Scheme 1-12. Maitlis proposal for FT chain growth	21
Scheme 1-13. Coupling of $\sigma\text{-vinyl}$ and $\mu\text{-CH}_2$ groups.....	22
Scheme 1-14. First stable transition metal $\mu\text{-CH}_2$ complex.....	23
Scheme 1-15. First transition metal $\mu\text{-CH}_2$ complex without a M–M bond.....	24
Scheme 1-16. Reactivity of $[\text{Ru}_2(\text{Cp})_2(\text{CO})_2(\text{NCCH}_3)(\mu\text{-CH}_2)]$	24
Scheme 1-17. Synthesis of $\mu\text{-CH}_2$ diphosphine-bridged complexes.....	25
Scheme 1-18. Methylene coupling at adjacent Rh/Os centres.....	25
Scheme 1-19. $[\text{RhM}'(\text{CO})_3(\mu\text{-CH}_2)(\text{dppm})_2]$ (M = Ru/Os) with alkynes and allene	26

Scheme 1-20. $[\text{RhM}^{\text{r}}(\text{CO})_3(\mu\text{-CH}_2)(\text{dppm})_2]$ (M = Ru/Os) reactivity with 1,1-dimethylallene	27
---	----

Chapter 2

Scheme 2-1. Formation of iridacyclic products (2 , 3 , 4 , and 5)	42
Scheme 2-2. Mechanism of iridacycle formation	48
Scheme 2-3. Acyl formation with 1,1-difluoroallene	50
Scheme 2-4. Coupling of allene and $\mu\text{-CH}_2$ to form 1,3-butadiene	54
Scheme 2-5. Multiple C–H bond activations of cumulenes	54
Scheme 2-6. Double C–H bond activation of allene	58

Chapter 3

Scheme 3-1. Geminal C–H bond activations of allene and methylallene	86
Scheme 3-2. Triple C–H bond activation of 1,1-dimethylallene	89
Scheme 3-3. Coordination of 1,1-difluoroallene	93
Scheme 3-4. Single C–H bond activation of monoolefins	95
Scheme 3-5. Attempts at vinylidene dihydride generation	97
Scheme 3-6. Formation of an allenyl hydride (23)	100
Scheme 3-7. Vinylidene to alkynyl-hydride transformation	102
Scheme 3-8. Proposed mechanism for geminal C–H bond activations of cumulenes	105

Chapter 4

Scheme 4-1. Formation of the methylene-bridged complex (28)	125
Scheme 4-2. Formation of C_3 -bridged Ir/Os complexes (30 , 31 , and 32)	130

Scheme 4-3. Formation of 33 by C–O bond formation.....	135
Scheme 4-4. Formation of a C ₄ -bridged complex (34).....	140
Scheme 4-5. Formation of C ₂ - and C ₃ -bridged Ir/Os complexes.....	142
Scheme 4-6. Mechanism of C–O bond formation in 33	149

Chapter 5

Scheme 5-1. Formation of trimethylenemethane isomers 41/41a	168
Scheme 5-2. Formation of isomers 42/42a	173
Scheme 5-3. Formation of 4-methyl-1,3-pentadiene and generation of 43	174
Scheme 5-4. Formation of $\mu\text{-}\eta^3\text{:}\kappa^1$ products 44 and 45	177
Scheme 5-5. Triple C–H bond activation of 1,1-dimethylallene	180
Scheme 5-6. Coordination of 1,1-difluoroallene	181
Scheme 5-7. Cumulene coordination and insertion products	184
Scheme 5-8. Scrambling of the CH ₂ label in trimethylenemethane	185

Appendix I

Scheme I-1. Formation of the double orthometallation product (48).....	214
--	-----

List of Symbols and Abbreviations

{X}	decoupled-nucleus X
\approx	approximately
1°	primary
2°	secondary
2D	two-dimensional
Å	Angström
APT	attached proton test
ASF	Anderson-Schulz-Flory
atm	pressure (in atmospheres)
<i>ca.</i>	approximately
cm ⁻¹	inverse centimetres (wavenumber)
Cp	cyclopentadiene
Cp*	pentamethylcyclopentadiene
Cy	cyclohexyl
d	day(s)
depmp	<i>bis</i> (diethylphosphino)methane
DMAD	dimethyl acetylenedicarboxylate
dppm	<i>bis</i> (diphenylphosphino)methane
Eq.	equation
equiv	equivalent(s)
Et	ethyl
FT	Fischer-Tropsch
g	gram
gCOSY	gradient-enhanced correlation spectroscopy
h	hour(s)
HFB	hexafluoro-2-butyne
HRMS	high resolution mass spectrometry
HSQC	heteronuclear single quantum coherence
Hz	hertz
<i>i</i> Pr	isopropyl

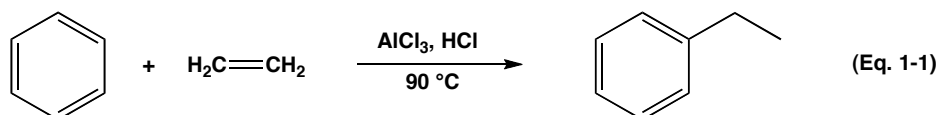
IR	infrared
M	molarity (moles per litre)
m/z	mass to charge ratio
M^+	molecular ion
Me	methyl
mg	milligram
MHz	megahertz
min	minute
mL	millilitre
mmol	millimole
n/a	not applicable
nbd	norbornadiene
NHC	<i>N</i> -heterocyclic carbene
${}^nJ_{AB}$	n-bond AB coupling constant
NMR	nuclear magnetic resonance
NOE	nuclear Overhauser effect
NOESY	nuclear Overhauser effect spectroscopy
η^x	hapticity of x continuous atoms
<i>o</i> -	ortho (1,2-)
°C	degree Celcius
ORTEP	Oak Ridge Thermal Ellipsoid Plot
OTf	triflate
Ph	phenyl
ppm	parts per million
s	second
SHOP	Shell Higher Olefins Process
<i>t</i>	time
THF	tetrahydrofuran
TMNO	trimethylamine <i>N</i> -oxide
TMS	tetramethylsilane
TOF	time of flight

vs.	versus
δ	chemical shift in ppm
Δ	addition of heat
κ^n-A	ligated by atom(s) A by n sites
$\mu-$	bridging
μL	microlitres
ν_{A-B}	A-B bond stretching frequency (cm^{-1})

Chapter 1: Introduction and Background Information

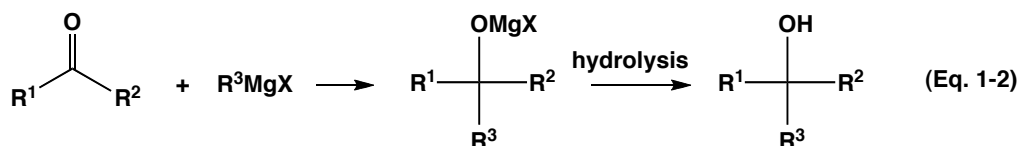
1.1 Carbon–Carbon Bond Formation

The formation of carbon-carbon (C–C) bonds is central to the chemistry of organic molecules, allowing the transformation of small, readily available hydrocarbons into larger, more complex products having important and useful chemical or physical properties. Such processes are used daily on the laboratory scale to carry out a wide range of organic transformations as chemists design new, more effective routes to important target molecules. Early C–C bond formation processes were dominated by Friedel-Crafts and Grignard reactions which are the basis of some important large-scale industrial processes for the production of new materials (polymers), important chemical feedstocks, and more specialized processes such as pharmaceutical production. One example of the use of classical Friedel-Crafts chemistry in industry, using AlCl_3 as the conventional catalyst, is the generation of ethylbenzene, and is one of the largest tonnage C–C bond-forming processes (Eq. 1-1).¹ This process is an example of a metal-catalyzed (albeit not transition metal) process used in industry.



In 1899 Barbier reported the first of what is now known as a Grignard reaction,² wherein methyl iodide, a methyl ketone, and magnesium metal in diethyl ether generated a tertiary alcohol. His student, Victor Grignard was the one who established the mechanism for this reaction,³ and devoted his career to the Grignard reaction, for which he was awarded the Nobel Prize in Chemistry in 1912. Traditionally, the Grignard reaction involved the addition of an organomagnesium halide (Grignard reagent) to a ketone or an aldehyde to form a tertiary or secondary alcohol, respectively (Eq. 1-2). However, since its discovery, the scope of the Grignard reaction has grown exponentially. The term Grignard reaction actually refers to two separate steps; first is the formation of the Grignard

reagent, followed by the reaction of this reagent with an organic or inorganic substrate to yield a product by either addition (Eq. 1-2) or substitution.⁴ The

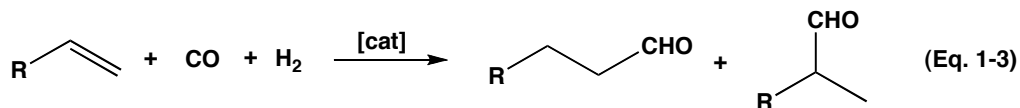


versatility of this reaction has made it a frequent choice for laboratory synthesis, for the production of value-added products such as specialty catalysts or intermediates in the pharmaceutical, flavour, fragrance, and food industries.

Although early processes of C–C bond formation relied heavily on main group metals, the majority of modern industrial processes use transition metal-based catalysts, a few examples of which are described below.

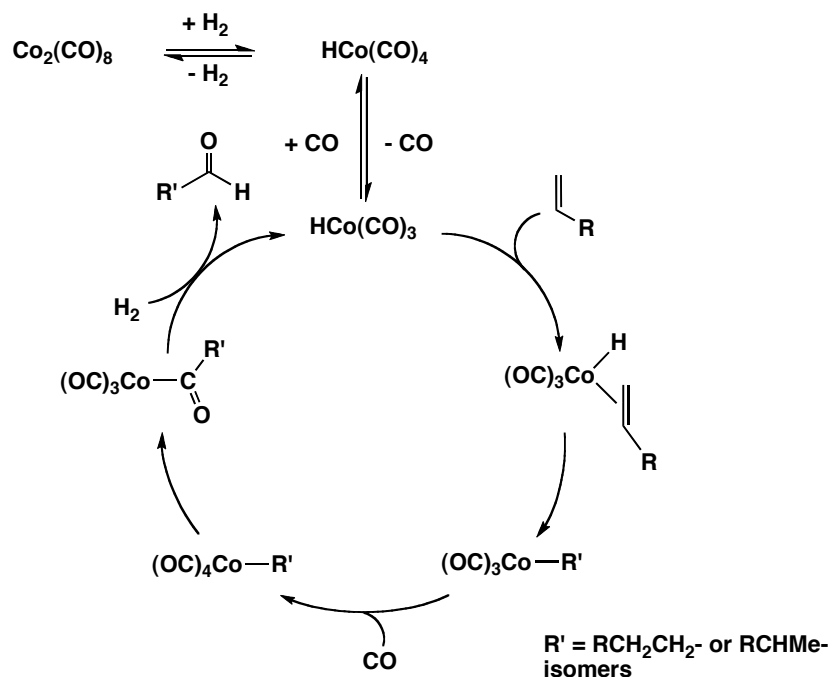
1.1.1 Olefin Hydroformylation and Methanol Carbonylation

Olefin hydroformylation is the addition of CO and H₂ to an olefin to generate an aldehyde (Eq. 1-3). The aldehydes produced can often be easily



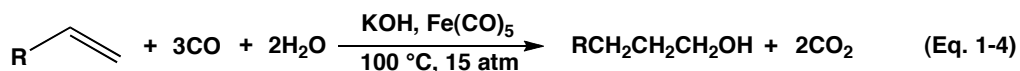
converted to secondary products, which then have applications as, for example, plasticizers and detergents.⁵ The first example of the hydroformylation of olefins to give aldehydes was reported in 1938 by Otto Roelen at Ruhrchemie,⁶ using Co₂(CO)₈ as the catalyst precursor. Although either 1° or 2° aldehydes are formed from the hydroformylation of α-olefins, the linear products are of higher commercial value. It was recognized soon after the discovery of this process that the catalytically active species was HCo(CO)₄,⁷ generated from the oxidative addition of H₂ to Co₂(CO)₈. The proposed catalytic cycle includes dissociation of a CO ligand to allow for the coordination of the olefin, after which olefin insertion occurs to generate an alkyl complex,⁸ as shown for the general mechanism in Scheme 1-1. Migratory insertion generates an acyl species, to which H₂ probably binds to give an H₂ complex followed by a heterolytic cleavage of H₂ to give the product aldehyde and regenerate the active catalyst.

Scheme 1-1



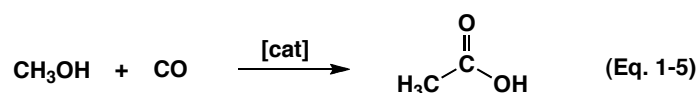
The problems of lack of selectivity of the above cobalt catalyst and the harsh reaction conditions necessary^{7a} were solved by Slauch and Mullineaux who discovered that the addition of sterically bulky phosphines, such as P(*n*-Bu)₃, favoured the formation of the more desirable, less hindered 1° aldehydes, and required only 5–10 atm pressures compare to 100–300 atm for the unmodified catalyst.⁹ Later it was discovered that rhodium tris(phosphine) complexes, first popularized by Wilkinson,¹⁰ were more effective hydroformylation catalysts, due to the lower temperatures and pressures required and to the increased selectivity.¹¹

Often, the product aldehydes from hydroformylation reactions are further reduced by H₂ to yield alcohol products. Walter Reppe studied the use of the water-gas shift reaction, catalyzed by Fe(CO)₅/base, to generate H₂ which could subsequently be used, along with an Fe-bound CO, for the hydroformylation of an olefin to an aldehyde and its subsequent reduction to an alcohol (Eq. 1-4).¹² Reppe's modification of classical hydroformylation did not significantly change



the mechanism of aldehyde production, for which Pettit and coworkers proposed reaction of an olefin with $(H)_2Fe(CO)_3$ to generate the alkyl metal carbonyl hydride, followed by migratory insertion of the alkyl group to CO, and reductive elimination of the aldehyde.¹³ The catalyst is subsequently regenerated by CO addition. In this reaction, however, it is easier to form the $H_2Fe(CO)_4$ from CO and H_2O , than it is by reacting $Fe(CO)_5$ with H_2 .

The carbonylation studies carried out by Reppe were influential in the development of related processes, notably the carbonylation of methanol (Eq. 1-5).



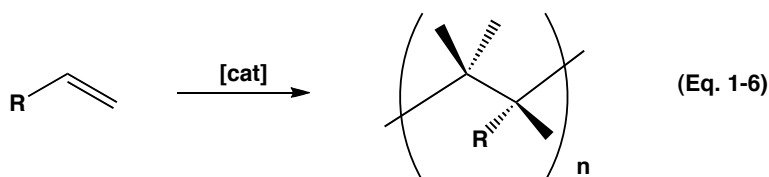
The first commercialized process for the carbonylation of methanol to acetic acid was introduced by BASF in the 1960's.^{11a} Initially, a cobalt/iodide catalyst was used, similar to early hydroformylation catalysts however, the applicability of the cobalt catalyst diminished rapidly with the introduction of the rhodium/iodide-catalyzed reaction by Monsanto.¹⁴ The cobalt catalyst was definitely cheaper than the rhodium catalyst, but had lower selectivity and required higher temperatures and pressures.¹⁵ The Monsanto Process produces over two million tons of acetic acid per annum by the carbonylation of methanol with greater than 99% selectivity using a rhodium/iodide catalyst.^{14b,16}

The next major modification of the process came in 1995 when BP Chemicals commercialized the Cativa™ process, using promoted iridium catalysts for methanol carbonylation.¹⁷ The effectiveness of iodide-promoted iridium catalysts had been noted in the original work at Monsanto, but only the rhodium process was commercialized.^{14a,15,18} The iridium-based process offers several advantages: not only is iridium approximately $\frac{3}{5}$ the cost of rhodium, but the iridium catalyst is also more robust and functions well under a broad range of conditions with higher reaction rates. Furthermore, less byproducts are produced, and the Cativa™ process can be promoted by a variety of compounds.^{17b,19}

The carbonylation of methanol is a rare process, in that all three of the group 9 metals have proven to be active catalysts and improvement in the catalyst activity has progressed down the group. The fact that iridium (Cativa™) is the best homogeneous industrial catalyst for this reaction is in some ways surprising, since the greater metal–ligand bond strengths of third-row metals²⁰ generally give rise to *less* labile systems having lower catalytic activity than their lighter congeners. In fact, it is this property that frequently prompts chemists to use Ir-based systems as stable models for first and second row catalytic systems.

1.1.2 Olefin Polymerization

One of the most important commercially used catalytic processes involves the polymerization of olefins (Eq. 1-6), and the development of polymerization catalysts is a well-researched field.²¹ Over the last 50 years, the production volume of polyolefin materials has increased considerably, to greater than 200 megatons per annum.²² The most recognized of all olefin polymerization catalysts are Ziegler-Natta catalysts, the development of which earned Ziegler and Natta the Nobel Prize in Chemistry in 1963.²³ Ziegler-Natta catalysts account for the production of more than 15 million tons of polyethylene and polypropylene per annum. Commercial Ziegler Natta catalysts are often high-valent early metal

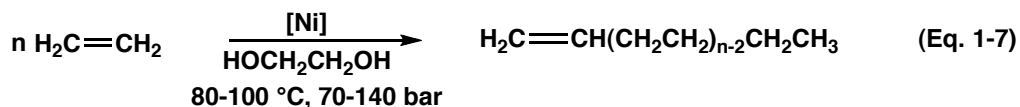


complexes on supports, such as the heterogeneous TiCl_3 catalyst, in which the active centres are on crystallites of TiCl_3 supported on MgCl_2 . Soon after the discovery of Ziegler Natta catalysts, homogeneous versions were developed. The general form of homogeneous Ziegler-Natta catalysts is $[\text{LL}'\text{MCl}_2]$ ($\text{M} = \text{Ti}, \text{Zr}, \text{Hf}$) in which L and L' were initially cyclopentadienyl (Cp) ligands, and therefore early homogeneous polymerization catalysts were termed metallocenes.^{21a} The catalysts for this process, however, can be varied such that L and L' are not necessarily Cp, and are therefore more commonly referred to as single-site

catalysts. This tunability allows for the control over the microstructure of the polymer as well as its polydispersity.

The polymerization of olefins occurs via successive migratory insertions of metal-bound alkyl groups to a metal-bound olefin. Most catalysts used for the polymerization of olefins are early transition metals, as later metals generally favour β -hydride elimination, which terminates chain growth. The greatest proportions of ethylene- and propylene-based polyolefin materials are found in packaging, building and construction supplies, transportation (lubricants, seals, transport tanks), electronic and electrical devices (cables, electrical home devices), agriculture supplies (twines, strings), medical supplies (blister packaging, medical devices), and sporting goods.²² The wide-spread applicability of polyolefins is due to a wide range in polymer characteristics and properties that can be generated depending on the catalyst and conditions used.

The Shell Higher Olefins Process (SHOP) is an industrial process based on homogeneous nickel catalysts discovered by Keim and coworkers.²⁴ Shell manufactures α -olefins from ethylene by oligomerization using a nickel catalyst in a polar solvent such as ethylene glycol, with elevated temperatures and pressures (Eq. 1-7).¹ The oligomerization is the first step in the SHOP



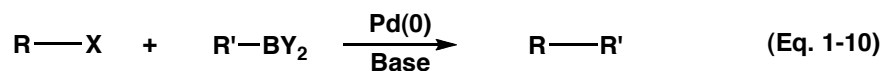
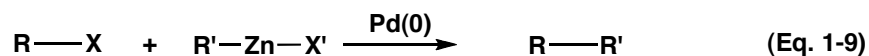
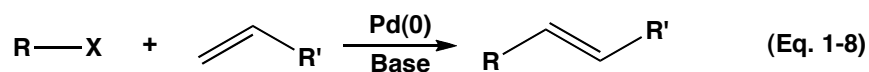
process and there are different applications for the different lengths of α -olefins. For example, the C_{10} – C_{14} oligomers are desirable feedstocks for use in detergent manufacturing, after hydroformylation to generate C_{11} – C_{15} alcohols.²⁵ The longer and shorter chains can then be manipulated by metathesis and isomerization over a heterogeneous catalyst to produce more of the C_{10} – C_{14} fragments.

1.1.3 Cross Coupling Reactions

Transition-metal catalyzed C–C bond formation has also demonstrated remarkable efficiency in cross coupling reactions, in which two different hydrocarbon fragments are coupled over a metal catalyst. Richard F. Heck, Ei-

ichi Negishi, and Akira Suzuki were awarded the 2010 Nobel Prize in Chemistry “for palladium-catalyzed cross couplings in organic synthesis” and have revolutionized fine chemical synthesis with their coupling reactions.²⁶ Specifically, the vinylation of aromatics has important applications in forming key precursors to fine chemicals. For example, the coupling of vinyl groups to aromatics can form intermediates to non-steroidal antirheumatic drugs, potent herbicides, and monomers for polymerization to electronic resins.¹

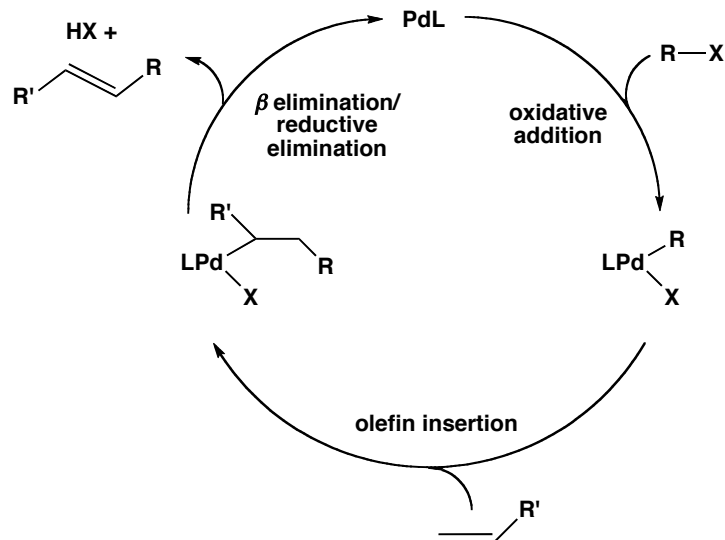
The classical Heck (Eq. 1-8),²⁷ Negishi (Eq. 1-9),²⁸ and Suzuki (or Suzuki-Miyaura) (Eq. 1-10)²⁹ couplings all involve Pd catalysts (also some Ni) and an alkyl, vinyl, or aryl halide, as shown below. Heck originally carried out his syntheses with arylmercuric compounds; however, Mizoroki soon after demonstrated that the reaction could be carried out with aryl iodide reagents,³⁰ hence the Heck reaction is often referred to as the Heck-Mizoroki reaction.



If one looks specifically at the Heck reaction, as an example, the overall mechanism of C–C bond formation appears to follow a pathway demonstrating fundamental elementary reaction steps, exemplifying some of the transformations commonly occurring at transition metal centres. The schematic mechanism shown below in Scheme 1-2 depicts: a) *oxidative addition* of the aryl or vinyl halide to the Pd centre, increasing the metal oxidation state by two; b) *olefin insertion* (involving an olefin containing an electron-withdrawing group) occurs into the Pd–R bond followed by; c) *β elimination* releasing the coupled fragment; and finally d) *reductive elimination* of the acid byproduct, regenerating the Pd

catalyst.²⁶ The highlighted transformations are possible due to the availability of more than one oxidation state and the ability of the metal centre to activate bonds between atoms, including those that are polar and those that are non-polar.

Scheme 1-2



1.1.4 Olefin Metathesis and Metal Alkylidenes

Olefin metathesis represents an unusual transformation in chemistry as it requires the cleavage of the very strong C=C double bond in the olefin.³¹ The breaking of the C=C double bond of an olefin generates carbene (RHC:) fragments which are exchanged between olefins. Yves Chauvin, Robert H. Grubbs and Richard R. Schrock were awarded the Nobel Prize in Chemistry in 2005 "for the development of the metathesis method in organic synthesis". Olefin metathesis is a valuable technology for the industrial production of olefins or the further conversion of olefins, as was described in the SHOP process. Metathesis is used in the production of bulk chemicals, specialty plastics and for fine chemical and pharmaceutical applications.²⁵

There are two main groups of organometallic catalysts for olefin metathesis, as shown in the representative examples in Chart 1-1. The Grubbs catalysts are Ru-based,^{31a,32} and have evolved such that replacement of a phosphine ligand in the first generation catalyst by an *N*-heterocyclic carbene

(NHC) generates the second generation catalyst.³³ Schrock catalysts are Mo- or W-based and are often used for asymmetric applications.^{31i,34} Although there are obvious differences between both types of catalysts, both contain a terminal alkylidene (=CRR') moiety, crucial for metathesis reactivity.

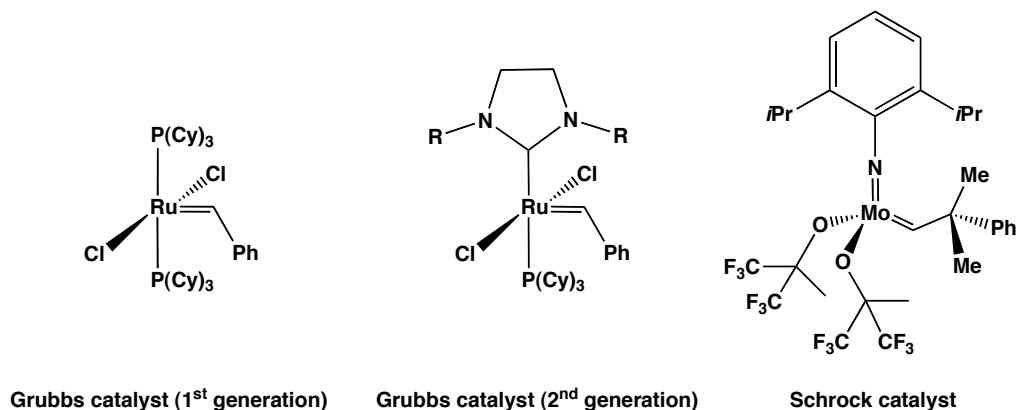
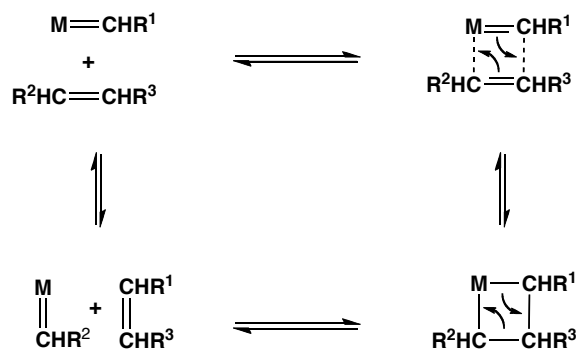


Chart 1-1. Olefin metathesis catalysts

The mechanism for olefin metathesis was correctly proposed by Hérisson and Chauvin in the early 1970's.³⁵ This mechanism, shown in Scheme 1-3, describes the formation of a metallacyclobutane from the 2+2 cycloaddition of the terminal alkylidene and the incoming olefin, which can either cleave reversibly to give the original reactants or, by cleavage of the original M–C and C–C bonds, generate a new olefin and a different alkylidene.²⁵

Scheme 1-3



As noted earlier, the terminal alkylidene moiety is critical in olefin metathesis reactions. Furthermore, metal complexes containing terminal

alkylidenes find many applications outside of metathesis reactions and are active in cyclopropanation reactions,³⁶ and the oligomerization of alkynes.³⁷ The majority of metal alkylidenes studied are of the form $L_nM=CRR'$ in which the alkylidene is terminal and bound to a single metal, much like those in the metathesis catalysts.³⁸ Complexes in which the alkylidene ligand bridges two metal centres,³⁹ have been much less studied and they differ from their terminal counterparts in that the bridging alkylidene has an approximately tetrahedral geometry and is formally saturated. As a result, bridging alkylidenes are expected to be less reactive than terminal unsaturated alkylidenes. Nonetheless, bridging alkylidenes have displayed interesting reactivity, particularly involving C–C bond formation with a variety of substrates.⁴⁰ The prototypical alkylidene – the methylene (CH_2) group which bridges adjacent metals on the catalyst surface – has also been implicated as the essential surface-bound species involved in carbon–carbon chain growth in Fischer-Tropsch chemistry.⁴¹

1.1.5 Fischer-Tropsch (FT) Chemistry

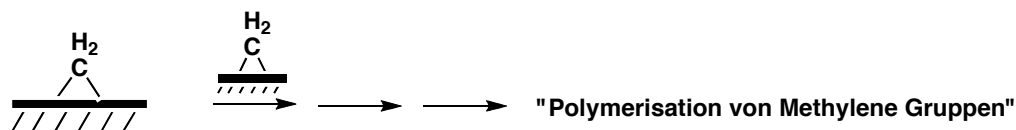
One fascinating example of C–C bond formation involves the conversion of two of the simplest molecules, CO and H_2 into a range of hydrocarbon products having uses as fuels and chemical feedstocks such as α -olefins, oxygenated hydrocarbons and alkanes, as shown below in Eq. 1-11. The component feedstock gases, CO and H_2 (syngas), required for FT chemistry are produced by the gasification of coal or the reforming of methane. The combination of these processes (syngas production and FT) are energy intensive and therefore the process is expensive. For FT chemistry to be economically viable, the cost of coal or natural gas must be low enough to offset the high cost of gasification.



Sabatier and Senderens first reported, in 1902, that passing syngas over a nickel catalyst produced methane.⁴² In 1923 Franz Fischer and Hans Tropsch in Germany reported the synthesis of linear aliphatic hydrocarbons at atmospheric pressure at 200–300 °C, by passing syngas over an iron or cobalt catalyst.⁴³ In these initial papers by Fischer and Tropsch, the reaction was described as the

initial formation of surface carbides, which were reduced by hydrogen to give surface-bound methylene groups ($\mu\text{-CH}_2$), which then polymerized to the hydrocarbon products (Scheme 1-4).

Scheme 1-4



The production of liquid petrochemicals synthesized with FT technology began in 1936, and it was used by Germany for the large-scale production of diesel fuel during World War II.⁴⁴ The economic feasibility of FT chemistry is directly related to the price of crude oil, which currently is the main source of liquid fuels. In the late 1940's, the limited amount of known oil reserves worldwide resulted in the prediction that the price would rise; however, massive deposits of crude oil were found in the Middle East, keeping the cost of oil from rising as many had anticipated.⁴⁴ This also slowed down further development of the FT process as a viable energy source. However, in the 1970's, the oil embargo placed on South Africa prompted the need for an alternate fuel supply, and interest in FT research was rekindled in this country. Currently, the price of crude oil is high enough for FT chemistry to be a viable technology for the production of fuels, as the cost of feedstocks (methane or coal) is still relatively low. Furthermore, with the depletion of conventional crude oil reserves and the abundance of coal and natural gas (see Table 1-1),⁴⁴ the increased usage of these abundant carbon reserves is inevitable.

Table 1-1. World reserves of "carbon" relative to oil

Source	Reserves, oil equivalent
Crude Oil	1.0
Tar Sands	0.7
Shale Oil	1.2
Natural Gas	1.5
Coal	26

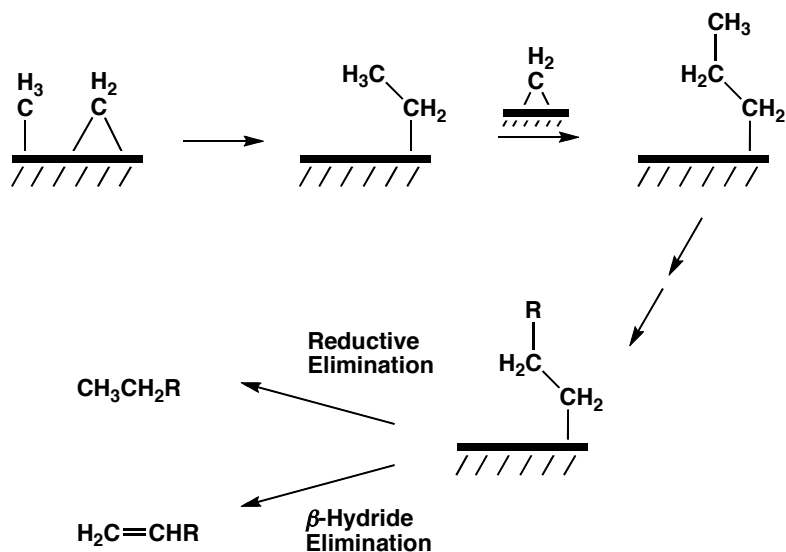
Classical FT chemistry often leads to the production of many different products, although the prominent products include α -olefins and aliphatic hydrocarbons. Small variations in catalyst, pressure, and temperature have profound impacts on product distribution. For example, a high temperature process (300 – 350 °C) with Fe-based catalysts is used for the production of gasoline and linear, low molecular mass olefins. The low temperature process (200 – 240 °C) with an Fe or Co catalyst is used for the production of high molecular mass linear waxes.⁴⁵ The mechanism of how C–C chain growth occurs in FT chemistry is not well understood, but mechanistic elucidation could allow for the tailoring of catalysts, conditions, and product distribution through rational design.

The first step in FT chemistry is the transformation of chemisorbed CO into a surface carbide to be hydrogenated, as was confirmed through surface studies (including labelling studies),⁴⁶ and organometallic models.⁴⁷ Although currently there is general agreement that the formation of a carbide species, followed by hydrogenation are the initial steps in the generation of hydrocarbons by FT chemistry, there is much less agreement on the important steps that result in the coupling of the CH₂ fragments. For example, Brady and Pettit discovered that passing CH₂N₂ and an inert gas over Ni, Pd, Fe, Co, Ru and Cu surfaces, only resulted in the decomposition of the CH₂N₂ to N₂ and ethylene.^{41c} They concluded that the simple reaction of μ -CH₂ groups was dimerization instead of polymerization. Interestingly, when H₂ was mixed with CH₂N₂, a range of hydrocarbon products, similar to the FT distribution, was observed over the same catalysts, suggesting that the original Fischer and Tropsch proposal of methylene oligomerization couldn't be correct.

Brady and Pettit proposed a different mechanism for chain propagation involving the migration of alkyl groups onto μ -CH₂ groups (Scheme 1-5).^{41c,d} Initiation occurs by migration of a methyl group (formed from the hydrogenation of surface-bound methylenes) onto a μ -CH₂ group to generate an ethyl group. Chain growth then occurs by migration of the ethyl fragment onto another μ -CH₂

group and continues, generating higher homologues, until reductive elimination occurs with a surface hydride to generate a linear alkane, or β -hydride elimination occurs to yield an α -olefin.

Scheme 1-5



Another inconsistency with the original mechanism is shown in a study of the statistics of product distribution. Anderson-Schulz-Flory (ASF) chain-length statistics imply that sequential chain propagation steps result in the hydrocarbon chain growing one carbon at a time, and that chain propagation and termination occur with probabilities independent of the length of the growing chain.⁴⁸ FT chemistry, if it occurs as originally proposed, should follow these chain-length statistics. Graphically, a plot of the log (W/N) (W = mass fraction and N = carbon number) versus N should give a straight line (dashed line, Figure 1-1). The mass fraction (W) decreases consistently as the number of carbons increases and, as such, the major product is the C_1 fragment (methane) followed by C_2 (ethane and ethylene), then C_3 hydrocarbons, and so on. As is shown, deviations from the ASF distribution of products occur when analyzing FT products (solid line, Figure 1-1).

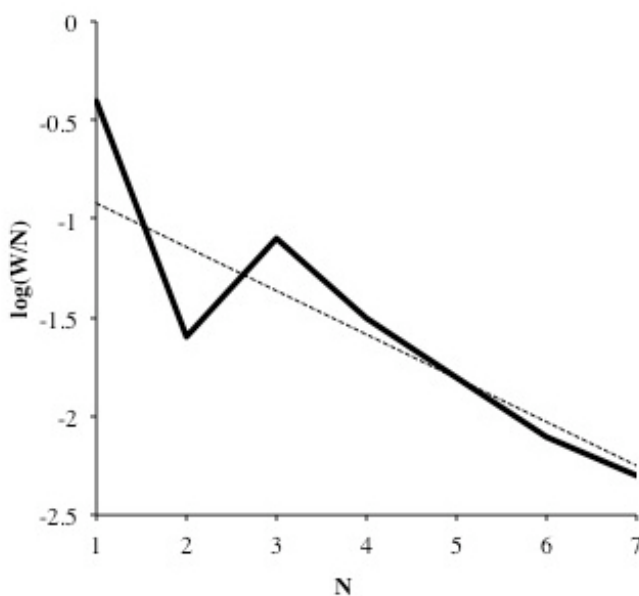
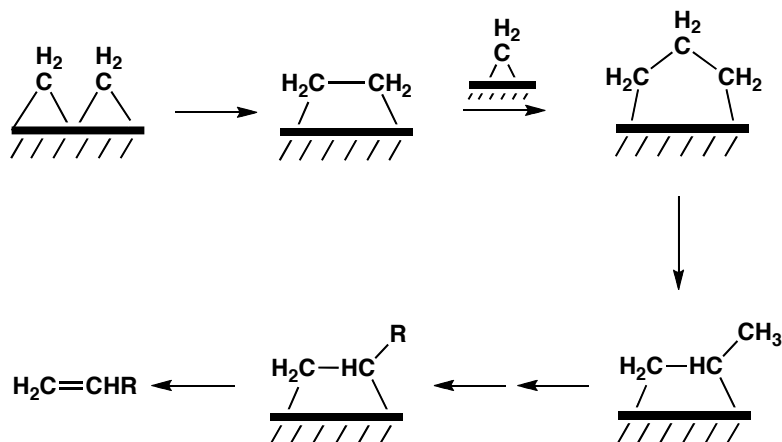


Figure 1-1. *A representative Anderson-Schulz-Flory plot for CO hydrogenation. The dashed line represents the theoretical plot for the polymerization of C₁ species; solid line represents the experimentally observed values based on a Rh/Ce/SiO₂ catalyst at 200 °C, 1 atm, CO:H₂ (1:2).⁴⁹*

The mechanism proposed by Brady and Pettit, like the original chain growth proposal, still failed to explain the anomalously low production of C₂ hydrocarbons. FT chemistry also results in the formation of a small amount of branched hydrocarbons, but the original proposal did not address the formation of such products. In a later proposal by Dry,^{41h,50} chain propagation occurs by the coupling of a surface-bound C₂ fragment (olefin) with a μ -CH₂ to generate a C₃ fragment, that isomerizes to a fragment that can be viewed as an adsorbed methyl-substituted C₂ olefinic fragment (propene), which is then available for further coupling (Scheme 1-6).^{41h,50} The subsequently added CH₂ groups add to the less hindered side of the olefinic growing chain and therefore desorption results in the formation of an α -olefin. This mechanism can also explain the lower than expected C₂ hydrocarbon production in in FT chemistry and the deviation from ASF statistics, because the C₂ surface-bound fragment has two metal-carbon bonds that are the same, and not hindered by steric effects at one end like those of

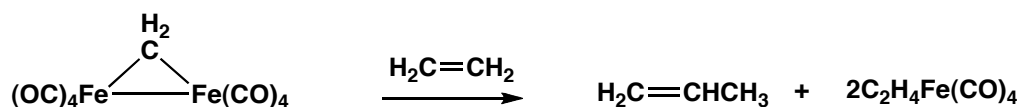
the C₃ and higher homologues (fragments). This means that the chain growth will occur at a rapid rate to form higher carbon fragments, relative to desorption.

Scheme 1-6



Dry's mechanism was also consistent with an earlier study by Brady and Pettit who used an $\text{Fe}_2(\text{CO})_8(\mu\text{-CH}_2)$ complex to investigate how ethylene coupled to a $\mu\text{-CH}_2$ group, as shown in Scheme 1-7.⁵¹ Presumably the loss of a CO ligand

Scheme 1-7



results in the generation of unsaturation required for the ethylene to bind to an Fe centre. This presumably is followed by ethylene insertion into the Fe-CH₂ bond to generate a bridging 1,3-propylene unit that undergoes β -hydride elimination to generate an allyl-hydride complex followed by reductive elimination to generate propylene. The proposed intermediates in this reaction were never observed,⁵¹ however, they do share a striking resemblance to the first steps of initiation and chain propagation of the Dry mechanism.

The FT process is obviously a heterogeneous process that has been investigated using heterogeneous metal surfaces as well as homogeneous metal complexes. As will be discussed, organometallic chemistry plays a significant role in investigating chain propagation for C-C bond formation in FT chemistry.

1.2 Heterogeneous vs. Homogeneous Catalysts

Although most of the processes discussed above are homogeneous, in which the catalysts are well-defined metal complexes dissolved in a solvent, many of the catalysts in industry are heterogeneous (such as in FT chemistry), in which the catalysts (generally a solid) and the reactants (usually liquids or gases) are in a different phase. Heterogeneous catalysts have the advantages of reasonable and even high activity, can be removed by simple physical methods such as filtration, do not contaminate the product, and are generally robust. Disadvantages of heterogeneous catalysts include harsh conditions (high reaction temperatures and pressures) in order to achieve high activities that are often necessary and the lack of selectivity, owing to the presence of many different types of active sites on a metal surface. Furthermore, the study of catalyst mechanisms in order to bring about rational improvement in catalyst design is difficult. The development and study of heterogeneous catalysts, regardless of whether or not a transition metal is involved, is often done empirically by employing a combinatorial or high-throughput approach in which multiple catalysts, conditions, and substrates can be tested and compared.⁵² Despite the obvious differences when comparing a soluble homogeneous metal complex to a heterogeneous catalyst, the same fundamental molecular transformations occur in both systems,⁵³ as proposed by E. L. Muetterties.

As noted, a variety of industrially catalyzed processes rely mainly on the use of heterogeneous catalysts. For example, the synthesis of ammonia is catalyzed over a heterogeneous Fe catalyst.⁵⁴ Petrochemical reforming processes including gasoline reforming (Pt/Re or Pt/Ir), hydrodesulfurization (using Co/Mo or Ni/Mo), and hydrocracking (Ni/Mo or Ni/W) all utilize heterogeneous catalysts.⁵⁵ Interestingly these last few catalysts contain two different metals, with presumably different properties.

Homogeneous systems are often used as models for heterogeneous catalysts,^{53a} and provide a number of advantages including solubility in organic solvents, the ease of catalyst modification, and the availability of standard

techniques for product characterization. The homogeneous catalysts discussed earlier are amenable to rational design by altering the steric and/or electronic properties of the catalyst. For example, the substitution of a $\text{P}(\text{Cy})_3$ ligand in Grubbs' 1st generation catalyst for an NHC ligand (2nd generation) generates a more active catalyst that is more tolerable to moisture and air.²³ Also, in the SHOP process, the substituents on the P,O chelating ligand in the nickel catalysts can be changed to dramatically affect the product distribution of oligomers/polymers.^{24b}

The facile tunability of homogeneous catalysts is also demonstrated with $[\text{RhCl}(\text{PPh}_3)_3]$, which was reported independently by three different groups in 1965,⁵⁶ and its use as a highly active hydrogenation catalyst was studied extensively by Wilkinson,^{10,57} and is therefore often referred to as Wilkinson's catalyst. The ligand system of this complex is amenable to rational design and was demonstrated with the synthesis of "Rh(diene) L_2^+ " catalysts first developed by Schrock and Osborn in 1979.⁵⁸ By evolving the ligand system, Schrock and Osborn were able to achieve the selective hydrogenation of alkynes to cis-olefins,⁵⁹ and dienes to monoenes.⁶⁰ The most important application of this work, however, is asymmetric catalysis.⁶¹ Some monometallic complexes have applicability as homogeneous catalysts, but these complexes are not generally reasonable models for surface catalysis because they lack a key component – an adjacent metal centre.

1.3 Surface Models and Multinuclear Complexes

1.3.1 Polynuclear Complexes

In the 1970's E. L. Muetterties made two bold assertions: that discrete metal cluster compounds were reasonable models for metal surfaces; and that surface chemistry was coordination chemistry, and the manipulation of organic molecules on a surface was organometallic chemistry.⁶² Clusters, having a number of adjacent metal centres provided an approximation to a portion of a metal surface, and in the presence of organic substrates could be effective models for the interaction of these substrates with the surface. However, in spite of the

relative ease of studying the reactivity of clusters under homogeneous conditions compared to heterogeneous reactions involving surfaces, the poor solubility of clusters and the presence of multiple metal centres still made it difficult to obtain detailed mechanistic information about the reactions involved. For these reasons there has been considerable interest in the organometallic chemistry of the relatively simple binuclear complexes. These complexes are relatively easy to study, while still having adjacent metals to allow the influence of these adjacent metals on substrate activation to be determined.

1.3.2 Bimetallic Complexes and Metal-Metal Cooperativity

Whether or not bimetallic complexes are effective models for surface catalysts, the availability of a second metal centre provides possible reactivity enhancement, or the possibility of metal-metal cooperativity which can give rise to reactivity enhancement compared to mononuclear systems. One of the best known examples of this was reported by Stanley and coworkers in 1993,⁶³ in which a dirhodium complex, $[\text{Rh}_2((\text{Et}_2\text{PCH}_2\text{CH}_2)(\text{Ph})\text{PCH}_2\text{P}(\text{Ph})(\text{CH}_2\text{CH}_2\text{PEt}_2))(\text{nbd})_2][\text{BF}_4]_2$ (nbd = norbornadiene), was shown to be a more effective hydroformylation catalyst (Chart 1-2), than closely comparable mononuclear systems. If the two metals could not get into close proximity, rate enhancement ceased, as was shown by synthesizing tetraphosphine ligands in which the central methylene bridge was replaced by larger spacers. With larger spacers, each Rh centre of the catalyst acted as an individual monomeric catalyst with poor activity and selectivity.

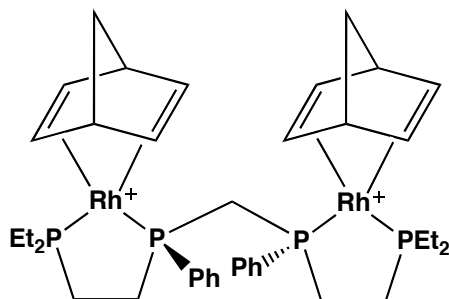
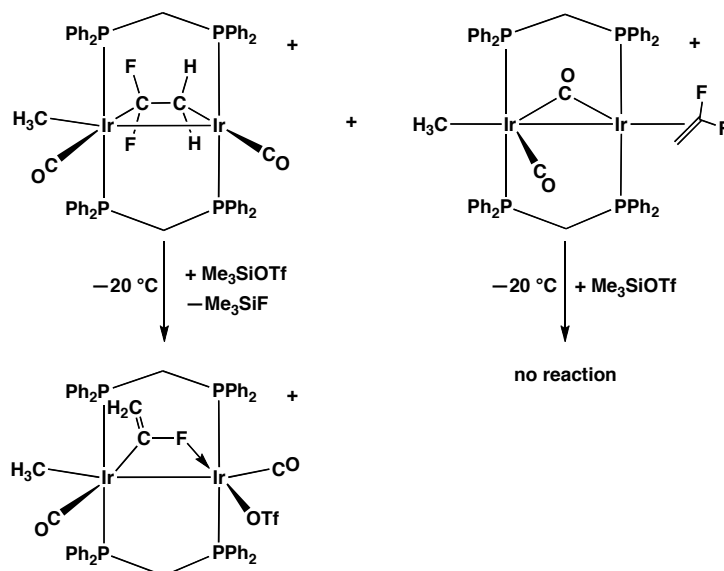


Chart 1-2. Stanley's bimetallic hydroformylation catalyst

Another interesting example of bimetallic cooperativity (albeit not catalytic) involves a diiridium system that has been shown to bind fluoroolefins in two coordination modes: terminally on Ir or in a bridging position between both Ir centres.⁶⁴ Upon addition of a fluoride ion abstractor to a mixture of isomers at $-40\text{ }^{\circ}\text{C}$, only the isomer with the bridging fluoroolefin reacts, while the other isomer remains unchanged,⁶⁵ as shown in Scheme 1-8. This observation was the

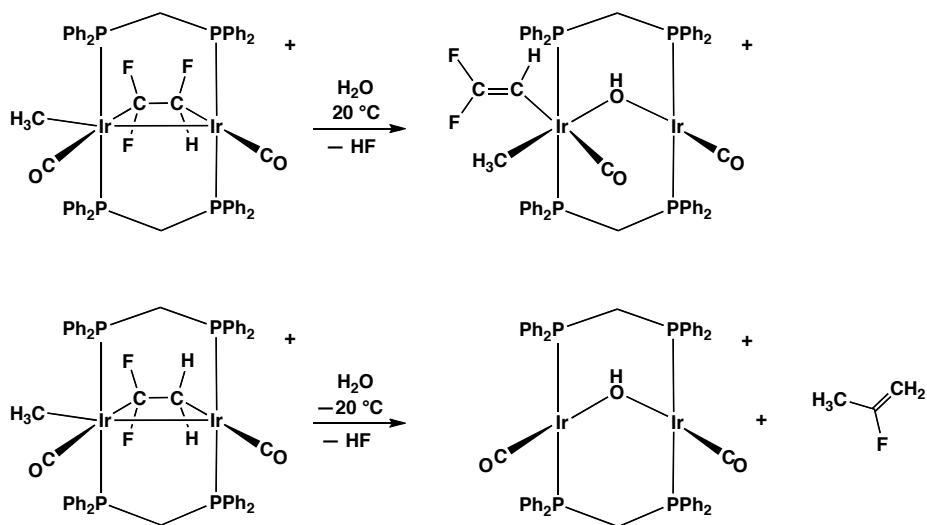
Scheme 1-8



first clear documentation of the enhanced reactivity of a bridging fluoroolefin over the terminal η^2 binding mode, attributed to cooperativity of the adjacent metal centres in substrate activation. It was later shown, that bridging trifluoroethylene or 1,1-difluoroethylene could be activated (even at low temperature) by water (Scheme 1-9, following page).⁶⁶

These examples, once again, illustrate how two adjacent metal centres can cooperate to facilitate the transformation of substrates. The bridging binding mode between two metal centres appears conducive to molecular transformations and activations, both on surfaces and in bimetallic complexes.

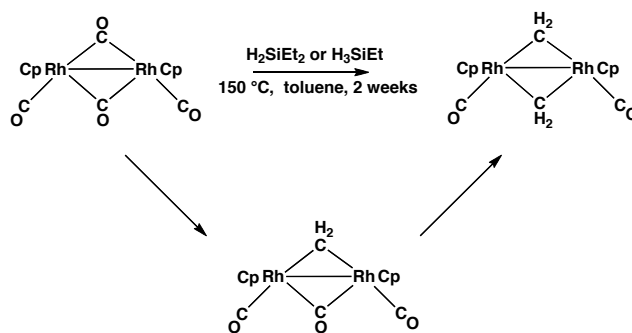
Scheme 1-9



1.3.3 Homogeneous Organometallic Complexes as Models for FT Chain-Growth

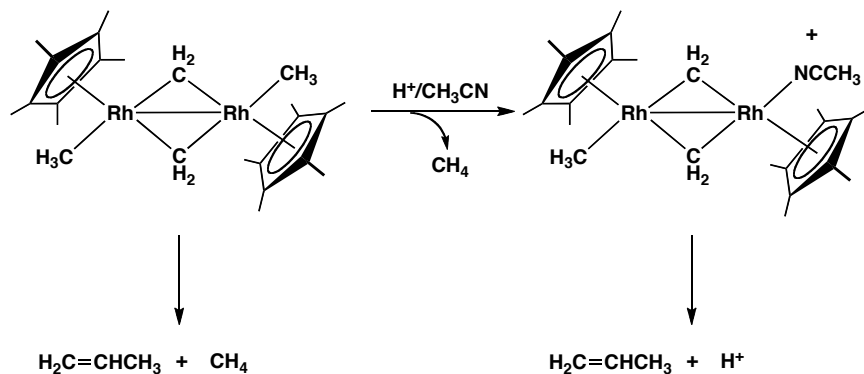
As noted earlier, there is general agreement that the first steps in FT chemistry involve the transformation of adsorbed CO to surface-bound carbides followed by H₂ reduction to μ -CH₂ groups bridging adjacent metals. This transformation of CO to CH₂ has been modeled in a bimetallic [Ru₂(Cp)₂(CO)₄] (Cp = η^5 -C₅H₅) complex by Akita and coworkers.⁶⁷ The addition of primary or secondary silanes to a toluene solution of the compound results in deoxygenative reduction to the bis(μ -CH₂) product [Ru₂(Cp)₂(CO)₂(μ -CH₂)₂] over 2 weeks, as shown in Scheme 1-10.⁶⁷

Scheme 1-10



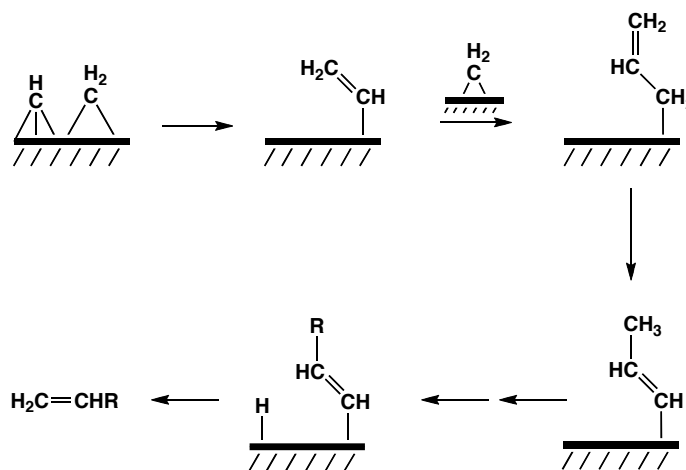
Most of the interest in the FT process by organometallic chemists has centred on the chain-propagating steps. Maitlis investigated FT-related C–C couplings using the decomposition of a $[\text{Cp}^*\text{Rh}(\mu\text{-CH}_2)(\text{Me})]_2$ ($\text{Cp}^* = \text{C}_5\text{Me}_5$) system to generate propylene, either thermally or with the addition of one-electron oxidants (Scheme 1-11).^{41f,68} Interestingly, a series of ^2H - and ^{13}C -labelling

Scheme 1-11



studies suggested that the simple coupling of C_1 fragments was probably not occurring but instead suggested the intermediacy of a σ -vinyl species, which then migrates to a $\mu\text{-CH}_2$ group to generate an allyl group. In the Maitlis proposal, initiation of chain growth starts by coupling of a surface-bound methyne ($\mu\text{-CH}$) and a $\mu\text{-CH}_2$ to generate a surface-bound alkenyl group (Scheme 1-12).^{41f,68f} This

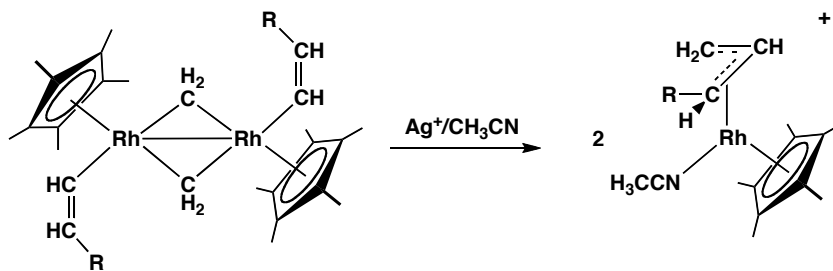
Scheme 1-12



alkenyl group can then migrate onto a μ -CH₂ group on the surface to give an allyl. Rearrangement via a 1,3-hydride shift results in isomerization to a substituted alkenyl unit and the migration onto another μ -CH₂ group can occur. Reductive elimination of the growing alkenyl fragment with a surface-bound hydride results in the linear olefin. In this mechanistic proposal, the initial formation of the vinyl species differs from the chain propagation steps, which would explain the anomalous C₂ production in FT chemistry according to ASF statistics.

The involvement of a vinyl moiety in carbon chain growth found support in subsequent studies in which σ -vinyl ligands were coupled to μ -CH₂ groups to give an allylic complex in the presence of a one-electron oxidant (Ag⁺) and acetonitrile (CH₃CN) as shown in Scheme 1-13.⁶⁹

Scheme 1-13



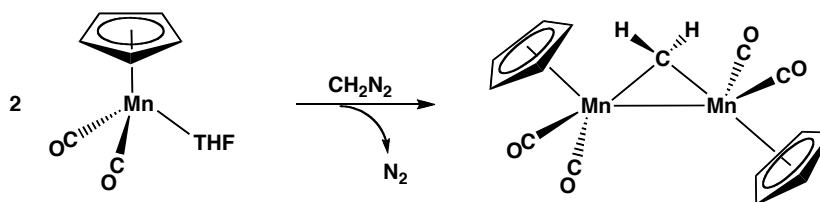
Although each mechanistic proposal discussed herein for chain growth in FT chemistry (Fischer-Tropsch, Brady-Pettit, Dry, Maitlis)⁴¹ is different in terms of the nature of the hydrocarbyl fragment that couples to the hydrogenated CO on the catalyst surface, all four proposals illustrate the importance of the μ -CH₂ functionality. Of particular interest to this thesis is the use of bimetallic, CH₂-bridged complexes containing group 8 and 9 metal centres to model the FT process. As previously mentioned, the FT product distribution differs, when, for example, Fe or Co is used as the catalytic metal.⁴⁵ This observation coupled with the possibility of metal-metal cooperativity discussed above, suggests that a bimetallic group 8/9 catalyst may have a substantial impact in FT chemistry, and an increase in activity and selectivity has been reported with such mixed-metal catalysts.⁷⁰ Studies have shown that a supported group 8/9 Co/Ru bimetallic

catalyst has increased activity and selectivity in the hydrogenation of CO than do samples incorporating only one metal, even when highly dispersed.⁷¹ Similar results have been shown with SiO₂-supported Fe/Rh, and Fe/Ir clusters derived from metal–carbonyl clusters.⁷² These aforementioned heterogeneous, mixed-metal catalysts show rate and selectivity enhancement over the single-metal catalysts, however, little is known about the role of each different metal in the FT process.

1.3.4 Methylene-Bridged Bimetallic Complexes

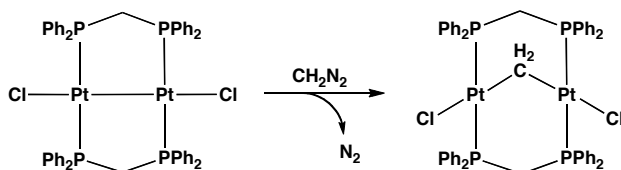
The bridging methylene group is pivotal to much of the research presented in this thesis. It has been shown that complexes in which the alkylidene unit bridges pairs of metal centres,³⁹ although not as reactive as the unsaturated terminal groups, nevertheless display interesting reactivity. The first, stable CH₂-bridged complex was reported by Herrmann and coworkers in 1975.⁷³ Treatment MnCp(CO)₂(THF) with CH₂N₂ resulted in the generation of Mn₂(Cp)₂(CO)₄(μ-CH₂) (Cp = η⁵-C₅H₅), as shown in Scheme 1-14. Herrmann and coworkers also

Scheme 1-14



synthesized an analogous Rh₂ complex, again by reaction of the precursor with CH₂N₂, and were able to obtain the first crystal structure determination of a methylene-bridged organometallic compound, which confirmed the distorted tetrahedral geometry at the bridging carbon.⁷⁴ The cases described above both have metal–metal bonds, but it is not a necessity. The first CH₂-bridged complex without a metal–metal bond was prepared using the same CH₂N₂ method described above wherein the CH₂ group inserts into a Pt–Pt bond (Scheme 1-15).⁷⁵ The bridging diphosphine in this case is important for maintaining the integrity of the complex by providing a rigid scaffold that holds the Pt centres

Scheme 1-15

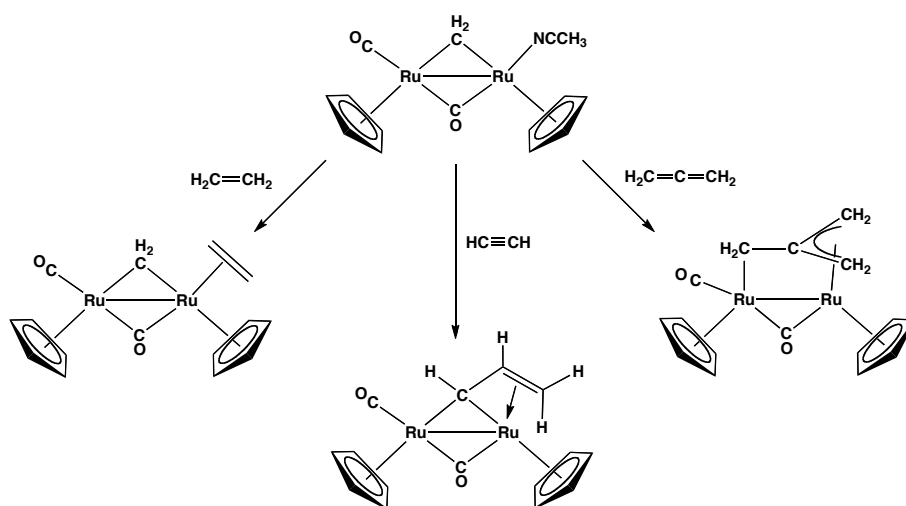


close enough to support the CH_2 group in the bridging position. Methylene-bridged complexes can also be synthesized by the double oxidative addition of a dihalogenomethane, as first reported by Balch and coworkers in 1981.⁷⁶ Throughout this thesis the preparation of $\mu\text{-CH}_2$ complexes will follow the CH_2N_2 method as opposed to the double oxidative addition route.

1.3.5 Carbon–Carbon Coupling Using Methylene-Bridged Complexes

The chemistry of CH_2 -bridged complexes obviously focuses heavily on the coupling of the CH_2 unit with other ligands, often resulting in C–C bond formation and various coordination modes of the resultant hydrocarbyl fragment.⁷⁷ Unsaturated substrates such as alkynes,^{40c,51b,78} cumulenes,⁷⁹ and olefins,^{51a,80} are particularly reactive with bridging methylene groups. Knox and coworkers studied the reactivity of $[\text{Ru}_2(\text{Cp})_2(\text{CO})_2(\text{NCCH}_3)(\mu\text{-CH}_2)]$ with a variety of unsaturated fragments (Scheme 1-16),^{40a,79a,81} noting that, for this

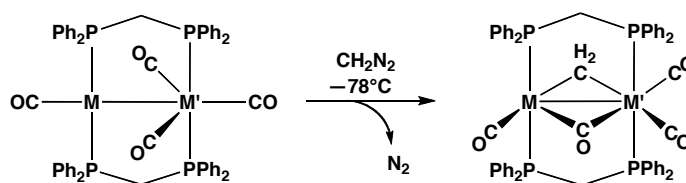
Scheme 1-16



system, facile coupling only occurred with the ligands that supplied more than two π -electrons. The coupling between the μ -CH₂ and propadiene (allene) resulted in a μ -trimethylenemethane moiety, which is believed to proceed through an unobserved, C₃-bridged intermediate generated by cumulene insertion into the Ru-CH₂ bond.

The putative intermediates in these C-C coupling processes were of interest to our group. Diphosphine-bridged systems of the Rh/Ru,⁸² Ir/Ru,⁸³ and Rh/Os⁸⁴ combinations, containing bridging methylene groups were synthesized by the conventional method of the addition of CH₂N₂ at low temperatures (Scheme 1-17).⁸⁵ Although the Rh/Ru and Ir/Ru systems yielded the same products over a

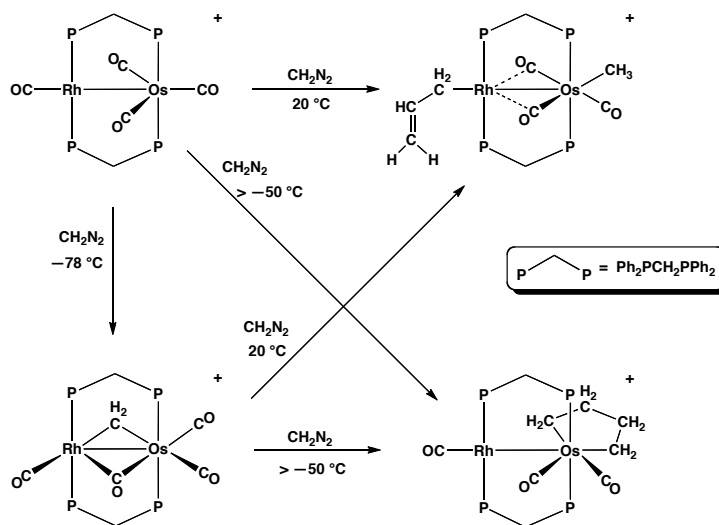
Scheme 1-17



M/M' = Rh/Ru, Rh/Os, Ir/Ru

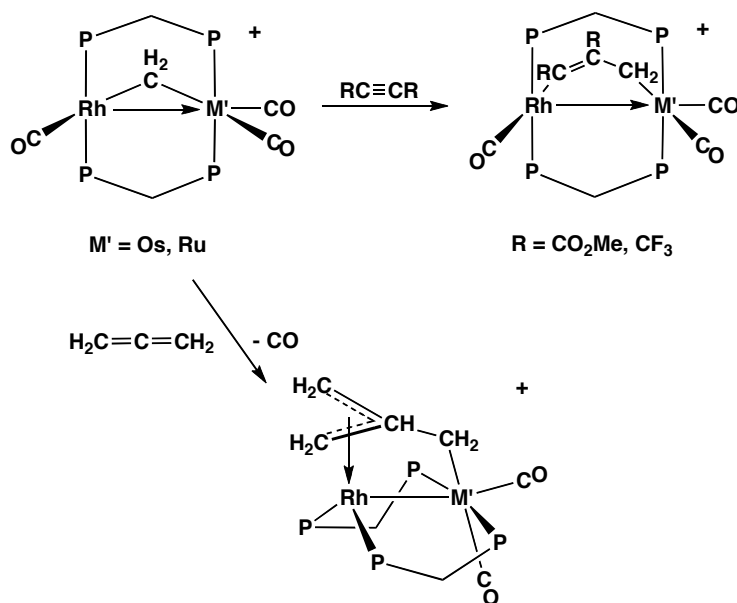
range of temperatures, up to ambient, the Rh/Os system requires low-temperature addition since at higher temperatures, CH₂ coupling (Scheme 1-18), occurred in

Scheme 1-18



which up to four CH₂ groups can be coupled,⁸⁴ resulting in the generation of either allyl and methyl, or butanediyl groups. The facile coupling of CH₂ groups suggests that our late-metal diphosphine-bridged systems may indeed prove valuable in modelling chemistry related to the FT process discussed above. Labelling studies involving this Rh/Os system implicated the involvement of bridging C₃- and C₄-hydrocarbyl intermediates. These putative hydrocarbyl intermediates remained elusive, as in the aforementioned Knox example,^{40a} but a stepwise incorporation of CH₂ groups was proposed. In attempts to model these intermediates, the addition of unsaturated substrates to [RhM'(CO)₃(μ-CH₂)(dppm)₂][X] (M' = Os, Ru, X = BF₄, CF₃SO₃) complexes was studied, in hopes of generating C₃-bridged complexes. In the reaction of both compounds with alkynes, the C₃-hydrocarbyl bridged complexes, as shown in Scheme 1-19, were successfully synthesized.^{78d,78k} The addition of another “CH₂” equivalent to the C₃-bridged Rh/Os complex generated a 5-membered rhodacycle, in which the 4-carbon hydrocarbyl fragment moved out of the bridging site to a chelating position on Rh.^{78k} Using allene as the unsaturated substrate in the Rh/Os

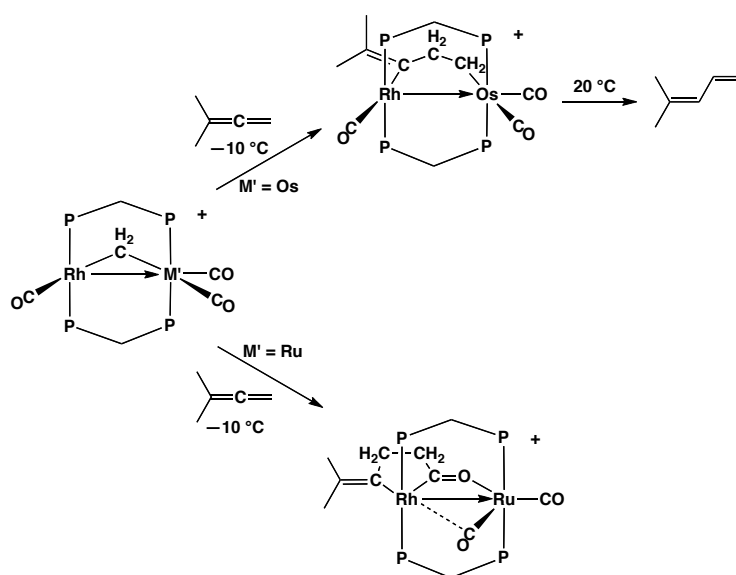
Scheme 1-19



and Rh/Ru systems discussed above, gave results resembling those reported by Knox with the generation of a μ -trimethylenemethane moiety,^{40a} but having the η^3 -bound fragment bound exclusively to the group 9 metal.

Reaction of $[\text{RhOs}(\text{CO})_3(\mu\text{-CH}_2)(\text{dppm})_2][\text{X}]$ ($\text{X} = \text{BF}_4, \text{CF}_3\text{SO}_3$) with 1,1-dimethylallene generated the C_3 -bridged intermediate, which at ambient temperature generated 4-methyl-1,3-pentadiene (Scheme 1-20).^{79c} The analogous Rh/Ru system also appeared to yield a C_3 -bridged fragment with 1,1-dimethylallene, although in this case migration of the hydrocarbonyl fragment to a CO ligand occurred, generating the corresponding acyl-bridged product.^{79c} These differences in reactivity are obviously due to the substitution of the group 8 metal centre (Os vs. Ru), as the reaction conditions and ancillary ligands are identical. Although such results can often be rationalized on the basis of the different metals used, the exact roles of each metal in these transformations remain to be determined. Developing a detailed understanding of the roles of the different metals and metal combinations will lead to an improved understanding of how metal–metal cooperativity can be used in organometallic chemistry ultimately leading to advances in catalyst development, including the move towards more function-directed catalysts.

Scheme 1-20

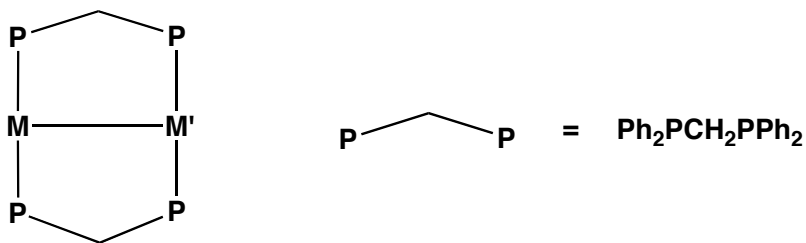


1.4 Goals of This Thesis

It is obvious that until the roles of the adjacent metals centres in the processes discussed herein are elucidated, the full benefits imparted by these heterobimetallic complexes, will not be exploited. It has for years been the contention of the Cowie group that in order to develop an understanding of the roles of the different metals in mixed-metal complexes, combinations of *all* metals involved need to be investigated. This is particularly true since the adjacent metal can significantly influence the reactivity at the other metal. Although the Rh/M' (M' = Os, Ru) combinations of μ -CH₂ complexes have been studied in detail and appear to function as useful models for the initial C–C bond coupling in FT chemistry, related systems involving Ir as the group 9 metal centre have been less studied. The potential benefits of changing to Ir include stronger metal–carbon bonds between the 3rd row Ir and the growing hydrocarbyl fragment. Although C₃-bridged complexes of Rh/Os and Rh/Ru have been isolated using alkynes as the C₂ fragment source, there have been no higher hydrocarbyl complexes observed in which the growing fragment bridges both metal centres. The implementation of Ir may promote the retention of the hydrocarbyl fragment at this metal and could allow for the additional growth of the hydrocarbyl fragment, which appears to happen only in the bridging position.⁸⁴ By incorporating Os as the accompanying group 8 metal, this pair of 3rd row metals, each having very strong M–C bonds, could optimize the possibility of retaining the bridging hydrocarbyl fragment.

In the work presented in this thesis, the focus is to generate Ir/M (M = Ru, Os) binuclear complexes in which the adjacent metals are held together by a linker ligand such that the metal–metal cooperativity, as mentioned above, can be exploited (Chart 1-3). Bis(diphenylphosphino)methane, or dppm, is a suitable ligand for the synthesis of bimetallic complexes wherein the role of the phosphine is to prevent dissociation of the bimetallic system into its monomeric components, while still being flexible enough to allow the formation and cleavage of metal–metal bonds.⁸⁶ This ligand also provides an added NMR handle available for

Chart 1-3



M/M' = Group 8/9 Metals

characterization, especially of non-isolable, labile intermediates, by providing information regarding the symmetry and connectivity within the bimetallic complex. The softer, late metals in low oxidation states tend to bind strongly to the phosphorus donor atoms, and this ligand system is relatively inert to the transformations occurring at the metal centres. Previous work in our group, however, has illustrated that the deprotonation of a methylene proton of the dppm backbone can occur,⁸⁷ and there has also been a recent case of dppm lability from a Rh centre.⁸⁸ In previous studies with Rh as the group 9 metal centre, the different metal environments could be distinguished by NMR. This thesis, however, focuses on Ir/M (M = Ru, Os) complexes, in which neither metal is observed in NMR studies, providing an additional challenge.

By studying the methylene-bridged systems of Ir/Ru, and Ir/Os (generated by CH_2N_2) and their reactivity with unsaturated substrates, we seek to provide information, that together with the extensive information already available on the Rh/M' systems discussed above, can help to elucidate the roles of the adjacent metals in these transformations, especially those relating to FT chemistry and C–C chain growth. We are also curious about the effect of replacing the group 9 metal with Ir, as this 3rd row metal has a greater tendency to undergo oxidative addition, particularly of C–H bonds. This reaction pathway could provide interesting competition to the C–C chain growth studied herein.

1.5 References

1. Calderazzo, F.; Catellani, M.; Chiusoli, G. P. In *Metal-catalysis in Industrial Organic Processes*; Chiusoli, G. P., Maitlis, P. M., Eds.; The Royal Society of Chemistry: Cambridge, 2006, p 163.
2. Barbier, P. *Compt. Rend.* **1899**, *128*, 110.
3. Grignard, V. *Compt. Rend.* **1900**, *130*, 1322.
4. Rakita, P. E. In *Handbook of Grignard Reagents*; Silverman, G. S., Rakita, P. E., Eds.; Marcel Dekker, Inc.: New York, 1996, p 1.
5. Bohnen, H.-W.; Cornils, B. *Adv. Catal.* **2002**, *47*, 1.
6. Cornils, B.; Herrmann, W. A.; Rasch, M. *Angew. Chem. Int. Ed.* **1994**, *33*, 2144.
7. (a) Adkins, H.; Krsek, G. *J. Am. Chem. Soc.* **1948**, *70*, 383. (b) Kirch, L.; Orchin, M. *J. Am. Chem. Soc.* **1959**, *81*, 3597.
8. Ziegler, T.; Versluis, L. *Adv. Chem. Ser.* **1992**, *230*, 75.
9. Slauch, L. H.; Mullineaux, R. D. *J. Organomet. Chem.* **1968**, *13*, 469.
10. Osborn, J. A.; Jardine, F. H.; Young, J. F.; Wilkinson, G. *J. Chem. Soc. A* **1966**, 1711.
11. (a) Maitlis, P. M.; Haynes, A. In *Metal-catalysis in Industrial Organic Processes*; Chiusoli, G. P., Maitlis, P. M., Eds.; The Royal Society of Chemistry: Cambridge, 2006, p 114. (b) Evans, D.; Osborn, J. A.; Wilkinson, G. *J. Chem. Soc. A* **1968**, 3133.
12. (a) Massoudi, R.; Kim, J. H.; King, R. B.; King Jr., A. D. *J. Am. Chem. Soc.* **1987**, *109*, 7428. (b) Reppe, J. W. *Justus Liebigs Ann. Chem.* **1953**, *582*, 116.
13. Kang, H. C.; Mauldin, C. H.; Sleiger, T. C. W.; Cann, K.; Pettit, R. *J. Am. Chem. Soc.* **1977**, *99*, 8323.
14. (a) Paulik, F. E.; Roth, J. F. *Chem. Commun.* **1968**, 1578. (b) Paulik, F. E., Hershman, A., Knox, W. R., Roth, J. E., Monsanto Company, *US Pat.*, 3 769 329, **1973**.
15. Roth, J. F.; Craddock, J. H.; Hershman, A.; Paulik, F. E. *Chem. Technol.* **1971**, 600.

16. (a) Forster, D. *Adv. Organomet. Chem* **1979**, *17*, 255. (b) Dekleva, T. W.; Forster, D. *Adv. Catal.* **1986**, *34*, 81.
17. (a) *Chem. Br.* **1996**, *32*, 7. (b) Jones, J. H. *Platinum Metals Rev.* **2000**, *44*, 94. (c) *Chem. Ind. (London)* **1996**, 483.
18. Robinson, K. K.; Hershman, A.; Craddock, J. H.; Roth, J. F. *J. Catal.* **1972**, *27*, 389.
19. (a) Maitlis, P. M.; Haynes, A.; Sunley, G. J.; Howard, M. J. *J. Chem. Soc. Dalton Trans.* **1996**, 2187. (b) Sunley, G. J.; Watson, D. J. *Catal. Today* **2000**, *58*, 293.
20. (a) Martinho Simões, J. A.; Beauchamp, J. L. *Chem. Rev.* **1990**, *90*, 629. (b) Hughes, A. K.; Wade, K. *Coord. Chem. Rev.* **2000**, *197*, 191. (c) Ziegler, T.; Tschinke, V. In *Bonding Energetics in Organometallic Compounds*; Marks, T. J., Ed.; American Chemical Society: Washington, DC, 1990, p 279. (d) Armentrout, P. B. In *Bonding Energetics in Organometallic Compounds*; Marks, T. J., Ed.; American Chemical Society: Washington, DC, 1990, p 18.
21. (a) Imanishi, Y.; Naga, N. *Prog. Polym. Sci.* **2001**, *26*, 1147. (b) Kaminsky, W. *Pure Appl. Chem.* **1998**, *70*, 1229. (c) Brintzinger, H. H.; Fischer, D.; Mülhaupt, R.; Rieger, B.; Waymouth, R. M. *Angew. Chem. Int. Ed.* **1995**, *34*, 1143. (d) Chen, E. Y.-X.; Marks, T. J. *Chem. Rev.* **2000**, *100*, 1391. (e) Jordan, R. F. Ed. *J. Mol. Catal.* **1998**, *128*, 1-337 (special issue on metallocene and single-site olefin catalysts). (f) Kaminsky, W.; Arndt, M. *Adv. Polym. Sci.* **1997**, *127*, 144. (g) Britovsek, G. J. P.; Gibson, V. C.; Wass, D. F. *Angew. Chem. Int. Ed.* **1999**, *38*, 428. (h) Bochmann, M. *J. Chem. Soc., Dalton Trans.* **1996**, 255.
22. Fink, G.; Brintzinger, H. H. In *Metal-catalysis in Industrial Organic Processes*; Chiusoli, G. P., Maitlis, P. M., Eds.; The Royal Society of Chemistry: Cambridge, 2006, p 218.
23. Crabtree, R. H. In *The Organometallic Chemistry of the Transition Metals*; 4th ed.; John Wiley & Sons, Inc.: Hoboken, 2005, p 343.

24. (a) Peuckert, M.; Keim, W. *Organometallics* **1983**, *2*, 594. (b) Hirose, K.; Keim, W. *J. Mol. Catal.* **1992**, *73*, 271.
25. Dwyer, C. L. In *Metal-catalysis in Industrial Organic Processes*; Chiusoli, G. P., Maitlis, P. M., Eds.; The Royal Society of Chemistry: Cambridge, 2006, p 201.
26. Wu, X.-F.; Anbarasan, P.; Neumann, H.; Beller, M. *Angew. Chem. Int. Ed.* **2010**, *49*, 9047.
27. (a) Heck, R. F. *J. Am. Chem. Soc.* **1968**, *90*, 5518. (b) Heck, R. F. *J. Am. Chem. Soc.* **1968**, *90*, 5526. (c) Heck, R. F. *J. Am. Chem. Soc.* **1968**, *90*, 5531. (d) Heck, R. F. *J. Am. Chem. Soc.* **1968**, *90*, 5535. (e) Heck, R. F. *J. Am. Chem. Soc.* **1968**, *90*, 5538. (f) Heck, R. F. *J. Am. Chem. Soc.* **1968**, *90*, 5542. (g) Heck, R. F. *J. Am. Chem. Soc.* **1968**, *90*, 5546.
28. King, A. O.; Okukado, N.; Negishi, E. *J. Chem. Soc. Chem. Commun.* **1977**, 683.
29. (a) Miyaura, N.; Suzuki, A. *J. Chem. Soc. Chem. Commun.* **1979**, 866. (b) Miyaura, N.; Yamada, K.; Suzuki, A. *Tetrahedron Lett.* **1979**, *20*, 3437. (c) Miyaura, N.; Suzuki, A. *Chem. Rev.* **1995**, *95*, 2457.
30. Mizoroki, T.; Mori, K.; Ozaki, A. *Bull. Chem. Soc. Japan* **1971**, *44*, 581.
31. (a) Grubbs, R. H. *Handbook of Metathesis*; Wiley-VCH: New York, 2003. (b) Ivin, K. J. *Olefin Metathesis*; Academic Press: London, 1983. (c) Grubbs, R. H.; Tumas, W. *Science* **1989**, *243*, 907. (d) Grubbs, R. H.; Wenzel, A. G.; Chatterjee, A. K. In *Comprehensive Organometallic Chemistry III*; Crabtree, R. H., Mingos, D. M. P., Eds.; Elsevier: 2007; Vol. 11, p 179. (e) Trnka, T. M.; Grubbs, R. H. *Acc. Chem. Res.* **2001**, *34*, 18. (f) Feldman, J.; Schrock, R. R. *Prog. Inorg. Chem.* **1991**, *39*, 1. (g) Breslow, D. S. *Prog. Polym. Sci.* **1993**, *18*, 1141. (h) Grubbs, R. H. *Tetrahedron* **2004**, *60*, 7117. (i) Schrock, R. R.; Murdzek, J. S.; Bazan, G. C.; Robbins, J.; DiMare, M.; O'Regan, M. *J. Am. Chem. Soc.* **1990**, *112*, 3875.
32. Schwab, P.; Grubbs, R. H.; Ziller, J. W. *J. Am. Chem. Soc.* **1996**, *118*, 100.

33. Scholl, M.; Ding, S.; Lee, C. W.; Grubbs, R. H. *Org. Lett.* **1999**, *1*, 953.
34. (a) Schrock, R. R. *Acc. Chem. Res.* **1986**, *19*, 342. (b) Hoveyda, A. H.; Schrock, R. R. *Chem. Eur. J.* **2001**, *7*, 945. (c) Schrock, R. R.; Hoveyda, A. H. *Angew. Chem. Int. Ed.* **2003**, *42*, 4592.
35. Hérisson, J.-L.; Chauvin, Y. *Makromol. Chem.* **1970**, *141*, 161.
36. (a) Maas, G. *Chem. Soc. Rev.* **2004**, *33*, 183. (b) Kirmse, W. *Angew. Chem. Int. Ed. Engl.* **2003**, *42*, 1088. (c) Brookhart, M.; Studabaker, W. B. *Chem. Rev.* **1987**, *87*, 411. (d) Basato, M.; Tubaro, C.; Biffis, A.; Bonato, M.; Buscemi, G.; Lighezzolo, F.; Lunardi, P.; Vianini, C.; Benetollo, F.; Del Zotto, A. *Chem. Eur. J.* **2009**, *15*, 1516.
37. (a) Schlund, R.; Schrock, R. R.; Crowe, W. E. *J. Am. Chem. Soc.* **1989**, *111*, 8004. (b) Park, L. Y.; Schrock, R. R.; Stieglitz, S. G.; Crowe, W. E. *Macromolecules* **1991**, *24*, 3489.
38. (a) Werner, H. *Organometallics* **2005**, *24*, 1036. (b) King, P. J. *Organomet. Chem.* **2002**, *30*, 282. (c) Whittlesey, M. K. *Organomet. Chem.* **2001**, *29*, 350. (d) Gallop, M. A.; Roper, W. R. *Adv. Organomet. Chem* **1986**, *25*, 121. (e) Bohle, D. S.; Clark, G. R.; Rickard, C. E. F.; Roper, W. R.; Wright, L. J. *J. Organomet. Chem.* **1988**, *358*, 411.
39. (a) Herrmann, W. A. *Adv. Organomet. Chem* **1982**, *20*, 159. (b) Puddephatt, R. J. *Polyhedron* **1988**, *7*, 767.
40. (a) Knox, S. A. R. *J. Cluster Sci.* **1992**, *3*, 385. (b) Dennett, J. N. L.; Knox, S. A. R.; Charmant, J. P. H.; Gillon, A. L.; Orpen, A. G. *Inorg. Chim. Acta* **2003**, *354*, 29. (c) Busetto, L.; Maitlis, P. M.; Zanotti, V. *Coord. Chem. Rev.* **2010**, *254*, 470. (d) Casey, C. P.; Audett, J. D. *Chem. Rev.* **1986**, *86*, 339.
41. (a) Fischer, F.; Tropsch, H. *Brennst. Chem.* **1926**, *7*, 97. (b) Fischer, F.; Tropsch, H. *Chem. Ber.* **1926**, *59*, 830. (c) Brady, R. C.; Pettit, R. *J. Am. Chem. Soc.* **1980**, *102*, 6181. (d) Brady, R. C.; Pettit, R. *J. Am. Chem. Soc.* **1981**, *103*, 1287. (e) Biloen, P.; Sachtler, W. M. H. *Adv. Catal.* **1981**, *30*, 165. (f) Maitlis, P. M.; Long, H. C.; Quayoum, R.; Turner, M. L.; Wang, Z.-Q. *Chem. Commun.* **1996**, *1*. (g) Long, H. C.; Turner, M. L.;

- Fornasiero, P.; Kaspar, J.; Graziani, M.; Maitlis, P. M. *J. Catal.* **1997**, *167*, 172. (h) Dry, M. E. *Appl. Catal. A* **1996**, *138*, 319.
42. Sabatier, P.; Senderens, J. B. *C. R. Acad. Sci.* **1902**, *134*, 514.
43. Fischer, F.; Tropsch, H. *Brennst. Chem.* **1923**, *4*, 276.
44. Dry, M. E. In *Handbook of Heterogeneous Catalysis*; 2nd ed.; Ertl, G., Knözinger, H., Schüth, F., Weitkamp, J., Eds.; WILEY-VCH Verlag GmbH & Co. KGaA: Weinheim, 2008, p 2965.
45. Dry, M. E. *Catal.Today* **2002**, *71*, 227.
46. (a) Wentrcek, P. R.; Wood, B. J.; Wise, H. *J. Catal.* **1976**, *43*, 363. (b) Araki, M.; Ponec, V. *J. Catal.* **1976**, *44*, 439. (c) Rabo, J. A.; Risch, A. P.; Poutsma, M. L. *J. Catal.* **1978**, *53*, 295. (d) Biloen, P.; Helle, J. N.; Sachtler, W. M. H. *J. Catal.* **1979**, *58*, 95. (e) Kaminsky, M. P.; Winograd, N.; Geoffroy, G. L. *J. Am. Chem. Soc.* **1986**, *108*, 1315.
47. (a) Shriver, D. F.; Sailor, M. J. *Acc. Chem. Res.* **1988**, *21*, 374. (b) Bradley, J. S. *Adv. Organomet. Chem* **1983**, *22*, 1. (c) Chisholm, M. H.; Hammond, C. E.; Johnston, V. J.; Streib, W. E.; Huffman, J. C. *J. Am. Chem. Soc.* **1992**, *114*, 7056.
48. Overett, M. J.; Hill, R. O.; Moss, J. R. *Coord. Chem. Rev.* **2000**, *206*, 581.
49. Turner, M. L.; Long, H. C.; Shenton, A.; Byers, P. K.; Maitlis, P. M. *Chem. Eur. J.* **1995**, *1*, 549.
50. Dry, M. E. *ACS Symp. Ser.* **1987**, *328*, 18.
51. (a) Sumner, C. E.; Riley, P. E.; Davis, R. E.; Pettit, R. *J. Am. Chem. Soc.* **1980**, *102*, 1752. (b) Sumner, C. E.; Collier, J. A.; Pettit, R. *Organometallics* **1982**, *1*, 1350.
52. (a) Creer, J. G.; Jackson, P.; Pandey, G.; Percival, G. G.; Seddon, D. *Appl. Catal.* **1986**, *22*, 85. (b) Richter, M.; Langpape, M.; Kolf, S.; Grubert, G.; Eckelt, R.; Radnik, J.; Schneider, M.; Pohl, M.-M.; Fricke, R. *Appl. Catal. B* **2002**, *36*, 261. (c) Caruthers, J. M.; Lauterbach, J. A.; Thomson, K. T.; Venkatasubramanian, V.; Snively, C. M.; Bhan, A.; Katare, S.; Oskarsdottir, G. *J. Catal.* **2003**, *216*, 98. (d) Woo, S. I.; Kim, K. W.; Cho, H. Y.; Oh, K. S.; Jeon, M. K.; Tarte, N. H.; Kim, T. S.; Mahmood, A.

- QSAR Comb. Sci.* **2005**, *24*, 138. (e) Gao, K.; Yuan, L.; Wang, L. *J. Comb. Chem.* **2006**, *8*, 247. (f) Weidenhof, B.; Reiser, M.; Stöwe, K.; Maier, W. F.; Kim, M.; Azurdia, J.; Gulari, E.; Seker, E.; Barks, A.; Laine, R. M. *J. Am. Chem. Soc.* **2009**, *131*, 9207. (g) Pescarmona, P. P.; Janssen, K. P. F.; Jacobs, P. A. *Chem. Eur. J.* **2007**, *13*, 6562. (h) Dehm, N. A.; Zhang, X.; Buriak, J. M. *Inorg. Chem.* **2010**, *49*, 2706.
53. (a) Copéret, C.; Chabanas, M.; Saint-Arroman, R. P.; Basset, J.-M. *Angew. Chem. Int. Ed.* **2003**, *42*, 156. (b) Muetterties, E. L.; Stein, J. *Chem. Rev.* **1979**, *79*, 479. (c) Locatelli, F.; Candy, J.-P.; Didillon, B.; Niccolai, G. P.; Uzio, D.; Basset, J.-M. *J. Am. Chem. Soc.* **2001**, *123*, 1658.
54. Shannon, I. R. In *Catalysis*; Kemball, C., Dowden, D. A., Eds.; The Chemical Society: London, 1978; Vol. 2, p 28.
55. (a) Satterfield, C. N. In *Heterogeneous Catalysis In Industrial Practice*; 2nd ed.; Nalven, F. G., Dahl, F., Eds.; McGraw-Hill Inc.: New York, 1991, p 339. (b) Dowden, D. A. In *Catalysis*; Kemball, C., Dowden, D. A., Eds.; The Chemical Society: London, 1978; Vol. 2, p 1.
56. (a) Young, J. F.; Osborn, J. A.; Jardine, F. H.; Wilkinson, G. *Chem. Commun.* **1965**, 131. (b) Jardine, F. H.; Osborn, J. A.; Wilkinson, G.; Young, J. F. *Chem. Ind. (London)* **1965**, 560. (c) Bennett, M. A.; Longstaff, P. A. *Chem. Ind. (London)* **1965**, 846. (d) ICI Ltd., Neth. Appl., 6 602 062 (*Chem. Abstr.*, **1967**, *66*, 10 556y).
57. (a) Stephenson, T. A.; Wilkinson, G. *J. Inorg. Nucl. Chem.* **1966**, *28*, 945. (b) Jardine, F. H.; Osborn, J. A.; Wilkinson, G. *J. Chem. Soc. A* **1967**, 1574.
58. Schrock, R. R.; Osborn, J. A. *J. Am. Chem. Soc.* **1976**, *98*, 2134.
59. Schrock, R. R.; Osborn, J. A. *J. Am. Chem. Soc.* **1976**, *98*, 2143.
60. Schrock, R. R.; Osborn, J. A. *J. Am. Chem. Soc.* **1976**, *98*, 4450.
61. (a) Burk, M. J. *Acc. Chem. Res.* **2000**, *33*, 363. (b) Noyori, R. *Angew. Chem. Int. Ed.* **2002**, *41*, 2008.

62. (a) Muetterties, E. L. *Science* **1977**, *196*, 839. (b) Muetterties, E. L. *Angew. Chem. Int. Ed.* **1978**, *17*, 545. (c) Muetterties, E. L.; Rhodin, T. N.; Band, E.; Brucker, C. F.; Pretzer, W. R. *Chem. Rev.* **1979**, *79*, 91.
63. Broussard, M. E.; Juma, B.; Train, S. G.; Peng, W.-J.; Laneman, S. A.; Stanley, G. G. *Science* **1993**, *260*, 1784.
64. Ristic-Petrovic, D.; Anderson, D. J.; Torkelson, J. R.; McDonald, R.; Cowie, M. *Organometallics* **2003**, *22*, 4647.
65. Anderson, D. J.; McDonald, R.; Cowie, M. *Angew. Chem. Int. Ed.* **2007**, *46*, 3741.
66. (a) Slaney, M. E.; Anderson, D. J.; Ferguson, M. J.; McDonald, R.; Cowie, M. *J. Am. Chem. Soc.* **2010**, *132*, 16544. (b) Slaney, M. E.; Anderson, D. J.; Ristic-Petrovic, D.; McDonald, R.; Cowie, M. *Accepted for publication in Chem. Eur. J. Nov. 8, 2011.*
67. (a) Akita, M.; Oku, T.; Moro-oka, Y. *J. Chem. Soc. Chem. Commun.* **1992**, 1031. (b) Akita, M.; Hua, R.; Oku, T.; Moro-oka, Y. *Organometallics* **1996**, *15*, 2548.
68. (a) Isobe, K.; Andrews, D. G.; Mann, B. E.; Maitlis, P. M. *J. Chem. Soc. Chem. Commun.* **1981**, 809. (b) Saez, I. M.; Andrews, D. G.; Maitlis, P. M. *Polyhedron* **1988**, *7*, 827. (c) Maitlis, P. M. *J. Organomet. Chem.* **1995**, *500*, 239. (d) Maitlis, P. M.; Quyoum, R.; Long, H. C.; Turner, M. L. *Appl. Catal. A* **1999**, *186*, 363. (e) Isobe, K.; Vázquez de Miguel, A.; Bailey, P. M.; Okeya, S.; Maitlis, P. M. *J. Chem. Soc. Dalton Trans.* **1983**, 1441. (f) Maitlis, P. M.; Ma, F.; Martinez, J.; Byers, P. K.; Saez, I.; Sunley, G. J. *Adv. Chem. Ser.* **1992**, *230*, 565.
69. (a) Martinez, J. M.; Adams, H.; Bailey, N. A.; Maitlis, P. M. *J. Chem. Soc. Chem. Commun.* **1989**, 286. (b) Martinez, J.; Gill, J. B.; Adams, H.; Bailey, N. A.; Saez, I. M.; Sunley, G. J.; Maitlis, P. M. *J. Organomet. Chem.* **1990**, *394*, 583.
70. Alexeev, O. S.; Gates, B. C. *Ind. Eng. Chem. Res.* **2003**, *42*, 1571.
71. Shen, G.-C.; Liu, A.-M.; Shido, T.; Ichikawa, M. *Top. Catal.* **1995**, *2*, 141.

72. Ichikawa, M.; Rao, L.-F.; Kimura, T.; Fukuoka, A. *J. Mol. Catal.* **1990**, *61*, 15.
73. Herrmann, W. A.; Reiter, B.; Biersack, H. *J. Organomet. Chem.* **1975**, *97*, 245.
74. Herrmann, W. A.; Krüger, C.; Goddard, R.; Bernal, I. *Angew. Chem. Int. Ed.* **1977**, *16*, 334.
75. (a) Brown, M. P.; Fisher, J. R.; Franklin, S. J.; Puddephatt, R. J.; Seddon, K. R. *J. Chem. Soc. Chem. Commun.* **1978**, 749. (b) Brown, M. P.; Fisher, J. R.; Puddephatt, R. J.; Seddon, K. R. *Inorg. Chem.* **1979**, *18*, 2808.
76. Balch, A. L.; Hunt, C. T.; Lee, C.-L.; Olmstead, M. M.; Farr, J. P. *J. Am. Chem. Soc.* **1981**, *103*, 3764.
77. Ritleng, V.; Chetcuti, M. J. *Chem. Rev.* **2007**, *107*, 797.
78. (a) Kaneko, Y.; Suzuki, T.; Isobe, K.; Maitlis, P. M. *J. Organomet. Chem.* **1998**, *554*, 155. (b) Akita, M.; Hua, R.; Nakanishi, S.; Tanaka, M.; Morooka, Y. *Organometallics* **1997**, *16*, 5572. (c) Adams, P. Q.; Davies, D. L.; Dyke, A. F.; Knox, S. A. R.; Mead, K. A.; Woodward, P. *J. Chem. Soc., Chem. Commun.* **1983**, 222. (d) Rowsell, B. D.; McDonald, R.; Ferguson, M. J.; Cowie, M. *Organometallics* **2003**, *22*, 2944. (e) Dyke, A. F.; Knox, S. A. R.; Naish, P. J.; Taylor, G. E. *J. Chem. Soc., Chem. Commun.* **1980**, 803. (f) Gracey, B. P.; Knox, S. A. R.; Macpherson, K. A.; Orpen, A. G.; Stobart, S. R. *J. Chem. Soc., Dalton Trans.* **1985**, 1935. (g) Colborn, R. E.; Dyke, A. F.; Knox, S. A. R.; Macpherson, K. A.; Orpen, A. G. *J. Organomet. Chem.* **1982**, *239*, C15. (h) Colborn, R. E.; Davies, D. L.; Dyke, A. F.; Knox, S. A. R.; Mead, K. A.; Orpen, A. G.; Guerchais, J. E.; Roué, J. *J. Chem. Soc., Dalton Trans.* **1989**, 1799. (i) Navarre, D.; Parlier, A.; Rudler, H.; Daran, J. C. *J. Organomet. Chem.* **1987**, *322*, 103. (j) Levisalles, J.; Rose-Munch, F.; Rudler, H.; Daran, J.-C.; Dromzee, Y.; Jeannin, Y.; Ades, D.; Fontanille, M. *J. Chem. Soc., Chem. Commun.* **1981**, 1055. (k) Wigginton, J. R.; Chokshi, A.; Graham, T. W.; McDonald, R.; Ferguson, M. J.; Cowie, M. *Organometallics* **2005**, *24*, 6398.

79. (a) Fildes, M. J.; Knox, S. A. R.; Orpen, A. G.; Turner, M. L.; Yates, M. I. *J. Chem. Soc., Chem. Commun.* **1989**, 1680. (b) Chetcuti, M. J.; Fanwick, P. E.; Grant, B. E. *Organometallics* **1991**, *10*, 3003. (c) Chokshi, A.; Rowsell, B. D.; Trepanier, S. J.; Ferguson, M. J.; Cowie, M. *Organometallics* **2004**, *23*, 4759. (d) Ristic-Petrovic, D.; Anderson, D. J.; Torkelson, J. R.; Ferguson, M. J.; McDonald, R.; Cowie, M. *Organometallics* **2005**, *24*, 3711. (e) Bai, T.; Ma, S.; Jia, G. *Coord. Chem. Rev.* **2009**, *253*, 423.
80. Motyl, K. M.; Norton, J. R.; Schauer, C. K.; Anderson, O. P. *J. Am. Chem. Soc.* **1982**, *104*, 7325.
81. (a) Doherty, N. M.; Howard, J. A. K.; Knox, S. A. R.; Terrill, N. J.; Yates, M. I. *J. Chem. Soc. Chem. Commun.* **1989**, 638. (b) Knox, S. A. R. *J. Organomet. Chem.* **1990**, *400*, 255.
82. Rowsell, B. D.; Trepanier, S. J.; Lam, R.; McDonald, R.; Cowie, M. *Organometallics* **2002**, *21*, 3228.
83. Dell'Anna, M. M.; Trepanier, S. J.; McDonald, R.; Cowie, M. *Organometallics* **2001**, *20*, 88.
84. (a) Trepanier, S. J.; Sterenberg, B. T.; McDonald, R.; Cowie, M. *J. Am. Chem. Soc.* **1999**, *121*, 2613. (b) Trepanier, S. J.; Dennett, J. N. L.; Sterenberg, B. T.; McDonald, R.; Cowie, M. *J. Am. Chem. Soc.* **2004**, *126*, 8046.
85. Herrmann, W. A. *Angew. Chem. Int. Ed.* **1978**, *17*, 800.
86. Puddephatt, R. J. *Chem. Soc. Rev.* **1983**, *12*, 99.
87. (a) Wells, K. D.; McDonald, R.; Ferguson, M. J.; Cowie, M. *Organometallics* **2011**, *30*, 2654. (b) Wells, K. D.; Ferguson, M. J.; McDonald, R.; Cowie, M. *Organometallics* **2011**, *30*, 815. (c) Torkelson, J. R.; Oke, O.; Muritu, J.; McDonald, R.; Cowie, M. *Organometallics* **2000**, *19*, 854. (d) Sterenberg, B. T.; Hilts, R. W.; Moro, G.; McDonald, R.; Cowie, M. *J. Am. Chem. Soc.* **1995**, *117*, 245.

88. Mobarok, M. H.; Oke, O.; Ferguson, M. J.; McDonald, R.; Cowie, M.
Inorg. Chem. **2010**, *49*, 11556.

Chapter 2: Facile Carbon-Carbon Bond Formation and Multiple Carbon-Hydrogen Bond Activations Promoted by Methylene-Bridged Iridium/Ruthenium Complexes*

2.1 Introduction

Transition-metal complexes containing alkylidene groups ($L_nM=CRR'$) have displayed a rich chemistry in carbon-carbon bond formation, including cyclopropanations,¹ olefin metathesis,² and the oligomerization of alkynes.³ Most alkylidenes studied are of the form $L_nM=CRR'$, where the alkylidene moiety is terminally bound to a metal centre.⁴ Bimetallic complexes, in which the alkylidene moiety bridges two metal centres, have been much less studied and are expected to be less reactive, owing to the formal saturation of these bridging units. Nevertheless, bridging alkylidene units have also shown interesting reactivity.⁵ In particular, the prototypical alkylidene unit, the methylene ($-CH_2-$) group, has been proposed to play a key role as a surface bound species in the sequential carbon-carbon bond formation that occurs in the Fischer-Tropsch (FT) process.⁶ In FT chemistry, the surface bound methylene groups are presumably bound in a bridging arrangement between a pair of adjacent metals and as such the chemistry of this bridging group should parallel that observed in methylene-bridged binuclear complexes.^{5a,5c,6f,7} Consequently, these well-defined methylene-bridged complexes can serve as useful models for heterogeneous FT chemistry, in keeping with the surface-cluster analogy initially proposed by E.L. Muetterties.⁸

As part of a study, the long-term goal of which is to determine the roles of the different metals in mixed-metal FT catalysts,⁹ we have investigated the chemistry of methylene-bridged complexes involving the Rh/Ru,^{7g,h,10} Ir/Ru,⁷ⁱ Rh/Os,^{7e,f,10} and Ir/Os¹¹ metal combinations. It is our contention that to fully understand the roles of the different metals and metal combinations in this

* A version of this chapter has been published. MacDougall, T. J.; Trepanier, S. J.; Dutton, J. L.; Ferguson, M. J.; McDonald, R.; Cowie, M. *Organometallics* **2011**, *30*, 5882.

chemistry, a careful comparison of different, but related combinations of metals is necessary. The Rh/Os system was found to be particularly reactive, coupling up to four methylene units to generate either allyl and methyl or butanediyl fragments at the metal centres,^{7e,f} mimicking aspects of FT reactivity. In this study we proposed that the key (although unobserved) intermediates in the methylene-coupling transformations were hydrocarbyl-bridged units, and that the stepwise addition of methylene groups occurred by insertion into the Rh–C bond of these bridging fragments. In order to learn more about the reactivity of these bridging hydrocarbyl groups and the roles played by the different metals in the growth of the carbon-carbon chain, we have investigated the stepwise coupling of methylene groups with a variety of unsaturated substrates.^{5c,7a,7d,7h,10-12}

In the study described herein we focus our investigation on methylene-bridged complexes involving the Ir/Ru metal combination, and their coupling with cumulenes. By implementing a third-row, group 9 metal, we sought to utilize the greater Ir–C bond strengths (compared to Rh in previous studies) in order to retain the growing hydrocarbyl fragments while utilizing the labile environment at ruthenium to allow for substrate transformations. We were also curious about the effect of replacing Rh by the less labile Ir centre on the insertion reactions and about the greater tendency of this 3rd-row metal to undergo oxidative addition, particularly of C–H bonds, in competition with carbon–carbon chain growth.

2.2 Results, Compound Characterization, and Discussion

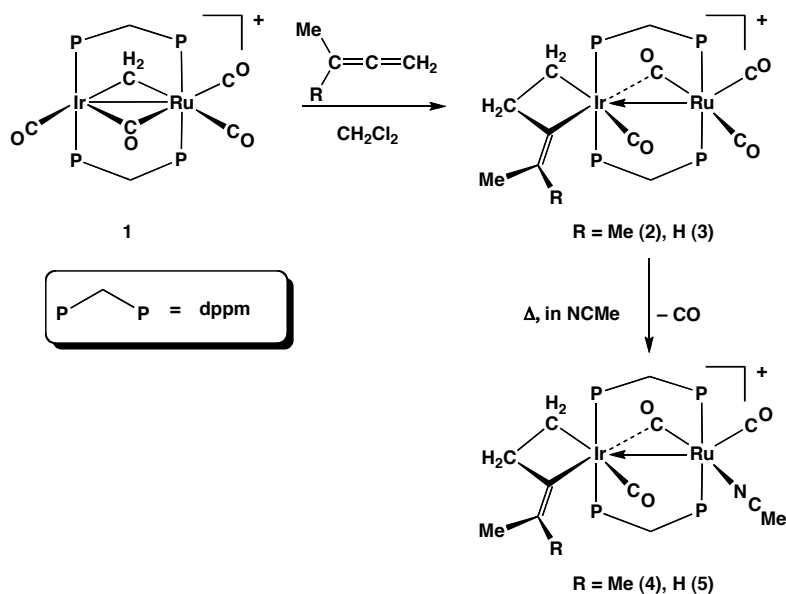
2.2.1 Carbon-Carbon Bond Formation

2.2.1.1 Alkyl Cumulenes

The methylene-bridged complex, $[\text{IrRu}(\text{CO})_4(\mu\text{-CH}_2)(\text{dppm})_2][\text{BF}_4]$ (**1**), reacts with either 1,1-dimethylallene or 1,2-butadiene (methylallene) at ambient temperature to generate the corresponding iridacycle-containing products, $[\text{IrRu}(\text{CO})_4(\kappa^1:\kappa^1\text{-Me}_2\text{C}=\text{CCH}_2\text{CH}_2)(\text{dppm})_2][\text{BF}_4]$ (**2**) or $[\text{IrRu}(\text{CO})_4(\kappa^1:\kappa^1\text{-MeCH}=\text{CCH}_2\text{CH}_2)(\text{dppm})_2][\text{BF}_4]$ (**3**), respectively, as outlined in Scheme 2-1. The reaction with the mono-substituted allene, methylallene, occurs

approximately twice as fast as with the disubstituted, 1,1-dimethylallene, presumably owing to inhibition resulting from the larger steric bulk of the

Scheme 2-1



disubstituted cumulene. In compound **3**, two isomers are possible, depending on whether the methyl group appears trans or cis to Ir. The trans arrangement, determined by an X-ray study of the related compound **5** (*vide infra*), is favoured by steric arguments allowing the methyl group to avoid the adjacent carbonyl ligand.

Both compounds **2** and **3** give rise to two resonances in the $^{31}\text{P}\{^1\text{H}\}$ NMR spectrum at approximately δ 26 and δ -14, consistent with the inequivalence of both ends of the bridging diphosphines, as shown in Figure 2-1 for **2**. As is usually observed,^{71,13} and as demonstrated for all compounds in this chapter as well as the following chapter (*vide infra*), the Ru-bound phosphorus resonances in both complexes appear downfield from the resonances due to the Ir-bound ends. The ^1H NMR spectra of **2** and **3** display two resonances for the dppm-methylene protons, a result of the absence of front-back symmetry about the IrRuP₄ plane, and display mutual two-bond coupling of *ca.* 15 Hz. The Ir-bound methylene (CH_2) protons appear as triplets of triplets (**2**: δ 0.98, **3**: δ 1.19), with three-bond

coupling to the Ir-bound ^{31}P nuclei and the adjacent CH_2 protons with an

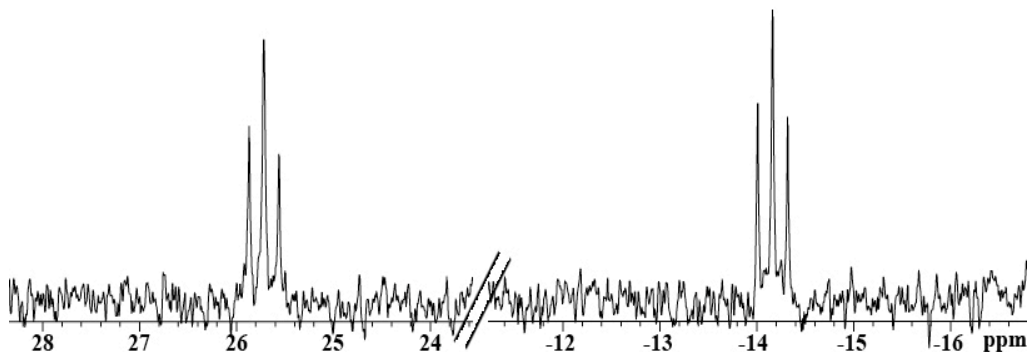


Figure 2-1. $^{31}\text{P}\{^1\text{H}\}$ NMR spectrum of $[\text{IrRu}(\text{CO})_4(\kappa^1:\kappa^1\text{-Me}_2\text{C}=\text{CCH}_2\text{CH}_2)\text{-}(\text{dppm})_2][\text{BF}_4]$ (**2**) in CD_2Cl_2 .

average coupling of 9.9 Hz and 7.3 Hz, respectively. The CH_2 protons on the carbon β to Ir appear as triplets at δ 2.15 (**2**) and δ 1.61 (**3**). The two methyl groups in **2** appear as broad singlets at δ 1.44 and δ 0.90 in the ^1H NMR spectrum while for **3** the single methyl group appears as a broad doublet at δ 0.90, displaying coupling of 5.8 Hz to the geminal proton, which in turn appears as a broad quartet at δ 4.96. All $^{31}\text{P}\{^1\text{H}\}$, ^1H and $^{13}\text{C}\{^1\text{H}\}$ NMR and IR data for all of the compounds in this chapter are given in the Experimental section.

In compound **2**, prepared from $[\text{IrRu}(^{13}\text{CO})_4(\mu\text{-}^{13}\text{CH}_2)(\text{dppm})_2][\text{BF}_4]$, the single Ir-bound carbonyl ligand appears in the $^{13}\text{C}\{^1\text{H}\}$ NMR spectrum as a broad triplet at δ 182.1, with resolvable coupling to only the Ir-bound ends of the diphosphines ($^2J_{\text{CP}} = 8.7$ Hz), while the Ir-bound carbon of the methylene group resonates at δ -17.8 ($^2J_{\text{CP}} = 6.3$ Hz) as a broad triplet. Two Ru-bound carbonyls appear as doublets of triplets at δ 212.7 and δ 207.3, in which the large two-bond $^{13}\text{C}\text{-}^{13}\text{C}$ coupling of 28.6 Hz suggests a mutually trans arrangement (the semi-bridging carbonyl is presumably the one at characteristically lower field), and the third Ru-bound CO appears at δ 188.7. The $^{13}\text{C}\{^1\text{H}\}$ NMR spectrum of **3** is closely comparable to **2** with the terminal carbonyl resonances at δ 208.8, δ 190.6, and δ 180.8 and the semi-bridging carbonyl resonance at δ 209.6. The $^{13}\text{CH}_2$ group of the iridacycle resonates characteristically upfield at δ -19.9 in **3**.

Attempts to obtain suitable single crystals of **2** and **3** have been unsuccessful; however, replacement of a Ru-bound carbonyl ligand in both compounds by an acetonitrile ligand either in refluxing acetonitrile, or by decarbonylation with trimethylamine *N*-oxide (TMNO) in acetonitrile yields the respective products, $[\text{IrRu}(\text{CO})_3(\text{NCCH}_3)(\kappa^1:\kappa^1\text{-Me}_2\text{C}=\text{CCH}_2\text{CH}_2)(\text{dppm})_2][\text{BF}_4]$ (**4**) and $[\text{IrRu}(\text{CO})_3(\text{NCCH}_3)(\kappa^1:\kappa^1\text{-MeCH}=\text{CCH}_2\text{CH}_2)(\text{dppm})_2][\text{BF}_4]$ (**5**; see Scheme 2-1), both of which yielded X-ray quality crystals. The structure determination of $[\text{IrRu}(\text{CO})_3(\text{NCCH}_3)(\kappa^1:\kappa^1\text{-Me}_2\text{C}=\text{CCH}_2\text{CH}_2)(\text{dppm})_2][\text{BF}_4]$ (**4**), as shown for the complex cation in Figure 2-2, verifies the proposed geometry in which the hydrocarbyl group is chelating on Ir. Although this hydrocarbyl moiety and the Ir-bound carbonyl ligand are disordered as explained in the Experimental section, refinement of the disordered model proceeded well. Selected bond lengths and angles for both disordered forms are presented in Table 2-1.

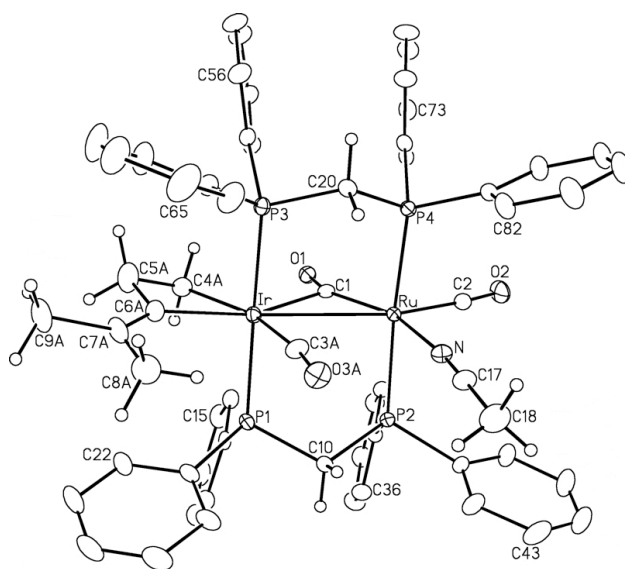


Figure 2-2. Perspective view of the complex cation of $[\text{IrRu}(\text{CO})_3(\text{NCCH}_3)(\kappa^1:\kappa^1\text{-Me}_2\text{C}=\text{CCH}_2\text{CH}_2)(\text{dppm})_2][\text{BF}_4]$ (**4**). Only the major disordered form (75% occupancy) is shown. Thermal ellipsoids are shown at the 20% probability level except for hydrogens, which are omitted for the phenyl groups but are shown arbitrarily small for the others.

Within the iridacycle moiety the parameters are as expected. The essentially trigonal planar arrangements of C(6A) and C(7A) together with their short separation (1.36(1) Å) are consistent with the olefinic formulation. Although the Ir–Ru separation (3.0006(3) Å) is long for a single bond between

Table 2-1. Selected Bond Lengths and Angles for the Both Disordered Forms of Compound 4

(a) Distance (Å)^a

atom 1	atom 2	distance	atom 1	atom 2	distance
Ir	Ru	3.0006(3)	Ru	N	2.184(3)
Ir	C1	2.455(4)	C4A	C5A	1.43(1)
Ir	C3A	1.905(7)	C4B	C5B	1.50(1)
Ir	C3B	1.94(3)	C5A	C6A	1.50(1)
Ir	C4A	2.11(1)	C5B	C6B	1.60(2)
Ir	C4B	2.21(3)	C6A	C7A	1.36(1)
Ir	C6A	2.116(6)	C6B	C7B	1.335(8)
Ir	C6B	2.19(2)	C7A	C8A	1.52(1)
Ru	C1	1.883(4)	C7B	C8B	1.50(1)
Ru	C2	1.864(4)	C7A	C9A	1.51(1)
C1	O1	1.184(4)	C7B	C9B	1.50(1)

(b) Angles (deg)^a

atom	atom 2	atom 3	angle	atom 1	atom	atom 3	angle
Ru	C1	O1	151.7(3)	Ir	C6A	C7A	137.0(8)
Ir	C1	O1	121.8(3)	Ir	C6B	C7B	145(1)
Ir	C4A	C5A	99.9(6)	C6A	C7A	C8A	126.0(8)
Ir	C4B	C5B	97(2)	C6B	C7B	C8B	119.4(6)
C4A	C5A	C6A	97.5(6)	C6A	C7A	C9A	122(1)
C4B	C5B	C6B	99(2)	C6B	C7B	C9B	119.5(6)
C5A	C6A	C7A	125.6(8)	C3A	Ir	C6A	98.5(3)
C5B	C6B	C7B	118(1)	C3B	Ir	C6B	93.4(9)
Ir	C6A	C5A	97.4(4)	C4A	Ir	C6A	62.7(3)
Ir	C6B	C5B	97(1)	C4B	Ir	C6B	66.3(8)

^aThe disordered groups are labelled “A” and “B”

these metals, one is proposed on the basis of electron counting, and this distance is slightly shorter than the non-bonding P–P distance of *ca.* 3.05 Å, suggesting a mutual attraction of the metals. Earlier in Scheme 2-1 we represented this as a

ductive Ru→Ir bond, in keeping with the favoured coordinatively saturated Ir(III)/Ru(0) oxidation-state assignment; also viable is an Ir(II)/Ru(I) formulation that would require a conventional Ir–Ru bond.

The X-ray structure of **5** as shown in Figure 2-3 displays a very similar structure to that of **4**, including a similar disorder. As suggested, earlier, the mutually trans arrangement of the methyl substituent and Ir across the olefinic bond in **5** is favoured over the cis arrangement, by placing the methyl

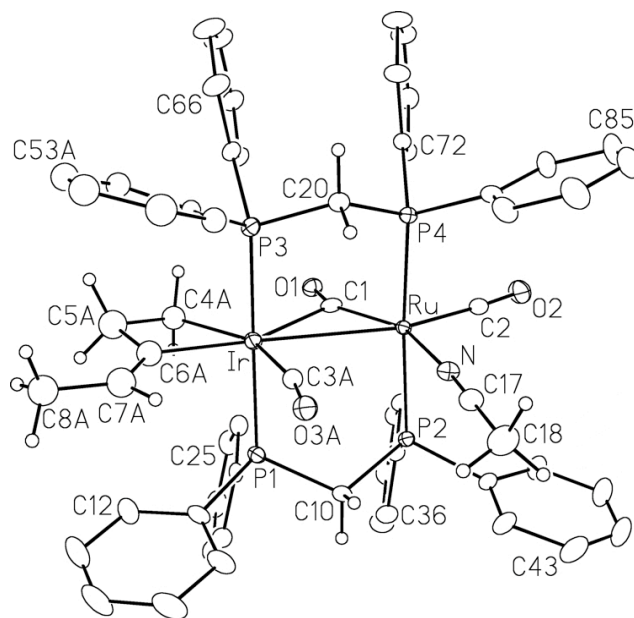


Figure 2-3. *Perspective view of the complex cation of $[\text{IrRu}(\text{CO})_3(\text{NCCH}_3)(\kappa^1:\kappa^1\text{-MeCH}=\text{CCH}_2\text{CH}_2)(\text{dppm})_2][\text{BF}_4]$ (**5**). Only the major disordered form (60 % occupancy) is shown. Thermal ellipsoids are as described in Figure 2-2.*

group in a less crowded environment, avoiding the adjacent carbonyl ligand. This is seen clearly in a comparison of the Ir–C(6A)–C(7A) ($137.0(8)^\circ$ in **4** and $130.8(9)^\circ$ in **5**) and C(3A)–Ir–C(6A) ($90.7(4)^\circ$ in **4** and $98.5(3)^\circ$ in **5**). Both of the angles are 6 – 8° larger for the dimethyl species, owing to repulsion between the methyl and carbonyl groups. The angles of the disordered forms of both **4** and **5** illustrate the same trend for the Ir–C(6B)–C(7B) ($145(1)^\circ$ in **4** and $134(1)^\circ$ in **5**)

and C(3B)–Ir–C(6B) (93.4(9)° in **4** and 87.7(7)° in **5**). Structurally, **5** is very similar in all aspects to that of **4**, and select bond lengths and angles can be found in Table 2-2.

Table 2-2. Selected Bond Lengths and Angles for the Both Disordered Forms of Compound 5

(a) Distance (Å)^a

atom 1	atom 2	distance	atom 1	atom 2	distance
Ir	Ru	2.9864(3)	Ru	N	2.167(3)
Ir	C1	2.453(4)	C3A	O3A	1.116(9)
Ir	C3A	1.903(7)	C3B	O3B	1.05(2)
Ir	C3B	1.94(2)	C4A	C5A	1.42(2)
Ir	C4A	2.08(1)	C4B	C5B	1.40(2)
Ir	C4B	2.10(2)	C5A	C6A	1.52(2)
Ir	C6A	2.11(1)	C5B	C6B	1.53(2)
Ir	C6B	2.15(2)	C6A	C7A	1.38(1)
Ru	C1	1.904(4)	C6B	C7B	1.40(2)
Ru	C2	1.857(4)	C7A	C8A	1.44(2)
C1	O1	1.183(5)	C7B	C8B	1.41(3)

(b) Angles (deg)^a

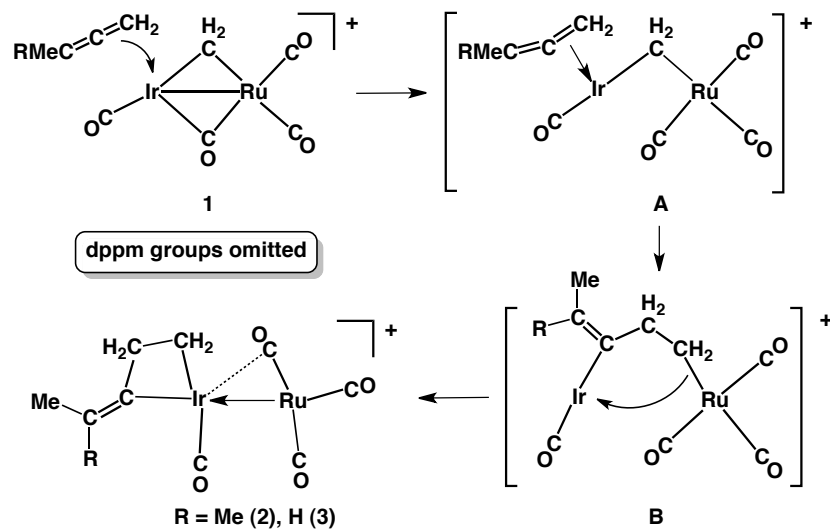
atom	atom 2	atom 3	angle	atom 1	atom	atom 3	angle
Ir	C1	O1	123.0(3)	Ir	C6B	C5B	100.1(9)
Ru	C1	O1	151.5(4)	Ir	C6A	C7A	130.8(9)
Ir	C4A	C5A	103.3(8)	Ir	C6B	C7B	134(1)
Ir	C4B	C5B	107(1)	C6A	C7A	C8A	124(1)
C4A	C5A	C6A	95.2(9)	C6B	C7B	C8B	135(2)
C4B	C5B	C6B	93(1)	C3A	Ir	C6A	90.7(4)
C5A	C6A	C7A	131(1)	C3B	Ir	C6B	87.7(7)
C5B	C6B	C7B	126(1)	C4A	Ir	C6A	62.5(5)
Ir	C6A	C5A	98.5(6)	C4B	Ir	C6B	59.9(6)

^aThe disordered groups are labelled “A” and “B”

We have considered three mechanistic possibilities for the observed coupling of the cumulenes and the μ -CH₂ group of **1**. The most obvious possibility involves initial cumulene coordination at Ir with subsequent insertion into the Ir–CH₂ bond to give the hydrocarbyl-bridged product, shown in structure **B** (Scheme 2-2). Bridged structures analogous to structure **B** are well

documented for related alkyne insertions.^{7h,11-12} Coordination at the saturated Ir centre in **1** is made possible by the incipient unsaturation at this metal, by movement of the bridging CO to Ru, concomitant with Ir–Ru bond cleavage (structure **A**). Migration of the resulting $\mu\text{-}\kappa^1\text{:}\kappa^1$ -hydrocarbyl fragment in **B** to a chelating position on Ir is presumably the result of the greater Ir–C bond strength

Scheme 2-2



compared to Ru–C.¹⁴ However, one troublesome aspect of this proposal is that the reaction of **1** with cumulenes occurs *more readily* than for its Rh/Ru and Rh/Os congeners which were generally unreactive unless promoted by carbonyl removal.¹⁰ We had expected the opposite on the basis of the generally lower lability of Ir species compared to the Rh analogues. Certainly, we have previously shown that nucleophilic displacement of a CO by PMe₃ is significantly slower for **1** than for the Rh/Ru and Rh/Os species.¹⁵

We therefore considered alternate mechanisms that did not involve prior cumulene coordination. In this context, we proposed direct nucleophilic attack of the $\mu\text{-CH}_2$ group on the cumulene. The CH₂ group is nucleophilic, as the addition of triflic acid (HOTf) to a solution of $[\text{IrRu}(\text{CO})_4(\mu\text{-CH}_2)(\text{dppm})_2]^+$ results in protonation of the methylene to generate the dicationic methyl complex, $[\text{IrRu}(\text{CH}_3)(\text{CO})_4(\text{dppm})_2]^{2+}$, even at $-80\text{ }^\circ\text{C}$.¹³ However, if nucleophilic attack

does occur at the cumulene, this should result in nucleophilic attack at the *central carbon*¹⁶ which would not give the observed product.

Inspection of the structure for **1**,⁷ⁱ in which the Ir–CH₂ bond (2.05(1) Å) is significantly shorter than Ru–CH₂ (2.31(1) Å), suggests a third possibility, which also does not require prior cumulene coordination. This weaker Ru–CH₂ interaction may be readily cleaved giving rise to an unobserved minor species having a terminal methylene group on Ir. Coupling of this Ir=CH₂ moiety and the cumulene could then occur via 2 + 2 cycloaddition. Such a possibility would give the iridacycle directly, without the involvement of a hydrocarbyl-bridged intermediate.

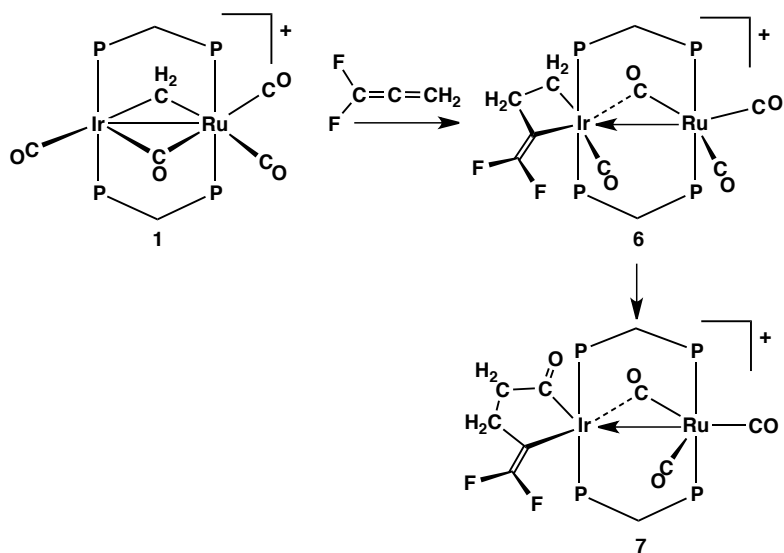
Although, as noted, the [RhM(CO)₄(μ-CH₂)(dppm)₂]⁺ (M = Ru, Os) congeners were unreactive towards most cumulenes investigated, their tricarbonyl analogues reacted readily to give μ-κ¹-η³-CH₂C(CH₂)CHR groups,¹⁰ having a very different geometry than observed in the present study. These different outcomes are a result of coupling of the μ-CH₂ group with either the central carbon or the terminal CH₂ group of the cumulene. Coupling to the central carbon would give the μ-κ¹-η³-geometry in the previous study, while coupling at the unsubstituted end would give the iridacycles in this study. It is not clear why this difference occurs, although the tricarbonyl species will be stronger nucleophiles than their tetracarbonyl analogues and as noted, such attack would be favoured at the central carbon. In attempts to carry out a comparison with the chemistry of the above tricarbonyl species of Rh/Ru and Rh/Os, we attempted the removal of a carbonyl from **1**, either in the presence of cumulene or in its absence, followed by cumulene addition, under a range of conditions. All attempts resulted in complex mixtures of unidentified products. Failure to prepare this methylene-bridged tricarbonyl species had previously been noted.⁷ⁱ

2.2.1.2 1,1-Difluoroallene

The addition of 1,1-difluoroallene to a solution of **1** in an NMR tube equipped with a J. Young valve results in its conversion, over a 24 h period to a 3:1 mixture of [IrRu(CO)₄(κ¹:κ¹-F₂C=CCH₂CH₂)(dppm)₂][BF₄] (**6**) and

$[\text{IrRu}(\text{CO})_3(\kappa^1:\kappa^1\text{-F}_2\text{C}=\text{CCH}_2\text{CH}_2\text{CO})(\text{dppm})_2][\text{BF}_4]$ (**7**), respectively, and allowing this mixture to stand for an additional 36 h period results in complete conversion to **7** (Scheme 2-3).

Scheme 2-3



The formation of **6** parallels that of **2** and **3** and all three products have similar NMR parameters. Compound **6** gives rise to two resonances in the $^{31}\text{P}\{^1\text{H}\}$ NMR spectrum at δ 24.8 and δ -14.8, as does compound **7** at δ 21.3 and δ -9.3. The slow conversion of **6** to **7** can be monitored by $^{31}\text{P}\{^1\text{H}\}$ spectroscopy, as shown in Figure 2-4. The Ir-bound CH_2 group resonates at δ 0.87 as a broad multiplet in the ^1H NMR spectrum; displaying coupling to both the Ir-bound ^{31}P nuclei and the adjacent CH_2 protons ($^3J_{\text{HP}} = 8.7$ Hz, $^3J_{\text{HH}} = 6.8$ Hz). This can be confirmed by selectively decoupled $^1\text{H}\{^{31}\text{P}\}$ NMR experiments as well as by a proton correlation NMR experiment (gCOSY). The other CH_2 group appears at δ 2.05 as a broad triplet, showing resolvable coupling to only the adjacent CH_2 protons. The resonances for the CO ligands in the $^{13}\text{C}\{^1\text{H}\}$ NMR spectrum are similar to those of **2** and **3**, while the original methylene carbon of **1** now appears at δ -19.6. The ^{19}F NMR spectrum shows two signals for the pair of geminal

fluorines, at δ -80.6 and δ -94.4 displaying mutual coupling of 84.2 Hz characteristic of two-bond fluorine-fluorine coupling.¹⁷

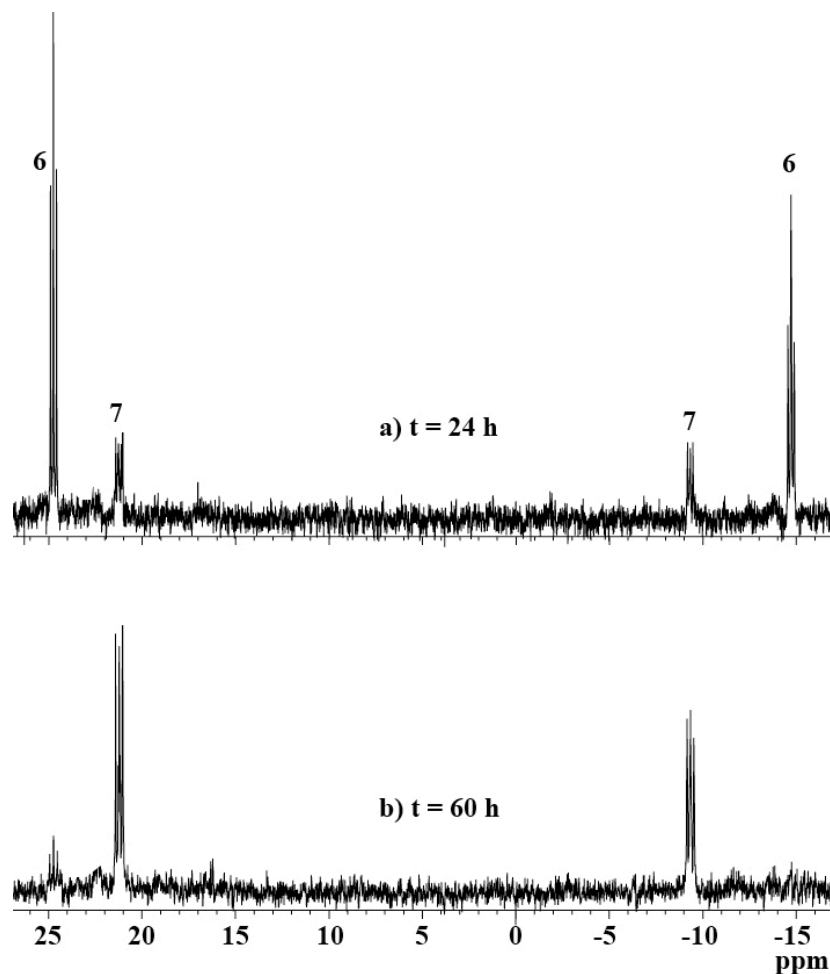


Figure 2-4. $^{31}\text{P}\{^1\text{H}\}$ NMR spectra of a mixture of **6** and **7** at 24 h and 60 h in CD_2Cl_2 .

The $^{13}\text{C}\{^1\text{H}\}$ NMR spectrum of compound **6** (^{13}CO and $^{13}\text{CH}_2$ -enriched) gives resonances for the terminal CO's at δ 195.9 , δ 191.7 , and δ 178.7 , a resonance for the semi-bridging CO at δ 211.2 , and a resonance for the $^{13}\text{CH}_2$ group at δ -19.6 . The $^{13}\text{C}\{^1\text{H}\}$ NMR spectrum of compound **7** (^{13}CO and $^{13}\text{CH}_2$ -enriched) is different from that of **6**, as it displays a distinctive¹⁸ low-field

resonance for the acyl carbon at δ 274.8, as a doublet of triplets, with coupling to the adjacent methylene carbon observed at δ 44.7 ($^1J_{CC} = 24.0$ Hz) and to the Ir-bound phosphorus nuclei ($^2J_{CP} = 7.3$ Hz). The acyl CO stretch also appears at characteristically low frequency (1705 cm^{-1}) in the IR spectrum, as confirmed by the isotope shift observed in the ^{13}C -enriched sample (1677 cm^{-1}). All CO ligands observed in the $^{13}\text{C}\{^1\text{H}\}$ NMR spectrum (δ 212.6, δ 186.8, and δ 176.7) are shown by selective ^{31}P -decoupling experiments to be Ru-bound. The ^1H NMR spectrum of a non-enriched sample of **7** is as expected, although now neither set of CH_2 protons (δ 2.79, δ 0.91) shows resolvable coupling to the Ir-bound ^{31}P nuclei, and only show mutual three-bond coupling of 7.6 Hz. The ^{19}F NMR signals shift slightly downfield from those of **6**, to δ -78.7 and δ -79.3, and display mutual coupling of 70.8 Hz.

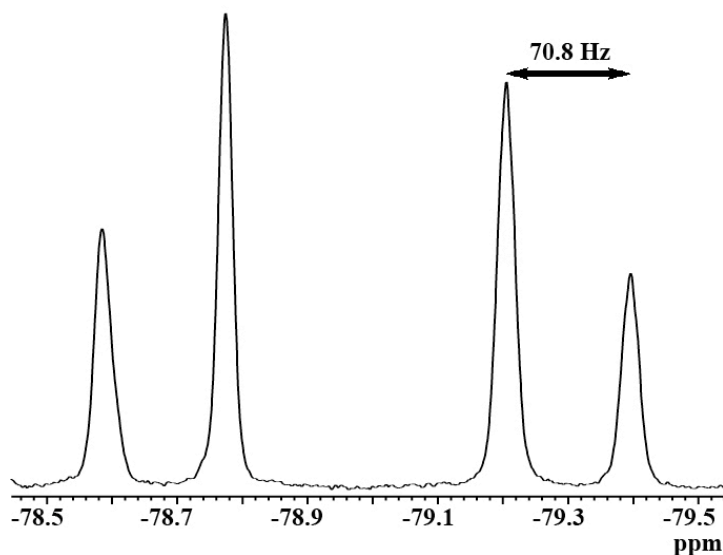


Figure 2-5. ^{19}F NMR spectrum of **7** in CD_2Cl_2 .

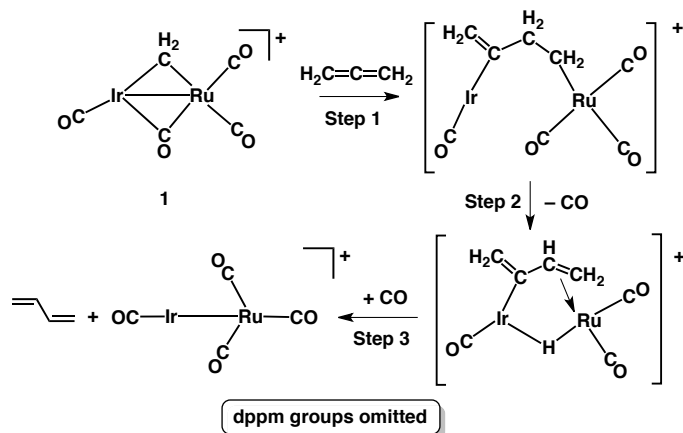
The migration of one end of the 1,1-difluorobutenyl moiety to a carbonyl group generates a more favourable, less strained 5-membered metallacycle. Presumably this migration occurs for the fluoro-substituted species, but not for the methyl-substituted analogues (**2** and **3**) owing to the electron-withdrawing effects of the fluorocarbyl unit, which leaves the carbonyl groups more electrophilic and more prone to migratory insertion, as a consequence of less back donation from Ir; this is evident in the higher frequency carbonyl stretches observed for **6**

(between 1999 and 2074 cm^{-1}) compared to **2** (between 1945 and 2048 cm^{-1}). Although the fluorovinyl group is adjacent to the Ir-bound CO in **6**, migratory insertion of these groups does not occur owing to the stronger Ir–fluorovinyl bond and to the lower nucleophilicity of the vinyl carbon (a function of both fluoro-substitution and the sp^2 hybridization of the α -carbon); instead migration of the more nucleophilic “CH₂” end to the adjacent semi-bridging carbonyl occurs, accompanied by slight rearrangements to give **7**.

2.2.1.3 Allene

The reaction of **1** with allene differs from the reactions involving the substituted cumulenes, noted above, in that no complex containing a hydrocarbyl moiety is observed in this case. Instead, the only products observed, over a wide temperature range, from $-80\text{ }^\circ\text{C}$ to ambient temperature, are the known tetracarbonyl complex, $[\text{IrRu}(\text{CO})_4(\text{dppm})_2][\text{BF}_4]^{7i}$ and 1,3-butadiene. Clearly, butadiene is a product of coupling of the C₃ fragment (allene) with the methylene group of **1**. We suggest that the formation of 1,3-butadiene results from a sequence of insertion, β -hydride elimination and reductive elimination steps, as outlined in Scheme 2-4. We rule out an iridacycle intermediate, such as observed in compounds **2** – **6**, since β -hydride elimination should not occur readily from a strained and inflexible 4-membered metallacycle.¹⁹ On the other hand, C₃-bridged units have been shown to be flexible to rotation about the metal-metal axis^{7h,11-12} giving more opportunity for β -elimination. The required 1,2-H shift that converts the bridging 2,4-butenediyl moiety to 1,3-butadiene is suggested to occur by β -hydride elimination (step 2) followed by reductive elimination of butadiene (step 3), although the exact nature of the proposed dienyl/hydride intermediate is not known. It is not clear why the reaction of with allene yields 1,3-butadiene, while the reactions involving the substituted allenes give metallacyclic products, but may suggest different mechanisms for cumulene incorporation.

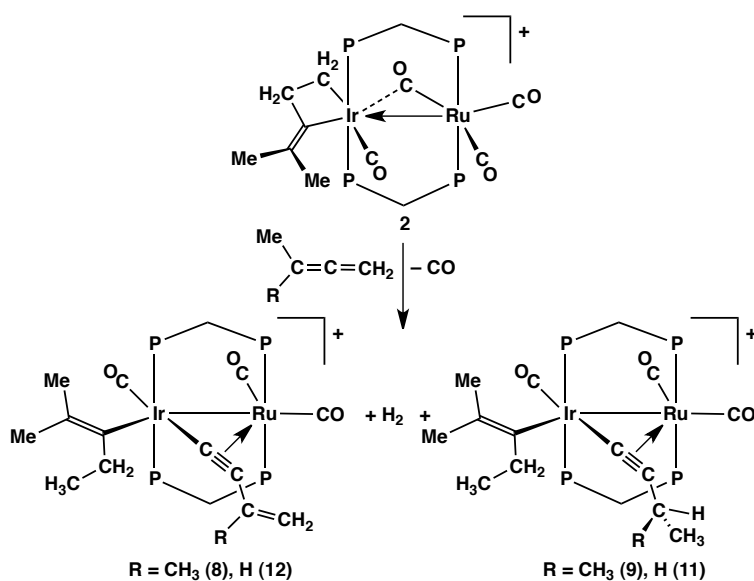
Scheme 2-4



2.2.2 Multiple Carbon–Hydrogen Bond Activations

The iridacyclic product (**2**) reacts further in the presence of excess 1,1-dimethylallene to give two products, $[\text{IrRu}(\text{CO})_3(\kappa^1\text{-C}(\text{CH}_2\text{CH}_3)=\text{C}(\text{CH}_3)_2)(\mu\text{-}\kappa^1:\eta^2\text{-C}\equiv\text{C}(\text{CH}_3)=\text{CH}_2)\text{-(dppm)}_2][\text{BF}_4]$ (**8**) and $[\text{IrRu}(\text{CO})_3(\kappa^1\text{-C}(\text{CH}_2\text{CH}_3)=\text{C}(\text{CH}_3)_2)(\mu\text{-}\kappa^1:\eta^2\text{-C}\equiv\text{C}(\text{H}(\text{CH}_3)_2)(\text{dppm)}_2][\text{BF}_4]$ (**9**), in an approximate 3:1 ratio, as outlined in Scheme 2-5. This product ratio appears to be highly dependent on reaction conditions, and ratios as high as 20:1 of these

Scheme 2-5



respective species have been obtained, without any obvious change in conditions. The reaction of **1** with excess 1,1-dimethylallene yields the same mixture of **8** and **9** over a 24 h period at ambient temperature, through the presumed intermediacy of **2**. Compound **8** is the result of the activation of three C–H bonds within the second equiv of dimethylallene and loss of a CO ligand; in addition to the activation of both geminal C–H bonds, activation of a methyl C–H bond has also occurred. Two of the hydrogens resulting from this triple C–H bond activation are lost as H₂, while the third has been eliminated with the “methylene end” of the iridacycle resulting in the formation of an Ir-bound κ^1 -alkenyl moiety. The minor product (**9**) has also resulted from CO loss and activation of the pair of geminal C–H bonds in the second equiv of dimethylallene. In this case one of the hydrogens is again transferred to the iridacycle to give the identical alkenyl group, while the other is transferred to the γ -carbon of the transformed cumulene fragment. Although **8** is related to **9** by the cleavage of two C–H bonds and H₂ loss, **9** is not an intermediate in the formation of **8**; leaving this product mixture for extended periods or warming to 40 °C does not result in the conversion of **9** to **8**. Furthermore, H₂ addition to **8** does not generate **9**, instead leaving **8** unreacted.

Complexes **8** and **9** have very similar ³¹P{¹H} resonances (δ 18.9 and δ –18.8 (**8**), δ 18.7 and δ –19.3 (**9**)), and the resonances for the Ru-bound ³¹P nuclei actually overlap slightly, as shown in Figure 2-6. Both complexes also have

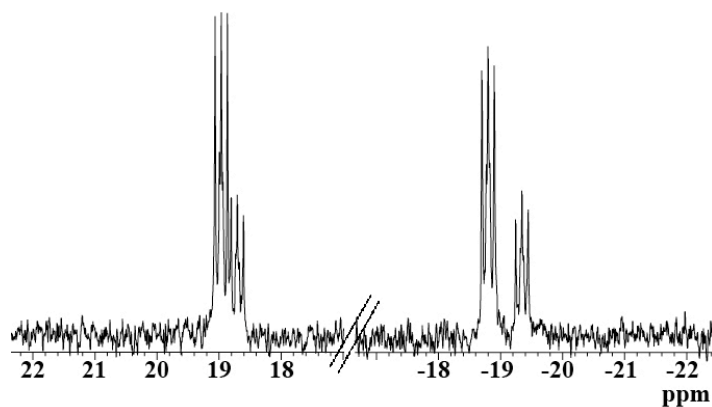


Figure 2-6. ³¹P{¹H} NMR spectrum of compounds **8** and **9** in CD₂Cl₂.

similar $^{13}\text{C}\{^1\text{H}\}$ NMR spectra, and $^{13}\text{C}\{^{31}\text{P}\}$ experiments confirm that each complex has one CO on Ir (δ 182.0 (**8**), δ 188.7 (**9**) and two on Ru (δ 207.8 and δ 199.4 (**8**), δ 208.6 and δ 200.4 (**9**)). ^1H NMR spectra are also consistent with the structures proposed. In compound **8**, the geminal olefinic protons appear at δ 4.49 and δ 4.10 as broad singlets, while distinct features of **9** include the presence of a septet at δ 2.63 ($^3J_{\text{HH}} = 7.2$ Hz), for the isopropyl proton, and the pair of isopropyl methyl groups as a corresponding doublet at δ 0.64.

An X-ray structure determination of **8**- CF_3SO_3 , in which the tetrafluoroborate anion has been exchanged with triflate, confirms the connectivity proposed for this product, the complex cation of which is shown in Figure 2-7. Within the alkynyl moiety, there is a 1:1 disorder between two positions for carbons numbered 11 through 14, as described in the Experimental Section. Selected bond lengths and angles for both disordered forms of **8**- CF_3SO_3 are presented in Table 2-3.

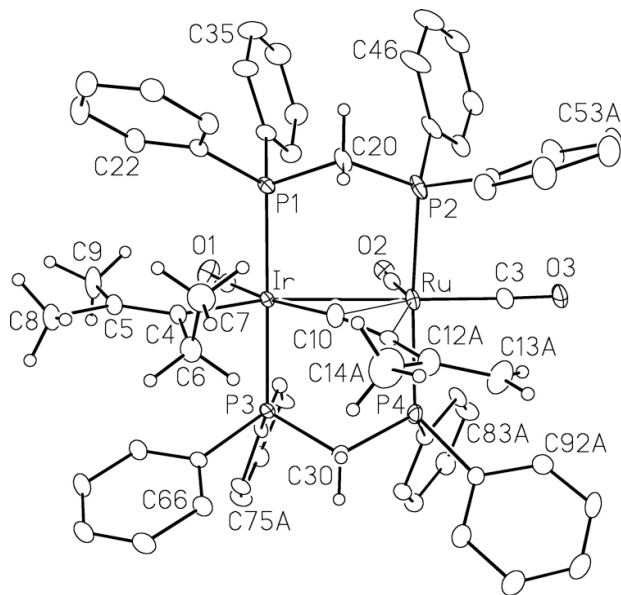


Figure 2-7. Perspective view of the complex cation of $[\text{IrRu}(\text{CO})_3(\kappa^1\text{-C}(\text{CH}_2\text{CH}_3)=\text{C}(\text{CH}_3)_2)(\mu\text{-}\kappa^1:\eta^2\text{-C}\equiv\text{CC}(\text{CH}_3)=\text{CH}_2)(\text{dppm})_2][\text{CF}_3\text{SO}_3]$ (**8**- CF_3SO_3), showing the atom labelling scheme. Thermal parameters are as described in Figure 2-2.

Within the Ir-bound κ^1 -alkenyl fragment, the C(4)–C(5) bond length of 1.341(4) Å is typical of a double bond,²⁰ while C(4)–C(6) (1.542(4) Å) corresponds to a single bond.²⁰⁻²¹ Within the vinylalkynyl moiety, the C(10)–C(11) bond lengths of 1.263(9) and 1.292(9) Å (for the two disordered forms) are intermediate between a triple and a double bond,²⁰⁻²¹ as a result of its η^2 -interaction with Ru. The C(12)–C(13) bond lengths (1.37(1), 1.36(1) Å) are somewhat longer than expected for a double bond while C(12)–C(14) (1.42(3), 1.47(2) Å) is shorter than expected for a single bond,²⁰⁻²¹ presumably a consequence of the disorder.

Table 2-3. Selected Bond Lengths and Angles for Both Disordered Forms of Compound 8-CF₃SO₃

(a) Distance (Å)^a

atom 1	atom 2	distance	atom 1	atom 2	distance
Ir	Ru	2.9687(3)	C10	C11A	1.263(9)
Ir	C4	2.138(2)	C10	C11B	1.292(9)
Ir	C10	1.992(3)	C11A	C12A	1.47(1)
Ru	C10	2.263(2)	C11B	C12B	1.47(1)
Ru	C11A	2.357(8)	C12A	C13A	1.37(1)
C4	C5	1.341(4)	C12B	C13B	1.36(1)
C4	C6	1.542(4)	C12A	C14A	1.42(3)
C5	C8	1.513(4)	C12B	C14B	1.47(2)
C5	C9	1.509(5)			

(b) Angles (deg)^a

atom	atom 2	atom 3	angle	atom 1	atom	atom 3	angle
Ir	C4	C5	129.1(2)	C10	C11A	C12A	151.3(7)
Ir	C4	C6	112.9(2)	C10	C11B	C12B	150.5(8)
C4	C5	C8	122.6(3)	C11A	C12A	C13A	121.8(7)
C4	C5	C9	126.5(3)	C11B	C12B	C13B	122.1(8)
Ir	C10	C11A	160.9(4)	C11A	C12A	C14A	114(1)
Ir	C10	C11B	159.5(4)	C11B	C12B	C14B	117(1)

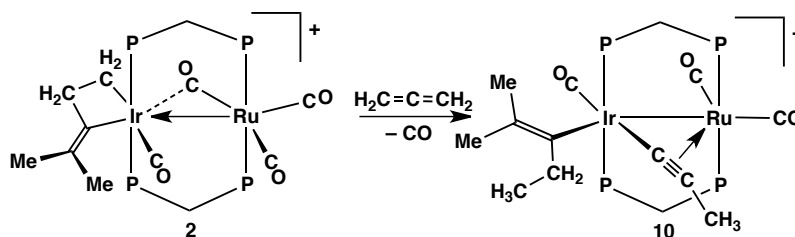
^aThe disordered groups are labelled “A” and “B”

The failure of compounds **8** and **9** to interconvert by H₂ loss/gain indicates that they are generated by competing pathways; however, we have no other

mechanistic information about the formation of these species, since no intermediates were detected in low-temperature NMR studies. Low-temperature studies of the reaction of **2** with a three-fold excess of 1,1-dimethylallene in the presence of trimethylamine *N*-oxide (TMNO) indicate the rapid formation of **8** and **9** at temperatures as low as $-20\text{ }^{\circ}\text{C}$, demonstrating that the rate determining step in this transformation involves the loss of a carbonyl from **2**. Although no intermediates were identified, we assume that geminal C–H activation results from dimethylallene coordination through the unsubstituted end at one metal (presumably accompanied by CO loss), followed by stepwise C–H activation involving the adjacent metal, and accompanying hydrogen transfer to the iridacyclic group. However, the stages at which H-transfer to the γ -carbon to yield **9** and H-abstraction from the methyl carbon to give **8** occur are not known.

In hopes of observing species that might model intermediates in the above transformations, we have investigated the stepwise reactions of **1** with different combinations of cumulenes. We first investigated the reactions of **2** (obtained from **1** and 1,1-dimethylallene) with either allene or 1,1-difluoroallene, neither of which can yield analogues of the “triple C–H activation product”, owing to the absence of the alkyl substituent necessary for the “third” activation, but which might instead yield analogues of **9**. In keeping with this assumption, the reaction of **2** with allene yields only one product, $[\text{IrRu}(\text{CO})_3(\kappa^1\text{-C}(\text{CH}_2\text{CH}_3)=\text{C}(\text{CH}_3)_2)(\mu\text{-}\kappa^1:\eta^2\text{-C}\equiv\text{CCH}_3)(\text{dppm})_2][\text{BF}_4]$ (**10**) – the result of double geminal C–H activation of allene accompanied by H-transfer to both the iridacycle and to the γ -carbon of the transformed C_3 -fragment, to give the propynyl-bridged product, shown in Scheme 2-6. The spectral data for **10** very much resemble that of **9**, apart from the methyl or isopropyl substituents on the respective alkynyl groups.

Scheme 2-6



An X-ray structure determination of **10**, as shown for the complex cation in Figure 2-8, verifies the connectivity proposed. Selected bond lengths and angles for **10** appear in Table 2-4, and an ORTEP diagram of an alternate view that includes all phenyl rings is shown in Figure 2-9. The structural parameters for **10** very much resemble those of **8**, in which the C(5)–C(6) distance

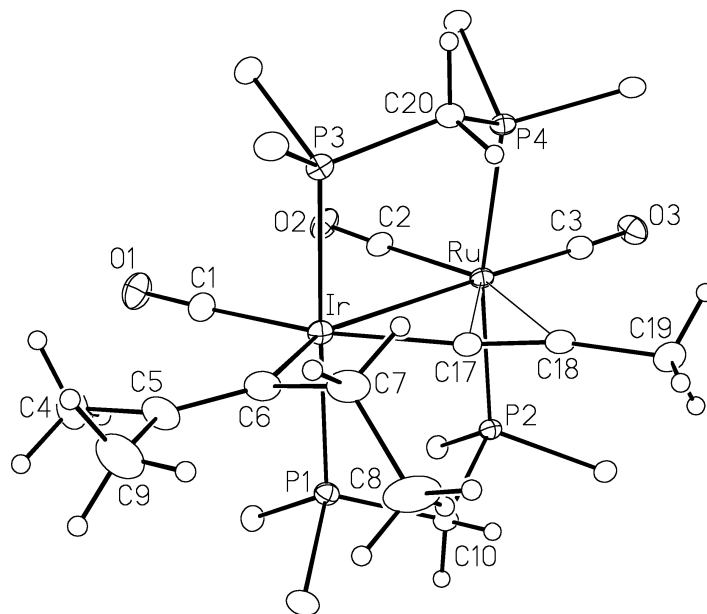


Figure 2-8. Perspective view of the complex cation of $[\text{IrRu}(\text{CO})_3(\kappa^1\text{-C}(\text{CH}_2\text{CH}_3)=\text{C}(\text{CH}_3)_2)(\mu\text{-}\kappa^1:\eta^2\text{-C}\equiv\text{CCH}_3)(\text{dppm})_2][\text{BF}_4]$ (**10**), showing the atom labeling scheme. Only the ipso carbons of the phenyl rings are shown. Thermal parameters are as described in Figure 2-2.

of 1.341(7) Å is as expected for a double bond and C(17)–C(18) (1.250(6) Å) corresponds to a triple bond that is somewhat elongated by the η^2 -interaction with Ru.²⁰⁻²¹ This latter interaction also leads to deviations in the Ir–C(17)–C(18) and C(17)–C(18)–C(19) angles from linearity. Within the Ir-bound alkenyl fragment the trigonal planar geometries at C(6) and C(5) are consistent with the olefinic formulation.

Table 2-4. Selected Bond Lengths and Angles of Compound 10

(a) Distance (Å)

atom 1	atom 2	distance	atom 1	atom 2	distance
Ir	Ru	2.9419(3)	C5	C6	1.341(7)
Ir	C6	2.136(4)	C5	C9	1.518(6)
Ir	C17	2.003(4)	C6	C7	1.534(6)
Ru	C17	2.275(4)	C17	C18	1.250(6)
Ru	C18	2.348(4)	C18	C19	1.486(6)
C4	C5	1.513(8)			

(b) Angles (deg)

atom	atom 2	atom 3	angle	atom 1	atom 2	atom 3	angle
C4	C5	C6	127.2(4)	Ir	C6	C7	112.8(3)
C4	C5	C9	111.1(5)	Ir	C17	C18	164.2(3)
C6	C5	C9	121.8(5)	C17	C18	C19	156.5(4)
Ir	C6	C5	127.1(3)				

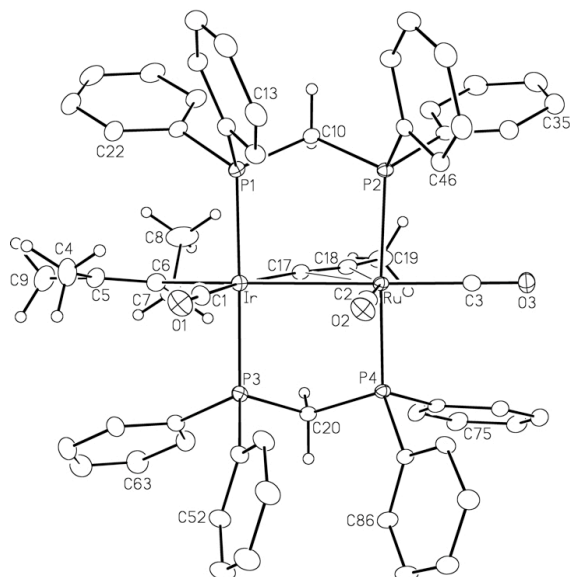


Figure 2-9. Alternate view of the complex cation of $[\text{IrRu}(\text{CO})_3(\kappa^1\text{-C}(\text{CH}_2\text{CH}_3)=\text{C}(\text{CH}_3)_2)(\mu\text{-}\kappa^1:\eta^2\text{-C}\equiv\text{CCH}_3)(\text{dppm})_2][\text{BF}_4]$ (**10**), with all phenyl carbons. Thermal parameters are as described in Figure 2-2.

Efforts to react complex **2** with 1,1-difluoroallene were unsuccessful; even the exposure of **2** to 10 equiv of the gaseous cumulene over 48 h at slightly elevated temperatures gave no reaction. The electronic difference imparted by the fluorine substituents, although remote from the expected C–H activation sites is apparently sufficient to hinder the reactivity observed with the other cumulenes. It may be that the electronegative fluorines result in strengthening of the distal C–H bonds²² enough to deactivate this cumulene to C–H bond cleavage.

In the reaction of **2** with methylallene, both pathways, observed in the reaction with 1,1-dimethylallene, are again accessible, yielding both $[\text{IrRu}(\text{CO})_3(\kappa^1\text{-C}(\text{CH}_2\text{CH}_3)=\text{C}(\text{CH}_3)_2)(\mu\text{-}\kappa^1\text{:}\eta^2\text{-C}\equiv\text{CCH}_2\text{CH}_3)(\text{dppm})_2][\text{BF}_4]$ (**11**) and $[\text{IrRu}(\text{CO})_3(\kappa^1\text{-C}(\text{CH}_2\text{CH}_3)=\text{C}(\text{CH}_3)_2)(\mu\text{-}\kappa^1\text{:}\eta^2\text{-C}\equiv\text{CCH}=\text{CH}_2)(\text{dppm})_2][\text{BF}_4]$ (**12**) in a 3:2 ratio, as shown earlier in Scheme 2-5. In this case, however, the major product is the double C–H activation product **11** in which the hydrogens resulting from geminal activation have migrated to the iridacycle, yielding the alkenyl group and to the γ -carbon of the activated allene. The lower proportion of the “methyl activated” product (**12**) compared to the dimethylallene reaction may, in part, reflect the statistical differences, having only one methyl group available in the present case, as opposed to two. Again, the interconversion of the two products (**11** and **12**) by H_2 loss or addition does not occur. The NMR spectral parameters are in agreement with those of compounds **9** and **8**, respectively, and are fully consistent with the structures shown.

Unfortunately, the X-ray structure determination of **11** revealed that it was badly disordered, so although the gross geometry was obvious, severe disorder of the bridging butynyl group did not allow its unambiguous identification. Nevertheless, the spectroscopy for this species is unambiguous, particularly regarding the ethyl substituent on the bridging alkynyl group. In the ^1H NMR spectrum this ethyl substituent resonates at δ 2.57 and δ 0.58 with mutual three-bond coupling of 7.3 Hz. The assignment of these resonances as such can be confirmed by 2D NMR spectroscopy (gCOSY).

Surprisingly, reversing the addition of methylallene and 1,1-dimethylallene by reacting **3** with dimethylallene did not yield the expected two

products analogous to those described above, but instead gave a mix of several unidentified products under a range of reaction conditions. One of these products (28 % yield) was identified as the product of the reaction of dimethylallene with $[\text{IrRu}(\text{CO})_4(\text{dppm})_2][\text{BF}_4]$, as will be described in the subsequent chapter.²³ The same reactivity pattern is observed with the addition of allene to **3**, in which one of the products (40 % yield) was identified as the product of allene addition to $[\text{IrRu}(\text{CO})_4(\text{dppm})_2][\text{BF}_4]$.²³ This reactivity pattern demonstrates the instability of compound **3** towards loss of the hydrocarbyl fragment under the reaction conditions. This also suggests that the tetracarbonyl complex, $[\text{IrRu}(\text{CO})_4(\text{dppm})_2]^+$, is active in multiple C–H bond activation processes as well as the methylene-bridged Ir/Ru complex discussed in this chapter.

2.3 Conclusions

In the reaction of $[\text{IrRu}(\text{CO})_4(\mu\text{-CH}_2)(\text{dppm})_2][\text{BF}_4]$ (**1**) with 1 equiv of the cumulenes studied there are two substantially different outcomes. With the substituted allenes, 1,1-dimethylallene, methylallene, and 1,1-difluoroallene the initial product obtained in each case is an iridacycle-containing species resulting from coupling of the $\mu\text{-CH}_2$ group and the unsubstituted end of the cumulene, while for allene itself no hydrocarbyl product is observed and instead the organic moiety resulting from allene/methylene coupling is eliminated as 1,3-butadiene. As discussed earlier, we consider two mechanisms for coupling of the methylene and cumulene groups to be viable. It is possible that the differing outcomes for the substituted and unsubstituted allenes arise due to these two different mechanisms (although we can offer no rationalization for why substituted and unsubstituted allenes should favour one mechanism over the other).

It is also possible that all cumulenes react via the same coupling mechanism to yield the same type of bridged intermediate (structure **B**, Scheme 2-2) and that the pathway followed is a consequence of the differing competitive rates of migration of the bridged unit to a chelating geometry on Ir and the $\beta\text{-H}$ elimination/reductive elimination pathway generating the 1,3-butadiene (Scheme 2-4). If this were the case, the methyl-substituted allenes could be less stable in

the bridging position, owing to their larger steric bulk and resulting steric repulsions with the μ -dppm groups, favouring migration to Ir, while the electronegative fluorine substituents in 1,1-difluoroallene strengthen the C–H bonds within this molecule, making C–H activation unfavourable with respect to chelate formation. Such a rationale would explain why the electronically different cumulenes (methyl- or fluorine-substituted) have similar outcomes. Although this study did not succeed in shedding light on this question, a study of the related Ir/Os system (which is presented in Chapters 4 and 5), containing strong Ir–C and Os–C bonds, may succeed in allowing a hydrocarbyl-bridged species to be observed and therefore may offer helpful insights.

The subsequent reactivities of the chelated product of methylene and 1,1-dimethylallene coupling, namely $[\text{IrRu}(\text{CO})_4(\kappa^1:\kappa^1\text{-Me}_2\text{C}=\text{CCH}_2\text{CH}_2)(\text{dppm})_2]^+$ (**2**), with methylallene, allene, or additional 1,1-dimethylallene were surprising and for each added cumulene appear to proceed in much the same way. All proceed by activation of two geminal C–H bonds of the cumulene followed by transfer of the resulting hydrogens to the existing iridacycle, yielding a κ^1 -alkenyl group, and to the γ -carbon of the activated cumulene, giving a bridging alkynyl group. When methyl substituents are present on the added cumulene a second pathway is competitive, in which one hydrogen from geminal activation is again transferred to the iridacycle. However, in this case, C–H activation of one of the methyl substituents also occurs, accompanied by H_2 loss, yielding a bridging vinylalkynyl group. Unfortunately, we were unable to obtain mechanistic information about these interesting transformations and additional studies are underway in hopes of resolving this issue.

As anticipated, the Ir/Ru metal combination has resulted in reactivity not seen with the other metal combinations. In particular, the lability of Ru combined with the greater bond strengths involving Ir have combined to yield the iridacyclic products, not previously seen with the other metal combinations.^{10,24} In addition, the tendency for low-valent Ir to undergo C–H activation is clearly evident in this study. Other aspects of reactivity, related to the relatively simple concept of carbonyl lability is not so easily rationalized, and appears not to depend on one

metal alone (for example in the comparison of Rh/Ru and Ir/Ru systems) but instead appears to depend on subtle influences of the adjacent metals. A full understanding of these and other observations must await additional studies needed to establish the mechanistic details of these transformations.

2.4 Experimental Section

2.4.1 General Comments

All solvents were dried using appropriate desiccants (given in Appendix II), distilled before use, and stored under a nitrogen atmosphere. Reactions were performed under an argon atmosphere using standard Schlenk techniques unless otherwise noted. Triruthenium dodecacarbonyl and ammonium hexachloroiridate (IV) were purchased from Strem Chemicals. The 1,2-butadiene (methylallene) was purchased from Organic Technologies, allene from Matrix Scientific, and 1,1-dimethylallene from Aldrich. The trimethylamine *N*-oxide dihydrate was also purchased from Aldrich and was dried according to the literature procedure.²⁵ Diazomethane was generated from Diazald,TM which was purchased from Aldrich, as was the ¹³C-enriched Diazald. ¹³C-enriched *N*-Methyl-*N*-nitroso-*p*-toluenesulfonamide was also prepared by using a modified version of the procedure for synthesizing the ¹⁴C-enriched radio-labelled analogue.²⁶ The ¹³CO was purchased from Isotech, Inc. Compound **1**, [IrRu(CO)₄(μ-CH₂)(dppm)₂][BF₄], was prepared by the literature procedure,⁷¹ with the exception that [Ir(CO)(dppm)₂][Cl]²⁷ was used instead of [IrCl(dppm)₂] in the synthesis. Complete multinuclear NMR characterization for **1** is presented in Table 2-5.

1,1-Difluoroallene was prepared using a modification of the published procedures,^{24,28} in which a solution of 100 μL of 2-bromo-3,3,3-trifluoro-1-propene (purchased from Aldrich) in 3 mL of diethyl ether was cooled to -90 °C in an acetone/liquid N₂ bath. To this was added dropwise 385 μL of a 2.5 M solution of *n*-butyllithium in hexanes (purchased from Aldrich), followed by stirring of the solution at this temperature for 30 min. The -90 °C bath was replaced by an acetonitrile/CO_{2(s)} bath (*ca.* -40 °C) and the solution was stirred for

15 min. The solution was then slowly warmed over 15 min to $-20\text{ }^{\circ}\text{C}$, resulting in the evolution of 1,1-difluoroallene gas.

The ^1H and $^{31}\text{P}\{^1\text{H}\}$ NMR spectra were recorded on a Varian Inova 400 spectrometer operating at 399.9 and 161.8 MHz, respectively. All low-temperature spectra and the heteronuclear decoupling experiments ($^{13}\text{C}\{^1\text{H}\}$ and $^{13}\text{C}\{^1\text{H}, ^{31}\text{P}\}$) were recorded on a Varian Unity spectrometer operating at 161.9 MHz for ^{13}C , 202.3 MHz for ^{31}P , and 499.8 MHz for ^1H . Infrared spectra were recorded in CH_2Cl_2 solution on a Nicolet Avatar 370 DTGS spectrometer. Mass spectrometry was performed on a Micromass ZabSpec TOF spectrometer by the mass spectrometry facility of this department, and elemental analyses were also carried out in the departmental facility.

2.4.2 Preparation of Compounds

Spectroscopic data for the compounds are presented in Table 2-5.

(a) $[\text{IrRu}(\text{CO})_4(\kappa^1:\kappa^1\text{-Me}_2\text{C}=\text{CCH}_2\text{CH}_2)(\text{dppm})_2][\text{BF}_4]$ (2).

Compound **1**, $[\text{IrRu}(\text{CO})_4(\mu\text{-CH}_2)(\text{dppm})_2][\text{BF}_4]$ (100 mg, 0.078 mmol) was dissolved in 20 mL of CH_2Cl_2 , affording a bright yellow/orange solution. To this solution was added 1,1-dimethylallene by micro-syringe (23 μL , 0.24 mmol). The reaction was stirred under an argon atmosphere at ambient temperature for 48 h, darkening to orange upon stirring. After stirring, the solution volume was reduced to 5 mL and to this was added 30 mL of diethyl ether to precipitate a yellow/orange solid that was washed with 2 x 5 mL of diethyl ether and dried in vacuo (90 % yield). HRMS: m/z calcd for $\text{C}_{60}\text{H}_{54}\text{IrO}_4\text{P}_4\text{Ru}$ (M^+), 1257.1640; found, 1257.1631 (M^+). Anal. Calcd for $\text{BC}_{60.41}\text{Cl}_{0.82}\text{F}_4\text{H}_{54.82}\text{IrO}_4\text{P}_4\text{Ru}$ ($2 \cdot 0.41 \text{ CH}_2\text{Cl}_2$): C, 52.66; H, 4.01. Found: C, 52.51; H, 4.05. ^1H NMR spectroscopy in CD_3CN confirmed the presence of dichloromethane of crystallization.

(b) $[\text{IrRu}(\text{CO})_4(\kappa^1:\kappa^1\text{-MeCH}=\text{CCH}_2\text{CH}_2)(\text{dppm})_2][\text{BF}_4]$ (3). Under an argon atmosphere, methylallene was passed through a stirred yellow/orange solution of **1** (100 mg, 0.078 mmol) in 20 mL of CH_2Cl_2 for

Table 2-5. Spectroscopic Data for the Compounds

Compound	IR (cm ⁻¹) ^b	NMR ^a		
		$\delta(^3\text{P}\{^1\text{H}\})^c$	$\delta(^1\text{H})^{d/e}$	$\delta(^{13}\text{C}\{^1\text{H}\})^{d/e}$
[IrRu(CO) ₄ (μ-CH ₂)(dppm) ₂][BF ₄] (1)	2039 (m), 1965 (s), 1783 (m)	30.1 (m, 2P), 3.1 (m, 2P)	3.90 (dm, 2H, ² J _{HH} = 14.6 Hz), 3.59 (tt, 2H, ³ J _{HP} = 11.4 Hz, ³ J _{HP} = 6.4 Hz), 3.13 (dm, 2H, ² J _{HH} = 14.6 Hz)	211.1 (dm, 1C, ² J _{CC} = 23.6 Hz), 195.7 (t, 1C, ² J _{CP} = 11.5 Hz), 191.3 (dt, 1C, ² J _{CC} = 23.6 Hz, ² J _{CP} = 11.5 Hz), 178.8 (t, 1C, ² J _{CP} = 11.1 Hz), 21.7 (m, 1C, ² J _{CP} = 13.3 Hz)
[IrRu(CO) ₄ (κ ¹ :κ ¹ -Me ₂ C=CCH ₂ CH ₂)-(dppm) ₂][BF ₄] (2)	2048 (s), 2032 (s), 2013 (s), 1945 (s)	25.7 (m, 2P), -14.2 (m, 2P)	4.61 (dm, 2H, ² J _{HH} = 14.1 Hz), 4.39 (dm, 2H, ² J _{HH} = 14.1 Hz), 2.15 (t, 2H, ³ J _{HH} = 7.9 Hz), 1.44 (bs, 3H), 0.98 (tt, 2H, ³ J _{HH} = 7.9 Hz, ³ J _{HP} = 8.9 Hz), 0.90 (bs, 3H)	212.7 (dt, 1C, ² J _{CC} = 28.6, ² J _{CP} = 14.9 Hz), 207.3 (dt, 1C, ² J _{CC} = 28.6 Hz, ² J _{CP} = 13.3 Hz), 188.7 (t, 1C, ² J _{CP} = 11.2 Hz), 182.1 (bt, 1C, ² J _{CP} = 8.7 Hz), -17.8 (bt, 1C, ² J _{CP} = 6.3 Hz)
[IrRu(CO) ₄ (κ ¹ :κ ¹ -MeHC=CCH ₂ CH ₂)-(dppm) ₂][BF ₄] (3)	2043 (s), 2032 (s), 1998 (s), 1981 (sh)	25.9 (m, 2P), -13.5 (m, 2P)	4.96 (bq, 1H, ³ J _{HH} = 5.8 Hz), 4.70 (dm, 2H, ² J _{HH} = 15.1 Hz), 4.32 (dm, 2H, ² J _{HH} = 15.1 Hz), 1.61 (t, 2H, ³ J _{HH} = 6.7 Hz), 1.19 (tt, ³ J _{HH} = 6.7 Hz, ³ J _{HP} = 10.9 Hz), 0.90 (bd, 3H, ³ J _{HH} = 5.8 Hz)	209.6 (dt, 1C, ² J _{CC} = 25.4 Hz, ² J _{CP} = 14.2 Hz), 208.8 (dt, 1C, ² J _{CC} = 25.4 Hz, ² J _{CP} = 12.2 Hz), 190.6 (t, 1C, ² J _{CP} = 10.7 Hz), 180.8 (bt, 1C, ² J _{CP} = 7.6 Hz), -19.9 (bt, 1C, ² J _{CP} = 7.1 Hz)
[IrRu(CO) ₃ (NCCCH ₃)(κ ¹ :κ ¹ -Me ₂ C=CCH ₂ CH ₂)(dppm) ₂][BF ₄] (4) ^f	n/a	31.3 (m, 2P), -16.9 (m, 2P)	4.40 (dm, 2H, ² J _{HH} = 13.7 Hz), 4.00 (dm, 2H, ² J _{HH} = 13.7 Hz), 2.85 (bt, ³ J _{HH} = 8.3 Hz), 1.38 (tt, 2H, ³ J _{HH} = 7.5 Hz, ³ J _{HP} = 9.3 Hz), 0.76 (bs, 3H), 0.41 (bs, 3H)	232.7 (t, 1C, ² J _{CP} = 11.1 Hz), 199.1 (t, 1C, ² J _{CP} = 13.4 Hz), 185.6 (dt, 1C, ² J _{CC} = 19.7 Hz, ² J _{CP} = 11.1 Hz), -11.6 (dm, 1C, ² J _{CC} = 19.7 Hz, ² J _{CP} = 5.8 Hz)

Table 2-5. Spectroscopic Data for the Compounds (Continued)

Compound	IR (cm ⁻¹) ^b	NMR ^a		
		$\delta(^3\text{P}\{^1\text{H}\})^c$	$\delta(^1\text{H})^{d/e}$	$\delta(^{13}\text{C}\{^1\text{H}\})^{d/e}$
[IrRu(CO) ₃ (NCCCH ₃)(κ ¹ :κ ¹ -MeHC=CCH ₂ CH ₂)(dppm) ₂][BF ₄] ^f (5) ^f	n/a	32.2 (m, 2P), -14.4 (m, 2P)	4.45 (dm, 2H, ² J _{HH} = 13.7 Hz), 3.94 (bq, 1H, ³ J _{HH} = 6.2 Hz), 3.78 (dm, 2H, ² J _{HH} = 13.7 Hz), 2.94 (bt, 2H, ³ J _{HH} = 9.1 Hz), 1.47 (t, 2H, ³ J _{HP} = 8.6 Hz, ³ J _{HH} = 9.1 Hz), 0.36 (bd, 3H, ³ J _{HH} = 6.2 Hz)	236.9 (t, 1C, ² J _{CP} = 9.0 Hz), 201.3 (t, 1C, ² J _{CP} = 14.3 Hz), 185.6 (dt, 1C, ² J _{CC} = 18.2 Hz, ² J _{CP} = 6.2 Hz), -16.2 (dm, 1C, ² J _{CC} = 18.2 Hz, ² J _{CP} = 5.8 Hz)
[IrRu(CO) ₃ (κ ¹ :κ ¹ -F ₂ C=CCH ₂ CH ₂)-(dppm) ₂][BF ₄] ^f (6)	2074 (s), 2060 (s), 2022 (m), 1999 (m)	24.8 (m, 2P), -14.8 (m, 2P)	4.74 (dm, 2H, ² J _{HH} = 14.7 Hz), 4.45 (dm, 2H, ² J _{HH} = 14.7 Hz), 2.05 (bt, 2H, ³ J _{HH} = 6.8 Hz), 0.87 (bm, 2H, ³ J _{HH} = 6.8 Hz, ³ J _{HP} = 8.7 Hz)	211.2 (m, 1C, ² J _{CC} = 11.0 Hz, ² J _{CP} = 8.9 Hz), 195.9 (dt, 1C, ² J _{CC} = 11.0 Hz, ² J _{CP} = 8.9 Hz), 191.7 (t, 1C, ² J _{CP} = 7.7 Hz), 178.7 (bt, 1C, ² J _{CP} = 10.2 Hz), -19.6 (m, 1C, ² J _{CP} = 5.6 Hz)
[IrRu(CO) ₃ (κ ¹ :κ ¹ -F ₂ C=CCH ₂ CH ₂ CO)-(dppm) ₂][BF ₄] ^f (7)	2031 (s), 1992 (s), 1939 (m), 1705 (m)	21.3 (m, 2P), -9.3 (m, 2P)	4.00 (dm, 2H, ² J _{HH} = 14.5 Hz), 3.17 (dm, 2H, ² J _{HH} = 14.5 Hz), 2.79 (bt, 2H, ³ J _{HH} = 7.6 Hz), 0.91 (bt, 2H, ³ J _{HH} = 7.6 Hz)	274.8 (dt, 1C, ¹ J _{CC} = 24.0 Hz, ² J _{CP} = 7.3 Hz), 212.6 (t, 1C, ² J _{CP} = 11.1 Hz), 186.8 (t, 1C, ² J _{CP} = 14.0 Hz), 176.7 (t, 1C, ² J _{CP} = 6.6 Hz), 44.7 (dt, ² J _{CC} = 24.0 Hz, ³ J _{CP} = 5.0 Hz)
[IrRu(CO) ₃ (κ ¹ -C(CH ₂ CH ₃)=C(CH ₃) ₂)(μ-κ ¹ :η ² -C≡CC(CH ₃)=CH ₂)(dppm) ₂][BF ₄] ^f (8)	2001 (s), 1977 (s), 1928 (m)	18.9 (m, 2P), -18.8 (m, 2P)	4.49 (bs, 1H), 4.35 (dm, 2H, ² J _{HH} = 13.8 Hz), 4.10 (bs, 1H), 3.34 (dm, 2H, ² J _{HH} = 13.8 Hz), 2.41 (q, 2H, ³ J _{HH} = 7.2 Hz), 1.96 (bs, 3H), 1.22 (bs, 3H), 0.90 (bs, 3H), 0.60 (t, 3H, ³ J _{HH} = 7.2 Hz)	207.8 (t, 1C, ² J _{CP} = 10.7 Hz), 199.4 (t, 1C, ² J _{CP} = 15.0 Hz), 182.0 (t, 1C, ² J _{CP} = 11.5 Hz), 13.4 (b, 1C)

Table 2-5. Spectroscopic Data for the Compounds (Continued)

Compound	NMR ^a		
	IR (cm ⁻¹) ^b	$\delta(^3\text{P}\{^1\text{H}\})^c$	$\delta(^{13}\text{C}\{^1\text{H}\})^{d,e}$
[IrRu(CO) ₃ (κ^1 -C(CH ₂ CH ₃)=C(CH ₃) ₂)(μ - κ^1 : η^2 -C≡CCH(CH ₃) ₂)(dppm) ₂][BF ₄] (9)	n/a	18.7 (m, 2P), -19.3 (m, 2P)	208.6 (t, 1C, ² J _{CP} = 11.1 Hz), 200.4 (t, 1C, ² J _{CP} = 14.4 Hz), 188.7 (t, 1C, ² J _{CP} = 11.3 Hz), 12.8 (b, 1C)
[IrRu(CO) ₃ (κ^1 -C(CH ₂ CH ₃)=C(CH ₃) ₂)(μ - κ^1 : η^2 -C≡CCH ₃)(dppm) ₂][BF ₄] (10), 1962 (s), 1938 (s), 1892 (m)	21.8 (m, 2P), -18.4 (m, 2P)	4.47 (dm, 2H, ² J _{HH} = 13.4 Hz), 3.43 (dm, 2H, ² J _{HH} = 13.4 Hz), 2.51 (q, 2H, ² J _{HH} = 7.3 Hz), 1.93 (t, 3H, ³ J _{HP} = 2.0 Hz), 0.92 (s, 3H), 0.83 (s, 3H), 0.72 (t, 3H, ² J _{HH} = 7.3 Hz)	208.1 (t, 1C, ² J _{CP} = 11.4 Hz), 198.9 (t, 1C, ² J _{CP} = 14.7 Hz), 181.8 (t, 1C, ² J _{CP} = 11.5 Hz), 12.9 (b, 1C)
[IrRu(CO) ₃ (κ^1 -C(CH ₂ CH ₃)=C(CH ₃) ₂)(μ - κ^1 : η^2 -C≡CCH ₂ CH ₃)(dppm) ₂][BF ₄] (11), n/a	21.4 (m, 2P), -19.6 (m, 2P)	4.51 (dm, 2H, ² J _{HH} = 13.3 Hz), 3.41 (dm, 2H, ² J _{HH} = 13.3 Hz), 2.57 (q, 2H, ³ J _{HH} = 7.3 Hz), 2.02 (qt, 2H, ⁵ J _{HP} = 2.9 Hz, ³ J _{HH} = 7.2 Hz), 1.16 (t, 3H, ³ J _{HH} = 7.2 Hz), 0.96 (bs, 3H), 0.79 (bs, 3H), 0.58 (t, 3H, ³ J _{HH} = 7.3 Hz)	207.8 (t, 1C, ² J _{CP} = 11.1 Hz), 199.0 (t, 1C, ² J _{CP} = 14.8 Hz), 181.5 (t, 1C, ² J _{CP} = 11.0 Hz), 13.8 (b, 1C)

Table 2-5. Spectroscopic Data for the Compounds (Continued)

Compound	IR (cm ⁻¹) ^b	NMR ^a		
		$\delta(^{31}\text{P}\{^1\text{H}\})^c$	$\delta(^1\text{H})^{d,e}$	$\delta(^{13}\text{C}\{^1\text{H}\})^{d,e}$
[IrRu(CO) ₃ (κ^1 -C(CH ₂ CH ₃)=C(CH ₃) ₂)(μ - κ^1 : η^2 -C≡CCH=CH ₂)(dppm) ₂][BF ₄] (12).	n/a	21.8 (m, 2P), -18.4 (m, 2P)	7.06 (d, 1H, ³ J _{HH} = 8.2 Hz), 6.98 (d, 1H, ³ J _{HH} = 15.8 Hz), 6.31 (dd, 1H, ³ J _{HH} = 15.8 Hz, ³ J _{HH} = 8.2 Hz), 4.46 (dm, 2H, ² J _{HH} = 13.3 Hz), 4.10 (bs, 1H), 3.42 (dm, 2H, ² J _{HH} = 13.3 Hz), 2.49 (q, 2H, ³ J _{HH} = 7.2 Hz), 0.92 (bs, 3H), 0.83 (bs, 3H), 0.73 (t, 3H, ³ J _{HH} = 7.2 Hz)	208.1 (t, 1C, ² J _{CP} = 11.4 Hz), 198.9 (t, 1C, ² J _{CP} = 13.3 Hz), 181.8 (t, 1C, ² J _{CP} = 11.6 Hz), 12.9 (b, 1C)

^a NMR abbreviations: s = singlet, d = doublet, t = triplet, q = quartet, m = multiplet, b = broad, sept = septet. NMR data at 27 °C in CD₂Cl₂ unless otherwise indicated. ^b IR abbreviations for ν_{CO} (cm⁻¹): s = strong, m = medium, sh = shoulder. Dichloromethane solution. ^c ³¹P chemical shifts referenced to external 85% H₃PO₄. ^d ¹H and ¹³C chemical shifts referenced to TMS. ^e Chemical shifts for the phenyl hydrogens and carbons not given. NMR data at 27 °C in CD₃CN.

1 min at a rate of approximately 0.1 mL/s and the solution was left to stir under a methylallene atmosphere for 24 h at ambient temperature. Upon stirring, the solution darkened slightly to orange. After 24 h, the solvent volume was reduced to 5 mL and the addition of 30 mL of diethyl ether precipitated a yellow solid that was washed with 2 x 5 mL of diethyl ether and dried in vacuo (94 % yield). HRMS: m/z calcd for $C_{58}H_{52}IrO_3P_4Ru$ ($M^+ - CO$), 1215.1493; found, 1215.1534 ($M^+ - CO$). Anal. Calcd for $BC_{59}F_4H_{52}IrO_4P_4Ru$: C, 53.32; H, 3.94. Found: C, 53.46; H, 3.87.

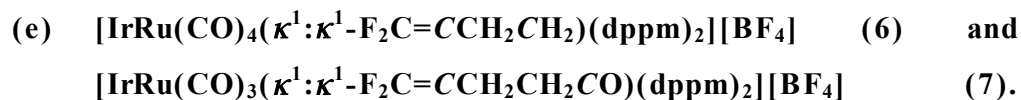
(c) **$[IrRu(CO)_3(NCCH_3)(\kappa^1:\kappa^1-Me_2C=CCH_2CH_2)(dppm)_2][BF_4]$ (4).**

Method iCompound **2** (50 mg, 0.037 mmol) was dissolved in 0.6 mL of CD_3CN in an NMR tube to afford an orange/yellow solution. To the NMR tube was added trimethylamine *N*-oxide (2.8 mg, 0.037 mmol) dissolved in 0.2 mL of CD_3CN , and the solution darkened. Compound **4** was identified as the only phosphorus-containing product by $^{31}P\{^1H\}$ spectroscopy. This product was not stable unless in the presence of CH_3CN or CD_3CN , and therefore, in order to obtain suitable 1H NMR data the reaction was carried out in CD_3CN ; as such, no 1H NMR resonance is reported for the coordinated solvent molecule. Compound **4** was characterized by NMR spectroscopy and X-ray crystallography. Although after many attempts a single crystal was grown suitable for X-ray analysis, solid samples, suitable for elemental analysis could not be obtained.

(d) **$[IrRu(CO)_3(NCCH_3)(\kappa^1:\kappa^1-MeCH=CCH_2CH_2)(dppm)_2][BF_4]$ (5).**

Compound **3** (50 mg, 0.038 mmol) was dissolved in 0.6 mL of CD_3CN in an NMR tube to afford an orange/yellow solution. To the NMR tube was added trimethylamine *N*-oxide (2.8 mg, 0.038 mmol) dissolved in 0.2 mL of CD_3CN , and the solution darkened. Compound **5** was identified as the only phosphorus-containing product by $^{31}P\{^1H\}$ NMR spectroscopy. This product was not stable unless in the presence of CH_3CN or CD_3CN , and therefore, in order to obtain suitable 1H NMR data the reaction was carried out in CD_3CN ; as such, no 1H NMR resonance is

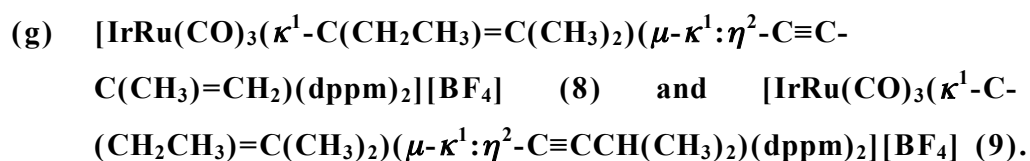
reported for the coordinated solvent molecule. Compound **5** was characterized by NMR spectroscopy and X-ray crystallography. Although a single crystal was grown suitable for X-ray analysis, solid samples, suitable for elemental analysis could not be obtained.



Compound **1** (50 mg, 0.039 mmol) was dissolved in 0.7 mL of CD_2Cl_2 in an NMR tube fitted with a J. Young valve. The solution was cooled to $-78\text{ }^\circ\text{C}$ and the headspace was evacuated and replaced with 1,1-difluoroallene, generated as described above. The NMR tube was warmed over 30 min to ambient temperature and left to react for 24 h after which time compounds **1**, **6**, and **7** were all present in the $^{31}\text{P}\{^1\text{H}\}$ NMR spectrum in a 2:2:1 ratio. Compound **6** could not be isolated from **1** and **7** at any point during the reaction; however, heating the reaction at $35\text{ }^\circ\text{C}$ for another 24 h, or leaving the reaction at ambient temperature for 36 h, resulted in complete conversion to **7**. The addition of 15 mL of diethyl ether and 5 mL of pentane precipitated a yellow-orange solid that was washed with 2 x 5 mL of diethyl ether and was dried in vacuo (80 % yield). HRMS: m/z calcd for **7**: $\text{C}_{58}\text{H}_{48}\text{F}_2\text{IrO}_4\text{P}_4\text{Ru}$ (M^+), 1265.1143; found, 1265.1138 (M^+). Anal. Calcd for $\text{BC}_{58}\text{F}_6\text{H}_{48}\text{IrO}_4\text{P}_4\text{Ru}$: C, 51.56; H, 3.58. Found: C, 51.47; H, 3.80. ^{19}F NMR for **6** (CD_2Cl_2): δ -80.6 (bd, 1F, $^2J_{\text{FF}} = 84.2$ Hz), δ -94.4 (bd, 1F, $^2J_{\text{FF}} = 84.2$ Hz); for **7** (CD_2Cl_2): δ -78.7 (bd, 1F, $^2J_{\text{FF}} = 70.8$ Hz), δ -79.3 (bd, 1F, $^2J_{\text{FF}} = 70.8$ Hz).

(f) **Reaction of 1 with allene.** Under an argon atmosphere, allene was passed through a stirring yellow/orange solution of **1** (40 mg, 0.031 mmol) in 5 mL of CH_2Cl_2 for 1 min at a rate of approximately 0.1 mL/s and the solution was left to stir under an allene atmosphere for 24 h at ambient temperature. Upon stirring, the solution darkened slightly to orange. After 24 h, the gases present in the headspace of the flask were condensed into an NMR tube containing CD_2Cl_2 at $-78\text{ }^\circ\text{C}$ and the ^1H NMR spectrum

determined the presence of 1,3-butadiene. ^1H NMR data for 1,3-butadiene (in CD_2Cl_2): δ 6.27 (dd, 2H, $^3J_{\text{HHtrans}} = 16.6$ Hz, $^3J_{\text{HHcis}} = 9.8$ Hz), δ 5.03 (dd, 2H, $^3J_{\text{HHtrans}} = 16.6$ Hz, $^2J_{\text{HHgem}} = 1.8$ Hz), δ 4.84 (dd, 2H, $^3J_{\text{HHcis}} = 9.8$ Hz, $^2J_{\text{HHgem}} = 1.8$ Hz). The solvent volume of the orange solution was then reduced to 2 mL and the addition of 30 mL of diethyl ether precipitated a yellow solid that was washed with 2 x 5 mL of diethyl ether and dried in vacuo (28 % yield). The solid product was identified as the known species, $[\text{IrRu}(\text{CO})_4(\text{dppm})_2][\text{BF}_4]$ by NMR.⁷ⁱ



Method (i). Compound **2** (50 mg, 0.037 mmol) was dissolved in 10 mL of CH_2Cl_2 affording an orange solution. To this stirred solution was added freshly distilled 1,1-dimethylallene by micro-syringe (50 equiv, 1.9 mmol, 182 μL), and the stirring was continued under an argon atmosphere at ambient temperature for 16 h, during which time the solution turned darker orange. The solution volume was reduced to 5 mL and the yellow/orange solid was precipitated by the addition of 30 mL of diethyl ether and 15 mL of pentane and washed with 3 x 5 mL of diethyl ether. The $^{31}\text{P}\{^1\text{H}\}$ NMR spectrum of the isolated product revealed a 3:1 mixture of phosphorus-containing products **8** and **9**, respectively. **Method (ii).** Compound **1** (50 mg, 0.039 mmol) was dissolved in 20 mL of CH_2Cl_2 , affording a yellow/orange solution. To this stirred solution was added freshly distilled 1,1-dimethylallene (100 equiv, 3.9 mmol, 382 μL) via syringe. This solution was left to stir for 24 h under an argon atmosphere at ambient temperature, during which time the solution darkened to deep orange. After 24 h, the solution volume was reduced to 5 mL and the addition of 30 mL of diethyl ether and 20 mL of pentane precipitated a yellow/orange solid that was washed with 3 x 5 mL of diethyl ether and was dried in vacuo (*ca.* 85 % yield). The $^{31}\text{P}\{^1\text{H}\}$ NMR spectrum of the isolated

product revealed the same 3:1 ratio of **8** and **9**, noted above. HRMS: *m/z* calcd for **8**: C₆₄H₆₀IrO₃P₄Ru (M⁺), 1295.2160; found, 1295.2196 (M⁺). Due to the isotope pattern overlap in the HRMS, only compound **8** could be identified. Elemental analysis was performed only on compound **8** as sufficient quantities of only this compound could be separated by crystallization from the mixture of **8** and **9** from CH₂Cl₂/Et₂O. Anal. Calcd for BC₆₄F₄H₆₀IrO₃P₄Ru: C, 55.66; H, 4.37. Found: C, 55.53; H, 4.38. Compound **9** was characterized by NMR spectroscopy.

- (h) [IrRu(CO)₃(κ¹-C(CH₂CH₃)=C(CH₃)₂)(μ-κ¹:η²-C≡CCH₃)-(dppm)₂][BF₄] (**10**). Under an argon atmosphere, allene was passed through a stirring yellow/orange solution of **2** (40 mg, 0.030 mmol) in 5 mL of CH₂Cl₂ for 1 min at a rate of approximately 0.1 mL/s and the solution was left to stir under an allene atmosphere for 24 h at ambient temperature. Upon stirring, the solution darkened to orange. After 24 h, the solvent volume was reduced to 2 mL and the addition of 30 mL of diethyl ether precipitated a yellow solid that was washed with 2 x 5 mL of diethyl ether and dried in vacuo (90 % yield). HRMS: *m/z* calcd for **10**: C₆₂H₅₈IrO₃P₄Ru (M⁺), 1269.2004; found, 1269.2005 (M⁺). Anal. Calcd for BC₆₄Cl₄F₄H₆₂IrO₃P₄Ru (**10**•2CH₂Cl₂): C, 50.41; H, 4.10. Found: C, 50.79; H, 4.08. The incorporation of 2 equiv of CH₂Cl₂ was supported by the X-ray crystal structure analysis.
- (i) [IrRu(CO)₃(κ¹-C(CH₂CH₃)=C(CH₃)₂)(μ-κ¹:η²-C≡CCH₂CH₃)-(dppm)₂][BF₄] (**11**) and [IrRu(CO)₃(κ¹-C(CH₂CH₃)=C(CH₃)₂)-(μ-κ¹:η²-C≡CCH=CH₂)(dppm)₂][BF₄] (**12**). Under an argon atmosphere, methylallene was passed through a stirred yellow/orange solution of **2** (50 mg, 0.037 mmol) in 10 mL of CH₂Cl₂ for 1 min at a rate of approximately 0.1 mL/s and the solution was left to stir under a methylallene atmosphere for 24 h at ambient temperature. Upon stirring, the solution darkened slightly to orange. After 24 h, the solvent volume was reduced to 5 mL and the addition of 30 mL of diethyl ether and 30 mL

of pentane precipitated a yellow solid that was washed with 2 x 5 mL of diethyl ether and dried in vacuo (*ca.* 87 % yield). The $^{31}\text{P}\{^1\text{H}\}$ NMR spectrum of the isolated product revealed the presence of **11** and **12** in a 3:2 ratio. HRMS: *m/z* calcd for **11**: $\text{C}_{63}\text{H}_{60}\text{IrO}_3\text{P}_4\text{Ru}$ (M^+), 1293.2160; found, 1283.2159 (M^+). Due to the isotope pattern overlap in the HRMS, only compound **11** could be identified. We were unable to obtain elemental analyses of either **11** or **12**, owing to our failure to separate them in sufficient quantity.

- (j) **Attempted reaction of 2 with 1,1-difluoroallene.** Compound **2** (30 mg, 0.022mmol) was dissolved in 0.7 mL of CD_2Cl_2 in an NMR tube fitted with a J. Young valve to afford a dark orange solution. The solution was cooled to $-78\text{ }^\circ\text{C}$ and the argon headspace was evacuated and replaced with 1,1-difluoroallene (prepared as described above, but using 200 μL of 2-bromo-3,3,3-trifluoro-1-propene and 770 μL of 2.5 M *n*-butyllithium in hexanes). The NMR tube was warmed over 30 min to ambient temperature and then left to react at $35\text{ }^\circ\text{C}$ for 48 h. No new product was observed in the $^{31}\text{P}\{^1\text{H}\}$ NMR spectrum, nor was the concentration of 1,1-difluoroallene decreased (as determined by integration of the ^1H NMR spectrum).

2.4.3 X-ray Structure Determinations

2.4.3.1 General

Crystals were grown via slow diffusion of diethyl ether into an acetonitrile/dichloromethane solution of the compound (**4**, **5**), diffusion of diethyl ether into a dichloromethane solution of the compound (**8-CF₃SO₃**), or diffusion of diethyl ether/pentane into a dichloromethane solution of the compound (**10**). Data were collected using a Bruker SMART 1000 CCD detector/PLATFORM diffractometer with the crystals cooled to $-80\text{ }^\circ\text{C}$ (**4**, **5**, **8-CF₃SO₃**) or with a Bruker APEX-II CCD detector/D8 diffractometer²⁹ with the crystals cooled to $-100\text{ }^\circ\text{C}$ (**10**); all data were collected using Mo $\text{K}\alpha$ radiation ($\lambda = 0.71073\text{ \AA}$). The data were corrected for absorption through Gaussian integration from indexing of

the crystal faces. Structures were solved using direct methods (*SHELXS-97*³⁰) (**4**, **5**, **10**), or Patterson search/structure expansion (*DIRDIF-99*³¹) (**8-CF₃SO₃**). Refinements were completed using the program *SHELXL-97*.³⁰ Hydrogen atoms attached to carbons were assigned positions based on the sp² or sp³ hybridization geometries of their attached carbons, and were given thermal parameters 20 % greater than those of their parent atoms. See Appendix III.1 for a listing of crystallographic experimental data for all structures in this chapter.

2.4.3.2 Special Refinement Conditions

(i) Compound **4**: Attempts to refine peaks of residual electron density as diethyl ether oxygen or carbon atoms were unsuccessful. The data were corrected for disordered electron density through use of the *SQUEEZE* procedure³² as implemented in *PLATON*.³³ A total solvent-accessible void volume of 513 Å³ with a total electron count of 103 (consistent with two molecules of solvent diethyl ether) was found in the unit cell. The B–F and F···F distances within the disordered tetrafluoroborate ion were restrained to be 1.35(1) and 2.20(1) Å, respectively. The Ir-bound metallacycle and the adjacent carbonyl group were disordered over two positions in a 3:1 ratio as shown in Figure 2-10. There was

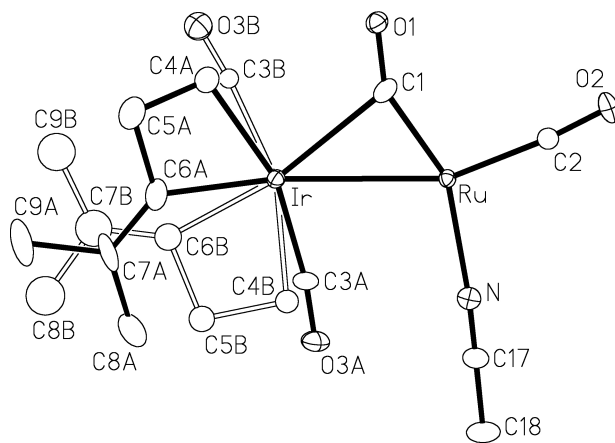


Figure 2-10. View of the complex cation of $[\text{IrRu}(\text{CO})_3(\text{NCCH}_3)(\kappa^2\text{-Me}_2\text{C}=\text{CCH}_2\text{CH}_2)(\text{dppm})_2][\text{BF}_4]$ (**4**) with the *dppm* ligands and hydrogens removed, showing both the major (solid bonds) and minor (hollow bonds) contributions involving the disordered carbonyl and 2-methylpent-2-ene-3,5-diyl groups.

also an accompanying disorder of the dppm phenyl rings. The geometry about carbon C7B in the minor part of the disordered 2-methylpent-2-ene-3,5-diyl fragment had the following distance restraints imposed during refinement: C7B–C8B and C7B–C9B, 1.50(1) Å; C8B···C9B, 2.60(1) Å; C6B–C8B and C6B–C9B, 2.45(1) Å.

(ii) Compound **5**: Attempts to refine peaks of residual electron density as solvent diethyl ether oxygen or carbon atoms were unsuccessful. The data were corrected for disordered electron density through use of the *SQUEEZE* procedure³² as implemented in *PLATON*.³³ A total solvent-accessible void volume of 538.4 Å³ with a total electron count of 105 (consistent with two molecules of solvent diethyl ether) was found in the unit cell. The Ir-bound metallacycle and the adjacent carbonyl group were disordered over two positions in a 3:2 ratio as shown in Figure 2-11, very similar to the disorder observed in **10**.

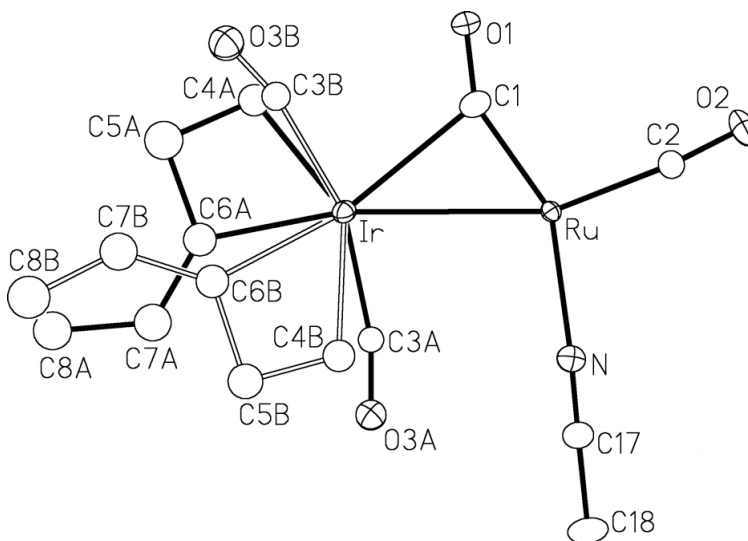


Figure 2-11. *View of the complex cation of [IrRu(CO)₃(NCCH₃)(κ²-MeCH=CCH₂CH₂)(dppm)₂][BF₄] (**5**) with the dppm ligands and hydrogens removed, showing both the major (solid bonds) and minor (hollow bonds) contributions involving the disordered carbonyl and pent-2-ene-3,5-diyl groups.*

2.5 References

1. (a) Maas, G. *Chem. Soc. Rev.* **2004**, *33*, 183. (b) Kirmse, W. *Angew. Chem. Int. Ed. Engl.* **2003**, *42*, 1088. (c) Brookhart, M.; Studabaker, W. B. *Chem. Rev.* **1987**, *87*, 411. (d) Basato, M.; Tubaro, C.; Biffis, A.; Bonato, M.; Buscemi, G.; Lighezzolo, F.; Lunardi, P.; Vianini, C.; Benetollo, F.; Del Zotto, A. *Chem. Eur. J.* **2009**, *15*, 1516.
2. (a) Ivin, K. J. *Olefin Metathesis*; Academic Press: London, 1983. (b) Grubbs, R. H.; Tumas, W. *Science* **1989**, *243*, 907. (c) Grubbs, R. H.; Wenzel, A. G.; Chatterjee, A. K. In *Comprehensive Organometallic Chemistry III*; Crabtree, R. H., Mingos, D. M. P., Eds.; Elsevier: 2007; Vol. 11, p 179. (d) Schrock, R. R. *Acc. Chem. Res.* **1990**, *23*, 158. (e) Trnka, T. M.; Grubbs, R. H. *Acc. Chem. Res.* **2001**, *34*, 18. (f) Feldman, J.; Schrock, R. R. *Prog. Inorg. Chem.* **1991**, *39*, 1. (g) Breslow, D. S. *Prog. Polym. Sci.* **1993**, *18*, 1141. (h) Fischmeister, C.; Custarlenas, R.; Bruneau, C.; Dixneuf, P. H. *NATO Science Series II: Math., Phys. Chem.* **2003**, *122*, 23. (i) Fischmeister, C.; Dixneuf, P. H. *NATO Science Series II: Math., Phys. Chem.* **2007**, *243*, 3. (j) Grubbs, R. H. *Tetrahedron* **2004**, *60*, 7117. (k) Schwab, P.; Grubbs, R. H.; Ziller, J. W. *J. Am. Chem. Soc.* **1996**, *118*, 100. (l) Schrock, R. R.; Murdzek, J. S.; Bazan, G. C.; Robbins, J.; DiMare, M.; O'Regan, M. *J. Am. Chem. Soc.* **1990**, *112*, 3875.
3. (a) Schlund, R.; Schrock, R. R.; Crowe, W. E. *J. Am. Chem. Soc.* **1989**, *111*, 8004. (b) Park, L. Y.; Schrock, R. R.; Stieglitz, S. G.; Crowe, W. E. *Macromolecules* **1991**, *24*, 3489. (c) Eisch, J. J.; Aradi, A. A.; Lucarelli, M. A.; Qian, Y. *Tetrahedron* **1998**, *54*, 1169.
4. (a) Gallop, M. A.; Roper, W. R. *Adv. Organomet. Chem.* **1986**, *25*, 121. (b) Werner, H. *Organometallics* **2005**, *24*, 1036. (c) Whittlesey, M. K. *Organomet. Chem.* **2001**, *29*, 350. (d) Bohle, D. S.; Clark, G. R.; Rickard, C. E. F.; Roper, W. R.; Wright, L. J. *J. Organomet. Chem.* **1988**, *358*, 411. (e) King, P. J. *Organomet. Chem.* **2002**, *30*, 282.

5. (a) Knox, S. A. R. *J. Cluster Sci.* **1992**, *3*, 385. (b) Dennett, J. N. L.; Knox, S. A. R.; Charmant, J. P. H.; Gillon, A. L.; Orpen, A. G. *Inorg. Chim. Acta* **2003**, *354*, 29. (c) Busetto, L.; Maitlis, P. M.; Zanotti, V. *Coord. Chem. Rev.* **2010**, *254*, 470. (d) Busetto, L.; Zanotti, V. *J. Organomet. Chem.* **2005**, *690*, 5430. (e) Casey, C. P.; Audett, J. D. *Chem. Rev.* **1986**, *86*, 339. (f) Herrmann, W. A. *Adv. Organomet. Chem* **1982**, *20*, 159. (g) Puddephatt, R. J. *Polyhedron* **1988**, *7*, 767.
6. (a) Fischer, F.; Tropsch, H. *Brennst. Chem.* **1926**, *7*, 97. (b) Fischer, F.; Tropsch, H. *Chem. Ber.* **1926**, *59*, 830. (c) Brady, R. C.; Pettit, R. *J. Am. Chem. Soc.* **1980**, *102*, 6181. (d) Brady, R. C.; Pettit, R. *J. Am. Chem. Soc.* **1981**, *103*, 1287. (e) Biloen, P.; Sachtler, W. M. H. *Adv. Catal.* **1981**, *30*, 165. (f) Maitlis, P. M.; Long, H. C.; Quyoum, R.; Turner, M. L.; Wang, Z.-Q. *Chem. Commun.* **1996**, *1*. (g) Long, H. C.; Turner, M. L.; Fornasiero, P.; Kaspar, J.; Graziani, M.; Maitlis, P. M. *J. Catal.* **1997**, *167*, 172. (h) Dry, M. E. *Appl. Catal. A* **1996**, *138*, 319.
7. (a) Sumner, C. E.; Collier, J. A.; Pettit, R. *Organometallics* **1982**, *1*, 1350. (b) Maitlis, P. M. *J. Organomet. Chem.* **2004**, *689*, 4366. (c) Torkelson, J. R.; McDonald, R.; Cowie, M. *J. Am. Chem. Soc.* **1998**, *120*, 4047. (d) Colborn, R. E.; Davies, D. L.; Dyke, A. F.; Knox, S. A. R.; Mead, K. A.; Orpen, A. G.; Guerschais, J. E.; Roué, J. *J. Chem. Soc., Dalton Trans.* **1989**, 1799. (e) Trepanier, S. J.; Sterenberg, B. T.; McDonald, R.; Cowie, M. *J. Am. Chem. Soc.* **1999**, *121*, 2613. (f) Trepanier, S. J.; Dennett, J. N. L.; Sterenberg, B. T.; McDonald, R.; Cowie, M. *J. Am. Chem. Soc.* **2004**, *126*, 8046. (g) Rowsell, B. D.; Trepanier, S. J.; Lam, R.; McDonald, R.; Cowie, M. *Organometallics* **2002**, *21*, 3228. (h) Rowsell, B. D.; McDonald, R.; Ferguson, M. J.; Cowie, M. *Organometallics* **2003**, *22*, 2944. (i) Dell'Anna, M. M.; Trepanier, S. J.; McDonald, R.; Cowie, M. *Organometallics* **2001**, *20*, 88. (j) Ritleng, V.; Chetcuti, M. J. *Chem. Rev.* **2007**, *107*, 797. (k) Colborn, R. E.; Dyke, A. F.; Knox, S. A. R.; Macpherson, K. A.; Orpen, A. G. *J. Organomet. Chem.* **1982**, *239*, C15.

- (l) Motyl, K. M.; Norton, J. R.; Schauer, C. K.; Anderson, O. P. *J. Am. Chem. Soc.* **1982**, *104*, 7325.
8. Muetterties, E. L.; Rhodin, T. N.; Band, E.; Brucker, C. F.; Pretzer, W. R. *Chem. Rev.* **1979**, *79*, 91.
9. (a) Sun, S.; Fujimoto, K.; Yoneyama, Y.; Tsubaki, N. *Fuel* **2002**, *81*, 1583. (b) Tsubaki, N.; Sun, S.; Fujimoto, K. *J. Catal.* **2001**, *199*, 236. (c) Maunula, T.; Ahola, J.; Salmi, T.; Haario, H.; Härkönen, M.; Luoma, M.; Pohjola, V. *J. Appl. Catal. B* **1997**, *12*, 287. (d) Adesina, A. A. *Appl. Catal. A* **1996**, *138*, 345. (e) Iglesia, E.; Soled, S. L.; Fiato, R. A.; Via, G. H. *J. Catal.* **1993**, *143*, 345.
10. Chokshi, A.; Rowsell, B. D.; Trepanier, S. J.; Ferguson, M. J.; Cowie, M. *Organometallics* **2004**, *23*, 4759.
11. MacDougall, T. J.; Llamazares, A.; Kuhnert, O.; Ferguson, M. J.; McDonald, R.; Cowie, M. *Organometallics* **2011**, *30*, 952.
12. Wigginton, J. R.; Chokshi, A.; Graham, T. W.; McDonald, R.; Ferguson, M. J.; Cowie, M. *Organometallics* **2005**, *24*, 6398.
13. Samant, R. G.; Trepanier, S. J.; Wigginton, J. R.; Xu, L.; Bierenstiel, M.; McDonald, R.; Ferguson, M. J.; Cowie, M. *Organometallics* **2009**, *28*, 3407.
14. (a) Armentrout, P. B. In *Bonding Energetics in Organometallic Compounds*; Marks, T. J., Ed.; American Chemical Society: Washington, DC, 1990, p 18. (b) Ziegler, T.; Tschinke, V. In *Bonding Energetics in Organometallic Compounds*; Marks, T. J., Ed.; American Chemical Society: Washington, DC, 1990, p 279.
15. Cowie, M. *Can. J. Chem.* **2005**, *83*, 1043.
16. Burkhard, O. J.; Eger, W. A.; Anders, E. *J. Org. Chem.* **2008**, *73*, 8265.
17. (a) Slaney, M. E.; Anderson, D. J.; Ferguson, M. J.; McDonald, R.; Cowie, M. *J. Am. Chem. Soc.* **2010**, *132*, 16544. (b) Slaney, M. E.; Anderson, D. J.; Ristic-Petrovic, D.; McDonald, R.; Cowie, M. *Accepted for publication in Chem. Eur. J. Nov. 8, 2011*. (c) Slaney, M. E.; Ferguson, M.

- J.; McDonald, R.; Cowie, M. *Accepted for publication in Organometallics*, January 11, 2012.
18. (a) Johnson, K. A.; Gladfelter, W. L. *Organometallics* **1990**, *9*, 2101. (b) Jeffery, J. C.; Orpen, A. G.; Stone, F. G. A.; Went, M. J. *J. Chem. Soc. Dalton Trans.* **1986**, 173. (c) Gao, Y.; Jennings, M. C.; Puddephatt, R. J. *Organometallics* **2001**, *20*, 1882. (d) Shafiq, F.; Kramarz, K. W.; Eisenberg, R. *Inorg. Chim. Acta* **1993**, *213*, 111. (e) Trepanier, S. J.; McDonald, R.; Cowie, M. *Organometallics* **2003**, *22*, 2638. (f) Rowsell, B. D.; McDonald, R.; Cowie, M. *Organometallics* **2004**, *23*, 3873.
 19. (a) McDermott, J. X.; White, J. F.; Whitesides, G. M. *J. Am. Chem. Soc.* **1973**, *95*, 4451. (b) McDermott, J. X.; White, J. F.; Whitesides, G. M. *J. Am. Chem. Soc.* **1976**, *98*, 6521.
 20. Allen, F. H.; Kennard, O.; Watson, D. G.; Brammer, L.; Orpen, A. G.; Taylor, R. *J. Chem. Soc., Perkin Trans. 2* **1987**, S1.
 21. $r_c(\text{sp}^3) = 0.77 \text{ \AA}$; $r_c(\text{sp}^2) = 0.74 \text{ \AA}$.
 22. Bent, H. A. *Chem. Rev.* **1961**, *61*, 275.
 23. MacDougall, T. J.; Samant, R. G.; Trepanier, S. J.; Ferguson, M. J.; McDonald, R.; Cowie, M. *Accepted to Organometallics*, **2012**.
 24. Ristic-Petrovic, D.; Anderson, D. J.; Torkelson, J. R.; Ferguson, M. J.; McDonald, R.; Cowie, M. *Organometallics* **2005**, *24*, 3711.
 25. Soderquist, J. A.; Anderson, C. L. *Tetrahedron Lett.* **1986**, *27*, 3961.
 26. Rhee, S. W.; Ryan, K. J.; Tracy, M.; Kelson, A. B.; Clizbe, L. A.; Chang, M.-H.; Park, J. S.; Roh, J.-K.; Kong, J.-Y.; Yang, J. G.; Kim, W.-B.; Ok, K.-D. *J. Labelled Compd. Radiopharm.* **1997**, *39*, 773.
 27. Miller, J. S.; Caulton, K. G. *J. Am. Chem. Soc.* **1975**, *97*, 1067.
 28. Drakesmith, F. G.; Stewart, O. J.; Tarrant, P. *J. Org. Chem.* **1968**, *33*, 280.
 29. Programs for diffractometer operation, unit cell indexing, data collection, data reduction and absorption correction were those supplied by Bruker.
 30. Sheldrick, G. M. *Acta Crystallogr.* **2008**, *A64*, 112.
 31. Beurskens, P. T.; Beurskens, G.; de Gelder, R.; Garcia-Granda, S.; Israel, R.; Gould, R. O.; Smits, J. M. M. *The DIRDIF-99 program system*;

Crystallography Laboratory, University of Nijmegen, The Netherlands, 1999.

32. van der Sluis, P.; Spek, A. L. *Acta Crystallogr.* **1990**, *A 46*, 194.
33. Spek, A. L. *Acta Crystallogr.* **1990**, *A 64*, C34. PLATON - a multipurpose crystallographic tool. Utrecht University, Utrecht, The Netherlands.

Chapter 3: Geminal Carbon–Hydrogen Bond Activation in Cumulenes Promoted by Adjacent Iridium/Ruthenium Centres *

3.1 Introduction

The activation of carbon–hydrogen bonds by late transition metal complexes is an important transformation in organometallic chemistry,¹ facilitating the selective conversion of inexpensive but relatively unreactive hydrocarbon feedstocks into value-added compounds. The target substrates for C–H bond activation are often alkanes, the major constituents of petroleum and natural gas, owing to the challenges presented by these inert molecules, for which there are few practical ways for their direct conversion into more useful products.^{1b} The activation of vinylic C–H bonds has also attracted considerable attention for the development of stoichiometric carbon–carbon bond forming reactions.^{1d,2} Alkenes are among the most abundant and commonly used organic feedstocks in industrial processes and have uses in carbon–carbon bond formation reactions by direct coupling of olefins with other unsaturated ligands and even alkyl groups, which often requires facile C–H bond activation of vinylic C–H bonds.^{1d,2a,2h,2j,3}

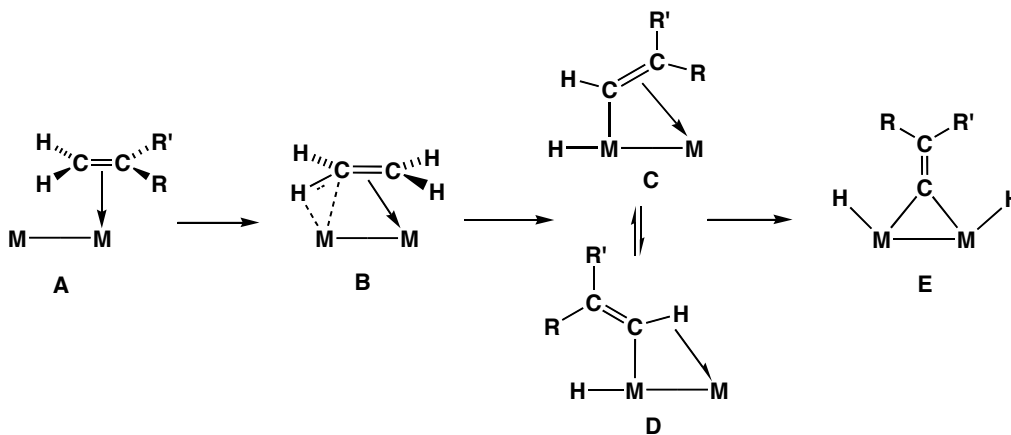
The activation of a single C–H bond in a range of organic substrates is a much studied transformation involving monometallic complexes.¹⁻² To achieve this single activation the generation of a highly reactive, coordinatively unsaturated species capable of performing the activation is often necessary. These species are often generated by ligand loss through photolysis,^{2b,c,2j,4} thermolysis,^{2a,2j,4b,5} or by hydrogen removal from a polyhydride precursor using sacrificial hydrogen acceptors.⁶ The simultaneous activation of two or more C–H bonds is a much less studied process,^{2e,6b,7} and, not surprisingly, presents a more challenging goal, particularly at a single metal centre.

* A version of this chapter has been accepted to *Organometallics* for publication. MacDougall, T. J.; Samant, R. G.; Trepanier, S. J.; Ferguson, M. J.; McDonald, R.; and Cowie, M. Manuscript ID: om-2011-01201h.

One strategy for the simultaneous activation of multiple C–H bonds involves the use of binuclear complexes having a pair of adjacent metals, which allows the oxidation of both metals by the substrate and can provide the necessary coordination sites for substrate activation. One transformation that is relatively rare, even in bimetallic complexes, is the activation of two C–H bonds on the same carbon atom. In the reported cases, most involve alkyl C–H bonds of non-innocent ancillary ligands or involve substrates that have a heteroatom capable of coordination before activation occurs.⁸ There are very few reports of the geminal C–H bond activation of hydrocarbon substrates such as α -olefins that do not contain heteroatoms.^{2e,6b,7} Of the few reports of activation of a pair of geminal C–H bonds in olefins, only one has been reported at a single metal.^{7a}

Although the reactivity of multimetal systems is fundamentally no different than that involving single metal centres, the availability of adjacent metals can offer pathways not available to monometallic systems. So although it has been shown that olefin C–H bond activation does not require prior π coordination,^{2c,9} one can envision that in binuclear complexes prior π coordination at one metal can orient the olefin favourably for subsequent C–H activation by the adjacent metal (structures **A** and **B**, Chart 3-1).^{6a} Following the first C–H activation by one metal, one can envision participation of the adjacent metal in the second C–H activation process through an intermediate such as **D**, leading to the vinylidene dihydride product (**E**).

Chart 3-1



Previous studies from our group have demonstrated the geminal C–H bond activation of butadiene by the cationic diiridium complex, $[\text{Ir}_2(\text{CH}_3)(\text{CO})_2(\text{dppm})_2][\text{CF}_3\text{SO}_3]$.^{2e} The observation, at low-temperature, of a butadiene adduct in which this diolefin binds through each olefinic group to a different metal centre, combined with the lack of reactivity with 2-methyl-1,3-butadiene or either cis- or trans-1,3-pentadiene, in which substitution at one olefinic bond presumably inhibits binding of that unit, suggested the involvement of both metals in the activation process. Additional support for this proposal came from the attempted activation of ethylene with this complex, for which only a π -adduct was observed.¹⁰ Although the same diiridium species also reacts readily with cumulenes, demonstrating a number of binding modes for these groups (including bridging modes), C–H bond activation of these substrates was not observed.¹¹

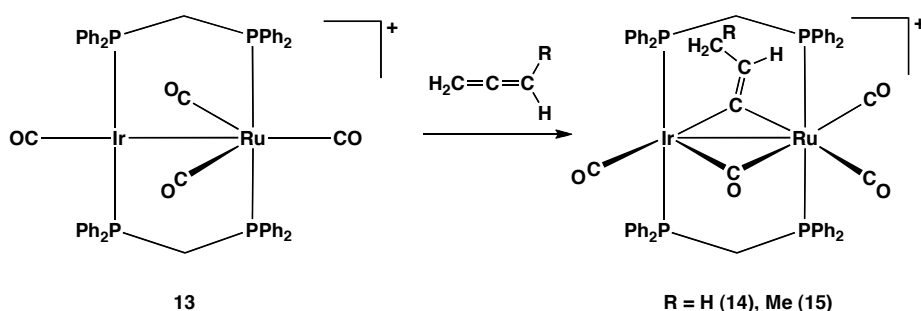
Multiple C–H bond activations involving a series of cumulenes have been observed in reactions with $[\text{IrRu}(\text{CO})_4(\mu\text{-CH}_2)(\text{dppm})_2]^+$,¹² as discussed in Chapter 2. However, two equivalents of cumulene were required; while the first equivalent inserted into the Ir–CH₂ bond to give a metallacycle, C–H bond activation occurred only with the second equivalent. Furthermore, two activation modes involving the cumulenes were observed; both modes involved activation of a pair of geminal C–H bonds, while for methyl-substituted cumulenes (1,2-butadiene and 1,1-dimethylallene) the activation of a methyl C–H bond was also observed. In order to obtain a better understanding of the roles of the different metals in these facile multiple C–H activation processes we have extended this study to include $[\text{IrRu}(\text{CO})_4(\text{dppm})_2]^+$ (**13**), anticipating that in the absence of the bridging CH₂ group involved in allene insertion in the previous study,¹² C–H bond activation might occur upon addition of only one equivalent of the allene. In addition, in this report we also extend the range of α -olefins investigated to include a few monoolefins and conjugated dienes.

3.2 Results and Compound Characterization

3.2.1 Activation of Propadiene and 1,2-Butadiene

The tetracarbonyl precursor, $[\text{IrRu}(\text{CO})_4(\text{dppm})_2][\text{BF}_4]$ (**13**), reacts with propadiene (allene) and 1,2-butadiene (methylallene) at ambient temperature to generate the alkylvinylidene-bridged products, $[\text{IrRu}(\text{CO})_4(\mu\text{-C}=\text{C}(\text{H})\text{R})(\text{dppm})_2][\text{BF}_4]$ ($\text{R} = \text{CH}_3$ (**14**); C_2H_5 (**15**)), respectively, within 24 h (Scheme 4-1). Both products have resulted from the activation of a pair of

Scheme 3-1



geminal, olefinic C–H bonds, accompanied by migration of one hydrogen to each of the β - and γ -carbons of the cumulene. Complex **14** can also be formed by the more conventional route involving the addition of propyne to a solution of **13**, requiring 8 h at ambient temperature. Presumably **15** can be generated analogously by reaction of **13** with 1-butyne, although this reaction was not attempted.

Complexes **14** and **15** display the expected two resonances in the $^{31}\text{P}\{^1\text{H}\}$ NMR spectrum (at approximately δ 29 and δ -1), consistent with the chemical inequivalence of both ends of the diphosphines. Although identification of these resonances is somewhat equivocal, with neither metal showing coupling to the ^{31}P nuclei, we assign them on the basis that the Ir-bound diphosphine ends are observed at higher field than those bound to Ru, as is often the case.¹²⁻¹³ Furthermore, this assignment is consistent with the $^{13}\text{C}\{^1\text{H}\}$ NMR spectrum, with accompanying selective ^{31}P decoupling which establishes that the pair of ^{13}C resonances at *ca.* δ 195 and δ 193 in both compounds, correspond to terminal

carbonyls that couple to the Ru-bound ^{31}P nuclei, while the carbonyl at *ca.* δ 182 is coupled to the Ir-bound ^{31}P nuclei. The bridging carbonyl, at *ca.* δ 209, displays coupling to both sets of ^{31}P nuclei, and in ^{13}CO -enriched samples, couples to the Ru-bound carbonyl at *ca.* δ 193 with mutual two-bond coupling of approximately 25 Hz, typical of a trans arrangement. The above assignment places the additional carbonyl on Ru, as established by the X-ray structure determination (*vide infra*).

In the ^1H NMR spectra of **14** and **15**, two signals represent the chemically inequivalent CH_2 protons of the dppm ligands (**14**: δ 4.01, δ 3.04, **15**: δ 4.19, δ 3.12), indicating the absence of “front-back” symmetry about the IrRuP_4 plane, consistent with the vinylidene group lying on one side of this plane. The protons of the newly formed methyl group of **14** appear at δ 0.78 as a doublet of triplets of triplets, coupling to the vinylic proton (6.4 Hz), while also displaying long-range coupling to both sets of ^{31}P nuclei (*ca.* 2 Hz). In compound **15** the ethyl moiety displays ^1H resonances at δ 1.06 and δ 0.36, having mutual three-bond coupling of 7.5 Hz. As expected, the vinylidene proton of **14** and **15** resonates downfield near δ 7, coupling to both sets ^{31}P nuclei (*ca.* 1.3 Hz) as well as to other protons of the vinylidene fragment.

An X-ray structure determination of **14-CF₃SO₃**, in which the tetrafluoroborate anion has been exchanged by a triflate anion, confirms the proposed connectivity, the complex cation of which is shown in Figure 3-1. Selected bond lengths and angles for **14-CF₃SO₃** appear in Table 3-1. As is usually the case, the dppm ligands bridge both metals in a mutually trans arrangement. Although the Ir–Ru separation of 2.9282(5) Å is longer than expected for a bond between these metals, it is somewhat shorter than the intraligand P–P separations of *ca.* 3.05, consistent with a mutual attraction of the metals. The Ir–C(5)–Ru angle of 88.4(2)° is acute for an sp^2 carbon (again suggesting the presence of a metal–metal bond), resulting in larger than expected Ir–C(5)–C(6) and Ru–C(5)–C(6) angles (141.4(4)° and 130.2(4)°, respectively). The asymmetry in these angles appears to result from repulsion of the methyl

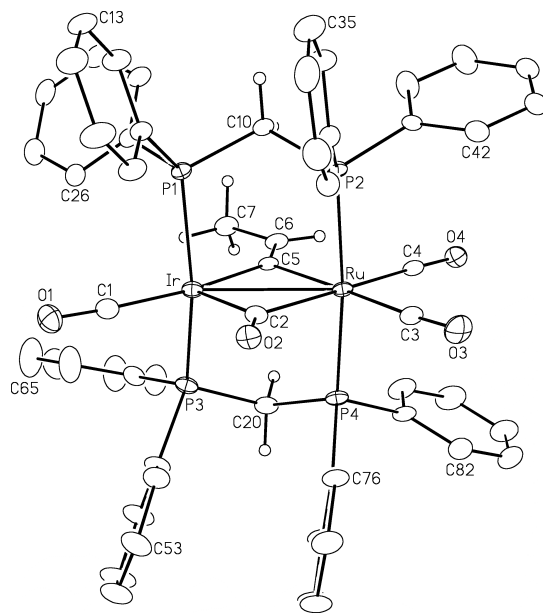


Figure 3-1. Perspective view of the complex cation of $[\text{IrRu}(\text{CO})_4(\mu\text{-C}=\text{C}(\text{H})\text{CH}_3)(\text{dppm})_2][\text{CF}_3\text{SO}_3]$ (**14-CF₃SO₃**). Thermal ellipsoids are shown at the 20 % probability level except for hydrogens, which are shown artificially small.

Table 3-1. Selected Bond Lengths and Angles for Compound 14-CF₃SO₃

(a) Distance (Å)

atom 1	atom 2	distance	atom 1	atom 2	distance
Ir	Ru	2.9282(5)	Ru	C(4)	1.907(5)
Ir	C(1)	1.886(6)	Ru	C(5)	2.141(5)
Ir	C(2)	1.998(5)	C(1)	O(1)	1.156(6)
Ir	C(5)	2.060(5)	C(4)	O(4)	1.143(6)
Ru	C(2)	2.178(5)	C(5)	C(6)	1.337(6)
Ru	C(3)	1.947(5)	C(6)	C(7)	1.471(7)

(b) Angles (deg)

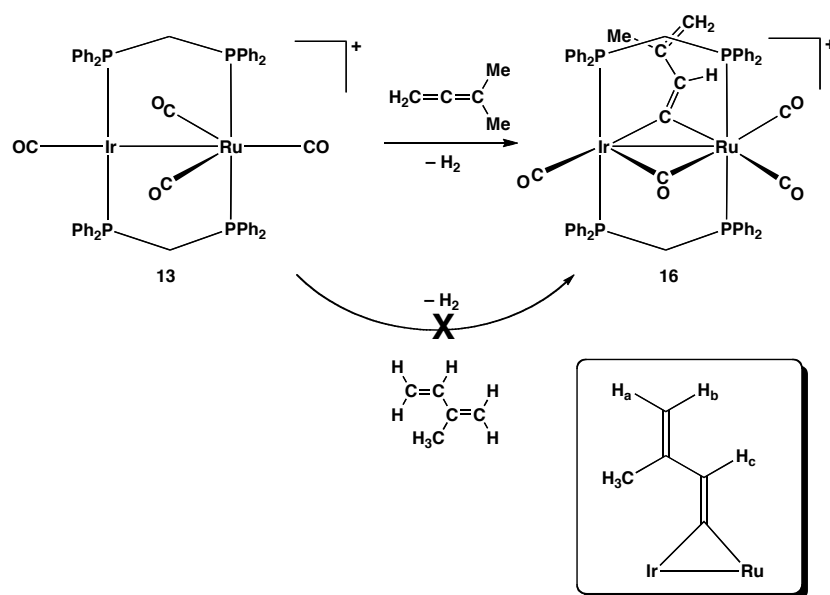
atom	atom 2	atom 3	angle	atom 1	atom 2	atom 3	angle
Ir	C(2)	O(2)	134.4(4)	Ir	C(5)	Ru	88.4(2)
Ir	C(2)	Ru	88.9(2)	Ru	C(5)	C(6)	130.2(4)
Ru	C(2)	O(2)	136.6(4)	C(5)	C(6)	C(7)	126.6(5)
Ir	C(5)	C(6)	141.4(4)	C(1)	Ir	C(5)	168.8(2)

substituent on the vinylidene ligand with the dppe phenyl groups. Within the vinylidene bridge, the C(5)–C(6) distance of 1.337(6) Å is typical of a double bond,¹⁴ while C(6)–C(7) (1.471(7) Å) is typical of a single bond between sp² and sp³ carbons.¹⁴⁻¹⁵ The C(5)–C(6)–C(7) angle (126.6(5)°) is also typical of sp² hybridization at C(6).

3.2.2 Activation of 1,1-Dimethylallene

Complex **13** also reacts with the disubstituted 1,1-dimethylallene at ambient temperature over 48 h to give [IrRu(CO)₄(μ-C=C(H)C(CH₃)=CH₂)(dppe)₂][BF₄] (**16**), having a bridging 3-methyl-1,3-butadienylidene fragment, as shown in Scheme 3-2. This product has resulted

Scheme 3-2



from the activation of *three* C–H bonds – the two geminal C–H bonds of the cumulene, much as observed in **14** and **15**, and one C–H bond of a methyl group. The longer reaction time compared to the above cumulenes appears to be due to the larger steric bulk of this disubstituted allene. In these C–H bond activations, one hydrogen is transferred to the β-carbon while the other two are lost as H₂.

All spectral parameters for **16**, apart from those of the vinylvinylidene fragment, are closely comparable to those of **14** and **15**. For this bridging hydrocarbyl group, four signals appear in the ^1H NMR spectrum (see Scheme 3-2 (inset) for the proton labelling): two doublets of multiplets at δ 4.74 (H_a) and δ 4.49 (H_b), a broad multiplet at δ 7.91 (H_c), and a multiplet at δ 0.46 (CH_3). A 2D ^1H correlation experiment shows unresolved spin-spin coupling between H_c and the methyl protons, which in turn show coupling to both H_a and H_b . Protons H_a and H_b show mutual two-bond coupling of 2.4 Hz, and NOESY experiments reveal strong NOE's between H_a and H_b , between H_a and the methyl protons, and between H_b and H_c .

An X-ray structure determination of **16-CF₃SO₃**, verifies the above formulation, as shown for the complex cation in Figure 3-2. Selected bond

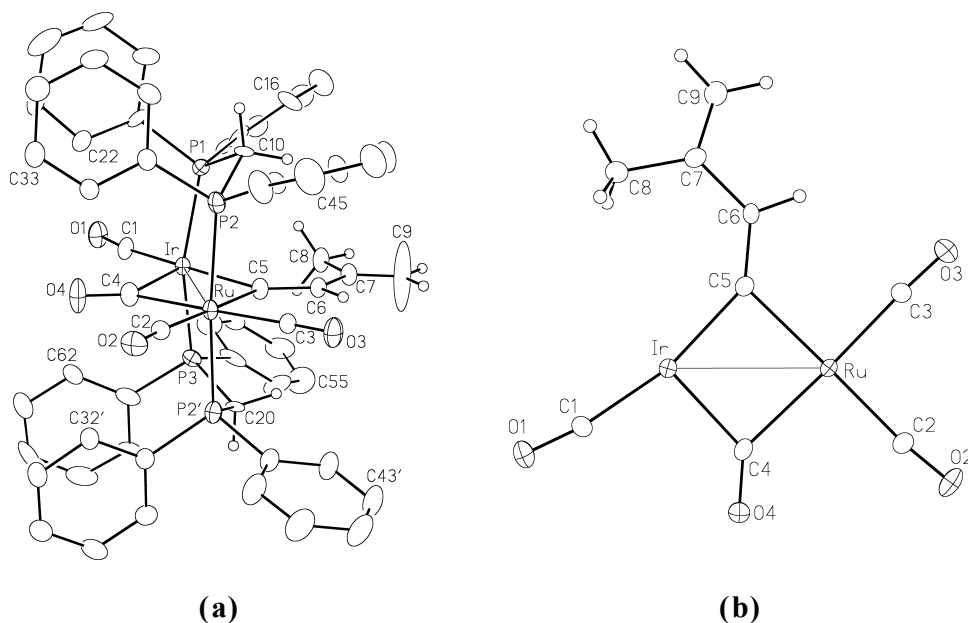


Figure 3-2. (a) Perspective view of the complex cation of $[\text{IrRu}(\text{CO})_4(\mu\text{-C}=\text{C}(\text{H})\text{C}(\text{CH}_3)=\text{CH}_2)(\text{dppm})_2][\text{CF}_3\text{SO}_3]$ (**16-CF₃SO₃**). Thermal ellipsoids are as described in Figure 3-1. Only the ipso carbon atoms of the dppm phenyl groups are shown. (b) Alternate view of the equatorial plane of the complex cation of **16-CF₃SO₃**, in which the dppm ligands above and below the plane of the drawing are omitted for clarity.

lengths and angles for **16-CF₃SO₃** appear in Table 3-2. A crystallographic mirror plane lies in the equatorial plane of the metals, essentially perpendicular to the metal-diphosphine vectors. Although Ru and its bound groups are ordered about this plane, the Ir-side of the complex is disordered on either side of this plane, as shown and described in the Experimental section. The elongated thermal ellipsoid for C(9) appears to disguise a disorder involving this atom. However, a simple disorder of this atom above and below the mirror plane is inconsistent with the well-behaved ellipsoids of the adjacent carbon atoms and may be a consequence of our inability to fully account for the disorder.

Table 3-2. Selected Bond Lengths and Angles for Compound 16-CF₃SO₃

(a) Distance (Å)

atom 1	atom 2	distance	atom 1	atom 2	distance
Ir	Ru	2.9553(6)	Ru	C(4)	2.166(8)
Ir	C(1)	1.88(1)	Ru	C(5)	2.158(7)
Ir	C(4)	2.051(7)	C(5)	C(6)	1.35(1)
Ir	C(5)	2.061(8)	C(6)	C(7)	1.45(1)
Ru	C(2)	1.946(7)	C(7)	C(8)	1.47(1)
Ru	C(3)	1.925(7)	C(7)	C(9)	1.24(2)

(b) Angles (deg)

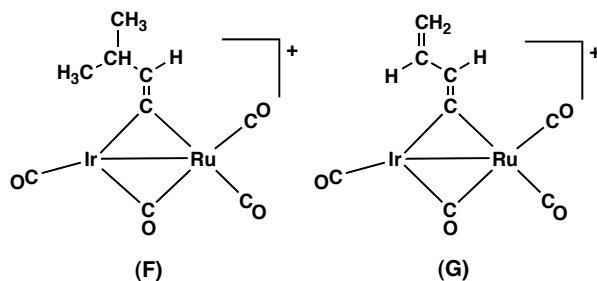
atom	atom 2	atom 3	angle	atom 1	atom	atom 3	angle
Ir	C(4)	Ru	88.9(3)	C(5)	C(6)	C(7)	130.1(7)
Ir	C(5)	C(6)	141.5(5)	C(6)	C(7)	C(8)	124.4(7)
Ir	C(5)	Ru	88.9(3)	C(6)	C(7)	C(9)	117.3(9)
Ru	C(5)	C(6)	129.1(5)	C(8)	C(7)	C(9)	118.3(9)

The geometry of **16** closely resembles that of **14**. Again, the Ir–Ru bond (2.9553(6) Å) is long, although is still shorter than the intraligand P–P separations. Within the vinylidene fragment the C(5)–C(6), and C(7)–C(9) bond lengths are typical of double bonds (1.35(1) Å and 1.24(2) Å, respectively; the latter is anomalously short owing to the disorder).¹⁴ The vinylidene unit is unsymmetrically bound, being more strongly bound to Ir (Ir–C(5) = 2.061(8) Å, Ru–C(5) = 2.158(7) Å), and is also tilted towards Ru (Ir–C(5)–C(6) = 141.5(5)°, Ru–C(5)–C(6) = 129.1(5)°), much as described

for **14**. This tilting presumably minimizes repulsions between the vinylidene methyl substituent and the phenyl rings 1 and 5.

Compound **16** can be viewed as resulting from the geminal activation of both C–H bonds at the unsubstituted end of 2-methyl-1,3-butadiene, with the accompanying loss of H₂; however attempts to generate **16** by reaction of **13** with this substrate does not occur in the presence of 100 equiv of the substrate over several days, even when carried out at slightly elevated temperatures (Scheme 3-2). The sterically less encumbered diene, 1,3-butadiene also does not react with compound **13**, under similar conditions. This is somewhat surprising given the double C–H activation of 1,3-butadiene by the similar compound [Ir₂(CH₃)(CO)₂(dppm)₂][CF₃SO₃]^{2e} but supports our previous proposal that this butadiene activation by the Ir₂ compound required prior coordination of both double bonds – one at each metal. In compound **13** the saturation at Ru and the greater steric crowding at this metal presumably does not allow such a coordination mode.

In a previous study discussed in Chapter 2, involving the related methylene-bridged complex, [IrRu(CO)₄(μ-CH₂)(dppm)₂][BF₄], reaction with 1 equiv of 1,1-dimethylallene proceeded without C–H bond activation to give a metallacyclic product resulting from coupling of the cumulene and the methylene group.¹² However, reaction of this intermediate with either a second equiv of 1,1-dimethylallene or with methylallene resulted in a triple C–H activation of the added cumulene accompanied by H₂ loss, analogous to that described above for **16**. In both of these previous triple C–H bond activations, a second product was also observed that involved activation of the pair of geminal C–H bonds *without* additional activation of the methyl group. In the current study with 1,1-dimethylallene we see no evidence of such a double C–H activation product which would have a structure as shown for **F** (dppm groups omitted), in which

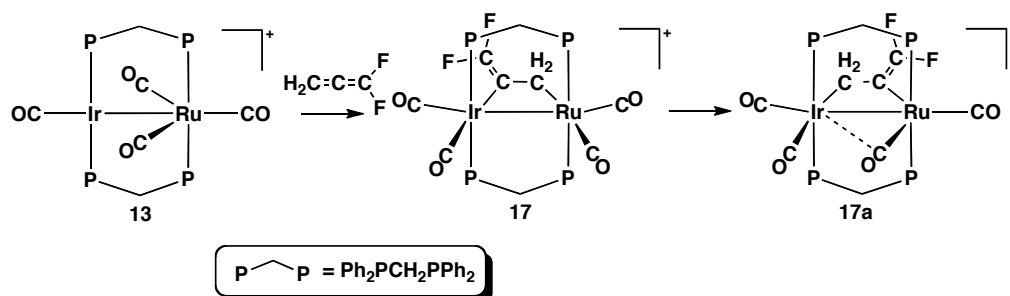


the hydrogens resulting from C–H activation have been transferred to the β - and γ -carbons, exactly as observed in compounds **14** and **15**. In this context it is also surprising that none of the triple C–H activation product was observed in the reaction of **13** with methylallene; such a product would have a structure shown as **G** (dppm groups omitted), fully analogous to **16**.

3.2.3 Reaction with 1,1-Difluoroallene

Compound **13** also reacts immediately with 1,1-difluoroallene at ambient temperature to generate the adduct, $[\text{IrRu}(\text{CO})_4(\mu\text{-}\kappa^1\text{-F}_2\text{C}=\text{C}-\text{CH}_2)(\text{dppm})_2][\text{BF}_4]$ (**17**) which converts to the isomer **17a** over a period of 24 h at ambient temperature (Scheme 3-3). Once all of **17** has been converted to **17a**, this isomer starts to decompose if left in solution at temperatures greater than $-20\text{ }^\circ\text{C}$ for more than 4 h. Attempts to isolate both **17** and **17a** independently at low temperatures failed and only decomposition resulted. For these reasons both **17** and **17a** were characterized by multinuclear NMR spectroscopy ($^{31}\text{P}\{^1\text{H}\}$, ^1H , ^{19}F , $^{13}\text{C}\{^1\text{H}\}$, and $^{13}\text{C}\{^1\text{H}, ^{31}\text{P}\}$) at $-20\text{ }^\circ\text{C}$.

Scheme 3-3



Both **17** and **17a** display very similar $^{31}\text{P}\{^1\text{H}\}$ NMR spectra (**17**: δ 26.6 and δ –18.4, **17a**: δ 25.5 and δ –20.8) and also have very similar ^1H NMR parameters. An important ^1H resonance for the differentiation between the two is the signal for the protons of the 1,1-difluoroallene ligand. For both isomers this resonance appears as a broad triplet, resulting from coupling of these protons to a pair of adjacent ^{31}P nuclei (**17**: $^3J_{\text{HP}} = 6.9\text{ Hz}$, **17a**: $^3J_{\text{HP}} = 9.1\text{ Hz}$). The appearance of a single resonance for both products defines that this allene is bound via the “C=CH₂” end. These isomers differ primarily in the orientation of the allene ligand. Selective decoupling of the Ru-bound

^{31}P nuclei in **17** results in a collapse of the allene CH_2 signal to a broad singlet, indicating that this moiety is adjacent to Ru, whereas the decoupling of the Ir-bound ^{31}P nuclei in **17a** results in a collapse of the CH_2 resonance to a singlet, confirming the opposite allene alignment as shown in Scheme 3-3. Binding of the 1,1-difluoroallene ligand through the “ $\text{C}=\text{CH}_2$ ” end is further supported by the appearance of *two* resonances in the ^{19}F NMR spectrum for both **17** and **17a**, demonstrating their chemical inequivalence as diagrammed in Scheme 3-3. The mutual two-bond coupling between these fluorines (58.6 Hz (**17**) and 66.5 Hz (**17a**)) is typical.^{11,16} Binding of 1,1-difluoroallene through the hydrogen-substituted double bond is its typical binding mode.^{11,17}

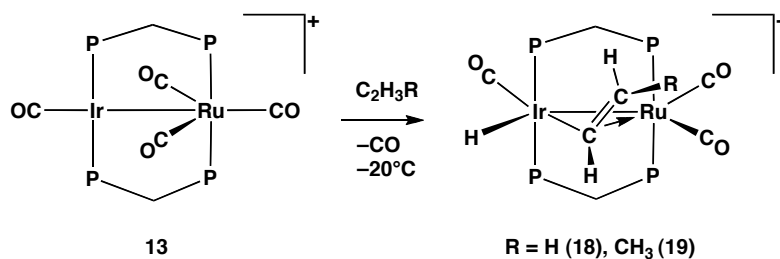
The difference in orientation of the difluoroallene ligands in isomers **17** and **17a** is accompanied by subtle differences in the carbonyl ligand geometries. In compound **17**, two carbonyls are bound to each metal, as determined by $^{13}\text{C}\{^1\text{H}\}$ NMR experiments employing selective ^{31}P -decoupling; those at δ 182.2 and δ 159.0 couple only to the Ir-bound ^{31}P nuclei, so are presumably bound to this metal, while those at δ 199.3 and δ 197.8 couple only to the Ru-bound ^{31}P nuclei. In **17a**, the carbonyls at δ 176.5 and δ 158.7 again couple only to the Ir-bound ^{31}P nuclei, while that at δ 195.5 is bound exclusively to Ru. However, in this case, the fourth carbonyl at δ 205.1 couples strongly to the Ru-bound ^{31}P nuclei ($^2J_{\text{CP}} = 8.4$ Hz) while also coupling weakly to the Ir-bound ^{31}P nuclei ($^2J_{\text{CP}} = 2.9$ Hz), indicating a ‘semi-bridging’ arrangement as shown in Scheme 3-3. Although no semi-bridging interaction of an Ir-bound carbonyl with Ru is shown for compound **17**, the carbonyl at significantly lower field is presumed to be adjacent to Ru,¹²⁻¹³ and may be interacting weakly with this metal. The semi-bridging CO arrangement in **17a** involves the metal that is bound to the more electron rich “ CH_2 ” end of the difluoroallene ligand, and is more capable of π back donating to a semi-bridging carbonyl.

No evidence of C–H activation involving the 1,1-difluoroallene ligand is observed upon warming above ambient temperature, suggesting that the $\mu\text{-}\kappa^1:\kappa^1$ arrangement may not be conducive to C–H activation of these groups.

3.2.4 C–H Bond Activation in Monoolefins

Unlike the reaction of **13** with the cumulenes, described above, no reaction of **13** is observed with ethylene or propylene, even with greater than 10 equiv of substrate at temperatures between $-78\text{ }^{\circ}\text{C}$ and ambient, after two days. However, at low-temperature in the presence of trimethylamine *N*-oxide (TMNO), the vinyl hydride products $[\text{IrRuH}(\text{CO})_3(\mu\text{-}\kappa^1\text{:}\eta^2\text{-C(H)=CHR})(\text{dppm})_2][\text{BF}_4]$ ($\text{R} = \text{H}$ (**18**), CH_3 (**19**)), shown in Scheme 3-4, are observed. No reaction is observed at temperatures below $-40\text{ }^{\circ}\text{C}$, owing to the limited solubility of TMNO at this temperature; however, warming to $-20\text{ }^{\circ}\text{C}$ generates the products **18** and **19** within 3 h.

Scheme 3-4



Both products have distinctive $^{31}\text{P}\{^1\text{H}\}$ NMR spectra that are characteristic of an ABCD spin system in which all ^{31}P nuclei are chemically inequivalent – a result of the orientation of the $\mu\text{-}\kappa^1\text{:}\eta^2\text{-vinyl}$ fragment – which leads to inequivalence of the ^{31}P nuclei above and below the Ir–Ru equatorial plane, combined with the inequivalence at each metal. In the $^{31}\text{P}\{^1\text{H}\}$ NMR spectra of **18** and **19**, the large mutual two-bond P–P coupling of at least 250 Hz observed for each ^{31}P resonance confirms the mutually trans orientation of both dppm groups at each metal. The $^{31}\text{P}\{^1\text{H}\}$ NMR spectrum of **18** is given on the following page as Figure 3-3. The lack of symmetry in compounds **18** and **19** also gives rise to four signals ranging from *ca.* δ 2.7 to δ 5.5 in the ^1H NMR spectrum representing the four inequivalent methylene protons of the dppm ligands. The proton attached to the α -carbon of the vinyl unit appears characteristically downfield in both cases at *ca.* δ 7 and couples to the trans proton ($^3J_{\text{HH}} > 10\text{ Hz}$), and in compound **18** also displays coupling (7.1 Hz) to the cis

proton in the vinyl fragment. The pair of geminal protons on the β -carbon of the vinyl unit display mutual two-bond coupling of 2.7 Hz. In **19**, no coupling is observed involving the methyl protons. Both **18** and **19** have characteristically

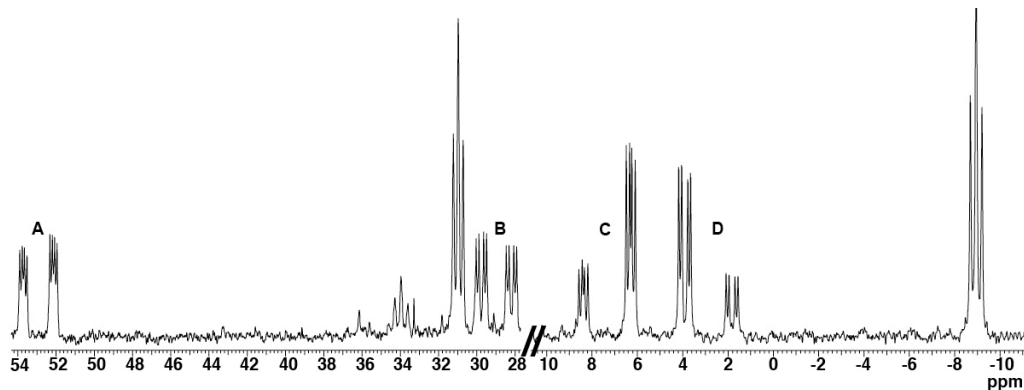


Figure 3-3. $^{31}\text{P}\{^1\text{H}\}$ NMR spectrum of a mixture of $[\text{IrRuH}(\text{CO})_3(\mu\text{-}\kappa^1\text{:}\eta^2\text{-C}(\text{H})=\text{CH}_2)(\text{dppm})_2][\text{BF}_4]$ (**18**) and $[\text{IrRu}(\text{CO})_4(\text{dppm})_2][\text{BF}_4]$ (**13**) in CD_2Cl_2 at $-20\text{ }^\circ\text{C}$. The four ^{31}P signals for **18** are labelled A, B, C, and D.

upfield hydride resonances ($\delta -9.57$ (**18**) and $\delta -9.95$ (**19**)), coupling to both of the inequivalent Ir-bound ^{31}P nuclei. If compound **18** is generated from $^{13}\text{C}_2$ -ethylene, the carbons of the vinyl moiety appear at $\delta 139.7$ (α -carbon) and 65.7 (β -carbon) in the $^{13}\text{C}\{^1\text{H}\}$ NMR spectrum, displaying mutual one-bond coupling of 39.7 Hz, intermediate between that of ethylene and ethane (67.6 and 34.6 Hz),¹⁸ consistent with the η^2 -coordination to Ru. Selective ^{31}P decoupling supports the binding mode shown in Scheme 3-4, as the signal for the α -carbon sharpens noticeably upon the decoupling of the Ir-bound ^{31}P nuclei, although the coupling is not resolved. There is also noticeable sharpening of the α -proton signal upon decoupling of the same Ir-bound ^{31}P nuclei, although it is more difficult to observe as this signal is partially obscured by the phenyl protons.

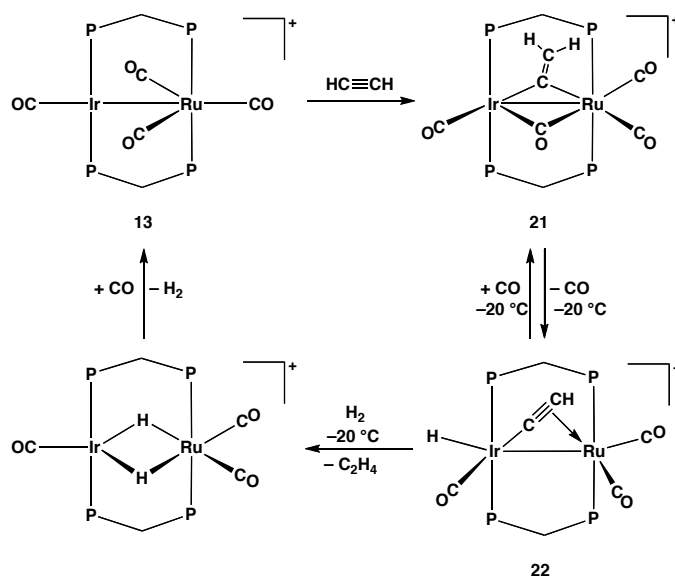
The need for TMNO to initiate these reactions indicates that they proceed through the tricarbonyl species $[\text{IrRu}(\text{CO})_3(\text{dppm})_2][\text{BF}_4]$ (**20**). Surprisingly, warming the solutions of **18** and **19** to $0\text{ }^\circ\text{C}$ does not bring about the anticipated activation of the second C–H bond to give the expected vinylidene-bridged dihydride (See Chart 3-1) and instead the olefin is lost upon warming via reductive elimination of the vinyl and hydride

moieties. Compound **20** subsequently decomposes in solution at ambient temperature over the period of one hour.

The addition of ethylene to compound **20** at $-78\text{ }^{\circ}\text{C}$ generates what we assume to be an ethylene adduct, in which the ethylene appears to be bound to the Ir centre. The signals for the ^{31}P nuclei are broad in the ^{31}P NMR spectrum, but the Ir-bound ^{31}P signal is particularly broad, spanning almost 500 Hz at $-78\text{ }^{\circ}\text{C}$, suggesting fluxionality at this metal, possibly due to the reversible coordination of the olefin. In the ^1H NMR spectrum at this temperature a very broad signal, typical for an Ir-bound ethylene group¹⁹ is observed at *ca.* δ 1.2 and one broad signal for the dpmm methylene protons appears at δ 4.06. Although the complex appears to have three carbonyls, the breadth of these resonances does not allow us to determine their arrangement in this product, therefore complete characterization by NMR was not possible. Warming this solution to $-20\text{ }^{\circ}\text{C}$ results in the conversion of this assumed ethylene adduct into **18** over a 3 h period.

Although we were unable to generate the vinylidene dihydride product from the geminal activation of ethylene, we attempted its synthesis by an indirect method by reaction of a preformed vinylidene product with H_2 . This targeted vinylidene complex, $[\text{IrRu}(\text{CO})_4(\mu\text{-C}=\text{CH}_2)(\text{dpmm})_2][\text{BF}_4]$ (**21**), is readily generated by reaction of **13** with acetylene, as shown in Scheme 3-5. For **21**, the vinylidene protons appear at

Scheme 3-5



δ 6.72 and δ 5.54 ($^2J_{\text{HH}} = 2.6$ Hz) in the ^1H NMR spectrum, and the X-ray structure determination of the triflate salt is shown for the complex cation in Figure 3-4. Selected bond lengths and angles for **21-CF₃SO₃** appear in Table 3-3. The geometry of **21-CF₃SO₃** closely resembles that of **14-CF₃SO₃** and **16-CF₃SO₃** in all aspects; the Ir–Ru separation of 2.9278(3) Å is the shortest in the series of compounds explored in this chapter although it remains larger than most such distances,¹³ and the C(5)–C(6) bond length is again typical of a double bond (1.309(5) Å).¹⁴ The asymmetry of the vinylidene unit is shown in the Ir–C(5)–C(6) and Ru–C(5)–C(6) angles (138.6(3)° and 133.1(3)° respectively) and the Ir–C(5) and Ru–C(5) bond lengths (2.050(3) Å and 2.151(3) Å). In this case the asymmetry is not a function of an unsymmetrical substitution pattern on the vinylidene but presumably reflects the greater crowding at Ru, which dictates the orientations of the dppm phenyl groups and their interactions with the vinylidene ligand.

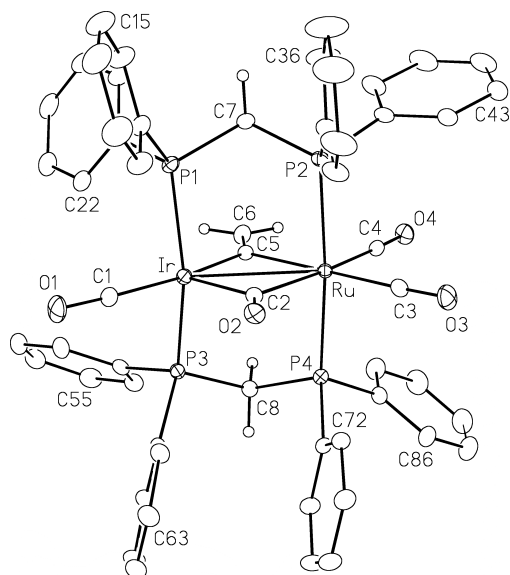


Figure 3-4. Perspective view of the complex cation of $[\text{IrRu}(\text{CO})_4(\mu\text{-C}=\text{CH}_2)(\text{dppm})_2][\text{CF}_3\text{SO}_3]$ (**21-CF₃SO₃**). Thermal ellipsoids are as described in Figure 3-1.

**Table 3-3. Selected Bond Lengths and Angles for Compound 21-
CF₃SO₃**

(a) Distance (Å)

atom 1	atom 2	distance	atom 1	atom 2	distance
Ir	Ru	2.9278(3)	Ru	C(3)	1.939(4)
Ir	C(1)	1.881(4)	Ru	C(4)	1.913(4)
Ir	C(2)	2.001(3)	Ru	C(5)	2.151(3)
Ir	C(5)	2.050(3)	C(5)	C(6)	1.309(5)
Ru	C(2)	2.194(3)			

(b) Angles (deg)

atom	atom 2	atom 3	angle	atom 1	atom	atom 3	angle
Ir	C(2)	Ru	88.5(1)	Ru	C(5)	C(6)	133.1(3)
Ir	C(5)	Ru	88.3(1)	C(1)	Ir	C(5)	166.9(2)
Ir	C(5)	C(6)	138.6(3)				

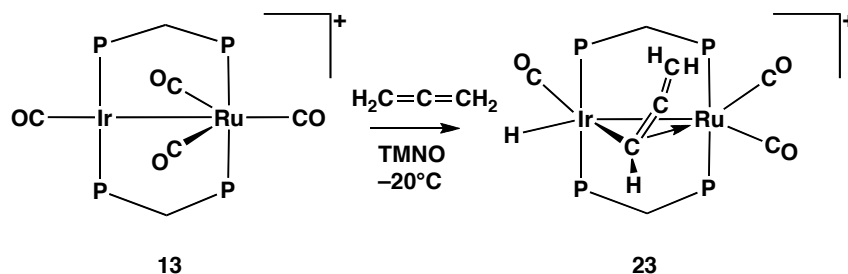
Attempts to displace a carbonyl in **21** by reaction with H₂ to give the targeted vinylidene-bridged dihydride did not succeed, with no reaction being observed at ambient temperature. In the absence of H₂, CO removal by the addition of TMNO at -20 °C results in the formation of the acetylide hydride complex, [IrRu(H)(CO)₃(μ-κ¹:η²-C≡CH)(dppm)₂][BF₄] (**22**), in which the acetylide moiety is σ-bound to Ir, while η²-bound to Ru; the addition of CO regenerates **21**. Compound **22** was characterized by multinuclear NMR spectroscopy at -20 °C. In the ¹H NMR spectrum the hydride appears at δ -9.63 with coupling to only the Ir-bound ³¹P nuclei (²J_{HP} = 11.1 Hz) while the acetylide proton appears as a broad singlet (*ca.* 10 Hz wide at half-height) at δ 3.77. Selective ³¹P-decoupling experiments suggest coupling to only the Ir-bound ³¹P nuclei. The orientation of the acetylide moiety is somewhat ambiguous since the weak coupling of the acetylide hydrogen to the Ir-bound phosphines could occur either via four-bond coupling through the σ-framework (as shown in Scheme 3-5) or via the π interaction if the acetylide were σ-bound to Ru. We represent the binding of this moiety as shown in Scheme 3-5, with the acetylide terminally

bound to Ir, as was the case for a similar Ir/Ru propynyl complex for which an X-ray structure was obtained and which displayed similar coupling to only the Ir-bound ^{31}P nuclei.¹² Three signals are observed in the $^{13}\text{C}\{^1\text{H}\}$ NMR spectrum for the carbonyl ligands. The Ru-bound carbonyls appear at δ 207.3 and δ 198.6, with the Ir-bound CO at δ 177.7; each carbonyl couples only to the pair of adjacent ^{31}P nuclei. Addition of H_2 to the solution of **22** at -20°C , in hopes of observing the vinylidene dihydride target, gives no reaction, and warming to ambient temperature in the presence of H_2 results in the slow appearance of the known dihydride-bridged complex $[\text{IrRu}(\text{CO})_3(\mu\text{-H})_2(\text{dppm})_2][\text{BF}_4]^{13\text{a}}$ (see Scheme 3-5). Within 2 h at ambient temperature, all of **22** has converted to this dihydride with the concomitant elimination of ethylene, as confirmed by ^1H NMR. This dihydride product can easily be converted back to $[\text{IrRu}(\text{CO})_4(\text{dppm})_2][\text{BF}_4]$ (**13**) by a CO purge overnight.^{13\text{a}}}

3.2.5 Mechanistic Insights into the Geminal Activation of Olefinic C–H Bonds

Low-temperature investigations of the reaction of **13** with cumulenes did not yield additional mechanistic information. However, the tricarbonyl complex **20** was used to investigate cumulene reactivity at -20°C . Compound **20**, generated *in situ* at -20°C , reacts with allene at this temperature to give the allenyl hydride product, $[\text{IrRu}(\text{H})(\text{CO})_3(\mu\text{-}\kappa^1\text{:}\eta^2\text{-CH=C=CH}_2)(\text{dppm})_2][\text{BF}_4]$ (**23**), analogous to **18** and **19**, within 1 h, as shown in Scheme 3-6. Compound **23** was characterized by multinuclear NMR spectroscopy at -20°C .

Scheme 3-6

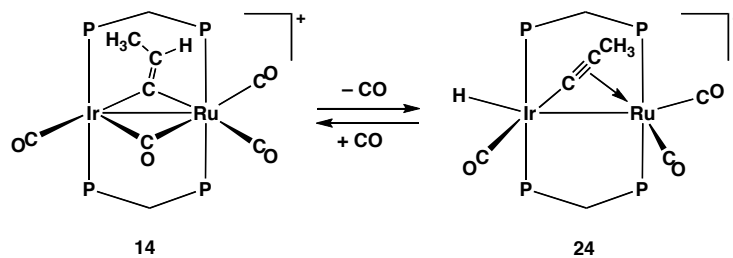


As was the case for compounds **18** and **19**, the $^{31}\text{P}\{^1\text{H}\}$ spectrum of **23** displays four signals (δ 45.0, δ 23.7, δ 3.8, and δ -12.7), with mutual two bond P–P couplings between pairs of resonances of greater than 250 Hz, indicating a trans arrangement of the dppm ligands. In the ^1H NMR spectrum, the hydride appears at δ -9.96 as a multiplet, with resolvable coupling to the Ir-bound ^{31}P nuclei (17.1 Hz). The three protons for the allenyl fragment are observed at δ 6.79, δ 4.88, and δ 4.57, with the latter two showing unresolved two-bond geminal H–H coupling, as confirmed by 2D NMR correlation studies. On the basis of $^{13}\text{C}\{^1\text{H}\}$ NMR spectra with accompanying selective ^{31}P -decoupling, the two downfield carbonyls (δ 205.2 and δ 196.2) are identified as bound to Ru, with the upfield carbonyl (δ 178.1) bound to Ir. Warming the solution above -20 °C results in the formation of many unidentified products, unless the solution is quickly purged with CO and left to react overnight, after which time complex **14** can be identified by $^{31}\text{P}\{^1\text{H}\}$ NMR (*ca.* 50 %) along with decomposition products. Apart from the formation of the final product (**14**) in low yield, no additional intermediates in its formation could be identified.

Our failure to bring about the second C–H bond activation by converting the alkenyl and allenyl hydrides (**18**, **19** and **23**) into the corresponding vinylidene and allenylidene dihydride products indicates that the conversion of the allenes to vinylidene products, noted above, does not proceed by a sequential pair of C–H activation steps. A clue to the nature of the steps that followed the first C–H activation came from a previous study¹² in which the conversion of a number of allenes into alkynyl-bridged products was observed. Furthermore, binuclear alkynyl hydride species are known to transform into vinylidene-bridged products in the conversion from alkynes,²⁰ suggesting these as viable intermediates. The propynyl hydride complex, $[\text{IrRu}(\text{H})(\text{CO})_3(\mu\text{-}\kappa^1\text{:}\eta^2\text{-C}\equiv\text{CCH}_3)(\text{dppm})_2][\text{BF}_4]$ (**24**), can be generated by removal of a carbonyl from the methyl vinylidene-bridged $[\text{IrRu}(\text{CO})_4(\mu\text{-C}=\text{C}(\text{H})\text{CH}_3)(\text{dppm})_2][\text{BF}_4]$ (**14**), as shown in Scheme 3-7, much as was observed upon carbonyl removal from the species **21** (see Scheme 3-5). The addition of CO to **24** also results in

reformation of **14** (80% of ^{31}P -containing products) along with some decomposition products, clearly demonstrating the reversible interconversion between alkynyl hydride and vinylidene species. The conversion of the vinylidene to alkynyl hydride occurs to alleviate the coordinative unsaturation

Scheme 3-7



upon CO loss, by converting a dianionic four-electron donor vinylidene into a pair of monoanionic donors that together donate six-electrons. Compound **24** is unstable in solution, decomposing within 1h at ambient temperature, so is unstable to workup, even at low temperature. To further support the alkynyl formulation for **24**, the addition of propyne to a solution of the tricarbonyl complex $[\text{IrRu}(\text{CO})_3(\text{dppm})_2][\text{BF}_4]$ (**20**) at 0 °C results in the facile generation of **24**. This reaction, along with the similar reaction discussed earlier (see Scheme 3-5), suggests that the CO ligand that is lost in the first C–H bond activation process subsequently recoordinates, generating the vinylidene complexes from the alkynyl hydride intermediates.

Compound **24** was characterized by multinuclear NMR spectroscopy at 0 °C. The $^{31}\text{P}\{^1\text{H}\}$ NMR spectrum displays two resonances at δ 32.6 and δ –9.9. In the ^1H NMR spectrum the hydride appears at δ –9.69 coupling only to the Ir-bound ^{31}P nuclei ($^2J_{\text{HP}} = 12.7$ Hz), consistent with its terminal binding to this metal. The propynyl protons appear at δ 0.76 and display weak coupling ($^5J_{\text{HP}} = 2.5$ Hz) to only the Ir-bound ^{31}P nuclei, as previously observed in similar compounds.¹² The $^{13}\text{C}\{^1\text{H}\}$ NMR spectrum is as expected with two resonances for the Ru-bound carbonyls (δ 208.1 and δ 198.8) and one for the lone carbonyl bound to Ir (δ 177.5).

In attempts to detect an allene adduct prior to the first C–H activation product (**23**), allene was added to a solution of **20** at $-78\text{ }^{\circ}\text{C}$ and monitored at this temperature by NMR spectroscopy. At this temperature, the allene adduct, $[\text{IrRu}(\text{CO})_4(\text{H}_2\text{C}=\text{C}=\text{CH}_2)(\text{dppm})_2][\text{BF}_4]$ (**25**) forms immediately. Surprisingly, this adduct has *four* carbonyl ligands (δ 210.8, δ 208.2, δ 190.3, δ 186.5), a result of CO scavenging from unobserved decomposition products. The use of an internal phosphorus standard (bis(triphenylphosphoranylidene) ammonium chloride) established a yield of **25** of less than 70 % with no other products observed, confirming the decomposition. NMR spectroscopic characterization of **25** at $-78\text{ }^{\circ}\text{C}$ proceeded much as described above, but was inconclusive regarding the allene coordination mode, being consistent with either an η^2 -mode on Ir or a bridging $\kappa^1:\kappa^1$ -mode analogous to **17a**, described earlier, in which Ru is bound to the central carbon with Ir bound to a terminal CH_2 group. However we do not discuss this species further since, in addition to the unresolved bonding ambiguity, this adduct is not an intermediate in the formation of **23**, since warming to $-60\text{ }^{\circ}\text{C}$ results in allene loss and regeneration of **13**. Interestingly, this adduct cannot be prepared directly from the addition of allene to the tetracarbonyl complex **13** at $-78\text{ }^{\circ}\text{C}$, suggesting that allene coordination requires initial (reversible) loss of a carbonyl ligand.

Adducts resembling compound **25** can be prepared by the addition of the alkyl cumulenes and 1,1-difluoroallene to a solution of **20** at $-78\text{ }^{\circ}\text{C}$, with the 1,1-difluoroallene being generated as described in the Experimental section. As with **25**, the alkyl cumulenes dissociate from the tetracarbonyl complexes at temperatures from $-40\text{ }^{\circ}\text{C}$ to ambient temperature, resulting in the reformation of $[\text{IrRu}(\text{CO})_4(\text{dppm})_2]^+$ (**13**) and decomposition products, while the 1,1-difluoroallene adduct generated, compound **17**, merely isomerizes to **17a**, as described earlier.

3.3 Discussion and Conclusions

As was observed for the related diiridium complex, $[\text{Ir}_2(\text{CH}_3)(\text{CO})_2(\text{dppm})_2]^+$, studied previously,^{2e} the mixed-metal complex,

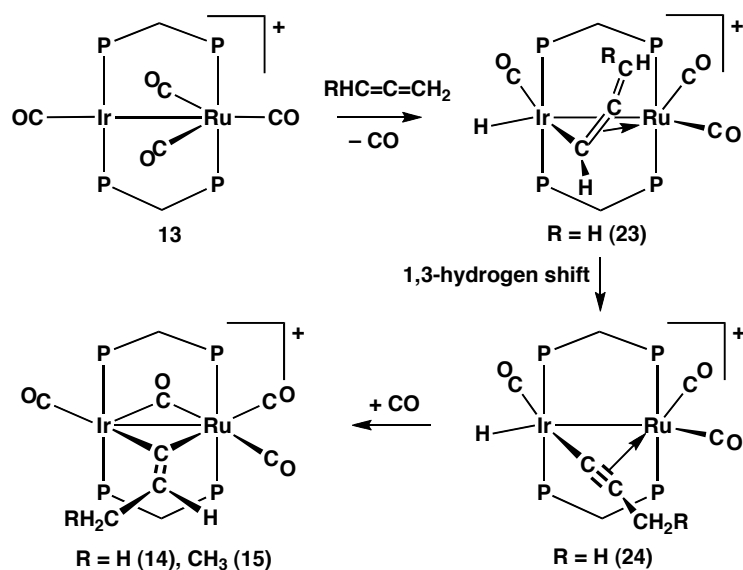
$[\text{IrRu}(\text{CO})_4(\text{dppm})_2]^+$ (**13**), is capable of double, geminal activation of select α -olefins under ambient conditions. However, the reactivities of these two complexes in this chemistry are somewhat orthogonal; whereas the Ir_2 complex was only observed to undergo double C–H activation with 1,3-butadiene, and yielded only adducts with cumulenes, the Ir/Ru species is unreactive towards butadiene, while readily undergoing C–H activation with allene, methylallene, and 1,1-dimethylallene. Both the Ir_2 complex and compound **13** are unreactive towards the monoolefins, ethylene and propylene, although removal of a carbonyl ligand from **13** in the presence of these olefins at $-20\text{ }^\circ\text{C}$ results in activation of a single C–H bond to give the vinyl hydride products, $[\text{IrRuH}(\text{CO})_3(\mu\text{-}\kappa^1\text{:}\eta^2\text{-CH=CHR})(\text{dppm})_2]^+$ ($\text{R} = \text{H}, \text{CH}_3$). Surprisingly however, warming these vinyl-bridged species does not result in activation of the second C–H bond, but results in olefin loss.

The failure of these vinyl hydride species, formed by single C–H activation of ethylene and propylene following CO loss from **13**, to undergo the second C–H activation to give the corresponding vinylidene hydride, combined with the failure of the allenyl hydride (**23**, see Scheme 3-6) to proceed to the allenylidene dihydride, suggests that the transformation from allene to vinylidene does not proceed by this route followed by subsequent transfers of the hydrides to the unsaturated hydrocarbyl fragment. Instead, these data, combined with the facile reversible conversion of vinylidene to alkynyl hydride upon the respective loss or gain of CO suggests that a route through an alkynyl hydride is feasible. This suggestion also finds support in our previous study,¹² in which double C–H activation of cumulenes yielded alkynyl-bridged products.

We therefore propose the sequence of transformations shown in Scheme 3-8, recognizing that a number of significant questions remain unanswered. Reaction of $[\text{IrRu}(\text{CO})_4(\text{dppm})_2]^+$ (**13**) with allene and methylallene results in loss of a carbonyl accompanied by activation of one of the geminal C–H bonds, yielding the corresponding allenyl ligands shown for compound **23**. The next important step involves a 1,3-hydrogen shift to give the propynyl hydride (**24**) or

butynyl hydride species. How this proposed metal-promoted shift occurs is not known. Recombination of CO results in the transformation of the alkynyl hydride to the vinylidene, as observed for the reversible transformations of **14** to **24** (Scheme 3-7) and **21** to **22** (Scheme 3-5).

Scheme 3-8



It seems clear that although $[\text{Ir}_2(\text{CH}_3)(\text{CO})_2(\text{dppm})_2]^+$ and $[\text{IrRu}(\text{CO})_4(\text{dppm})_2]^+$ are both capable of geminal C–H activation in olefins, each achieves this by a different mechanism. We suggest that the previously studied diiridium species^{2e} effects this double C–H activation by a mechanism related to that shown in Chart 3-1, in which the pair of metals bring about the stepwise activation of the adjacent C–H bonds. In a recent study, the related species, $[\text{Ir}_2(\text{CO})_3(\mu\text{-H})(\text{depmp})_2]^+$ ($\text{depmp} = \text{Et}_2\text{PCH}_2\text{PEt}_2$), has been shown to bring about geminal C–H activation in a number of α -olefins, and is proposed to proceed in the same manner.²¹ In contrast, the current Ir/Ru species is believed to effect double C–H activation in the allenes studied by a more complicated sequence as described above, proceeding through an alkynyl hydride species. On this basis it is hardly surprising that this Ir/Ru complex is unable to doubly activate monoolefins or conjugated olefins, which are unable to readily access an alkynyl intermediate. Interestingly, the primary reactivity in both systems (Ir₂ or Ir/Ru)

occurs at the same group 9 metal centre (Ir), and the significant differences in reactivity for the two classes of compounds, with regards to geminal C–H activation, indicates that changing one metal from group 9 to group 8 can have a profound influence on the chemistry.

The last major question that remains unanswered is how the third C–H activation, involving a methyl group in 1,1-dimethylallene occurs. Related to this question, we do not understand why in this study the single methyl group in methylallene does not also undergo the analogous third C–H activation to give the vinyl vinylidene-bridged structure, shown earlier as structure **G**, although this latter issue may just reflect a significantly slower rate involving activation of the third C–H bond.

3.4 Experimental Section

3.4.1 General Comments

All solvents were dried using appropriate desiccants (given in Appendix II), distilled before use, and stored under a nitrogen atmosphere. Reactions were performed under an argon atmosphere using standard Schlenk techniques unless otherwise noted. The following reagents were purchased from the suppliers given in parentheses: triruthenium dodecacarbonyl and ammonium hexachloroiridate (IV) (Strem Chemicals), propylene, and propyne (Praxair), 1,2-butadiene (Organic Technologies), propadiene (Matrix Scientific), 1,1-dimethylallene and 1,3-butadiene (Aldrich), ethylene and acetylene (Matheson), isoprene (Alfa Aesar), $^{13}\text{C}_2$ -ethylene (Cambridge Isotopes), and ^{13}CO (Isotech, Inc). The trimethylamine *N*-oxide dihydrate was purchased from Aldrich and was dried according to the literature procedure.²² Compound **13**, $[\text{IrRu}(\text{CO})_4(\text{dppm})_2][\text{BF}_4]$, was prepared by the literature procedure,^{13a} except that $[\text{Ir}(\text{CO})(\text{dppm})_2][\text{Cl}]$ ²³ was substituted for $[\text{IrCl}(\text{dppm})_2]$ in the original synthesis.

1,1-Difluoroallene was prepared using a modification of the published procedures,^{11,24} in which a solution of 100 μL of 2-bromo-3,3,3-trifluoro-1-propene (Aldrich) in 3 mL of diethyl ether was cooled to $-90\text{ }^\circ\text{C}$ in an acetone/liquid N_2 bath. To this was added dropwise 385 μL of a 2.5 M solution of

n-butyllithium in hexanes (Aldrich), followed by stirring of the solution at this temperature for 30 min. The $-90\text{ }^{\circ}\text{C}$ bath was replaced by an acetonitrile/ $\text{CO}_{2(\text{s})}$ bath (*ca.* $-40\text{ }^{\circ}\text{C}$) and the solution was stirred for 15 min. The solution was then slowly warmed over 15 min to $-20\text{ }^{\circ}\text{C}$, resulting in the evolution of 1,1-difluoroallene gas.

The ^1H NMR and $^{31}\text{P}\{^1\text{H}\}$ NMR spectra were recorded on a Varian Inova 400 spectrometer operating at 399.9 MHz and 161.9 MHz, respectively. All low temperature spectra and the heteronuclear decoupling experiments ($^{13}\text{C}\{^1\text{H}\}$ and $^{13}\text{C}\{^1\text{H},^{31}\text{P}\}$) were recorded on a Varian Unity spectrometer operating at 161.9 MHz for ^{13}C , 202.3 MHz for ^{31}P , and 499.8 MHz for ^1H . Infrared spectra were recorded in CH_2Cl_2 solution on a Nicolet Avatar 370 DTGS spectrometer. Mass Spectrometry was performed on a Micromass ZabSpec TOF spectrometer by the mass spectrometry facility of this department, and elemental analyses were also carried out in the departmental facility.

3.4.2 Preparation of Compounds

Spectroscopic data for the compounds are presented in Table 3-4.

- (a) **[IrRu(CO) $_4$ (μ -C=C(H)CH $_3$)(dppm) $_2$][BF $_4$] (14). Method i.** A stirred yellow solution of compound **13** (100 mg, 0.079 mmol) in 5 mL of CH_2Cl_2 was saturated with propadiene (allene) gas and left to stir under an atmosphere of the gas. No colour change was noted, but after 16 h of stirring at ambient temperature, the $^{31}\text{P}\{^1\text{H}\}$ NMR spectrum revealed compound **14** as the only phosphorus-containing product. After reduction of the solvent volume by 50 %, addition of 20 mL of diethyl ether followed by 20 mL of pentane resulted in the precipitation of a yellow solid that was washed with 3 x 10 mL of diethyl ether and dried in vacuo (85 % yield). HRMS: *m/z* calcd for $\text{C}_{56}\text{H}_{48}\text{IrO}_3\text{P}_4\text{Ru}$ ($\text{M}^+ - \text{CO}$), 1186.1218; found, 1186.1221 ($\text{M}^+ - \text{CO}$). Elemental analyses for **14-CF $_3$ SO $_3$** , obtained from **14** by tetrafluoroborate anion exchange for a triflate ion. Anal. Calcd for $\text{C}_{62.5}\text{ClF}_3\text{H}_{59}\text{IrO}_8\text{P}_4\text{RuS}$: C, 50.73; H, 4.02. Found: C, 50.31; H, 3.73. The inclusion of one equiv of diethyl ether and

Table 3-4. Spectroscopic Data for the Compounds

Compound	IR (cm ⁻¹) ^a	NMR ^b		
		$\delta(^{31}\text{P}\{\text{H}\})^c$	$\delta(^{13}\text{C}\{\text{H}\})^{d,e}$	
[IrRu(CO) ₄ (μ -C=C(H)CH ₃ - (dppm) ₂][BF ₄] (14)	2048 (s), 1996 (s), 1984 (s), 1799 (m)	28.8 (m, 2P), -1.4 (m, 2P)	$\delta(^1\text{H})^{d,e}$ 6.91 (qdt, 1H, ³ J _{HH} = 6.4 Hz, ⁴ J _{HP} = 1.5 Hz, 1.0 Hz), 4.01 (dm, 2H, ² J _{HH} = 12.9 Hz), 3.04 (dm, 2H, ² J _{HH} = 12.9 Hz), 0.78 (dt, 3H, ³ J _{HH} = 6.4 Hz, ⁴ J _{HP} = 1.8 Hz, 1.8 Hz)	$\delta(^{13}\text{C}\{\text{H}\})^{d,e}$ 209.0 (dtt, 1C, ² J _{CC} = 24.5 Hz, ² J _{CP} = 9.0 Hz, 6.5 Hz), 195.0 (t, 1C, ² J _{CP} = 10.7 Hz), 192.8 (dt, 1C, ² J _{CC} = 24.5 Hz, ² J _{CP} = 11.2 Hz), 182.2 (t, 1C, ² J _{CP} = 11.6 Hz)
[IrRu(CO) ₄ (μ -C=C(H)CH ₃ - CH ₃)(dppm) ₂][BF ₄] (15)	2047 (s), 2030 (s), 1995 (s), 1780 (s)	28.7 (m, 2P), -1.2 (m, 2P)	$\delta(^1\text{H})^{d,e}$ 6.74 (tt, 1H, ³ J _{HH} = 6.5 Hz, ⁴ J _{HP} = 1.0 Hz, 1.2 Hz), 4.19 (dm, 2H, ² J _{HH} = 12.6 Hz), 3.12 (dm, 2H, ² J _{HH} = 12.6 Hz), 1.06 (m, 2H, ³ J _{HH} = 7.5 Hz, 6.5 Hz), 0.36 (t, 3H, ³ J _{HH} = 7.5 Hz)	$\delta(^{13}\text{C}\{\text{H}\})^{d,e}$ 208.9 (m, 1C, ² J _{CC} = 24.2 Hz, ² J _{CP} = 9.3 Hz, 5.8 Hz), 194.8 (t, 1C, ² J _{CP} = 11.0 Hz), 192.5 (m, 1C, ² J _{CC} = 24.2 Hz, ² J _{CP} = 12.6 Hz), 182.1 (t, 1C, ² J _{CP} = 12.2 Hz)
[IrRu(CO) ₄ (μ -C=C(H)C- (CH ₃)=CH ₂)(dppm) ₂][BF ₄] (16)	2051 (s), 2000 (s), 1978 (s), 1792 (m)	26.5 (m, 2P), -4.4 (m, 2P)	$\delta(^1\text{H})^{d,e}$ 7.91 (bs, 1H), 4.74 (dm, 1H, ² J _{HH} = 2.4 Hz), 4.49 (dm, 1H, ² J _{HH} = 2.4 Hz), 3.96 (dm, 2H, ² J _{HH} = 12.8 Hz), 3.05 (dm, 2H, ² J _{HH} = 12.8 Hz), 0.46 (m, 3H)	$\delta(^{13}\text{C}\{\text{H}\})^{d,e}$ 211.5 (m, 1C, ² J _{CC} = 25.1 Hz, ² J _{CP} = 13.3 Hz), 193.5 (bt, 1C, ² J _{CP} = 10.9 Hz), 191.6 (dt, 1C, ² J _{CC} = 25.1 Hz, ² J _{CP} = 3.0 Hz), 182.2 (t, 1C, ² J _{CP} = 12.5 Hz)
[IrRu(CO) ₄ (μ - κ^1 - κ^1 -F ₂ C=C- CH ₂)(dppm) ₂][BF ₄] (17) ^f	n/a	26.6 (m, 2P), -18.4 (m, 2P)	$\delta(^1\text{H})^{d,e}$ 4.48 (dm, 2H, ² J _{HH} = 14.3 Hz), 4.10 (dm, 2H, ² J _{HH} = 14.3 Hz), 1.29 (bt, 2H, ³ J _{HP} = 6.9 Hz)	$\delta(^{13}\text{C}\{\text{H}\})^{d,e}$ 199.3 (t, 1C, ² J _{CP} = 9.5 Hz), 197.7 (t, 1C, ² J _{CP} = 12.8 Hz), 182.2 (bt, 1C, ² J _{CP} = 7.3 Hz), 159.0 (bt, 1C, ² J _{CP} = 10.0 Hz)
[IrRu(CO) ₄ (μ - κ^1 - κ^1 -H ₂ C- C=CF ₂)(dppm) ₂][BF ₄] (17a) ^f	n/a	25.5 (m, 2P), -20.8 (m, 2P)	$\delta(^1\text{H})^{d,e}$ 4.60 (dm, 2H, ² J _{HH} = 14.4 Hz), 4.14 (dm, 2H, ² J _{HH} = 14.4 Hz), 1.99 (bt, 2H, ³ J _{HP} = 9.1 Hz)	$\delta(^{13}\text{C}\{\text{H}\})^{d,e}$ 205.1 (m, 1C, ² J _{CP} = 8.4 Hz, ² J _{CP} = 2.9), 195.5 (t, 1C, ² J _{CP} = 14.1 Hz), 176.5 (t, 1C, ² J _{CP} = 6.8 Hz), 158.7 (t, 1C, ² J _{CP} = 9.1 Hz)

Table 3-4. Spectroscopic Data for the Compounds (Continued)

Compound	IR (cm ⁻¹) ^a	NMR ^b		
		$\delta(^{31}\text{P}\{\text{H}\})^c$	$\delta(\text{H})^{d/e}$	$\delta(^{13}\text{C}\{\text{H}\})^{d/e}$
[IrRu(H)(CO) ₃ (μ - κ^1 - η^2 -C(H)=CH ₂)(dppm) ₂][BF ₄] (18) ^f	n/a	52.9 (ddd, 1P, ² J _{pp} = 255.1 Hz, ² J _{pp} = 39.1 Hz, ³ J _{pp} = 21.6 Hz), 29.0 (ddd, 1P, ² J _{pp} = 255.5 Hz, ² J _{pp} = 62.0 Hz, ³ J _{pp} = 21.9 Hz), 7.3 (ddd, 1P, ² J _{pp} = 337.8 Hz, ² J _{pp} = 39.1 Hz, ³ J _{pp} = 23.1 Hz), 2.9 (ddd, 1P, ² J _{pp} = 337.8 Hz, ² J _{pp} = 62.2 Hz, ³ J _{pp} = 21.0 Hz)	7.13 (m, 1H, ³ J _{HH(trans)}} = 11.0 Hz, ³ J _{HH(cis)}} = 7.1 Hz), 5.49 (dm, 1H, ² J _{HH} = 15.2 Hz), 4.48 (m, 1H, ³ J _{HH(trans)}} = 11.0 Hz, ² J _{HH(gem)}} = 2.7 Hz), 4.38 (dm, 1H, ² J _{HH} = 15.0 Hz), 3.87 (dm, 1H, ² J _{HH} = 15.0 Hz) 3.14 (m, 1H, ³ J _{HH(cis)}} = 7.1 Hz, ² J _{HH(gem)}} = 2.7 Hz), 2.69 (dm, 1H, ² J _{HH} = 15.2 Hz), -9.57 (dd, 1H, ² J _{HP} = 14.5 Hz, ² J _{HP} = 9.4 Hz)	207.4 (dd, 1C, ² J _{CP} = 12.5 Hz, ² J _{CP} = 10.3 Hz), 198.5 (dd, 1C, ² J _{CP} = 13.6 Hz, ² J _{CP} = 7.9 Hz), 178.9 (dd, 1C, ² J _{CP} = 8.0 Hz, ² J _{CP} = 6.9 Hz)
[IrRu(H)(CO) ₃ (μ - κ^1 - η^2 -C(H)=C(H)CH ₃)(dppm) ₂][BF ₄] (19) ^f	n/a	46.1 (ddd, 1P, ² J _{pp} = 252.7 Hz, ² J _{pp} = 38.8 Hz, ³ J _{pp} = 16.6 Hz), 24.8 (ddd, 1P, ² J _{pp} = 252.7 Hz, ² J _{pp} = 62.1 Hz, ³ J _{pp} = 19.4 Hz), 5.2 (ddd, 1P, ² J _{pp} = 335.9 Hz, ² J _{pp} = 38.8 Hz, ³ J _{pp} = 19.4 Hz), -11.0 (ddd, 1P, ² J _{pp} = 335.9 Hz, ² J _{pp} = 62.1 Hz, ³ J _{pp} = 16.6 Hz)	7.10 (bm, 1H, ³ J _{HH} = 15.3 Hz), 4.84 (dm, 1H, ² J _{HH} = 13.0 Hz), 4.56 (bd, 1H, ² J _{HH} = 15.3 Hz), 4.04 (dm, 1H, ² J _{HH} = 14.8 Hz), 3.91 (dm, 1H, ² J _{HH} = 14.8 Hz), 2.96 (dm, 1H, ² J _{HH} = 13.0 Hz), 2.27 (b, 3H), -9.95 (dd, 1H, ² J _{HP} = 16.9 Hz, ² J _{HP} = 5.3 Hz)	209.3 (dd, 1C, ² J _{CP} = 14.3 Hz, ² J _{CP} = 10.1 Hz), 194.7 (dd, 1C, ² J _{CP} = 11.8 Hz, ² J _{CP} = 9.8 Hz), 192.7 (dd, 1C, ² J _{CP} = 11.5 Hz, ² J _{CP} = 9.6 Hz)
[IrRu(CO) ₃ (dppm) ₂][BF ₄] (20) ^g	n/a	33.1 (m, 2P), 18.2 (m, 2P)	4.15 (bm, 4H)	205.3 (t, 1C, ² J _{CP} = 12.0 Hz), 196.2 (t, 1C, ² J _{CP} = 15.8 Hz), 171.0 (t, 1C, ² J _{CP} = 10.9 Hz)

Table 3-4. Spectroscopic Data for the Compounds (Continued)

Compound	IR (cm ⁻¹) ^a	NMR ^b		
		$\delta(^{31}\text{P}\{\text{H}\})^c$	$\delta(\text{H})^{d,e}$	$\delta(^{13}\text{C}\{\text{H}\})^{d,e}$
[IrRu(CO) ₄ (μ -C=CH ₂)-(dppm) ₂][BF ₄] (21)	2048 (s), 1999 (s), 1947 (s), 1805 (s)	30.2 (m, 2P), 3.3 (m, 2P)	6.72 (bd, 1H, ² J _{HH} = 2.6 Hz), 5.54 (d, 1H, ² J _{HH} = 2.6 Hz), 4.02 (dm, 2H, ² J _{HH} = 13.4 Hz), 2.99 (dm, 2 H, ² J _{HH} = 13.4 Hz)	203.5 (dtt, 1C, ² J _{CC} = 21.7 Hz, ² J _{CP} = 7.4 Hz, ² J _{CP} = 5.2 Hz), 195.9 (t, 1C, ² J _{CP} = 9.3 Hz), 192.9 (dt, 1C, ² J _{CC} = 21.7 Hz, ² J _{CP} = 10.3 Hz), 179.2 (t, 1C, ² J _{CP} = 10.1 Hz)
[IrRu(H)(CO) ₃ (μ - κ^1 - η^2 -C≡CH)(dppm) ₂][BF ₄] (22) ^f	n/a	27.7 (m, 2P), -12.7 (m, 2P)	4.31 (dm, 2H, ² J _{HH} = 14.1 Hz), 3.77 (bs, 1H), 3.24 (dm, 2H, ² J _{HH} = 14.1 Hz), -9.63 (t, 1H, ² J _{HP} = 11.1 Hz)	207.3 (t, 1C, ² J _{CP} = 11.3 Hz), 198.6 (t, 1C, ² J _{CP} = 14.2 Hz), 177.7 (t, 1C, ² J _{CP} = 9.3 Hz)
[IrRu(H)(CO) ₃ (μ - κ^1 - η^2 -CH=C=CH ₂)(dppm) ₂][BF ₄] (23) ^f	n/a	45.0 (ddd, 1P, ² J _{PP} = 254.5 Hz, ² J _{PP} = 41.3 Hz, ³ J _{PP} = 13.8 Hz), 23.7 (ddm, 1P, ² J _{PP} = 254.5 Hz, ² J _{PP} = 60.2 Hz), 3.8 (ddm, 1P, ² J _{PP} = 335.3 Hz, ² J _{PP} = 41.3 Hz), -12.7 (ddd, 1P, ² J _{PP} = 335.5 Hz, ² J _{PP} = 60.2 Hz, ³ J _{PP} = 13.8 Hz)	6.79 (m, 1H), 4.88 (m, 1H), 4.74 (dm, 1H, ² J _{HH} = 12.8 Hz), 4.57 (m, 1H), 4.04 (dm, 1H, ² J _{HH} = 14.4 Hz), 3.91 (dm, 1H, ² J _{HH} = 12.8 Hz), 3.09 (dm, 1H, ² J _{HH} = 14.4 Hz), -9.96 (dm, 1H, ² J _{HP} = 17.1 Hz)	205.2 (t, 1C, ² J _{CP} = 14.3 Hz), 196.2 (t, 1C, ² J _{CP} = 11.3 Hz), 178.1 (t, 1C, ² J _{CP} = 7.0 Hz)
[IrRu(H)(CO) ₃ (μ - κ^1 - η^2 -C≡CC(H ₃)(dppm) ₂][BF ₄] (24) ^h	n/a	32.6 (m, 2P), -9.9 (m, 2P)	4.45 (dm, 2H, ² J _{HH} = 14.7 Hz), 3.17 (dm, 2H, ² J _{HH} = 14.7 Hz), 0.76 (t, 3H, ⁵ J _{HP} = 2.5 Hz), -9.69 (t, 1H, ² J _{HP} = 12.7 Hz)	208.1 (t, ² J _{CP} = 11.8 Hz), 198.8 (t, 1C, ² J _{CP} = 14.5 Hz), 177.5 (t, 1C, ² J _{CP} = 8.7 Hz)

Table 3-4. Spectroscopic Data for the Compounds (Continued)

Compound	NMR ^b		
	IR (cm ⁻¹) ^a	$\delta(^{31}\text{P}\{^1\text{H}\})^c$	$\delta(^{13}\text{C}\{^1\text{H}\})^{d,e}$
[IrRu(CO) ₄ (H ₂ C=C=CH ₂)- (dppm) ₂][BF ₄] ^f (25) ^g	n/a	28.6 (m, 2P), -4.6 (m, 2P)	5.97 (s, 1H), 5.23 (s, 1H), 4.31 (dm, 2H, ² J _{HH} = 15.1 Hz), 4.13 (dm, 2H, ² J _{HH} = 15.1 Hz), 0.63 (bt, 2H, ³ J _{HP} = 7.1 Hz)
			210.8 (b, 1C), 208.2 (b, 1C), 190.3 (b, 1C), 186.5 (b, 1C)

^a IR abbreviations: s = strong, m = medium. Dichloromethane solution; in units of cm⁻¹. ^b NMR abbreviations: s = singlet, d = doublet, t = triplet, q = quartet, m = multiplet, b = broad. NMR data at 27 °C in CD₂Cl₂ unless otherwise indicated. ^c ³¹P chemical shifts referenced to external 85% H₃PO₄. ^d ¹H and ¹³C chemical shifts referenced to TMS. ^e Chemical shifts for the phenyl carbons and protons not given. ^f Data acquired at -20 °C. ^g Data acquired at -78 °C. ^h Data acquired at 0 °C.

0.5 equiv of dichloromethane was confirmed by X-ray crystal structure analysis. **Method ii.** A stirred yellow solution of compound **13** (100 mg, 0.079 mmol) in 5 mL of CH₂Cl₂ was saturated with propyne gas, and left to stir under a propyne atmosphere. No colour change was noted, but after 8 h of stirring at ambient temperature, the ³¹P {¹H} NMR spectrum revealed compound **14** as the only phosphorus-containing product. After reduction of the solvent volume by 50%, the addition of 20 mL of diethyl ether followed by 20 mL of pentane resulted in the precipitation of a yellow solid that was rinsed with 3 x 10 mL of diethyl ether and dried in vacuo.

- (b) **[IrRu(CO)₄(μ-C=C(H)CH₂CH₃)(dppm)₂][BF₄] (15).** A stirred yellow solution of **13** (92 mg, 0.073 mmol) in 5 mL of CH₂Cl₂ was saturated with 1,2-butadiene (methylallene) gas and was left to stir under an atmosphere of the gas for 24 h, after which time the colour had darkened to deep orange. Slow addition of 50 mL of pentane resulted in the precipitation of an orange solid that was rinsed with 2 x 5 mL of pentane and dried in vacuo (80 % yield). HRMS: *m/z* calcd for C₅₈H₅₀IrO₄P₄Ru (M⁺), 1229.1327; found, 1229.1331 (M⁺). Elemental analyses were carried out on **15-CF₃SO₃**. Anal. Calcd for C₅₉F₃H₅₀IrO₇P₄RuS: C, 51.38; H, 3.63. Found: C, 51.03; H, 3.98.
- (c) **[IrRu(CO)₄(μ-C=C(H)C(CH₃)=CH₂)(dppm)₂][BF₄] (16).** Compound **13** (73 mg, 0.058 mmol) was dissolved in 4 mL of 1:1 CH₂Cl₂/THF to afford a yellow slurry. To this yellow slurry was added 100 μL of 1,1-dimethylallene (1.0 mmol, 18 equiv) by micro-syringe. The solution was left to stir under Ar for 48 h at ambient temperature. Addition of 20 mL of diethyl ether followed by 40 mL of pentane resulted in the precipitation of a yellow solid that was rinsed with 3 x 10 mL of diethyl ether and dried in vacuo (88 % yield). HRMS: *m/z* calcd for C₅₉H₅₀IrO₄P₄Ru (M⁺), 1241.1327; found, 1241.1327 (M⁺). Elemental analyses were carried out on **16-CF₃SO₃**. Anal. Calcd for C₆₀F₃H₅₀IrO₇P₄RuS: C, 51.87; H, 3.63. Found: C, 51.41; H, 3.96.

- (d) $[\text{IrRu}(\text{CO})_4(\mu\text{-}\kappa^1\text{:}\kappa^1\text{-F}_2\text{C}=\text{C}-\text{CH}_2)(\text{dppm})_2][\text{BF}_4]$ (17) and $[\text{IrRu}(\text{CO})_4(\mu\text{-}\kappa^1\text{:}\kappa^1\text{-H}_2\text{C}-\text{C}=\text{CF}_2)(\text{dppm})_2][\text{BF}_4]$ (17a).

Compound **13** (50 mg, 0.040 mmol) was partially dissolved in 0.7 mL of CD_2Cl_2 in an NMR tube fitted with a J. Young valve to afford a yellow slurry. The NMR tube was cooled to $-78\text{ }^\circ\text{C}$ and the 1,1-difluoroallene, generated as described above, was condensed into the tube. Warming the NMR tube to ambient temperature over 20 min revealed, by ^{31}P NMR, the formation of the 1,1-difluoroallene adduct, $[\text{IrRu}(\text{CO})_4(\mu\text{-}\kappa^1\text{:}\kappa^1\text{-F}_2\text{C}=\text{C}-\text{CH}_2)(\text{dppm})_2][\text{BF}_4]$ (**17**), which was characterized by multinuclear NMR at $-20\text{ }^\circ\text{C}$. Warming **17** to ambient temperature resulted in the formation of the isomer $[\text{IrRu}(\text{CO})_4(\mu\text{-}\kappa^1\text{:}\kappa^1\text{-H}_2\text{C}-\text{C}=\text{CF}_2)(\text{dppm})_2][\text{BF}_4]$ (**17a**) within 24 h, which was also characterized by multinuclear NMR at $-20\text{ }^\circ\text{C}$. At temperatures above $-20\text{ }^\circ\text{C}$ compound **17a** decomposed within 4 h. ^{19}F NMR of **17** ($-20\text{ }^\circ\text{C}$): δ -72.2 (bd, 1F, $^2J_{\text{FF}} = 58.6$ Hz), δ -91.6 (bd, 1F, $^2J_{\text{FF}} = 58.6$ Hz). ^{19}F NMR of **17a** ($-20\text{ }^\circ\text{C}$): δ -68.7 (bd, 1F, $^2J_{\text{FF}} = 66.5$ Hz), δ -94.3 (bd, 1F, $^2J_{\text{FF}} = 66.5$ Hz). No HRMS or elemental analyses could be obtained for either of these products due to their instability at ambient temperature.

- (e) $[\text{IrRuH}(\text{CO})_3(\mu\text{-}\kappa^1\text{:}\eta^2\text{-C(H)=CH}_2)(\text{dppm})_2][\text{BF}_4]$ (**18**). A mixture of anhydrous trimethylamine *N*-oxide (TMNO) (0.75 equiv, 2.0 mg, 0.027 mmol) that was dried according to the literature procedure,²² and compound **13** (45 mg, 0.036 mmol) was partially dissolved in 0.7 mL of CD_2Cl_2 in an NMR tube fitted with a J. Young valve to afford a yellow slurry, and was quickly cooled to $-78\text{ }^\circ\text{C}$. The argon headspace of the NMR tube was then evacuated at $-78\text{ }^\circ\text{C}$, filled with ethylene gas (6 mL via gastight syringe), warmed to $-20\text{ }^\circ\text{C}$ and left to react at this temperature for 2 h. The sample was inserted into an NMR probe which had been precooled to $-20\text{ }^\circ\text{C}$ (in previous experiments, no new species were observed below $-20\text{ }^\circ\text{C}$). At $-20\text{ }^\circ\text{C}$ compound **18** was observed in a 3:1 ratio with compound **13** (based on integration of the $^{31}\text{P}\{^1\text{H}\}$ NMR

resonances). Less than 1 equiv of TMNO was used as compound **18** decomposed readily in the presence of excess TMNO. Compound **18** could not be isolated and purified due to instability at ambient temperature, so its characterization was based on multinuclear NMR spectroscopy at $-20\text{ }^{\circ}\text{C}$.

- (f) **[IrRuH(CO)₃(μ - κ^1 : η^2 -C(H)=C(H)CH₃)(dppm)₂][BF₄] (19).** A mixture of anhydrous TMNO (0.75 equiv, 2.0 mg, 0.027 mmol) and compound **13** (45 mg, 0.036 mmol) was partially dissolved in 0.7 mL of CD₂Cl₂ in an NMR tube fitted with a J. Young valve to afford a yellow slurry, and was quickly cooled to $-78\text{ }^{\circ}\text{C}$. The argon headspace of the NMR tube was then evacuated at $-78\text{ }^{\circ}\text{C}$, filled with propylene gas (6 mL, via gastight syringe), warmed to $-20\text{ }^{\circ}\text{C}$ and left to react at that temperature for 2 h. The sample was inserted into an NMR probe which had been precooled to $-20\text{ }^{\circ}\text{C}$, (below which, no new species were observed). At $-20\text{ }^{\circ}\text{C}$ compound **19** formed in a 3:1 ratio with compound **13**. Less than 1 equiv of TMNO was used as compound **19** decomposed readily in the presence of excess TMNO. Compound **19** could not be isolated or purified due to its instability at ambient temperature, so characterization was based on multinuclear NMR spectroscopy at $-20\text{ }^{\circ}\text{C}$.
- (g) **[IrRu(CO)₃(dppm)₂][BF₄] (20).** Compound **13** (50 mg, 0.040 mmol) was dissolved in 5 mL of CH₂Cl₂ to afford a yellow solution. Anhydrous TMNO (1.0 equiv, 0.040 mmol, 3.0 mg) was dissolved in 1 mL of CH₂Cl₂ in an NMR tube affording a clear, colourless solution. The TMNO solution was transferred dropwise, via cannula, to the Schlenk flask containing the stirring yellow solution of **13** and the solution turned orange immediately. The addition of 30 mL of diethyl ether followed by 20 mL of pentane resulted in the precipitation of an orange solid that was washed with 3 x 10 mL of diethyl ether and dried in vacuo (67 % yield). Owing to the instability of **20** (even as a solid product), its characterization was based on multinuclear NMR spectroscopy at $-80\text{ }^{\circ}\text{C}$.

- (h) **[IrRu(CO)₄(μ -C=CH₂)(dppm)₂][BF₄] (21).** A stirred yellow solution of **13** (100 mg, 0.079 mmol) in 5 mL of CH₂Cl₂ was saturated with acetylene gas and left to stir under an atmosphere of the gas for 4 h, resulting in a colour change to orange. The addition of 20 mL of diethyl ether followed by 40 mL of pentane resulted in the precipitation of an orange solid that was washed with 3 x 10 mL of diethyl ether and dried in vacuo (90 % yield). HRMS: *m/z* calcd for C₅₆H₄₆IrO₄P₄Ru (M⁺), 1201.1014; found, 1201.1049 (M⁺). Elemental analyses were done using **21-CF₃SO₃**, in which the tetrafluoroborate anion had been exchanged for triflate. Anal. Calcd for C_{57.5}ClF₃H₅₁IrO₇P₄RuS: C 49.48; H 3.68. Found: C 49.55; H 3.43. Incorporation of 0.5 equiv of CH₂Cl₂ was confirmed by the X-ray crystal structure analysis.
- (i) **[IrRu(H)(CO)₃(μ - κ^1 : η^2 -C \equiv CH)(dppm)₂][BF₄] (22).** Compound **21** (50 mg, 0.039 mmol) was dissolved in 0.5 mL of CD₂Cl₂ in an NMR tube to afford an orange solution and cooled to 0 °C. To this solution was added anhydrous TMNO (1 equiv, 0.039 mmol, 2.9 mg) as a solution in CD₂Cl₂, resulting in no obvious colour change. The reaction was left for 1 h at -20 °C after which time the sample was inserted into an NMR spectrometer precooled to -20 °C. Compound **22** was the only phosphorus-containing product observed and was characterized by multinuclear NMR spectroscopy at -20 °C, as the compound was only stable in solution at lower than ambient temperatures and decomposed upon attempted work up.
- (j) **[IrRu(H)(CO)₃(μ - κ^1 : η^2 -CH=C=CH₂)(dppm)₂][BF₄] (23).** A mixture of anhydrous TMNO (0.75 equiv, 2.0 mg, 0.027 mmol) and compound **13** (45 mg, 0.036 mmol) was partially dissolved in 0.7 mL of CD₂Cl₂ in an NMR tube fitted with a J. Young valve to afford a yellow slurry, and was quickly cooled to -20 °C. The argon headspace of the NMR tube was then evacuated at -20 °C, filled with allene gas (6 mL, via gastight syringe), and left to react at that temperature for 1 h. The sample

was inserted into an NMR probe which had been precooled to $-20\text{ }^{\circ}\text{C}$, (below which, no new species were observed). At $-20\text{ }^{\circ}\text{C}$ up to 67 % of the phosphorus-containing products were assigned to **23**. Less than 1 equiv of TMNO was used as compound **23** decomposed readily in the presence of excess TMNO. Compound **23** could not be isolated or purified due to its instability at ambient temperature, so its characterization was based on multinuclear NMR spectroscopy at $-20\text{ }^{\circ}\text{C}$.

- (k) **[IrRu(H)(CO)₃(μ - κ^1 : η^2 -C \equiv CCH₃)(dppm)₂][BF₄] (24). Method i.** Compound **14** (30 mg, 0.023 mmol) was dissolved in 0.5 mL of CD₂Cl₂ in an NMR tube to afford a yellow/orange solution and cooled to 0 °C. To this solution was added anhydrous TMNO (1 equiv, 0.023 mmol, 1.7 mg) as a solution in CD₂Cl₂, resulting in no obvious colour change. The reaction was left for 1 h at 0 °C after which time the sample was inserted into an NMR spectrometer precooled to 0 °C. Compound **24** was the only phosphorus-containing product and was characterized by multinuclear NMR spectroscopy at 0 °C, as the compound was only stable in solution at lower than ambient temperatures, decomposing upon attempted work up. **Method ii.** Compound **20** (25 mg, 0.020 mmol) was dissolved in 0.7 mL of CD₂Cl₂ in an NMR tube. The NMR tube was cooled to 0 °C and the solution was purged with propyne for 1 min and left to react at 0 °C for 1 h, after which time the sample was placed in a precooled NMR spectrometer. Compound **24** was the only phosphorus-containing product identified by ³¹P{¹H} NMR at that temperature.
- (l) **Variable temperature NMR study of [IrRu(CO)₃(dppm)₂][BF₄] (20) and allene: generation of [IrRu(CO)₄(H₂C=C=CH₂)-(dppm)₂][BF₄] (25).** Compound **20** (27 mg, 0.022 mmol) was dissolved in 0.7 mL of CD₂Cl₂ in an NMR tube equipped with a J. Young valve to afford an orange solution. The tube was quickly cooled to $-78\text{ }^{\circ}\text{C}$ and the headspace of the tube was evacuated and allene gas was added (5 mL via gastight syringe). The sample was placed into the NMR

spectrometer precooled to $-78\text{ }^{\circ}\text{C}$. At this temperature, the entire sample had converted to the allene adduct, $[\text{IrRu}(\text{CO})_4(\eta^2\text{-H}_2\text{C}=\text{C}=\text{CH}_2)(\text{dppm})_2][\text{BF}_4]$ (**25**), by scavenging a CO ligand from decomposition of one-third of compound **20**, as determined by integration of the ^{31}P resonances using a ^{31}P standard, bis(triphenylphosphoranylidene) ammonium chloride. At temperatures as low as $-60\text{ }^{\circ}\text{C}$ the weakly bound allene dissociated from the complex, leaving only the tetracarbonyl complex $[\text{IrRu}(\text{CO})_4(\text{dppm})_2]^+$ (**13**).^{13a}

- (m) Attempted reaction of 1 with 2-methyl-1,3-butadiene.** Compound **13** (20 mg, 0.016 mmol) was dissolved in 0.5 mL CD_2Cl_2 in an NMR tube. To the yellow solution was added 151 μL of 2-methyl-1,3-butadiene (100 equiv, 1.51 mmol) by micro-syringe. The solution was left to react at ambient temperature for one week and after this time the ^{31}P NMR spectrum revealed compound **13** as the only phosphorus-containing product. Slightly elevated temperatures did not result in any reaction.

3.4.3 X-ray Structure Determinations

3.4.3.1 General

Crystals were grown via slow diffusion of diethyl ether into a dichloromethane solution of the compound (**14-CF₃SO₃**, **21-CF₃SO₃**) or by diffusion of pentane into a tetrahydrofuran solution of the compound (**16-CF₃SO₃**). Data were collected using a Bruker SMART 1000 CCD detector/PLATFORM diffractometer with the crystals cooled to $-80\text{ }^{\circ}\text{C}$ (**14-CF₃SO₃**, **21-CF₃SO₃**) or with a Bruker APEX II CCD detector/D8 diffractometer²⁵ with the crystals cooled to $-100\text{ }^{\circ}\text{C}$ (**16-CF₃SO₃**); all data were collected using Mo $K\alpha$ radiation ($\lambda = 0.71073\text{ \AA}$). The data were corrected for absorption via a multi-scan method (**14-CF₃SO₃**, **21-CF₃SO₃**) or through Gaussian integration from indexing of the crystal faces (**16-CF₃SO₃**). Structures were solved using direct methods (*SHELXS-97*)²⁶ and least-squares refinements were completed using the program *SHELXL-97*.²⁶ Hydrogen atoms attached to carbons were assigned positions based on the sp^2 or sp^3 hybridization geometries

of their attached carbons, and were given thermal parameters 20 % greater than those of their parent atoms. See Appendix III.2 for a listing of crystallographic experimental data for all structures in this chapter.

3.4.3.1 Special Refinement Conditions

i) Compound **14-CF₃SO₃**: Attempts to refine peaks of residual electron density as solvent dichloromethane or diethyl ether molecules were unsuccessful. The data were corrected for disordered electron density through use of the *SQUEEZE* procedure²⁷ as implemented in *PLATON*.²⁸ A total solvent-accessible void volume of 1885 Å³ with a total electron count of 685 (consistent with one equivalent of diethyl ether and 0.5 equivalents of dichloromethane per unit of the complex cation) was found in the unit cell. Bond distances and angles within the minor (25 %) orientation of the disordered triflate were restrained during refinement to be equal to the corresponding values within the major orientation by use of the *SHELXL-97*²⁶ SAME instruction.

(ii) Compound **16-CF₃SO₃**: Attempts to refine peaks of residual electron density as disordered or partial-occupancy solvent tetrahydrofuran carbon or oxygen atoms were unsuccessful. The data were corrected for disordered electron density through use of the *SQUEEZE*²⁷ procedure as implemented in *PLATON*.²⁸ A total solvent-accessible void volume of 1715.9 Å³ with a total electron count of 566 (consistent with 14 molecules of tetrahydrofuran, or 3.5 molecules per formula unit of the IrRu complex) was found in the unit cell. A crystallographic mirror plane perpendicular to the metal phosphorus vectors contains the Ru atom. However, the iridium position is disordered on either side of this mirror plane. As a result of this disorder involving the Ir position the ligands attached to this metal are similarly disordered above and below the mirror plane, as shown in Figure 3-5. Twinning was not detected in this crystal.

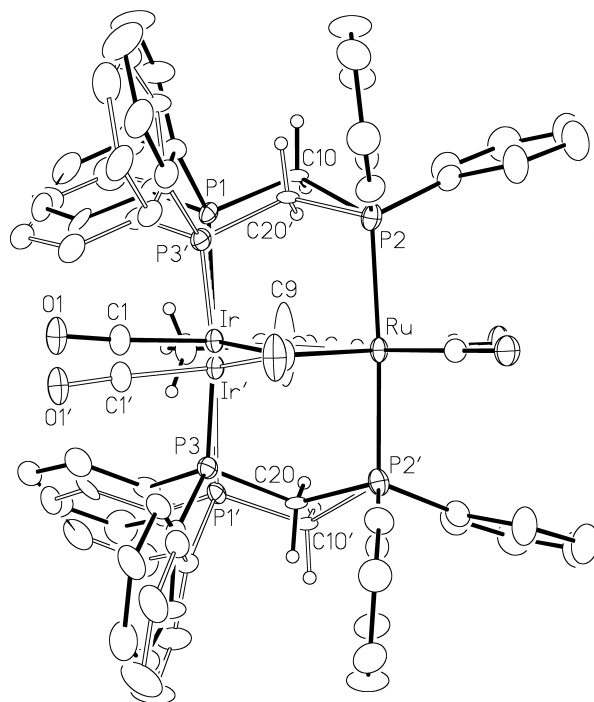


Figure 3-5. *View of the complex cation of $[\text{IrRu}(\text{CO})_4(\mu\text{-C}=\text{C}(\text{H})\text{C}(\text{CH}_3)=\text{CH}_2)(\text{dppm})_2][\text{CF}_3\text{SO}_3]$ (**16-CF₃SO₃**), showing the disorder across the mirror plane that predominately affects the Ir half of the cation. One disordered molecule is connected by solid bonds while the other is connected by open bonds.*

(iii) **21-CF₃SO₃**: The triflate ion was determined to be disordered over two different sites. At one of these (at approximate crystal coordinates [0.38, 0.46, 0.52]) the triflate ion was defined with two sets of equally-abundant (25 % occupancy) positions ($\{\text{S}(2\text{A}), \text{F}(94\text{A}), \text{F}(95\text{A}), \text{F}(96\text{A}), \text{O}(94\text{A}), \text{O}(95\text{A}), \text{O}(96\text{A}), \text{C}(92\text{A})\}$ and $\{\text{S}(2\text{B}), \text{F}(94\text{B}), \text{F}(95\text{B}), \text{F}(96\text{B}), \text{O}(94\text{B}), \text{O}(95\text{B}), \text{O}(96\text{B}), \text{C}(92\text{B})\}$). Distances within these sets of atoms were restrained during refinement: $d(\text{S}-\text{O}) = 1.45(1) \text{ \AA}$; $d(\text{S}-\text{C}) = 1.80(1) \text{ \AA}$; $d(\text{F}-\text{C}) = 1.35(1) \text{ \AA}$; $d(\text{F}\cdots\text{F}) = 2.20(1) \text{ \AA}$; $d(\text{O}\cdots\text{O}) = 2.37(1) \text{ \AA}$. At the same site is located a solvent dichloromethane molecule (refined with an occupancy factor of 50 %) to which the following restraints were applied: $d(\text{Cl}-\text{C}) = 1.80(1) \text{ \AA}$; $d(\text{Cl}\cdots\text{Cl}) = 2.95(1) \text{ \AA}$. (The atoms at the other triflate ion site [0.76, 0.42, 0.0], located near the

crystallographic twofold rotational axis $[3/4, y, 0]$, were refined with an occupancy factor of 50 % and with no geometric restraints applied.)

3.5 References

- (a) Dyker, G. *Handbook of C-H Transformations*; Wiley-VCH: Weinheim, 2005. (b) Labinger, J. A.; Bercaw, J. E. *Nature* **2002**, *417*, 507. (c) Lewis, J. C.; Bergman, R. G.; Ellman, J. A. *Acc. Chem. Res.* **2008**, *41*, 1013. (d) Slugovc, C.; Padilla-Martínez, I.; Sirol, S.; Carmona, E. *Coord. Chem. Rev.* **2001**, *213*, 129. (e) Jones, W. D. In *Comprehensive Organometallic Chemistry III*; 3rd ed.; Parkin, G., Ed.; Elsevier: New York, 2007, p 699.
- (a) Lim, Y.-G.; Kang, J.-B.; Kim, Y. H. *Chem. Commun.* **1996**, 585. (b) Stoutland, P. O.; Bergman, R. G. *J. Am. Chem. Soc.* **1988**, *110*, 5732. (c) Stoutland, P. O.; Bergman, R. G. *J. Am. Chem. Soc.* **1985**, *107*, 4581. (d) Papenfuhs, B.; Dirnberger, T.; Werner, H. *Can. J. Chem.* **2006**, *84*, 205. (e) Ristic-Petrovic, D.; Torkelson, J. R.; Hilts, R. W.; McDonald, R.; Cowie, M. *Organometallics* **2000**, *19*, 4432. (f) Peng, T.-S.; Gladysz, J. A. *Organometallics* **1995**, *14*, 898. (g) Cao, D. H.; Stang, P. J.; Arif, A. M. *Organometallics* **1995**, *14*, 2733. (h) Bhalla, G.; Oxgaard, J.; Goddard III, W. A.; Periana, R. A. *Organometallics* **2005**, *24*, 5499. (i) Dirnberger, T.; Werner, H. *Organometallics* **2005**, *24*, 5127. (j) Alvarado, Y.; Boutry, O.; Gutiérrez, E.; Monge, A.; Nicasio, M. C.; Poveda, M. L.; Pérez, P. J.; Ruíz, C.; Bianchini, C.; Carmona, E. *Chem. Eur. J.* **1997**, *3*, 860.
- Lee, D.-H.; Kwon, K.-H.; Yi, C. S. *Science* **2011**, *333*, 1613.
- (a) Bell, T. W.; Brough, S.-A.; Partridge, M. G.; Perutz, R. N.; Rooney, A. D. *Organometallics* **1993**, *12*, 2933. (b) Bianchini, C.; Barbaro, P.; Meli, A.; Peruzzini, M.; Vacca, A.; Vizza, F. *Organometallics* **1993**, *12*, 2505.
- Ghosh, C. K.; Hoyano, J. K.; Krentz, R.; Graham, W. A. G. *J. Am. Chem. Soc.* **1989**, *111*, 5480.

6. (a) Fryzuk, M. D.; Jones, T.; Einstein, F. W. B. *Organometallics* **1984**, *3*, 185. (b) Suzuki, H.; Omori, H.; Hwan Lee, D.; Yoshida, Y.; Fukushima, M.; Tanaka, M.; Moro-oka, Y. *Organometallics* **1994**, *13*, 1129. (c) Suzuki, H.; Omori, H.; Moro-oka, Y. *Organometallics* **1988**, *7*, 2759. (d) Jia, G.; Meek, D. W.; Gallucci, J. D. *Organometallics* **1990**, *9*, 2549.
7. (a) Bell, T. W.; Haddleton, D. M.; McCamley, A.; Partridge, M. G.; Perutz, R., N.; Willner, H. *J. Am. Chem. Soc.* **1990**, *112*, 9212. (b) Boncella, J. M.; Green, M. L. H. *J. Organomet. Chem.* **1987**, *325*, 217. (c) Boncella, J. M.; Green, M. L. H.; O'Hare, D. *J. Chem. Soc., Chem. Commun.* **1986**, 618. (d) Deeming, A., J.; Hasso, S.; Underhill, M.; Canty, A. J.; Johnson, B. F. G.; Jackson, W. G.; Lewis, J.; Matheson, T. W. *J. C. S. Chem. Comm.* **1974**, 807. (e) Deeming, A., J.; Underhill, M. *J. C. S. Chem. Comm.* **1973**, 277. (f) Deeming, A., J.; Underhill, M. *J. C. S. Dalton* **1974**, 1415. (g) Deeming, A. J.; Underhill, M. *J. Organomet. Chem.* **1972**, *42*, C60. (h) Takemori, T.; Inagaki, A.; Suzuki, H. *J. Am. Chem. Soc.* **2001**, *123*, 1762.
8. (a) Kee, T. P.; Gibson, V. C.; Clegg, W. *J. Organomet. Chem.* **1987**, *325*, C14. (b) Gutiérrez-Puebla, E.; Monge, Á.; Nicasio, M. C.; Pérez, P. J.; Poveda, M. L.; Carmona, E. *Chem. Eur. J.* **1998**, *4*, 2225. (c) Slugovc, C.; Mereiter, K.; Trofimenko, S.; Carmona, E. *Angew. Chem. Int. Ed.* **2000**, *39*, 2158. (d) Slugovc, C.; Mereiter, K.; Trofimenko, S.; Carmona, E. *Helv. Chim. Acta.* **2001**, *84*, 2868. (e) Lee, D.-H.; Chen, J.; Faller, J. W.; Crabtree, R. H. *Chem. Comm.* **2001**, 213. (f) Gusev, D. G.; Lough, A. J. *Organometallics* **2002**, *21*, 2601. (g) Kakiuchi, F.; Chatani, N. *Adv. Synth. Catal.* **2003**, *345*, 1077. (h) Clot, E.; Chen, J.; Lee, D.-H.; Sung, S. Y.; Appelhans, L. N.; Faller, J. W.; Crabtree, R. H.; Eisenstein, O. *J. Am. Chem. Soc.* **2004**, *126*, 8795. (i) Crabtree, R. H. *J. Organomet. Chem.* **2004**, *689*, 4083. (j) Grotjahn, D. B.; Hoerter, J. M.; Hubbard, J. L. *J. Am. Chem. Soc.* **2004**, *126*, 8866. (k) Rankin, M. A.; McDonald, R.; Ferguson, M. J.; Stradiotto, M. *Angew. Chem. Int. Ed.* **2005**, *44*, 3603.

- (l) Hong, S. H.; Chlenov, A.; Day, M. W.; Grubbs, R. H. *Angew. Chem. Int. Ed.* **2007**, *46*, 5148.
9. Silvestre, J.; Calhorda, M. J.; Hoffman, R.; Stoutland, P. O.; Bergman, R. G. *Organometallics* **1986**, *5*, 1841.
 10. Torkelson, J. R. PhD. Thesis, University of Alberta, 1998, Chapter 4.
 11. Ristic-Petrovic, D.; Anderson, D. J.; Torkelson, J. R.; Ferguson, M. J.; McDonald, R.; Cowie, M. *Organometallics* **2005**, *24*, 3711.
 12. MacDougall, T. J.; Trepanier, S. J.; Dutton, J. L.; Ferguson, M. J.; McDonald, R.; Cowie, M. *Organometallics* **2011**, *30*, 5882.
 13. (a) Dell'Anna, M. M.; Trepanier, S. J.; McDonald, R.; Cowie, M. *Organometallics* **2001**, *20*, 88. (b) Samant, R. G.; Trepanier, S. J.; Wigginton, J. R.; Xu, L.; Bierenstiel, M.; McDonald, R.; Ferguson, M. J.; Cowie, M. *Organometallics* **2009**, *28*, 3407.
 14. Allen, F. H.; Kennard, O.; Watson, D. G.; Brammer, L.; Orpen, A. G.; Taylor, R. *J. Chem. Soc., Perkin Trans. 2* **1987**, S1.
 15. $r_c(\text{sp}^3) = 0.77 \text{ \AA}$; $r_c(\text{sp}^2) = 0.74 \text{ \AA}$.
 16. Slaney, M. E.; Anderson, D. J.; Ferguson, M. J.; McDonald, R.; Cowie, M. *J. Am. Chem. Soc.* **2010**, *132*, 16544.
 17. (a) Lentz, D.; Willemsen, S. *Organometallics* **1999**, *18*, 3962. (b) Lentz, D.; Nickelt, N.; Willemsen, S. *Chem. Eur. J.* **2002**, *8*, 1205. (c) Lentz, D. *J. Fluorine Chem.* **2004**, *125*, 853.
 18. Maciel, G. E.; McIver Jr., J. W.; Ostlund, N. S.; Pople, J. A. *J. Am. Chem. Soc.* **1970**, *92*, 11.
 19. (a) Antwi-Nsiah, F.; Cowie, M. *Organometallics* **1992**, *11*, 3157. (b) Ristic-Petrovic, D.; Anderson, D. J.; Torkelson, J. R.; McDonald, R.; Cowie, M. *Organometallics* **2003**, *22*, 4647.
 20. Bruce, M. I. *Chem. Rev.* **1991**, *91*, 197.
 21. Slaney, M. E.; Anderson, D. J.; Ferguson, M. J. D.; McDonald, R.; Cowie, M. *Accepted for publication in Organometallics, January 16, 2012.*
 22. Soderquist, J. A.; Anderson, C. L. *Tetrahedron Lett.* **1986**, *27*, 3961.
 23. Miller, J. S.; Caulton, K. G. *J. Am. Chem. Soc.* **1975**, *97*, 1067.

24. Drakesmith, F. G.; Stewart, O. J.; Tarrant, P. *J. Org. Chem.* **1968**, *33*, 280.
25. Programs for diffractometer operation, unit cell indexing, data collection, data reduction and absorption correction were those supplied by Bruker.
26. Sheldrick, G. M. *Acta Crystallogr.* **2008**, *A64*, 112.
27. van der Sluis, P.; Spek, A. L. *Acta Crystallogr.* **1990**, *A46*, 194.
28. Spek, A. L. *Acta Crystallogr.* **1990**, *A64*, C34. PLATON - a multipurpose crystallographic tool. Utrecht University, Utrecht, The Netherlands.

Chapter 4: Alkyne/Methylene Coupling at Adjacent Iridium/Osmium Centres: Facile Carbon–Carbon and Carbon–Oxygen Bond Formation*

4.1 Introduction

Continuing with the investigation of the methylene-bridged bis(diphosphine) complexes of Ir/M (M = Ru, Os), this chapter describes forays into the relatively unexamined Ir/Os metal combination. In the previous chapters, it has been demonstrated that the introduction of Ir to the bimetallic complex often leads to C–H bond activation reactions as well as C–C bond formation, however, the disparity between the Ir–C and Ru–C bond strengths often results in the hydrocarbyl fragment not bridging the complex, but chelating on the iridium centre.¹ The search for the metal combination that will allow for the careful study of hydrocarbyl-bridged fragments important for processes such as the Fischer-Tropsch (FT) chemistry,² then continues. Exploiting the greater bond strengths involving these third-row metals (Ir/Os), we hoped might stabilize species not observed with the other metal combinations, allowing us to study them in greater detail in terms of possible involvement in carbon-carbon chain growth in FT chemistry.²⁻³

Changing the group 8 metal to Ru appears to have provided a more labile metal centre as the adjacent Ir participated in multiple C–H bond activations.¹ Considering that only the Rh/Os⁴ combination demonstrated incorporation of up to four methylene groups, the next logical system was Ir/Os. In this chapter, we outline our attempts to generate C₃- and C₄-bridged hydrocarbyl fragments, by reactions of either the methylene-bridged (C₁) complexes [IrOs(CO)_n(μ-CH₂)(dppm)₂][X] (*n* = 3, 4; R = CF₃, CO₂Me; X = BF₄, CF₃SO₃) with alkynes, or by reaction of the alkyne-bridged (C₂) precursors [IrOs(CO)_n(μ-κ¹:κ¹-

* A version of this chapter has been published. MacDougall, T. J.; Llamazares, A.; Kuhnert, O.; Ferguson, M. J.; McDonald, R.; Cowie, M. *Organometallics* **2011**, *30*, 952.

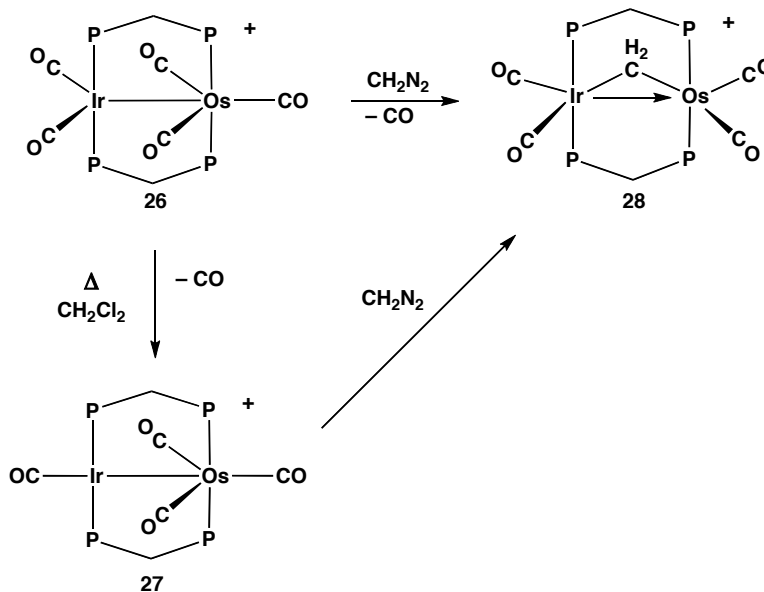
$\text{RC}=\text{CR})(\text{dppm})_2][\text{CF}_3\text{SO}_3]$ ($n = 3, 4$; $\text{R} = \text{CF}_3, \text{CO}_2\text{Me}$) with diazomethane. The reactivity of this system is also compared to the related work involving the other metal combinations.⁴⁻⁵

4.2 Results and Compound Characterization

4.2.1 Methylene-Bridged Precursor

The precursor methylene-bridged complex, $[\text{IrOs}(\text{CO})_4(\mu\text{-CH}_2)(\text{dppm})_2][\text{CF}_3\text{SO}_3]$ (**28**), is readily prepared by reaction of either $[\text{IrOs}(\text{CO})_5(\text{dppm})_2][\text{CF}_3\text{SO}_3]$ (**26**) or $[\text{IrOs}(\text{CO})_4(\text{dppm})_2][\text{CF}_3\text{SO}_3]$ (**27**) with diazomethane at ambient temperature (see Scheme 4-1). One carbonyl in compound **26** is labile and readily lost in the reaction, generating the identical product as in the reaction of **27**, under identical conditions. Both reactions proceed instantly, even at $-78\text{ }^\circ\text{C}$. No incorporation of additional methylene groups is observed when the reaction is carried out at ambient temperature.

Scheme 4-1



Complex **28** produces the expected pattern in the $^{31}\text{P}\{^1\text{H}\}$ NMR spectrum, characteristic of an $\text{AA}'\text{BB}'$ spin system, corresponding to the Ir- and Os-bound ends of the diphosphines. With both resonances ($\delta -5.5$ and $\delta -6.5$) so close in

chemical shift, as shown in Figure 4-1, which resonance corresponds to the Ir- or Os-bound ends of the diphosphines is not clear.

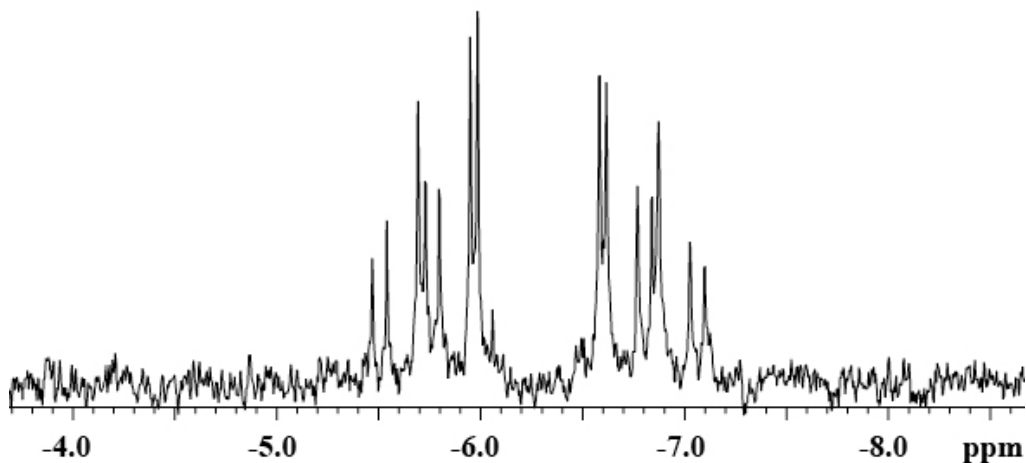


Figure 4-1. $^{31}\text{P}\{^1\text{H}\}$ NMR spectrum of $[\text{IrOs}(\text{CO})_4(\mu\text{-CH}_2)(\text{dppm})_2][\text{CF}_3\text{SO}_3]$ (**28**) in CD_2Cl_2

Through the use of $^{13}\text{C}\{^1\text{H}, ^{31}\text{P}\}$ NMR techniques in which the phosphorus resonances are selectively decoupled, we can determine that two carbonyls display spin-spin coupling with each end of the diphosphine units, so are attached two to each metal, but we are unable to identify which set of ^{31}P resonances is which. The two ^{13}C resonances at δ 185.1 and δ 178.2 correspond to the carbonyls on one metal while those at δ 181.7 and δ 170.0 correspond to the carbonyls on the other; all carbonyls appear to be terminally bound as supported by the IR spectrum in which all carbonyl bands fall in the region above 1900 cm^{-1} . A $^{13}\text{CH}_2$ -enriched sample of **28** shows the $\mu\text{-CH}_2$ carbon in the $^{13}\text{C}\{^1\text{H}\}$ NMR spectrum at δ 46.6 as a very broad multiplet displaying couplings of 9.0 Hz and 8.2 Hz to the chemically inequivalent ^{31}P nuclei. In the ^1H NMR spectrum of **28**, two signals at δ 4.77 and δ 3.36 represent the chemically inequivalent CH_2 protons of the dppm ligands, indicating the absence of “front-back” symmetry on either side of the IrOsP_4 plane. These protons display mutual two-bond coupling of 14.0 Hz. The protons of the newly introduced methylene bridge appear as a

multiplet at δ 4.75. Due to the overlap in the ^1H NMR spectrum between the methylene protons of the dppm ligands and the newly introduced methylene group protons, a 2D HSQC NMR experiment was used to correlate the carbon signal at δ 46.6 to the proton signal at δ 4.75.

An X-ray structure determination of **28**, as shown for the complex cation in Figure 4-2, verifies the bridging arrangement of the methylene group and the symmetrical ligand arrangement having two carbonyls on each metal. Selected bond lengths and angles are presented in Table 4-1.

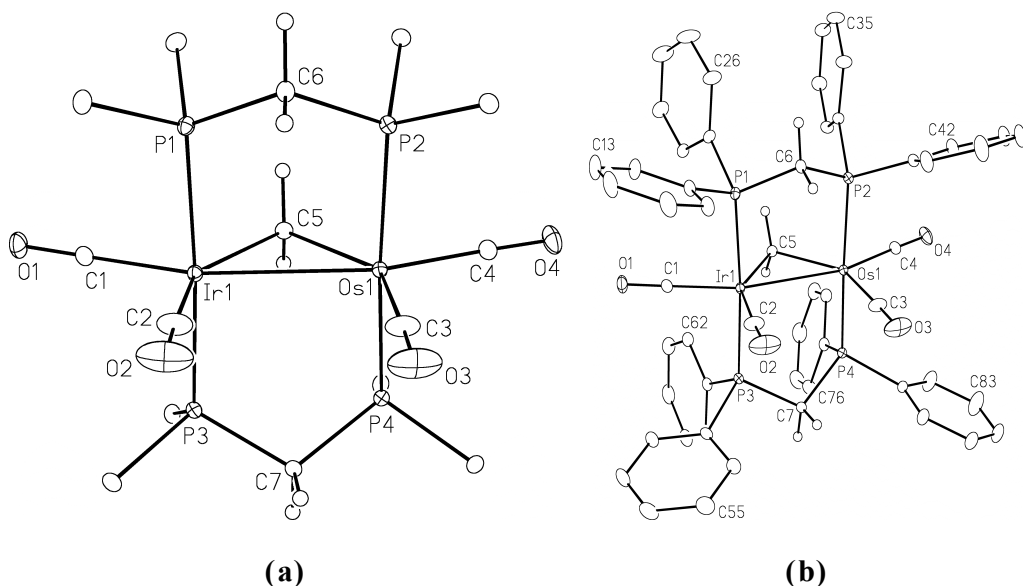


Figure 4-2. (a) Perspective view of the complex cation of $[\text{IrOs}(\text{CO})_4(\mu\text{-CH}_2)(\text{dppm})_2][\text{CF}_3\text{SO}_3]$ (**28**). Thermal ellipsoids are shown at the 20 % probability level except for hydrogens, which are shown artificially small. Only the ipso carbons of the phenyl rings are shown. (b) Same as (a), with all phenyl carbons shown.

As is typical with these A-frame-like complexes, the dppm ligands bridge both metals in a mutually trans arrangement. The Ir–Os separation of 2.8345(1) Å is consistent with a metal–metal bond and is significantly shorter than the intraligand P–P separation of *ca.* 3.00 Å, indicating compression along the Ir–Os

axis due to mutual attraction of the metals. The geometry at both metals is a distorted octahedron in which the distortion in the equatorial plane arises from the acute angles formed by the introduction of the methylene bridge (C(5)–Ir–Os = 48.82(5)° and C(5)–Os–Ir = 48.32(5)°). There is no significant twisting around the metal-metal axis in the complex cation, resulting in an eclipsed conformation of both metals. Torsion angles relating the eclipsed ligands are between *ca.* 3° and 6°. The disorder of the metals, noted in the Experimental section presumably gives rise to a slight, unresolved disorder of the carbonyl ligands which probably gives rise to the somewhat elongated thermal ellipsoids for C(2)O(2) and C(3)O(3).

Table 4-1. Selected Bond Lengths and Angles for Compound 28

(a) Distance (Å)

atom 1	atom 2	distance	atom 1	atom 2	distance
Ir	Os	2.8345(1)	Os	C(4)	1.881(2)
Ir	C(1)	1.887(2)	Os	C(5)	2.150(2)
Ir	C(2)	1.919(3)	C(2)	O(2)	1.139(3)
Ir	C(5)	2.134(2)	C(3)	C(3)	1.144(3)
Os	C(3)	1.919(3)			

(b) Angles (deg)

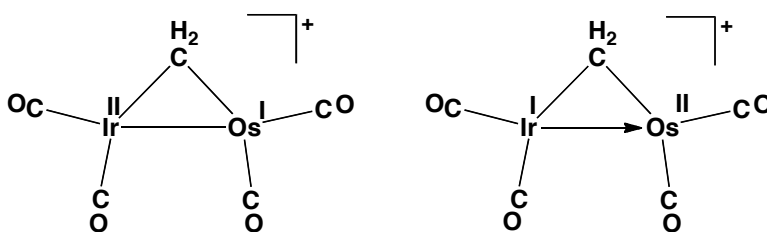
atom	atom 2	atom 3	angle	atom 1	atom 2	atom 3	angle
Ir	C(2)	O(2)	177.3(3)	Os	Ir	C(2)	97.50(10)
Os	C(3)	O(3)	177.8(3)	Ir	Os	C(3)	95.64(10)
Ir	C(5)	Os	82.86(7)	Ir	Os	C(4)	158.63(7)
C(5)	Ir	Os	48.82(5)	C(5)	Os	Ir	48.32(5)
Os	Ir	C(1)	157.74(7)				

The structure of **28** differs significantly from those of its congeners, involving the Rh/Ru, Rh/Os, and Ir/Ru combinations of metals which all have a carbonyl ligand in a site bridging the metals. The absence of a bridging carbonyl in the Ir/Os species (**28**) is consistent with the lower tendency of third-row metals

to support bridging carbonyl ligands.⁶ As such, compound **28** more closely resembles the mono-phosphine analogues $[\text{MM}'(\text{PMe}_3)(\text{CO})_3(\mu\text{-CH}_2)(\text{dppm})_2]^+$ ($\text{MM}' = \text{RhRu},^{5\text{a}} \text{RhOs},^{4\text{b}} \text{IrRu}^{5\text{c}}$), which also have two terminal ligands on each metal.

The bonding in **28** can be described by either of the valence-bond formulations shown in Chart 4-1. In the Ir(II)/Os(I) formulation the metals are connected by a conventional metal–metal bond, while in the Ir(I)/Os(II) formulation the coordinatively saturated Ir centre forms a dative bond to Os to give the latter its favoured $18e^-$ configuration. We favour this latter description, in keeping with the preferred oxidation states of these metals.

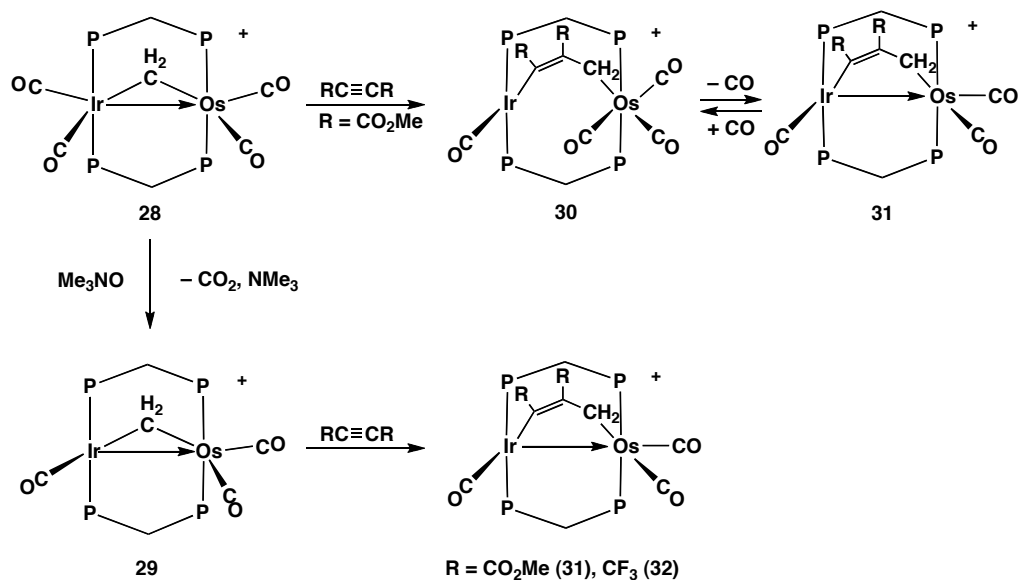
Chart 4-1



4.2.2 C₃-Bridged Species from $[\text{IrOs}(\text{CO})_x(\mu\text{-CH}_2)(\text{dppm})_2][\text{CF}_3\text{SO}_3]$ ($x = 3$ or 4)

The addition of dimethyl acetylenedicarboxylate (DMAD) to the methylene-bridged tetracarbonyl complex $[\text{IrOs}(\text{CO})_4(\mu\text{-CH}_2)(\text{dppm})_2][\text{CF}_3\text{SO}_3]$ (**28**) under ambient conditions results in the insertion of the alkyne into the Ir–CH₂ bond yielding $[\text{IrOs}(\text{CO})_4(\mu\text{-}\kappa^1:\kappa^1\text{-C}(\text{CO}_2\text{CH}_3)=\text{C}(\text{CO}_2\text{CH}_3)\text{CH}_2)(\text{dppm})_2][\text{CF}_3\text{SO}_3]$ (**30**) and $[\text{IrOs}(\text{CO})_3(\mu\text{-}\kappa^1:\kappa^1\text{-C}(\text{CO}_2\text{CH}_3)=\text{C}(\text{CO}_2\text{CH}_3)\text{CH}_2)(\text{dppm})_2][\text{CF}_3\text{SO}_3]$ (**31**), (Scheme 4-2), in a 7:3 ratio, as shown in the $^{31}\text{P}\{^1\text{H}\}$ NMR spectrum in Figure 4-3. The fourth carbonyl ligand of **30** is readily displaced under an argon purge, converting it to **31**, while addition of $\text{CO}_{(\text{g})}$ to the **30/31** mix yields only **30**.

Scheme 4-2



Unlike the facile reaction with DMAD, hexafluorobutyne (HFB) does not react with **28** at ambient temperature. However, decarbonylation of **28** by reaction with sublimed anhydrous trimethylamine *N*-oxide (TMNO) generates the unstable complex $[\text{IrOs}(\text{CO})_3(\mu\text{-CH}_2)(\text{dppm})_2][\text{CF}_3\text{SO}_3]$ (**29**), which undergoes facile alkyne insertion of either DMAD or HFB to generate $[\text{IrOs}(\text{CO})_3(\mu\text{-}\kappa^1:\kappa^1\text{-C}(\text{R})=\text{C}(\text{R})\text{CH}_2)(\text{dppm})_2][\text{CF}_3\text{SO}_3]$ ($\text{R} = \text{CO}_2\text{Me}$ (**31**) or CF_3 (**32**), respectively,

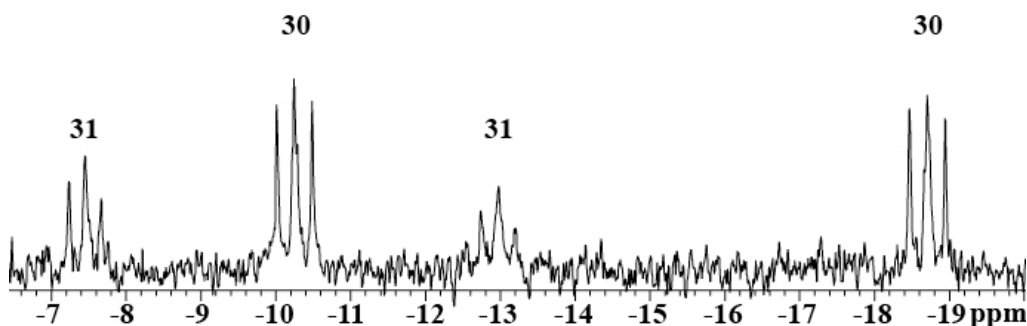


Figure 4-3. $^{31}\text{P}\{^1\text{H}\}$ NMR spectrum of $[\text{IrOs}(\text{CO})_4(\mu\text{-}\kappa^1:\kappa^1\text{-C}(\text{CO}_2\text{CH}_3)=\text{C}(\text{CO}_2\text{CH}_3)\text{CH}_2)(\text{dppm})_2][\text{CF}_3\text{SO}_3]$ (**30**) and $[\text{IrOs}(\text{CO})_3(\mu\text{-}\kappa^1:\kappa^1\text{-C}(\text{CO}_2\text{CH}_3)=\text{C}(\text{CO}_2\text{CH}_3)\text{CH}_2)(\text{dppm})_2][\text{CF}_3\text{SO}_3]$ (**31**) in CD_2Cl_2 .

see Scheme 4-2). The presence of adventitious water, present in unsublimed TMNO, results in the formation of unwanted hydroxide-containing byproducts.

In the case of compounds **30**, **31**, and **32**, their unsymmetrical carbonyl distribution allows the ^{31}P resonances to be identified as Ir- or Os-bound on the basis of ^{13}C NMR experiments employing selective ^{31}P -decoupling, since coupling is only observed between adjacent ^{31}P and ^{13}C moieties. The metal having the greater number of carbonyls is identified as Os on the basis of its greater tendency to be coordinatively saturated. The structures shown in Scheme 4-2 are assigned on the basis of these experiments. A ^{13}CO -enriched sample of **30** displays four terminal CO resonances in the $^{13}\text{C}\{^1\text{H}\}$ NMR spectrum at δ 184.4, δ 177.8, and δ 160.0, corresponding to the Os-bound CO ligands with coupling to the Os-bound phosphorus nuclei of between 5.5 Hz and 7.0 Hz, while one at δ 174.8, corresponds to the sole Ir-bound CO, displaying 10.4 Hz coupling to the Ir-bound phosphorus atoms. A $^{13}\text{CH}_2$ -enriched sample of **30** shows the Os-bound CH_2 carbon in the $^{13}\text{C}\{^1\text{H}\}$ NMR spectrum at approximately δ 47 as a very broad multiplet. This multiplet sharpens noticeably (as seen in line width at 50 % peak height) upon decoupling of the Os-bound phosphorus signal at δ -18.7, but shows no effect upon decoupling the Ir-bound phosphorus signal. In the ^1H NMR spectrum of **30**, two signals at δ 5.13 and δ 4.86 represent the chemically inequivalent CH_2 protons of the dppm ligands, while the Os-bound CH_2 protons appear as a triplet at δ 2.20 with 11.1 Hz coupling to only the two phosphorus nuclei bound to this metal. The absence of coupling of these μ - CH_2 protons to the Ir-bound phosphorus nuclei is consistent with alkyne insertion into the Ir- CH_2 bond. In addition to the above resonances, compound **30** displays two separate resonances for the CH_3 groups of the inserted DMAD molecule at δ 2.38 and δ 1.29.

For compounds **31** and **32**, ^{13}CO -enriched samples each display two resonances at *ca.* δ 185 and δ 180 corresponding to the Os-bound CO ligands showing coupling to only the Os-bound phosphorus atoms of *ca.* 9.4 Hz, while one at *ca.* δ 168 corresponds to the Ir-bound CO, coupling to only the Ir-bound

phosphorus atoms (${}^2J_{CP} = 9.5$ Hz). Again, a ${}^{13}\text{C}_2$ -enriched sample of **31** and **32** shows the Os-bound CH_2 carbons in the ${}^{13}\text{C}\{\text{H}\}$ NMR spectrum as broad multiplets at δ 10.3 and δ 8.0, respectively. In the ${}^1\text{H}$ NMR spectra of **31**, the Os-bound CH_2 protons appear as a triplet at δ 1.53 with 11.4 Hz coupling to the Os-bound ${}^{31}\text{P}$ nuclei, while in **32** these protons appear as a more complex triplet of quartets at δ 1.86 with 8.9 Hz coupling to phosphorus as well as coupling of 2.5 Hz to one CF_3 group. As above, the absence of coupling between these CH_2 protons and the Ir-bound phosphorus nuclei is consistent with alkyne insertion into the Ir- CH_2 bond. In the case of compound **32**, the ${}^{19}\text{F}$ NMR spectrum displays two resonances for the CF_3 groups of the inserted HFB group, as shown in Figure 4-4.

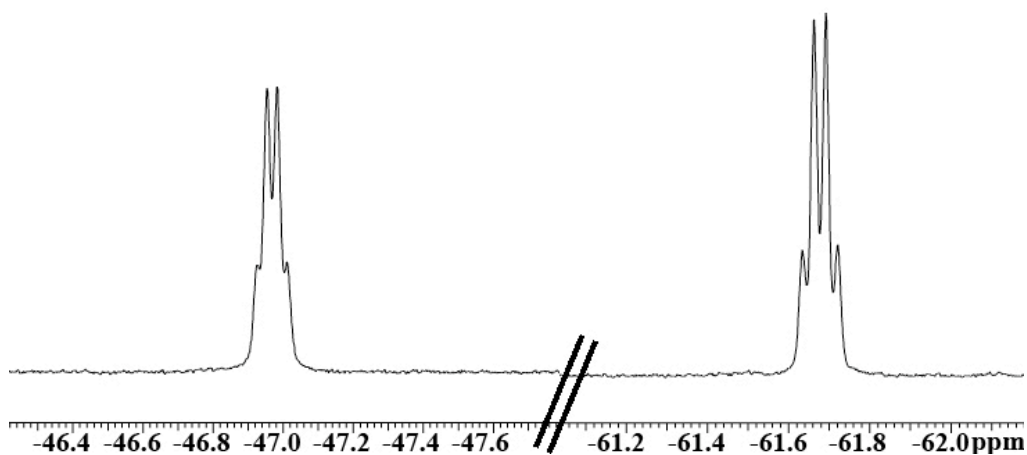


Figure 4-4. Select regions of the ${}^{19}\text{F}$ NMR spectrum of $[\text{IrOs}(\text{CO})_3(\mu\text{-}\kappa^1:\kappa^1\text{-C}(\text{CF}_3)=\text{C}(\text{CF}_3)\text{CH}_2)(\text{dppm})_2][\text{CF}_3\text{SO}_3]$ (**32**) in CD_2Cl_2 .

An X-ray structure determination of **32**, shown for the complex cation in Figure 4-5, verifies that alkyne insertion into the Ir- CH_2 bond has occurred as was proposed based on the above spectroscopic studies. Selected bond lengths and angles are presented in Table 4-2. The geometry at Os is shown to be a rather undistorted octahedron while that at Ir is best described as a tetragonal pyramid in which the axial site corresponds to the Ir-Os bond. Although the nature of the metal-metal bond (2.7910(7) Å) and the corresponding oxidation states of the metals can be ambiguous in such complexes, we again favour an Ir(I)/Os(II)

formulation in which the occupied dz^2 orbital of the square planar Ir forms a dative bond to Os, as is shown in Scheme 4-2. Although the dppm ligands occupy the typical bridging positions, close-to-mutually trans at both metals, they are significantly twisted with respect to each other, resulting in a staggered conformation at both metals, in which the torsion angles about the Ir–Os bond range from $23.48(3)^\circ$ to $28.09(3)^\circ$.

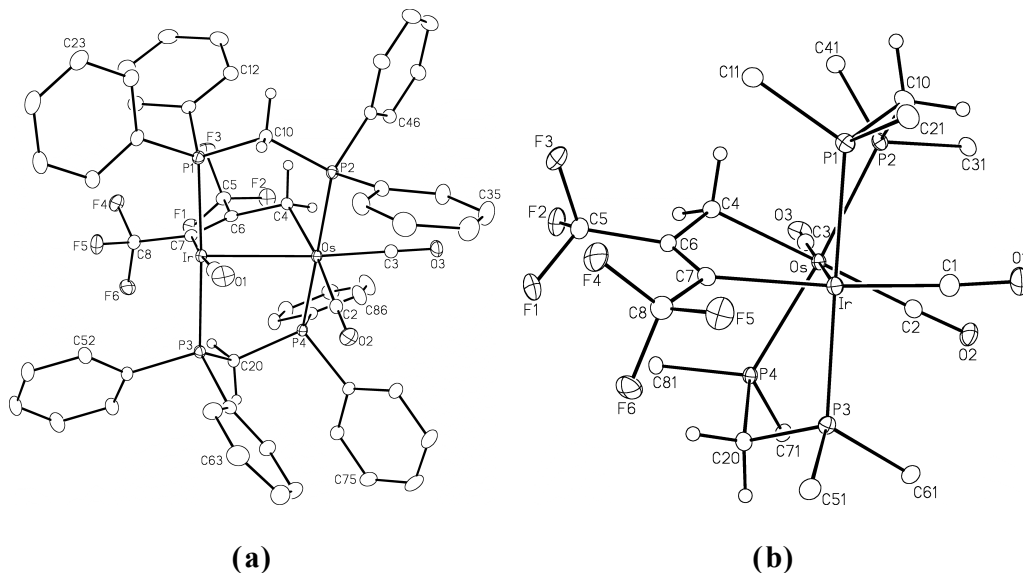


Figure 4-5. (a) Perspective view of the complex cation of $[\text{IrOs}(\text{CO})_3(\mu\text{-}\kappa^1:\kappa^1\text{-C}(\text{CF}_3)=\text{C}(\text{CF}_3)\text{CH}_2)(\text{dppm})_2][\text{CF}_3\text{SO}_3]$ (**32**). Thermal ellipsoids are as described in Figure 4-2. Only the ipso carbons of the phenyl rings are shown. (b) Alternate view of the complex cation of $[\text{IrOs}(\text{CO})_3(\mu\text{-}\kappa^1:\kappa^1\text{-C}(\text{CF}_3)=\text{C}(\text{CF}_3)\text{CH}_2)(\text{dppm})_2][\text{CF}_3\text{SO}_3]$ (**32**) with all phenyl carbons shown. Thermal ellipsoids are as described in Figure 4-2.

Within the bridging C_3 fragment the $\text{C}(6)\text{--C}(7)$ bond length of $1.344(5)$ Å is characteristic of a double bond,⁷ while $\text{C}(6)\text{--C}(4)$ ($1.512(4)$ Å) is indicative of a single bond between sp^2 and sp^3 carbons.⁷⁻⁸ All angles within the C_3 fragment ($\text{Ir}\text{--C}(7)\text{--C}(6) = 122.3(2)^\circ$, $\text{C}(4)\text{--C}(6)\text{--C}(7) = 122.1(3)^\circ$, and $\text{Os}\text{--C}(4)\text{--C}(6) = 115.5(2)^\circ$) are slightly larger than those predicted for undistorted sp^2 and sp^3

angles, and together with the acute the Ir–Os–C(4) and Os–Ir–C(7) angles of 82.40(9)° and 85.88(9)°, respectively, suggest significant strain within the dimetallacyclopentene moiety. Presumably, the staggered arrangement of the two coordination spheres along the metal-metal axis occurs to alleviate further strain; an eclipsed conformation, while maintaining the observed metal-metal distance, would exacerbate the strain within this moiety. This structure closely resembles those of the related species, $[\text{RhM}(\text{CO})_3(\mu-\kappa^1:\kappa^1\text{-C}(\text{CF}_3)=\text{C}(\text{CF}_3)\text{CH}_2)(\text{dppm})_2]^+$ (M = Ru,^{5b} Os^{5d}). An alternate view with all phenyl carbons shown is given in Figure 4-5(b).

Table 4-2. Selected Bond Lengths and Angles for Compound 32

(a) Distance (Å)

atom 1	atom 2	distance	atom 1	atom 2	distance
Ir	Os	2.7910(2)	Os	C(4)	2.185(3)
Ir	C(1)	1.876(4)	C(4)	C(6)	1.512(4)
Ir	C(7)	2.102(3)	C(5)	C(6)	1.515(5)
Os	C(2)	1.937(3)	C(6)	C(7)	1.344(5)
Os	C(3)	1.862(3)	C(7)	C(8)	1.511(5)

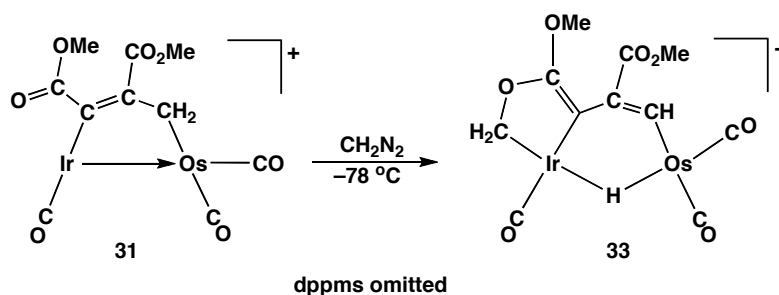
(b) Angles (deg)

atom	atom 2	atom 3	angle	atom 1	atom 2	atom 3	angle
Os	C(4)	C(6)	115.5(2)	Ir	C(7)	C(6)	122.3(2)
C(4)	C(6)	C(5)	113.6(3)	Ir	C(7)	C(8)	114.2(2)
C(4)	C(6)	C(7)	122.1(3)	C(1)	Ir	C(7)	175.4(1)
C(5)	C(6)	C(7)	123.8(3)	Os	Ir	C(7)	85.88(9)
C(6)	C(7)	C(8)	123.3(3)	Ir	Os	C(4)	82.40(9)

Compounds **30** and **31** react with a second equiv of CH₂N₂; however, instead of the anticipated insertion into the Ir–C bond of the strained bridging C₃ unit, a new C–O bond is formed to yield $[\text{IrOs}(\text{CO})_3(\mu\text{-H})(\mu-\kappa^1:\kappa^1:\kappa^1\text{-CH}_2\text{OC}(\text{OCH}_3)=\text{CC}(\text{CO}_2\text{CH}_3)=\text{CH})(\text{dppm})_2][\text{CF}_3\text{SO}_3]$ (**33**), as illustrated in Scheme 4-3. The reactions of compounds **30** and **31** with CH₂N₂ to generate **33**

occur readily. Although **30** requires prior CO loss to generate **31** before reacting to form **33**, as shown by $^{31}\text{P}\{^1\text{H}\}$ NMR spectroscopy at $-78\text{ }^\circ\text{C}$, the relative rates of reaction of **30** and **31** are comparable, attesting to the extreme lability of the fourth CO in the former.

Scheme 4-3



The defining feature of the ^1H NMR spectrum of **33** is the hydride resonance at $\delta -18.9$, appearing as a quintet with equal coupling of 8.4 Hz to all four phosphorus nuclei of the dppm ligands, confirming its bridging arrangement, as shown in Figure 4-6. The proton of the CH group appears as a triplet at $\delta 5.10$, showing coupling to only the Os-bound phosphorus nuclei of 11.2 Hz, while the Ir-bound CH_2 group appears at $\delta 4.10$, with coupling to only the Ir-bound phosphorus nuclei of 10.6 Hz. The protons of the dppm methylene groups appear as two signals at $\delta 5.10$ and $\delta 4.85$ ($^2J_{\text{HH}} = 13.4\text{ Hz}$).

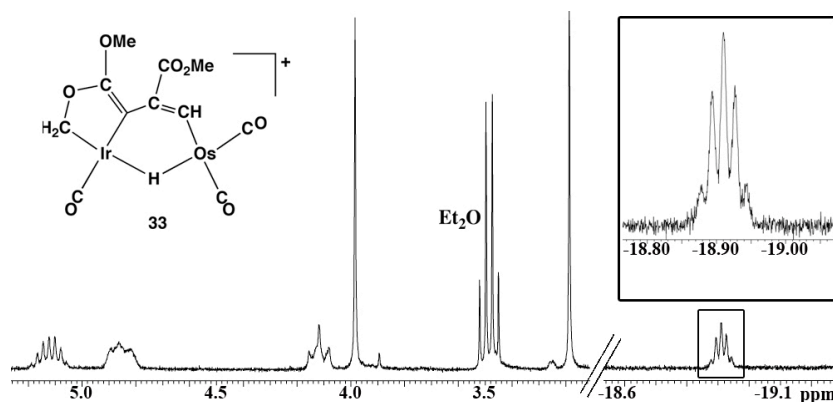


Figure 4-6. ^1H NMR spectrum of $[\text{IrOs}(\text{CO})_3(\mu\text{-H})(\mu\text{-}\kappa^1:\kappa^1:\kappa^1\text{-CH}_2\text{OC}(\text{OCH}_3)=\text{CC}(\text{CO}_2\text{CH}_3)=\text{CH})(\text{dppm})_2][\text{CF}_3\text{SO}_3]$ (**33**) in CD_2Cl_2 (hydride resonance inset).

In a ^{13}C -enriched sample of **33** two signals for the three CO ligands appear in the $^{13}\text{C}\{^1\text{H}\}$ NMR spectrum at δ 184.3 (1C) for the Ir-bound CO coupling to only the adjacent phosphorus nuclei ($^2J_{\text{CP}} = 4.7$ Hz), and δ 174.4 (2C, coincidentally overlapped) for the two Os-bound CO ligands, coupling to the Os-bound phosphorus nuclei ($^2J_{\text{CP}} = 7.4$ Hz). In a sample of **31** in which the Os-bound CH_2 group was ^{13}C -enriched, reaction with $^{12}\text{CH}_2\text{N}_2$ resulted in ^{13}C enrichment only at the Os-bound methyne group (Scheme 4-3). This carbon appears at δ 115.2 in the $^{13}\text{C}\{^1\text{H}\}$ NMR spectrum and is shown by APT to be bound to a single proton. In addition, this proton, noted above, now displays coupling to the labelled carbon of 148.0 Hz in the ^1H NMR spectrum. Experiments in which $^{13}\text{CH}_2\text{N}_2$ was added to unlabelled **31** gives rise to a $^{13}\text{C}\{^1\text{H}\}$ resonance at δ 60.4. In the ^1H NMR spectrum the added methylene resonance appears as a doublet of triplets at δ 4.10 with coupling to the ^{13}C of 147.2 Hz. These experiments confirm that C–H activation involves the CH_2 group of the original $\mu\text{-C}_3$ fragment and not the added CH_2 group. Low temperature NMR studies did not yield additional information on the transformation of **31** to **33**, since no additional species were observed.

Although these NMR data clearly established the fate of the original CH_2 group in the precursor **31**, it did not establish how the newly added CH_2 group was incorporated into the complex. However, the connectivity was clearly established by the X-ray structure determination of **33**, and a representation of the complex cation is shown in Figure 4-7. Clearly shown in this figure are the C_3 -bridged unit (C(6)–C(7)–C(8)), in which the original CH_2 unit has been converted to CH and the bridging hydride, together with the new 5-membered ring involving the added methylene group, the carbonyl group of the ester functionality from the DMAD, and the Ir centre (Ir–C(4)–O(4)–C(5)–C(6)). Selected bond lengths and angles are presented in Table 4-3.

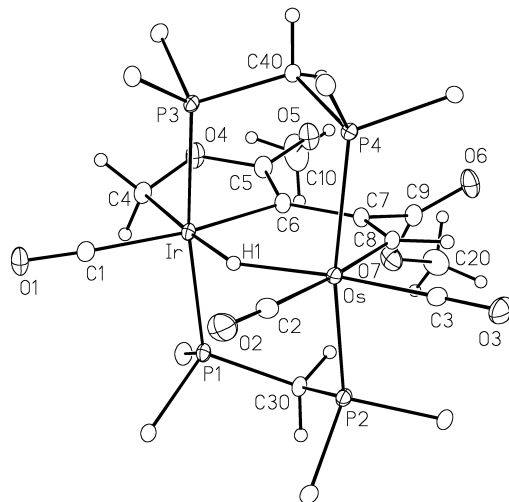


Figure 4-7. Perspective view of the complex cation of $[\text{IrOs}(\text{CO})_3(\mu\text{-H})(\mu\text{-}\kappa^1:\kappa^1:\kappa^1\text{CH}_2\text{OC}(\text{OCH}_3)=\text{CC}(\text{CO}_2\text{CH}_3)=\text{CH})(\text{dppm})_2][\text{CF}_3\text{SO}_3]$ (**33**). Only the ipso carbons of the phenyl rings are shown. Thermal ellipsoids are as described in Figure 4-2.

Both metals display a pseudo-octahedral geometry, with all angles between adjacent groups of approximately 90° . The most significant distortions from octahedral geometries result from the non-linearity of the P(1)–Ir–P(3) ($172.13(3)^\circ$) and P(2)–Os–P(4) ($158.81(4)^\circ$) units of the diphosphines, which are bent towards the bridging hydrocarbonyl fragment. This bending occurs to minimize contacts between the almost vertical dppm phenyl rings on the same face as the bridging hydride, and the carbonyl ligands, and is aided by the phenyl group orientations on the opposite face which lie almost parallel to the bridging “C₃” moiety (Figure 4-8). One carbonyl on Os lies opposite the bridging hydride ligand and another is trans to the methyne carbon of the C₃-bridging unit.

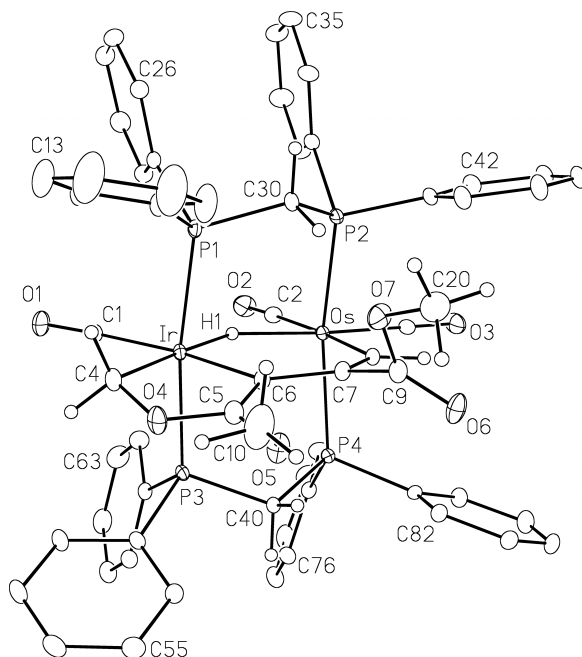


Figure 4-8. Perspective view of the complex cation of $[\text{IrOs}(\text{CO})_3(\mu\text{-H})(\mu\text{-}\kappa^1:\kappa^1:\kappa^1\text{CH}_2\text{OC}(\text{OCH}_3)=\text{CC}(\text{CO}_2\text{CH}_3)=\text{CH})(\text{dppm})_2][\text{CF}_3\text{SO}_3]$ (**33**). Thermal ellipsoids are as described in Figure 4-2.

Within the bridging hydrocarbyl fragment the bond lengths are most consistent with the canonical form shown in Scheme 4-3 in which the C(5)–C(6) and C(7)–C(8) bonds (1.348(6) and 1.344(6) Å) are typical of double bonds, while C(6)–C(7), a double bond in the precursor (**31**), has now lengthened to 1.464(5) Å, typical of a single bond between sp^2 hybridized carbons.⁷ The length of the newly formed C(4)–O(4) bond (1.447(5) Å), and the C(5)–O(4) bond (1.349(5) Å), are as expected, with the latter being typical for an enol ester.⁷ The unsymmetrical metal-hydride distances (Ir–H(1) = 1.61(5) Å, Os–H(1) = 1.84(5) Å) suggest a stronger interaction with Ir, although the uncertainties in accurately defining the hydrogen position by X-ray methods leaves this interpretation in some doubt, and certainly the equal spin–spin coupling of the hydride to both ends of the diphosphines in the ^1H NMR spectrum is suggestive of a close-to-symmetric hydride bridge in solution. Incorporation of the hydride bridge results in a substantial lengthening of the metal-metal separation to 3.2956(3) Å from

approximately 2.8 Å in the precursor (estimated from the analogous species **32**), as expected for a 3-centre 2-electron interaction.

Table 4-3. Selected Bond Lengths and Angles for Compound 33

(a) Distance (Å)

atom 1	atom 2	distance	atom 1	atom 2	distance
Ir	C(1)	1.904(4)	O(4)	C(5)	1.349(5)
Ir	C(4)	2.128(4)	C(5)	C(6)	1.348(6)
Ir	C(6)	2.101(4)	C(6)	C(7)	1.464(5)
Ir	H(1)	1.61(5)	C(7)	C(8)	1.344(6)
Os	C(2)	1.938(4)	C(7)	C(9)	1.497(6)
Os	C(3)	1.879(4)	C(9)	O(6)	1.201(5)
Os	C(8)	2.115(4)	C(9)	O(7)	1.347(6)
Os	H(1)	1.84(5)	O(7)	C(20)	1.455(6)
C(4)	O(4)	1.447(5)			

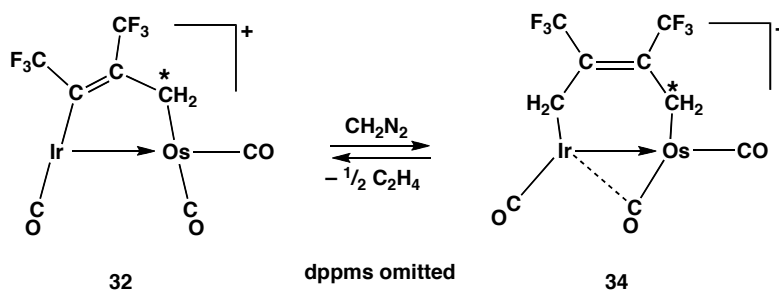
(b) Angle (deg)

atom 1	atom 2	atom 3	angle	atom 1	atom 2	atom 3	angle
O(4)	C(5)	C(6)	122.7(4)	Ir	H(1)	Os	145(4)
O(4)	C(5)	C(6)	122.7(4)	C(1)	Ir	C(4)	89.21(18)
C(5)	C(6)	C(7)	120.8(4)	C(4)	Ir	C(6)	77.86(16)
C(6)	C(7)	C(8)	125.1(4)	C(4)	O(4)	C(5)	113.1(3)
C(7)	C(8)	Os	129.1(3)	C(5)	O(5)	C(10)	115.0(4)

In a previous study on the related Rh/Os system we had reported the conversion of the C₃-bridged species, [RhOs(CO)₃(μ-κ¹:κ¹-RC=C(R)CH₂)-(dppm)₂]⁺ (R = CO₂Me), to the C₄-bridged product by methylene insertion into the Rh–carbon bond of the bridging hydrocarbyl fragment, and had been surprised that the HFB analogue (R = CF₃) had not reacted similarly.^{5d} We now find that the former proposal of methylene insertion into the Rh–hydrocarbyl bond had been in error, as is unambiguously shown in the current study, for which the spectroscopy matches very closely to that in the Rh/Os study.

The hexafluorobutyne-containing analogue (**32**) also reacts with diazomethane, but in this case, yields a very different product, $[\text{IrOs}(\text{CO})_3(\mu\text{-}\kappa^1:\kappa^1\text{-CH}_2\text{C}(\text{CF}_3)=\text{C}(\text{CF}_3)\text{CH}_2)(\text{dppm})_2][\text{CF}_3\text{SO}_3]$ (**34**), which is only stable at temperatures below $-20\text{ }^\circ\text{C}$; upon warming to ambient temperature quantitative regeneration of **32** occurs, also generating ethylene, as seen in the ^1H NMR spectrum (Scheme 4-4).

Scheme 4-4



Compound **34** appears to be the originally anticipated product, in which methylene insertion into the Ir–C bond of the C_3 -bridged fragment has occurred. Both hydrocarbyl methylene groups of **34** appear in the ^1H NMR spectrum at δ 4.01 and δ 2.27. The former resonance appears as a triplet (see Figure 4-9) for which selective decoupling of the Ir-bound ^{31}P resonances leads to its collapse to a singlet, while no effect is seen in the other resonance. The second CH_2 signal appears as a multiplet, which simplifies to a poorly resolved quartet, displaying coupling to the adjacent CF_3 group ($^4J_{\text{HF}} = 2.5\text{ Hz}$) upon decoupling the Os-bound ^{31}P nuclei; decoupling of these ^{31}P nuclei leads to no noticeable change in the other CH_2 resonance. The small fluorine-hydrogen coupling noted is typical of what we would expect from 4-bond coupling⁹ and indicates that the C_3 unit of the precursor (**32**) has remained intact.

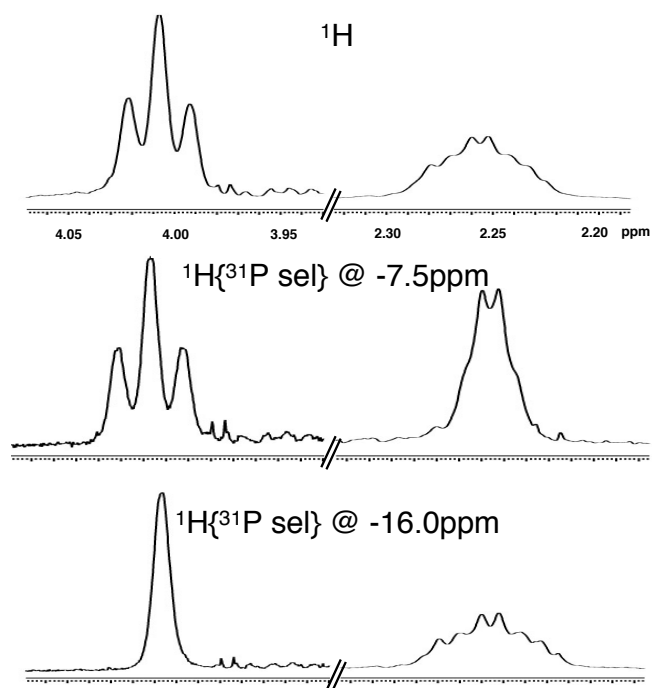


Figure 4-9. Select regions of the ^1H and $^1\text{H}\{^{31}\text{P}\}$ NMR spectra showing the resonances for the two CH_2 groups of the C_4 -bridge of compound **34** in CD_2Cl_2 .

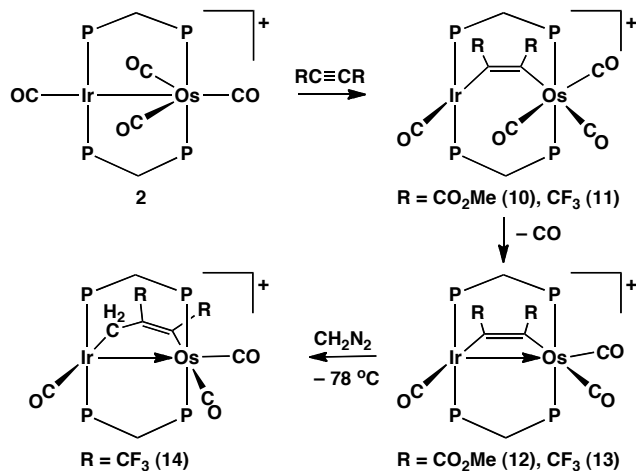
In a ^{13}C -enriched sample of **34** three resonances are observed in the $^{13}\text{C}\{^1\text{H}\}$ NMR spectrum at δ 187.9, δ 184.0, and δ 178.0. The two upfield resonances each appear as triplets having *ca.* 9 Hz coupling to different pairs of phosphorus nuclei; the one at δ 184.0 couples to the Ir-bound ends of the diphosphines while the one at δ 178.0 displays coupling to the Os ends. The slightly downfield ^{13}C resonance displays *ca.* 8 Hz coupling to the Os-bound ^{31}P nuclei, but sharpens slightly upon ^{31}P decoupling at the Ir end suggesting a weak semi-bridging interaction. When all carbonyls and both methylene groups are ^{13}C -enriched this low-field carbonyl resonance shows *ca.* 15 Hz coupling to the Os-bound methylene group, suggesting a mutually trans arrangement; however, no ^{13}C - ^{13}C coupling is observed for the Ir-bound methylene group and the carbonyl resonating at δ 184.0, suggesting at least some deviation from a rigorous trans arrangement.

Using bis(triphenylphosphoranylidene)ammonium chloride as an internal phosphorus standard, it is evident that all of **34** is transformed back to the C₃-bridged species (**32**) via loss of the CH₂ unit (Scheme 4-4). The methylene unit lost from **32** is observed as ethylene in the ¹H NMR spectrum at δ 5.41. The conversion of **34** to **32** occurs even in the absence of excess diazomethane, so incorporation of an additional CH₂ group is not necessary and does not precede ethylene formation.

4.2.3 C₂-Bridged Species

Attempts to obtain isomers of **31** and **32**, having an “Ir-CH₂-(alkyne)-Os” core led us to investigate CH₂ insertion into alkyne-bridged Ir/Os species, on the assumption that CH₂ insertion into the Ir-alkyne bond would occur. The alkyne-bridged precursors, [IrOs(CO)₄(μ-R₂C=CR)(dppm)₂][CF₃SO₃] (R = CO₂Me (**35**), CF₃ (**36**)), were obtained by addition of the respective alkynes to the tetracarbonyl complex [IrOs(CO)₄(dppm)₂][CF₃SO₃] (**27**) (Scheme 4-5).

Scheme 4-5



Again, the ³¹P resonances are not readily identified as Ir- or Os-bound without the ¹³C{³¹P} experiments which establish that the ¹³CO resonances at δ 180.0 (**35**) and δ 177.0 (**36**) correspond to the lone Ir-bound carbonyl in each complex while the three other carbonyls in both compounds are terminally bound to Os. The IR spectra of these compounds reveal the CO stretches in the range

2075 to 1957 cm^{-1} , offering further support that all are terminally bound. In the ^1H NMR spectrum the dppm CH_2 groups resonate between *ca.* δ 4.7 and δ 4.2. In the case of **35**, the CH_3 protons on the bridging alkyne fragment appear at δ 3.32 and δ 2.48. A carbonyl can be removed from both **35** and **36** by the addition of TMNO or by refluxing in THF, yielding the C_2 -bridged tricarbonyl species $[\text{IrOs}(\text{CO})_3(\mu\text{-}\kappa^1:\kappa^1\text{-C(R)=CR})(\text{dppm})_2][\text{CF}_3\text{SO}_3]$ ($\text{R} = \text{CO}_2\text{Me}$ (**37**), CF_3 (**38**)), as shown in Scheme 4-5; we propose that loss of an Os-bound CO is accompanied by formation of an $\text{Ir}\rightarrow\text{Os}$ dative bond. All spectroscopic parameters are in keeping with the A-frame nature of these species as is confirmed by the X-ray structure determination of **37**, which shows the bridging $\kappa^1:\kappa^1$ arrangement of the alkyne (Figure 4-10). Selected bond lengths and angles are presented in Table 4-4.

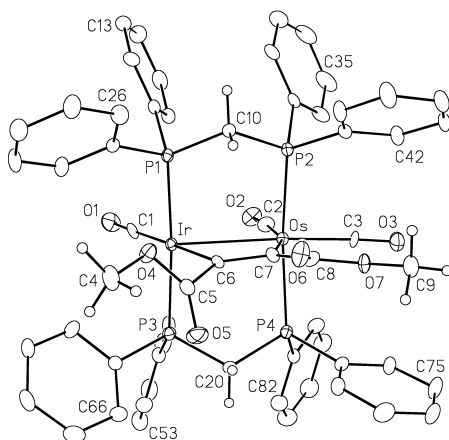


Figure 4-10. Perspective view of the complex cation of $[\text{IrOs}(\text{CO})_3(\mu\text{-}\kappa^1:\kappa^1\text{-C}(\text{CO}_2\text{Me})=\text{C}(\text{CO}_2\text{Me}))(\text{dppm})_2][\text{CF}_3\text{SO}_3]$ (**37**). Phenyl hydrogens omitted. Thermal ellipsoids are as described in Figure 4-2.

Complex **37** has a pseudo-octahedral Os centre in which the sixth coordination site is occupied by the dative $\text{Ir}\rightarrow\text{Os}$ bond from an otherwise square-planar Ir(I) centre, much as discussed earlier for compound **32**. The $\text{Ir}\text{-Os}$ bond length of 2.8610(6) Å is typical of a single bond, and is significantly shorter than the non-bonded $\text{P}\text{-P}$ distances. The alkyne bridges the two metals almost parallel to the metal-metal axis, in which the $\text{C}(6)\text{-C}(7)$ bond length of 1.345(11) Å is

typical of a double bond and the C(5)–C(6)–C(7) and C(6)–C(7)–C(8) angles are all near the expected 120°.

Table 4-4. Selected Bond Lengths and Angles of Compound 37

(a) Distance (Å)

atom 1	atom 2	distance	atom 1	atom 2	distance
Ir	Os	2.8610(6)	C(6)	C(5)	1.516(11)
Ir	C(1)	1.906(9)	C(6)	C(7)	1.345(11)
Ir	C(6)	2.110(8)	C(5)	O(5)	1.203(11)
Os	C(2)	1.936(9)	C(5)	O(4)	1.312(11)
Os	C(3)	1.858(8)	O(4)	C(4)	1.447(10)
Os	C(7)	2.090(8)	C(7)	C(8)	1.471(11)

(b) Angle (deg)

atom 1	atom 2	atom 3	angle	atom 1	atom 2	atom 3	angle
Ir	C(6)	C(7)	118.6(6)	Os	Ir	C(6)	64.8(2)
C(6)	C(7)	Os	103.5(6)	Ir	Os	C(2)	87.7(3)
C(1)	Ir	C(6)	179.1(3)	Ir	Os	C(3)	175.7(3)
Os	Ir	C(1)	115.4(2)	Ir	Os	C(7)	72.6(2)

Using the same methodology as discussed previously, diazomethane can be used to introduce a CH₂ group into the Ir-carbon bond of the “IrOs(μ -RC=CR)” moiety of **38** to give **39** (Scheme 4-5), as determined by the 8.8 Hz coupling between the CH₂ protons and the Ir-bound ³¹P nuclei. In this case, coupling of the CH₂ protons and the fluorine nuclei of the adjacent CF₃ group is not observed in either the ¹H or the ¹⁹F NMR spectrum, although small couplings of 2 Hz or less could be masked by the width of the observed peaks. The three carbonyl ligands are terminally bound as witnessed by their IR stretches in the range of 1991 to 1910 cm⁻¹ and in a ¹³CO-enriched sample of **39** the three carbonyl resonances are observed between δ 177.1 and 195.2 in the ¹³C NMR spectrum. Selective ³¹P decoupling identifies the downfield resonance as the lone Ir-bound carbonyl. In a ¹³CH₂-enriched sample the Ir-bound methylene unit appears in the ¹³C{¹H} NMR spectrum at δ 67.8. Although spin-spin coupling between the CH₂ unit and the ³¹P nuclei bound to Ir is not directly observed,

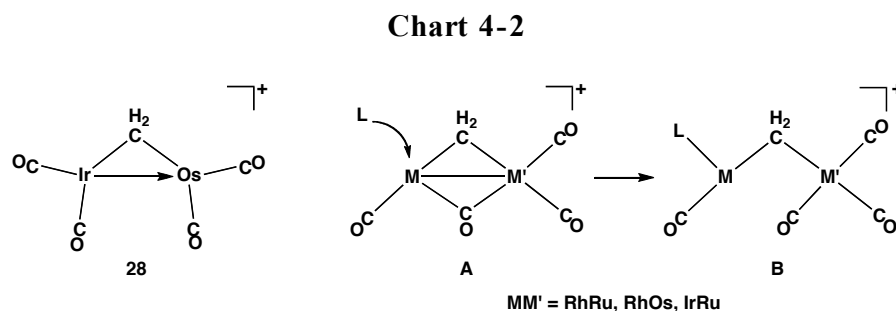
owing to the breadth of the signal; sharpening of the peak is observed upon ^{31}P decoupling of the Ir-bound ^{31}P nuclei. This C₃-bridged product, $[\text{IrOs}(\text{CO})_3(\mu\text{-}\kappa^1:\kappa^1\text{-CH}_2(\text{CF}_3)\text{C}=\text{CCF}_3)(\text{dppm})_2][\text{CF}_3\text{SO}_3]$ (**39**), does not react with additional CH_2N_2 . Compound **39** is unstable, and warming to ambient temperature results in its disappearance, accompanied by quantitative reformation of **38**. This loss of the methylene unit, as ethylene, was also observed upon warming, as was also noted in the transformation of **34** to **32**.

Reaction of the DMAD-bridged species (**37**) with CH_2N_2 does not parallel the reaction with **38** but instead yields multiple unidentified products, unchanged by varying the reaction conditions. One of the products yielded a single crystal from solution; however the badly disordered structure did not refine acceptably. Nevertheless, the connectivity determined from the preliminary structure determination indicates the formation of a bond between the added methylene group and the carbonyl oxygen of the adjacent end of the bridging DMAD group, much as observed for compound **34**, suggesting one reason for the divergence in the reactivities of **37** and **38**.

4.3 Discussion

In many ways, the reactivity of the Ir/Os species, described in this paper, parallels that described earlier for the analogous Rh/Ru, Rh/Os, and Ir/Ru systems, although significant differences are observed depending on the metal combination. In the generation of the methylene-bridged precursor $[\text{IrOs}(\text{CO})_4(\mu\text{-CH}_2)(\text{dppm})_2]^+$ by reaction of $[\text{IrOs}(\text{CO})_4(\text{dppm})_2]^+$ with diazomethane, the reactivity parallels that of the Rh/Ru and Ir/Ru systems, while differing substantially from that of the Rh/Os system. Whereas the three systems, $[\text{MM}'(\text{CO})_4(\text{dppm})_2]^+$ ($\text{MM}' = \text{RhRu}, \text{IrRu}, \text{IrOs}$) incorporate only a single methylene group, irrespective of temperature, the Rh/Os system is much more reactive with diazomethane, incorporating up to four methylene groups at temperatures above $-60\text{ }^\circ\text{C}$, yielding the mono-methylene species, as the exclusive product, only at temperatures below this.

The structure of $[\text{IrOs}(\text{CO})_4(\mu\text{-CH}_2)(\text{dppm})_2]^+$ (**28**), as noted, is very different from the structures of its congeners, $[\text{MM}'(\text{CO})_4(\mu\text{-CH}_2)(\text{dppm})_2]^+$ ($\text{MM}' = \text{RhRu}, \text{RhOs}, \text{IrRu}$). Whereas these latter three species have unsymmetrical structures, having a bridging carbonyl, one terminal CO on Rh or Ir and two terminal COs on Ru or Os, as shown for structure **A** in Chart 4-2 (dppm groups not shown), compound **28** has a close-to-symmetric structure having two carbonyls on each metal. Although these different structure types should give rise to different reactivity patterns, their reactivities with additional diazomethane appears, at first glance, to bear little relationship to their structures, recalling that of these four compounds, only the Rh/Os member reacted with additional diazomethane.⁴



We had previously rationalized the differing reactivities of the Rh/Ru, Rh/Os and Ir/Ru species (having similar structures) on the basis of incipient coordinative unsaturation.^{4b,5c,10} Although both metals in **A** are saturated, a comparison of the structures of these three compounds showed that the only one to react further with diazomethane (Rh/Os) had the bridging carbonyl interacting the weakest with the group 9 metal. This led to the suggestion that this weak Rh-($\mu\text{-CO}$) interaction was a source of incipient unsaturation being readily displaced from Rh by nucleophilic attack at the vacant coordination site, as shown in Chart 4-2. This weaker interaction allowed even the weak nucleophile, diazomethane, to displace this bridging carbonyl, while presumably for the Rh/Ru and Ir/Ru analogues, the stronger interactions of the group 9 metal with the bridging carbonyl did not allow diazomethane to displace this CO, resulting in no reactivity. These ideas were supported by the relative rates of substitution of a

carbonyl by PMe_3 at $-25\text{ }^\circ\text{C}$, for which the rates decreased in the order: rate (RhOs) $\approx 30 \times$ rate (RhRu) $\approx 36 \times$ rate (IrRu),¹⁰ paralleling the increasing strength of the group 9–(μ -CO) interaction.

We can now extend these ideas to include the lack of reactivity of **28** with diazomethane. As shown in Chart 4-2, compound **28** is again saturated at both metals, and the all-terminal-carbonyl arrangement observed should be less able to transfer an Ir-bound CO to Os, making it the least susceptible to nucleophilic attack at Ir. Furthermore, although structure **A** is formally saturated, it has a vacant site opposite the bridging carbonyl and adjacent to the methylene group, while compound **28** has no accessible coordination site. In keeping with this logic, **28** is unreactive towards diazomethane.

In order to test the above idea that Ir/Os should be the least susceptible to nucleophilic attack of the series, we compared its reactivity with PMe_3 to that of the Ir/Ru analogue (the slowest of the previous series). Under identical conditions at ambient temperature, the rate of substitution of a carbonyl in $[\text{IrRu}(\text{CO})_4(\mu\text{-CH}_2)(\text{dppm})_2][\text{CF}_3\text{SO}_3]$, by PMe_3 was found to be approximately 1.5 \times the rate of substitution in **28** (monitored by $^{31}\text{P}\{^1\text{H}\}$ NMR spectroscopy) to generate $[\text{IrOs}(\text{CO})_3(\text{PMe}_3)(\mu\text{-CH}_2)(\text{dppm})_2][\text{CF}_3\text{SO}_3]$ (**40**), consistent with the ideas of coordinative saturation noted above.

These structural arguments, however, do not explain the relative reactivities of this tetracarbonyl series with dimethyl acetylenedicarboxylate (DMAD), nor the failure of hexafluorobutyne (HFB) to react with any of the tetracarbonyl precursors. The most reactive species with diazomethane and PMe_3 (Rh/Os) is unreactive towards DMAD,^{5d} while both the Ir/Os(**28**) and Rh/Ru analogues^{5b} react readily with DMAD at ambient temperature.

In most studies involving the insertion of unsaturated substrates into a metal– CH_2 bond of a bridging methylene group, a vacant coordination site, adjacent to the bond into which insertion occurs, is assumed.^{5b,5d,11} Certainly the regioselectivity of these insertions in our MM' series, which always occurs into the group 9 metal– CH_2 bond,^{5b,5d} is consistent with incipient coordinative

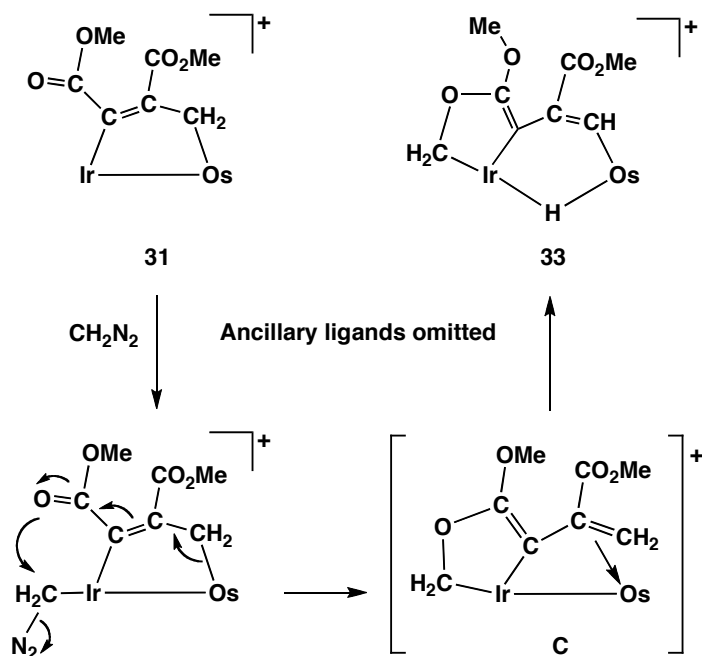
unsaturation at this metal, and furthermore, insertion is significantly more facile for the tricarbonyl analogues $[\text{MM}'(\text{CO})_3(\mu\text{-CH}_2)(\text{dppm})_2]^+$ than for the tetracarbonyl species. The reactivity trend in our tetracarbonyl series and in particular the facile reactivity of the saturated species **28** with DMAD, which can occur without carbonyl loss, suggests that coordinative unsaturation is not required to initiate the insertion. Furthermore, these electron-deficient alkynes are not particularly nucleophilic.

The bridging methylene group in these late-metal species is nucleophilic,^{5d,12} so we suggest that nucleophilic attack of this bridging group at the electron-deficient alkynes, HFB and DMAD, may initiate the insertion; this reactivity is more in line with the electrophilic nature of both alkynes. At first glance, this proposal seems inconsistent with the higher reactivity noted here and elsewhere,^{5b,5d,13} of DMAD compared to HFB; on the basis of the higher group electronegativity of CF_3 ,¹⁴ the opposite would be expected. However, we suggest that the potential for the carboxylate group to offer additional resonance stabilization results in DMAD being more electrophilic. In the tetracarbonyl complex **28** the additional carbonyl (compared to **29**) lowers the nucleophilicity of the complex, lowering its reactivity towards the less electrophilic alkyne, HFB, which reacts with **29** but not with **28**. We do not fully understand what subtle factors might give rise to the differences in nucleophilicity of the $\mu\text{-CH}_2$ group in this closely related series.

Differences in reactivity between DMAD and HFB, noted above, are even more noticeable in the reactions of the C_3 -bridged species $[\text{IrOs}(\text{CO})_3(\mu\text{-}\kappa^1:\kappa^1\text{-RC}=\text{C}(\text{R})\text{CH}_2)(\text{dppm})_2]^+$ ($\text{R} = \text{CO}_2\text{Me}$ (**31**), CF_3 (**32**)) with diazomethane which proceed *very* differently. Whereas **32** reacts with diazomethane to give the anticipated C_4 -bridged product, shown in Scheme 4-4, compound **31** yields the dimetallacycle **33** by C–O bond formation, as shown in Scheme 4-3. We propose that the reaction involving **31** proceeds as outlined in Scheme 4-6, in which the carboxylate carbonyl adjacent to the site of diazomethane coordination displaces N_2 via nucleophilic attack at the coordinated diazomethane, generating the O– CH_2

bond, leading to the unobserved intermediate **C** having a terminal olefin moiety as shown. Carbon-hydrogen bond activation of the α -olefin moiety could then generate the final hydrido-bridged compound **33**.

Scheme 4-6



On this basis, the different reactivity of the HFB-inserted product **32** with diazomethane is understandable. With no adjacent carbonyl functionality, the favoured reactivity in this case is the anticipated insertion into the Ir-C(sp²) bonds of the “ μ -C₃” fragment. The instability of this species, reverting to the precursor and ethylene, must result from the more favourable Ir-C(sp²) bond of the precursor (**32**) than the Ir-C(sp³) bond of the product, and **32** is presumably also favoured, having the electronegative CF₃ group on the α -carbon, which further strengthens this Ir-C bond. We also suggest that the additional strain within the 6-membered dimetallacycle of **34** further destabilizes this product.

Our second strategy for yielding C₄-bridged species was through double methylene insertion into the Ir-C(sp²) bond of alkyne-bridged species. Although this again would lead to replacement of an Ir-C(sp²) bond by a less favourable Ir-C(sp³) bond, we reasoned that the relief in strain, progressing from a four-

membered C₂-bridged to a five-membered C₃-bridged species might favour the insertion product. Certainly this strategy had proven successful for the Rh/Os system. However, in the current Ir/Os system the DMAD-bridged precursor yields a mixture of uncharacterized products, while the C₃-bridged product obtained from the HFB-bridged precursor, namely, [IrOs(CO)₃(μ - κ^1 : κ^1 -CH₂(CF₃)C=CCF₃)(dppm)₂][CF₃SO₃] (**39**), is unstable at temperatures above -20 °C, reverting to the HFB-bridged precursor; unlike the analogous RhOs species, compound **39** failed to insert a second methylene group.

4.4 Conclusions

The methylene-bridged Ir/Os complex reflects the trend of third row metals to tend not to support bridging-carbonyl ligands, and therefore adopts a different structure than the other combinations of metals studied previously in our group. The insertion of the alkyne substrates into the Ir-CH₂ bond is as expected, however, our proposal that the stronger metal-carbon bonds of this system could help retain the growing hydrocarbyl fragments does not seem to have come to fruition. Attempts at coupling multiple methylene-groups and adding methylene groups to C₃-bridges failed.

Characterization of the Ir/Os complexes described herein relied heavily on NMR spectroscopy. Crystallographically, the one electron difference between the two third-row group 8 and 9 metals made it difficult to assign which metal Ir and which was Os. The drive for the Os to be coordinatively saturated helped us to assign the metal centres, as did refining crystallographic models in which the metals were switched and obtaining higher R-factors for those.

Besides the reactivity differences observed by changing the metal combination, we also observed differences in the reactivity of the organic substrates on the basis of different R groups on the alkyne (RC≡CR). The carboxylate group of the DMAD alkyne provides a nucleophile to attack coordinated diazomethane. The HFB, however, does not have an ancillary reactive functionality and therefore reacts in a relatively predictable fashion for these late-metal methylene-bridged complexes.

Clearly, the factors involved in the transformations investigated are subtle and changes in the metal combination can have a significant effect on reactivity. These factors, which are not fully understood, are more complex than in monometallic systems, and will need to be understood before the potential of mixed-metal systems can be fully utilized.

4.5 Experimental Section

4.5.1 General Comments

All solvents were dried using appropriate desiccants (given in Appendix II), distilled before use, and stored under a nitrogen atmosphere. Reactions were performed under an argon atmosphere using standard Schlenk techniques. Diazomethane was generated from Diazald,TM which was purchased from Aldrich, as was the ¹³C-enriched Diazald,TM dimethyl acetylenedicarboxylate (DMAD) and bis(triphenylphosphoranylidene)-ammonium chloride (PPNCl), while the hexafluorobutyne (HFB) was purchased from PCR Inc. ¹³C-enriched *N*-methyl-*N*-nitroso-*p*-toluenesulfonamide was prepared by using a modified version of the procedure for synthesizing the ¹⁴C-enriched radio-labelled analogue.¹⁵

The ¹H and ³¹P{¹H} NMR spectra were recorded on a Varian Inova 400 spectrometer operating at 399.9 and 161.8 MHz, respectively. All low-temperature spectra and the heteronuclear decoupling experiments (¹³C{¹H} and ¹³C{¹H, ³¹P}) were recorded on a Varian Unity spectrometer operating at 161.9 MHz for ¹³C, 202.3 MHz for ³¹P, and 499.8 MHz for ¹H. Infrared spectra were recorded in CH₂Cl₂ solution on a Nicolet Avatar 370 DTGS spectrometer. Mass spectrometry was performed on a Micromass ZabSpec TOF spectrometer by the mass spectrometry facility of this department, and elemental analyses were also carried out in the departmental facility.

4.5.2 Preparation of Compounds

Spectroscopic data for the compounds are presented in Table 4-5.

(a) [IrOs(CO)₅(dppm)₂][CF₃SO₃] (**26**) and [IrOs(CO)₄(dppm)₂]-[CF₃SO₃] (**27**). Compound **26** was prepared according to the published

Table 4-5. Spectroscopic Data for the Compounds

Compound	NMR ^a		
	IR (cm ⁻¹) ^b	$\delta(^{31}\text{P}\{^1\text{H}\})^c$	$\delta(^{13}\text{C}\{^1\text{H}\})^{d,e}$
[IrOs(CO) ₄ (μ -CH ₂)(dppm) ₂][CF ₃ SO ₃] (28)	2039(w), 2028(wsh)	-5.8 (m, 2P), -6.9 (m, 2P)	4.77 (dm, 2H, ² J _{HH} = 14.1 Hz), 4.75 (m, 2H), 3.36 (dm, 2H, ² J _{HH} = 14.0 Hz)
	1994(s), 1926(m)		185.1 (m, 1C, ² J _{CP} = 9.0 Hz, ² J _{CC} = 7.8 Hz), 181.7 (dt, 1C, ² J _{CP} = 9.3 Hz, ² J _{CC} = 7.4 Hz), 178.2 (dt, 1C, ² J _{CP} = 9.7 Hz, ² J _{CC} = 8.0 Hz), 170.0 (dt, 1C, ² J _{CP} = 10.8 Hz, ² J _{CC} = 7.4 Hz), 46.6 (m, 1C, ² J _{CP} = 9.0 Hz, ² J _{CC} = 8.2 Hz, ² J _{CC} = 7.8 Hz)
[IrOs(CO) ₃ (μ -CH ₂)(dppm) ₂][CF ₃ SO ₃] (29)	n/a	19.3 (m, 2P), 2.9 (m, 2P)	5.41 (m, 2H, ² J _{HP} = 10.6 Hz), 4.16 (dm, 2H, ² J _{HH} = 15.0 Hz), 3.65 (dm, 2H, ² J _{HH} = 15.0 Hz)
			195.2 (dt, 1C, ² J _{CP} = 13.1 Hz, ² J _{CC} = 10.2 Hz), 187.6 (m, 1C, ² J _{CP} = 11.8 Hz), 174.3 (dt, 1C, ² J _{CP} = 9.3 Hz), 70.1 (m, 1C, ² J _{CP} = 9.2 Hz, ² J _{CC} = 12.2 Hz)
[IrOs(CO) ₄ (μ - κ^1 : κ^1 -C(CO ₂ CH ₃)=C(CO ₂ CH ₃)CH ₂ -)(dppm) ₂][CF ₃ SO ₃] (30)	2025(s), 1998(s), 1946(m), 1923(msh)	-10.3 (m, 2P), -18.7 (m, 2P)	5.13(dm, 2H, ² J _{HH} = 13.5 Hz), 4.86 (dm, 2H, ² J _{HH} = 13.5 Hz), 2.38 (s, 3H), 2.20 (t, 2H, ³ J _{HP} = 11.1 Hz), 1.29 (s, 3H)
			184.4 (dt, 1C, ² J _{CC} = 14.3 Hz, ² J _{CP} = 7.0 Hz), 177.8 (t, 1C, ² J _{CP} = 7.0 Hz), 174.8 (bt, 1C, ² J _{CP} = 10.4 Hz), 160.0 (m, 1C, ² J _{CC} = 5.5 Hz), 46.5 (b, 1C)
[IrOs(CO) ₃ (μ - κ^1 : κ^1 -C(CO ₂ CH ₃)=C(CO ₂ CH ₃)CH ₂ -)(dppm) ₂][CF ₃ SO ₃] (31)	2006(s), 1980(m), 1917(s)	22.3 (m, 2P), -3.9 (m, 2P)	4.69 (dm, 2H, ² J _{HH} = 14.8 Hz), 3.79 (dm, 2H, ² J _{HH} = 14.8 Hz), 3.14 (s, 3H), 2.70 (s, 3H), 1.53 (t, 2H, ³ J _{HP} = 11.4 Hz)
			187.2 (t, 1C, ² J _{CP} = 8.8 Hz), 181.3 (dm, 1C, ² J _{CP} = 12.7 Hz, ² J _{CC} = 16.9 Hz), 167.8 (t, 1C, ² J _{CP} = 9.6 Hz), 10.2 (dt, 1C, ² J _{CP} = 9.6 Hz, ² J _{CC} = 16.5 Hz)

Table 4-5. Spectroscopic Data for the Compounds (Continued)

Compound	IR (cm ⁻¹) ^b	NMR ^a	
		$\delta(^1\text{P}\{\text{H}\})^c$	$\delta(^{13}\text{C}\{\text{H}\})^{d,e}$
[IrOs(CO) ₃ (μ - κ^1 : κ^1 -C(CF ₃)=C(CF ₃)(CH ₂)(dppm) ₂]-[CF ₃ SO ₃] (32)	2032 (s), 2004 (m), 1951 (s)	20.8 (m, 2P), -4.8 (m, 2P)	4.29 (dm, 2H, ² J _{HH} = 14.5 Hz), 3.99 (dm, 2H, ² J _{HH} = 14.5 Hz), 1.86 (tq, 2H, ³ J _{HF} = 8.9 Hz, ⁴ J _{HF} = 2.5 Hz)
			185.0 (t, 1C, ² J _{CP} = 9.8 Hz), 179.8 (dt, 1C, ² J _{CP} = 6.9 Hz, ² J _{CC} = 16.3 Hz), 167.7 (t, 1C, ² J _{CP} = 9.4 Hz), 8.0 (m, 1C, ² J _{CP} = 8.6 Hz, ² J _{CC} = 16.3 Hz)
[IrOs(CO) ₃ (μ -H)(μ - κ^1 : κ^1 -CH ₂ OC(OCH ₃)=C-C(CO ₂ CH ₃)=CH)(dppm) ₂][CF ₃ SO ₃] (33)	2034(s), 1975(m), 1928(w)	-8.7 (om, 4P)	5.12 (t, 1H, ³ J _{HF} = 11.2 Hz), 5.10 (dm, 2H, ² J _{HH} = 13.4 Hz), 4.85 (dm, 2H, ² J _{HH} = 13.3 Hz), 4.10 (t, 2H, ² J _{HF} = 10.6 Hz), 3.98 (s, 3H), 3.19 (s, 3H), -18.91 (quin, 1H, ² J _{HF} = 8.4 Hz)
			184.3 (dd, 1C, ² J _{CP} = 4.7 Hz, ² J _{CC} = 16.4 Hz), 174.4 (d, 2C, ² J _{CP} = 7.4 Hz), 115.2 (dt, 1C, ² J _{CC} = 16.4 Hz, ² J _{CP} = 13.4 Hz), 60.4 (bm, 1C)
[IrOs(CO) ₃ (μ - κ^1 : κ^1 -CH ₂ C(CF ₃)=C(CF ₃)(CH ₂)(dppm) ₂]-[CF ₃ SO ₃] (34) ^f	n/a	-7.7 (m, 2P), -15.5 (m, 2P)	5.25 (dm, 2H, ² J _{HH} = 14.7 Hz), 4.79 (dm, 2H, ² J _{HH} = 14.7 Hz), 4.01 (t, 2H, ³ J _{HF} = 7.4 Hz, ⁴ J _{HF} = 1.3 Hz), 2.27 (m, 2H, ³ J _{HF} = 11.4 Hz, ⁴ J _{HF} = 2.5 Hz)
			187.9 (bm, 1C, ² J _{CP} = 7.5 Hz, ² J _{CC} = 14.8 Hz), 184.0 (bt, 1C, ² J _{CP} = 8.6 Hz), 178.0 (t, 1C, ² J _{CP} = 8.9 Hz), 78.4 (b, 1C), -12.7 (dt, 1C, ² J _{CP} = 7.3 Hz, ² J _{CC} = 14.8 Hz)
[IrOs(CO) ₃ (μ - κ^1 : κ^1 -C(CO ₂ CH ₃)=C(CO ₂ CH ₃)-(dppm) ₂][CF ₃ SO ₃] (35)	2058(m), 2027(s), 2001(s), 1961(m)	-17.7 (m, 2P), -28.0 (m, 2P)	4.74 (dm, 2H, ² J _{HH} = 13.5 Hz), 4.20 (dm, 2H, ² J _{HH} = 13.5 Hz), 3.32 (s, 3H), 2.48 (s, 3H)
			182.6 (t, 1C, ² J _{CP} = 9.9 Hz), 180.0 (t, 1C, ² J _{CP} = 6.3 Hz), 173.2 (m, 1C, ² J _{CP} = 6.2 Hz, ² J _{CC} = 3.8 Hz), 154.0 (m, 1C, ² J _{CP} = 10.3 Hz, ² J _{CC} = 3.8 Hz)
[IrOs(CO) ₃ (μ - κ^1 : κ^1 -C(CF ₃)=C(CF ₃)(dppm) ₂]-[CF ₃ SO ₃] (36)	2075(m), 2032(s), 2017(s), 1957(s)	-22.6 (m, 2P), -31.2 (m, 2P)	4.49 (dm, 2H, ² J _{HH} = 14.4 Hz), 4.30 (dm, 2H, ² J _{HH} = 14.4 Hz)
			185.2 (bm, 1C, ² J _{CP} = 7.5 Hz), 177.0 (bm, 1C, ² J _{CP} = 7.4 Hz), 174.3 (bm, 1C), 154.4 (bm, 1C)

Table 4-5. Spectroscopic Data for the Compounds (Continued)

Compound	IR (cm ⁻¹) ^b	NMR ^a		
		$\delta(^3\text{P}\{^1\text{H}\})^e$	$\delta(^1\text{H})^{d,e}$	$\delta(^{13}\text{C}\{^1\text{H}\})^{d,e}$
[IrOs(CO) ₃ (μ - κ^1 : κ^1 -C(CO ₂ CH ₃)=C(CO ₂ CH ₃))- (dppm) ₂][CF ₃ SO ₃] (37)	2026(s), 2007(s), 1951(m)	13.1 (m, 2P), -10.7 (m, 2P) 1951(m)	4.90 (dm, 2H, ² J _{HH} = 13.2 Hz), 4.14 (dm, 2H, ² J _{HH} = 13.2 Hz), 2.85 (s, 3H), 2.52 (s, 3H)	193.3 (t, 1C, ² J _{CP} = 10.8 Hz), 191.1 (t, 1C, ² J _{CP} = 5.2 Hz), 167.5 (t, 1C, ² J _{CP} = 10.3 Hz)
[IrOs(CO) ₃ (μ - κ^1 : κ^1 -C(CF ₃)=C(CF ₃))(dppm) ₂]- [CF ₃ SO ₃] (38)	2033(s), 2011(s), 1958(m)	9.6 (m, 2P), -17.0 (m, 2P)	4.02 (dm, 2H, ² J _{HH} = 13.1 Hz), 3.58 (dm, 2H, ² J _{HH} = 13.1 Hz)	191.4 (t, 1C, ² J _{CP} = 9.5 Hz), 190.5 (bm, 1C, ² J _{CP} = 6.7 Hz), 166.4 (t, 1C, ² J _{CP} = 8.7 Hz)
[IrOs(CO) ₃ (μ - κ^1 : κ^1 -CH ₂ C(CF ₃)=C(CF ₃))(dppm) ₂]- [CF ₃ SO ₃] (39) ^b	1991(s), 1962(s), 1910(m)	-16.7 (m, 2P), -19.9 (m, 2P)	4.55 (dm, 2H, ² J _{HH} = 14.2 Hz), 4.18 (dm, 2H, ² J _{HH} = 14.2 Hz), 3.57 (tq, 2H, ³ J _{HP} = 8.8 Hz, ⁴ J _{HF} = 2.5 Hz)	195.2 (bt, 1C, ² J _{CP} = 7.2 Hz), 182.2 (t, 1C, ² J _{CP} = 9.3 Hz), 177.1 (t, 1C, ² J _{CP} = 9.6 Hz), 67.8 (bm, 1C)
[IrOs(CO) ₃ (PMe ₃)(μ -CH ₂)(dppm) ₂][CF ₃ SO ₃] (40)	1988(s), 1962(s), 1921(s)	-13.2 (m, 2P), -15.0 (m, 2P), -78.8 (m, 1P)	4.15 (dm, 2H, ² J _{HH} = 14.6 Hz), 4.07 (m, 2H, ³ J _{HP} = 11.5 Hz, ³ J _{HP} = 8.7 Hz), 3.35 (dm, 2H, ² J _{HH} = 14.6 Hz), 0.95 (d, 9H, ² J _{HP} = 9.1 Hz)	187.7 (dt, 1C, ² J _{CP} = 5.1 Hz, ² J _{CC} = 10.5 Hz), 182.9 (ddt, 1C, ² J _{CP} = 4.7 Hz, ² J _{CP} = 16.2 Hz, ² J _{CC} = 10.5 Hz), 180.5 (ddt, 1C, ² J _{CP} = 14.1 Hz, ² J _{CP} = 5.5 Hz, ² J _{CC} = 14.3 Hz), 53.0 (bm, 1C)

^a NMR abbreviations: s = singlet, d = doublet, t = triplet, q = quartet, m = multiplet, b = broad, quin = quintet. NMR data at 27 °C in CD₂Cl₂ unless otherwise indicated. ^b IR abbreviations for ν_{CO} (cm⁻¹): s = strong, m = medium, w = weak, sh = shoulder. Dichloromethane solution. ^c ³P{¹H} chemical shifts are referenced vs. external 85% H₃PO₄. ^d ¹H and ¹³C chemical shifts are referenced vs. external TMS. ^e Chemical shifts for the phenyl hydrogens and carbons are not given. ^f Spectroscopic data obtained at -78 °C.

procedure¹⁶ with the slight modification described herein. The protonation step to generate $[\text{IrOs}(\text{CO})_3(\mu\text{-H})_2(\text{dppm})_2][\text{X}]$ was carried out using HOSO_2CF_3 (HOTf) instead of $\text{HBF}_4\cdot\text{Et}_2\text{O}$ as follows. A solution of HOTf in Et_2O (1 equiv in 10 mL of Et_2O) was added to an orange solution of $[\text{IrOs}(\text{H})_2(\text{CO})_3(\mu_2\text{-}\kappa^1:\kappa^1\text{-}(o\text{-C}_6\text{H}_4)\text{PhPCH}_2\text{PPh}_2)(\text{dppm})]^{16}$ in benzene, resulting in the gradual precipitation of a yellow powder. To ensure complete precipitation of the product, excess diethyl ether was added. Furthermore, instead of purging a solution of $[\text{IrOs}(\text{CO})_3(\mu\text{-H})_2(\text{dppm})_2][\text{CF}_3\text{SO}_3]$ in CH_2Cl_2 , a slurry of the complex in THF and CH_2Cl_2 was purged with $\text{CO}_{(\text{g})}$ for 16 h to afford **26**. Compound **27** was prepared by the published procedure,¹⁶ using CH_2Cl_2 as solvent with recrystallization from CH_2Cl_2 /diethyl ether.

- (b) **$\text{IrOs}(\text{CO})_4(\mu\text{-CH}_2)(\text{dppm})_2][\text{CF}_3\text{SO}_3]$ (**28**). **Method (i).** Compound **26** (50 mg, 0.035 mmol) was dissolved in 5 mL of CH_2Cl_2 . Diazomethane, generated from 200 mg of Diazald,TM was passed through the solution at ambient temperature, causing the solution colour to change from light yellow to bright yellow. The solvent was evaporated to 2 mL, and 30 mL of diethyl ether was added to precipitate a bright yellow solid. This solid was recrystallized from CH_2Cl_2 /diethyl ether, washed with 2 x 5 mL of diethyl ether, and dried in vacuo (91 % yield). HRMS: m/z calcd for $\text{C}_{55}\text{H}_{46}\text{IrO}_4\text{OsP}_4$ (M^+), 1279.1585; found, 1279.1585 (M^+). Anal. Calcd for $\text{C}_{59}\text{F}_3\text{H}_{53.5}\text{IrO}_{7.75}\text{OsP}_4\text{S}$ (**28**·0.75 $\text{C}_4\text{H}_{10}\text{O}$): C, 47.82; H, 3.64. Found: C, 47.83; H, 3.68. ¹H NMR spectroscopy in CDCl_3 confirmed the presence of ether of crystallization. **Method (ii).** Compound **27** (40 mg, 0.028 mmol) was dissolved in 5 mL of CH_2Cl_2 and cooled to -78 °C. Diazomethane, generated from 200 mg of Diazald,TM was passed through the solution, causing a colour change from orange to bright yellow. The solvent was evaporated to 2 mL, and 30 mL of diethyl ether was added to precipitate a bright yellow solid, which was recrystallized from CH_2Cl_2 /diethyl ether, washed with 2 x 5 mL of diethyl ether, and dried in vacuo (92 % yield).**

- (c) **[IrOs(CO)₃(μ -CH₂)(dppm)₂][CF₃SO₃] (29).** Compound **28** (22 mg, 0.015 mmol) was dissolved in 5 mL of CH₂Cl₂, the solution was cooled to 0 °C, and anhydrous TMNO (1.74 mg, 0.023 mmol, 1.50 equiv) was added, resulting in an immediate colour change from yellow to dark red. The solution was warmed to ambient temperature, the solvent was evaporated to 2 mL, and 10 mL of diethyl ether together with 30 mL of pentane were added to precipitate a red solid, which was recrystallized from CH₂Cl₂/diethyl ether/pentane (1:3:5), washed with 2 x 5 mL of pentane, and dried in vacuo (78 % yield). HRMS: *m/z* calcd for C₅₄H₄₆IrO₃OsP₄ (M⁺), 1251.1635; found, 1251.1636 (M⁺). Due to the instability of this compound, satisfactory elemental analyses could not be obtained.
- (d) **[IrOs(CO)₄(μ - κ^1 : κ^1 -C(CO₂CH₃)=C(CO₂CH₃)CH₂)(dppm)₂]-[CF₃SO₃] (30).** **Method (i).** Compound **28** (50 mg, 0.035 mmol) was dissolved in 10 mL of CH₂Cl₂, and to it was added dimethyl acetylenedicarboxylate (DMAD; 5.5 μ L, 0.045 mmol). The solution was stirred at ambient temperature for 3 h, resulting in a gradual colour change from yellow to light orange. The solution was purged with CO_(g) for 3 min with no resulting colour change. The solvent was evaporated to 3 mL and to it was added 10 mL of diethyl ether and 30 mL of pentane to precipitate a light orange solid. The solid was recrystallized from CH₂Cl₂/diethyl ether/pentane (1:3:5), washed with 2 x 5 mL of pentane, and dried in vacuo (90 % yield). HRMS: *m/z* calcd for C₆₀H₅₂IrO₇OsP₄ (M⁺ - CO), 1393.1902; found, 1393.1902 (M⁺ - CO). Anal. Calcd for C₆₂F₃H₅₂IrO₁₁OsP₄S: C, 47.48; H, 3.34. Found: C, 47.69; H, 3.64. **Method (ii).** Compound **31** (20 mg, 0.013 mmol) was dissolved in 0.7 mL of CD₂Cl₂ in an NMR tube to afford an orange solution, which was purged by CO_(g) for 1 min, resulting in a slight lightening of the solution. Conversion of **31** to **30** was monitored by ³¹P NMR spectroscopy and was observed to be quantitative under the CO atmosphere.

- (e) **[IrOs(CO)₃(μ - κ^1 : κ^1 -C(CO₂CH₃)=C(CO₂CH₃)CH₂)(dppm)₂]-[CF₃SO₃] (31).** Compound **29** (25 mg, 0.018 mmol) was dissolved in 5 mL of CH₂Cl₂, and to it was added DMAD (2.6 μ L, 0.021 mmol), resulting in a colour change from red to yellow. The solvent was evaporated to 2 mL and 10 mL of diethyl ether and 20 mL of pentane were added to precipitate a yellow-orange solid. The solid was recrystallized from CH₂Cl₂/diethyl ether/pentane (1:3:5), washed with 2 x 5 mL of pentane, and dried in vacuo (89 % yield). HRMS: *m/z* calcd for C₆₀H₅₂IrO₇OsP₄ (M⁺), 1393.1905; found, 1393.1902 (M⁺). Anal. Calcd for C₆₁F₃H₅₂IrO₁₀OsP₄S: C, 47.56; H, 3.40. Found: C, 47.73; H, 3.74.
- (f) **[IrOs(CO)₃(μ - κ^1 : κ^1 -C(CF₃)=C(CF₃)CH₂)(dppm)₂][CF₃SO₃] (32).** Compound **29** (55 mg, 0.039 mmol) was dissolved in 10 mL of CH₂Cl₂. Hexafluoro-2-butyne (HFB) was passed vigorously through the solution for 2 min, resulting in a colour change from red to orange. The solvent was evaporated to 2 mL and 10 mL of diethyl ether and 20 mL of pentane were added to precipitate an orange solid. The solid was recrystallized from CH₂Cl₂/diethyl ether/pentane (1:3:3), washed with 2 x 5 mL of pentane, and dried in vacuo (87 % yield). HRMS: *m/z* calcd for C₅₉H₄₆F₆IrO₃OsP₄ (M⁺), 1413.1539; found, 1413.1541 (M⁺). Anal. Calcd for C_{59.25}Cl_{0.5}F₉H_{46.5}IrO₆OsP₄S (**32**·0.25 CH₂Cl₂): C, 44.99; H, 2.96. Found: C, 44.80; H, 3.09. ¹H NMR spectroscopy in CDCl₃ confirmed the presence of dichloromethane of crystallization. ¹⁹F NMR (in CD₂Cl₂): δ -47.0 (quartet, 3F, ⁵J_{FF} = 13.8 Hz), δ -61.7 (quartet of triplets, 3F, ⁵J_{FF} = 13.7 Hz, ⁴J_{FH} = 2.6 Hz), δ -79.2 (singlet, 3F).
- (g) **[IrOs(CO)₃(μ -H)(μ - κ^1 : κ^1 : κ^1 CH₂OC(OCH₃)=CC-(CO₂CH₃)=CH)(dppm)₂][CF₃SO₃] (33).** An orange solution of **31** (34 mg, 0.023 mmol) in 5 mL of CH₂Cl₂ was cooled to -78 °C. Diazomethane, generated from 200 mg of Diazald,TM was passed through the solution at this temperature, resulting in no observable colour change. The solution was slowly warmed to ambient temperature, the solvent was

evaporated to 2 mL and to it was added 10 mL of diethyl ether and 20 mL of pentane to precipitate a light orange solid, which was recrystallized from CH₂Cl₂/diethyl ether/pentane (1:3:5) and dried in vacuo (86 % yield). HRMS: *m/z* calcd for C₆₁H₅₄IrO₇OsP₄ (M⁺), 1407.2061; found, 1407.2059 (M⁺). Anal. Calcd for C₆₂F₃H₅₄IrO₁₀OsP₄S: C, 47.90; H, 3.50. Found: C, 47.85; H, 3.91.

- (h) **[IrOs(CO)₃(μ-κ¹:κ¹-CH₂C(CF₃)=C(CF₃)CH₂)(dppm)₂][CF₃SO₃]** (**34**). An orange solution of **32** (40 mg, 0.026 mmol) in 5 mL of CH₂Cl₂ was cooled to -78 °C. Diazomethane, generated from 200 mg of Diazald,TM was passed through the solution at this temperature, resulting in a colour change from orange to yellow. The solution was kept at -78 °C and the product was characterized by low-temperature NMR since it was not stable upon warming to ambient temperature. ¹⁹F NMR (-78 °C in CD₂Cl₂): δ -49.9 (quartet of triplets, 3F, ⁵J_{FF} = 15.8 Hz, ⁴J_{FH} = 2.6 Hz), δ -59.8 (quartet of triplets, 3F, ⁵J_{FF} = 16.5 Hz, ⁴J_{FH} = 1.3 Hz), δ -79.6 (singlet, 3F).
- (i) **[IrOs(CO)₄(μ-κ¹:κ¹-C(CO₂CH₃)=C(CO₂CH₃))(dppm)₂]-[CF₃SO₃]** (**35**). A solution of DMAD (4.5 μL, 0.036 mmol) in 5 mL of CH₂Cl₂ was cooled to -78 °C and was added dropwise via cannula over 30 min to a solution of compound **27** (51 mg, 0.036 mmol) in 5 mL of CH₂Cl₂ at -78 °C. The mixture was stirred at this temperature for 30 min and then slowly warmed to ambient temperature. After an additional 2 h of stirring the solvent was evaporated to 2 mL, and to it was added 10 mL of diethyl ether and 20 mL of pentane to precipitate a light orange solid. The solid was recrystallized from CH₂Cl₂/pentane, washed with 2 x 5 mL of pentane, and dried in vacuo (75 % yield). HRMS: *m/z* calcd for C₅₉H₅₀IrO₇OsP₄ (M⁺ - CO), 1379.1741; found, 1379.1746 (M⁺ - CO). Anal. Calcd for C₆₁F₃H₅₀IrO₁₁OsP₄S: C, 47.13; H, 3.24. Found: C, 46.87; H, 3.06.

(j) **[IrOs(CO)₄(μ - κ^1 : κ^1 -C(CF₃)=C(CF₃))(dppm)₂][CF₃SO₃] (36).**

An orange solution of **27** (60 mg, 0.043 mmol) in 10 mL of CH₂Cl₂ was cooled to -78 °C. The argon headspace of the flask was evacuated and replaced with a slight overpressure of HFB. The reaction was stirred at -78 °C for 1 h and then slowly warmed to ambient temperature and stirred for 12 h, resulting in a gradual colour change to yellow. The solvent was evaporated to 2 mL, and to it was added 20 mL of pentane to precipitate a light orange solid, which was recrystallized from CH₂Cl₂/pentane, washed with 2 x 5 mL of pentane, and dried in vacuo (94 % yield). HRMS: *m/z* calcd for C₅₇H₄₄F₆IrO₃OsP₄ (M⁺ - CO), 1399.1382; found, 1399.1384 (M⁺ - CO). Anal. Calcd for C_{59.175}Cl_{0.35}F₉H_{44.35}IrO₇OsP₄S (**36**·0.175CH₂Cl₂): C, 44.30; H, 2.83. Found: C, 44.09; H, 2.76. ¹H NMR spectroscopy in CDCl₃ confirmed the presence of dichloromethane of crystallization. ¹⁹F NMR (in CD₂Cl₂): δ -52.7 (quartet, 3F, ⁵J_{FF} = 13.6 Hz), δ -53.1 (quartet, 3F, ⁵J_{FF} = 13.6 Hz), δ -79.3 (singlet, 3F).

(k) **[IrOs(CO)₃(μ - κ^1 : κ^1 -C(CO₂CH₃)=C(CO₂CH₃))(dppm)₂]-**

[CF₃SO₃] (37). A solution of anhydrous TMNO (0.023 mmol, 1.7 mg) in 3 mL of CH₂Cl₂ was added dropwise over a period of 30 min to a stirred solution of **35** (30 mg, 0.019 mmol) in 5 mL of CH₂Cl₂, resulting in a gradual darkening of the solution. The solvent was evaporated to 2 mL, and to it was added 10 mL of diethyl ether and 20 mL of pentane to precipitate an orange solid, which was recrystallized from CH₂Cl₂/diethyl ether/pentane (1:3:5), washed with 2 x 3 mL of pentane and dried in vacuo (86 % yield). HRMS: *m/z* calcd for C₅₉H₅₀IrO₇OsP₄ (M⁺), 1379.1746; found, 1379.1739 (M⁺). Anal. Calcd for C₆₀F₃H₅₀IrO₁₀OsP₄S: C, 47.21; H, 3.30. Found: C, 47.20; H, 3.44.

(l) **[IrOs(CO)₃(μ - κ^1 : κ^1 -C(CF₃)=C(CF₃))(dppm)₂][CF₃SO₃] (38).**

Compound **36** (40 mg, 0.026 mmol) was dissolved in 3 mL of CH₂Cl₂, and to the solution was added dropwise over a period of 30 min anhydrous TMNO (2.3 mg, 0.031 mmol) in 2 mL of CH₂Cl₂, resulting in a gradual

colour change from orange to dark orange-red. The solvent was evaporated to 2 mL, and to it was added 20 mL of diethyl ether to precipitate an orange solid. The solid was recrystallized from CH₂Cl₂/diethyl ether, washed with 2 x 3 mL of diethyl ether and dried in vacuo (82 % yield). HRMS: *m/z* calcd for C₅₇H₄₄F₆IrO₃OsP₄ (M⁺), 1399.1384; found, 1399.1394 (M⁺). Anal. Calcd for C₅₈F₉H₄₄IrO₆OsP₄S: C, 45.05; H, 2.87. Found: C, 45.18; H, 2.97. ¹⁹F NMR (in CD₂Cl₂): δ –45.9 (quartet, 3F, ⁵J_{FF} = 11.2 Hz), δ –51.2 (quartet, 3F, ⁵J_{FF} = 11.2 Hz), δ –79.3 (singlet, 3F).

- (m) **[IrOs(CO)₃(μ-κ¹:κ¹-CH₂C(CF₃)=C(CF₃))(dppm)₂][CF₃SO₃]** (**39**). A dark orange solution of **38** (33 mg, 0.021 mmol) in 5 mL of CH₂Cl₂ was cooled to –78 °C. Diazomethane generated from 200 mg of Diazald,TM was passed through the solution at low-temperature, resulting in a colour change to yellow. This compound was stable in solution at low-temperature only, and was characterized by NMR at –78 °C. ¹⁹F NMR (–78 °C): δ –51.5 (quartet, 3F, ⁵J_{FF} = 16.6 Hz), δ –52.2 (quartet of triplets, 3F, ⁵J_{FF} = 16.6 Hz, ⁴J_{FH} = 2.5 Hz), δ –79.2 (singlet, 3F).
- (n) **[IrOs(CO)₃(PMe₃)(μ-CH₂)(dppm)₂][CF₃SO₃]** (**40**). Compound **28** (100 mg, 0.070 mmol) was dissolved in 5 mL of CH₂Cl₂, and to the solution was added neat PMe₃ (14.5 μL, 0.140 mmol). The solution was stirred at ambient temperature for 6 h, resulting in a lightening of the solution. The solvent was evaporated to 2 mL, and to it was added 10 mL of diethyl ether and 20 mL of pentane to precipitate a light yellow solid, which was recrystallized from CH₂Cl₂/diethyl ether/pentane (1:3:5) and dried in vacuo (91 % yield). Anal. Calcd for C₅₈F₃H₅₅IrO₆OsP₅S: C, 47.25; H, 3.76. Found: C, 47.80; H, 3.79.
- (o) **Relative Rates for the Reactions of 28 and [IrRu(CO)₄(μ-CH₂)(dppm)₂][CF₃SO₃] with PMe₃**. Compound **28** (30 mg, 0.021 mmol) was dissolved in 0.7 mL of CD₂Cl₂ in an NMR tube. [IrRu(CO)₄(μ-CH₂)(dppm)₂][CF₃SO₃] (**1-CF₃SO₃**) (28 mg, 0.021 mmol)

was dissolved in 0.7 mL of CD₂Cl₂ in an NMR tube to yield a solution of identical concentration to that of **28** in CD₂Cl₂. To both tubes was added neat PMe₃ (4.4 μL, 0.042 mmol) simultaneously (*t* = 0 h). The reaction was monitored each hour (including *t* = 0 h) by ³¹P{¹H} spectroscopy, monitoring the relative rates of conversions of **28** and the Ir/Ru analogue to their corresponding PMe₃-substitution products.

4.5.3 X-ray Structure Determinations

4.5.3.1 General

Crystals were grown by slow diffusion of diethyl ether into an acetonitrile solution of the compound (**28**) or diffusion of diethyl ether into a CH₂Cl₂ solution of the compound (**32**, **33-BF₄**, **37-BF₄**). Data were collected using a Bruker APEX-II CCD detector/D8 diffractometer¹⁷ with the crystals cooled to -100 °C (**28**, **32**, **33-BF₄**) or using an Enraf-Nonius CAD4 diffractometer¹⁷ with the crystals cooled to -50 °C (**37-BF₄**); all data were collected using Mo Kα radiation ($\lambda = 0.71073 \text{ \AA}$). The data were corrected for absorption through Gaussian integration from indexing of the crystal faces (**28**, **33-BF₄**, **37-BF₄**) or through use of a multiscan model (SADABS¹⁷) (**32**). Structures were solved using Patterson search/structure expansion (DIRDIF-2008¹⁸) (**28**), direct methods/structure expansion (SIR97¹⁹) (**32**), or direct methods (SHELXS-97²⁰) (**33-BF₄**, **37-BF₄**). Refinements were completed using the program SHELXL-97.²⁰

Hydrogen atoms attached to carbons were assigned positions based on the sp² or sp³ hybridization geometries of their attached carbons and were given thermal parameters 20 % greater than those of their parent atoms (the hydrido ligand of **33-BF₄** was located from a difference Fourier map and was assigned a fixed isotropic displacement parameter while its coordinates were freely refined). See Appendix III.3 for a listing of crystallographic experimental data for all structures within this chapter.

4.5.3.2 Special Refinement Conditions

(i) Compound **28**: The metals were found to be equally disordered over both positions, so each was refined as 50 % Ir and 50 % Os, sharing each site. (ii) Compound **32**: The Cl–C and Cl \cdots Cl distances within the disordered solvent dichloromethane molecules were restrained to be 1.80(1) and 2.80(1) Å, respectively.

(iii) Compound **33-BF₄**: Restraints were applied to achieve idealized geometries within the two conformers of the disordered tetrafluoroborate ion; F–B distances were constrained to be equal (within 0.03 Å) during refinement, as were the F \cdots F distances of F–B–F angles.

(iv) Compound **37-BF₄**: Restraints were applied to distances within the two conformers of the disordered tetrafluoroborate ion in the same manner as for **33-BF₄** above. The Cl–C distances within the disordered solvent dichloromethane molecule were constrained to be equal (within 0.03 Å) during refinement, as were the Cl \cdots Cl distances within each disordered moiety.

(v) Assignments of metal centres in complexes **32**, **33-BF₄**, **37-BF₄**: For each of the complexes in which the metals have dissimilar coordination environments, the final models were tested by switching the identities of the metal atom centres (Ir for Os and vice versa) and refining these to completion. In each case, the final indices became subtly but noticeably worse for the ‘reversed-metals’ models (**32**: from $R_1 = 0.0262$, $wR_2 = 0.0674$ to $R_1 = 0.0264$, $wR_2 = 0.0691$; **33-BF₄**: from $R_1 = 0.0299$, $wR_2 = 0.0792$ to $R_1 = 0.0306$, $wR_2 = 0.0806$; **37-BF₄**: from $R_1 = 0.0458$, $wR_2 = 0.1489$ to $R_1 = 0.0460$, $wR_2 = 0.1498$). For **33-BF₄**, the position of the hydrido ligand (H(1)) could not be freely refined after reversing the identities of the metals, and that model would only converge after distance restraints were applied ($d(\text{Ir–H}(1)) = 1.61(1)$ Å; $d(\text{Os–H}(1)) = 1.85(1)$ Å) that were based on the distances observed for the freely-refined hydrido ligand of the original model.

4.6 References

1. MacDougall, T. J.; Trepanier, S. J.; Dutton, J. L.; Ferguson, M. J.; McDonald, R.; Cowie, M. *Organometallics* **2011**, *30*, 5882.
2. (a) Fischer, F.; Tropsch, H. *Brennst. Chem.* **1926**, *7*, 97. (b) Fischer, F.; Tropsch, H. *Chem. Ber.* **1926**, *59*, 830.
3. (a) Brady, R. C.; Pettit, R. *J. Am. Chem. Soc.* **1980**, *102*, 6181. (b) Brady, R. C.; Pettit, R. *J. Am. Chem. Soc.* **1981**, *103*, 1287. (c) Biloen, P.; Sachtler, W. M. H. *Adv. Catal.* **1981**, *30*, 165. (d) Maitlis, P. M.; Long, H. C.; Quyoum, R.; Turner, M. L.; Wang, Z.-Q. *Chem. Commun.* **1996**, *1*. (e) Long, H. C.; Turner, M. L.; Fornasiero, P.; Kaspar, J.; Graziani, M.; Maitlis, P. M. *J. Catal.* **1997**, *167*, 172. (f) Dry, M. E. *Appl. Catal. A* **1996**, *138*, 319.
4. (a) Trepanier, S. J.; Sterenberg, B. T.; McDonald, R.; Cowie, M. *J. Am. Chem. Soc.* **1999**, *121*, 2613. (b) Trepanier, S. J.; Dennett, J. N. L.; Sterenberg, B. T.; McDonald, R.; Cowie, M. *J. Am. Chem. Soc.* **2004**, *126*, 8046.
5. (a) Rowsell, B. D.; Trepanier, S. J.; Lam, R.; McDonald, R.; Cowie, M. *Organometallics* **2002**, *21*, 3228. (b) Rowsell, B. D.; McDonald, R.; Ferguson, M. J.; Cowie, M. *Organometallics* **2003**, *22*, 2944. (c) Dell'Anna, M. M.; Trepanier, S. J.; McDonald, R.; Cowie, M. *Organometallics* **2001**, *20*, 88. (d) Wigginton, J. R.; Chokshi, A.; Graham, T. W.; McDonald, R.; Ferguson, M. J.; Cowie, M. *Organometallics* **2005**, *24*, 6398.
6. (a) Cotton, F. A.; Wilkinson, G.; Gaus, P. L. In *Basic Inorganic Chemistry*; 3rd ed.; John Wiley & Sons, Inc.: New York, 1995, p 646. (b) Housecroft, C. E.; Sharpe, A. G. In *Inorganic Chemistry*; 2nd ed.; Prentice Hall: Harlow, England, 2005, p 713. (c) Elschenbroich, C. In *Organometallics*; 3rd ed.; Wiley-VCH: Weinheim, Germany, 2006, p 360.
7. Allen, F. H.; Kennard, O.; Watson, D. G.; Brammer, L.; Orpen, A. G.; Taylor, R. *J. Chem. Soc., Perkin Trans. 2* **1987**, S1.
8. $r_c(\text{sp}^3) = 0.77 \text{ \AA}$; $r_c(\text{sp}^2) = 0.74 \text{ \AA}$.

9. (a) Emsley, J. W.; Phillips, L.; Wray, V. *Prog. N.M.R. Spectroscopy* **1976**, *10*, 83. (b) Foris, A. *Magn. Reson. Chem.* **2004**, *42*, 534. (c) Wray, V.; Lincoln, D. N. *J. Chem. Soc. Perkin Trans. 2* **1976**, *2*, 1307.
10. Cowie, M. *Can. J. Chem.* **2005**, *83*, 1043.
11. (a) Akita, M.; Hua, R.; Knox, S. A. R.; Moro-oka, Y.; Nakanishi, S.; Yates, M. I. *J. Organomet. Chem.* **1998**, *569*, 71. (b) Dyke, A. F.; Knox, S. A. R.; Naish, P. J.; Taylor, G. E. *J. Chem. Soc., Chem. Commun.* **1980**, 803. (c) Gracey, B. P.; Knox, S. A. R.; Macpherson, K. A.; Orpen, A. G.; Stobart, S. R. *J. Chem. Soc., Dalton Trans.* **1985**, 1935.
12. (a) Samant, R. G.; Trepanier, S. J.; Wigginton, J. R.; Xu, L.; Bierenstiel, M.; McDonald, R.; Ferguson, M. J.; Cowie, M. *Organometallics* **2009**, *28*, 3407. (b) Gao, Y.; Jennings, M. C.; Puddephatt, R. J. *Organometallics* **2001**, *20*, 1882.
13. (a) Corrigan, P. A.; Dickson, R. S. *Aust. J. Chem.* **1979**, *32*, 2147. (b) King, P. J.; Knox, S. A. R.; Legge, M. S.; Orpen, A. G.; Wilkinson, J. N.; Hill, E. A. *J. Chem. Soc., Dalton Trans.* **2000**, 1547.
14. Campanelli, A. R.; Domenicano, A.; Ramondo, F.; Hargittai, I. *J. Phys. Chem. A* **2004**, *108*, 4940.
15. Rhee, S. W.; Ryan, K. J.; Tracy, M.; Kelson, A. B.; Clizbe, L. A.; Chang, M.-H.; Park, J. S.; Roh, J.-K.; Kong, J.-Y.; Yang, J. G.; Kim, W.-B.; Ok, K.-D. *J. Labelled Compd. Radiopharm.* **1997**, *39*, 773.
16. Hilts, R. W.; Franchuk, R. A.; Cowie, M. *Organometallics* **1991**, *10*, 1297.
17. (a) For compounds **3**, **7**, and **8-BF₄**, programs for diffractometer operation, data collection, data reduction, and absorption correction were those supplied by Bruker. (b) For compound **12-BF₄**, programs for diffractometer operation and data collection were those supplied by Enraf-Nonius. The data were reduced using the program XCAD4 (Harms, K.; Wocadlo, S. University of Marburg, 1995). Absorption corrections were applied using programs of the SHELXTL system (Bruker, 2008).

18. Beurskens, P. T.; Beurskens, G.; de Gelder, R.; Garcia-Granda, S.; Israel, R.; Gould, R. O.; Smits, J. M. M. *The DIRDIF-99 program system*; Crystallography Laboratory, University of Nijmegen, The Netherlands, 1999.
19. Altomare, A.; Burla, M. C.; Camalli, M.; Cascarano, G. L.; Giacovazzo, C.; Guagliardi, A.; Moliterni, A. G. G.; Polidori, G.; Spagna, R. *J. Appl. Crystallogr.* **1999**, *32*, 115.
20. Sheldrick, G. M. *Acta Crystallogr.* **2008**, *A64*, 112.

Chapter 5: Reactions of Iridium/Osmium Complexes with Cumulenes: A Comparative Study

5.1 Introduction

The use of methylene-bridged heterobimetallic complexes by the Cowie group to model the formation of carbon–carbon bonds occurring on a metal surface in the Fischer-Tropsch (FT) reaction, as described in Chapters 2 and 4, has met with mixed success.¹ Among the successes, a study from our group involving the Rh/Os metal combination demonstrated the facile coupling of diazomethane-generated methylene units to generate either butanediyl or allyl and methyl fragments at the bimetallic core, which under H₂ subsequently underwent hydrogenolysis to yield the respective products, *n*-butane, propene, and methane,^{1a,b} giving a sampling of FT-type products. The intermediates in C–C bond formation are proposed to involve the stepwise incorporation of methylene units to yield bridging ethylene and propanediyl groups before the pathway diverges to generate the allyl and methyl or butanediyl fragments. The propanediyl-bridged fragment appears to be a pivotal intermediate in this methylene coupling transformation. Such species have been observed² and are proposed as unstable intermediates in the coupling of ethylene with a methylene group to yield propene.³ In our studies, the addition of ethylene to the “M'(μ-CH₂)M” (M' = Ir, Rh; M = Ru, Os) complexes also did not yield the targeted propanediyl species, owing to the facile elimination of propene.^{1a,b,1f} We therefore investigated the stepwise coupling of methylene groups with a variety of unsaturated substrates,^{1c,1e,1g,4} that could lead to C₃-bridged fragments analogous to the propanediyl fragments. Although the insertion of alkynes to generate C₃-bridged fragments works well, unsaturation is present within the C₃-bridge, that is not present in the actual propanediyl targets. We therefore sought to model the propanediyl fragment more closely by using cumulenes as unsaturated fragments, in hopes of generating insertion products in which the unsaturation remains *exo* to the C₃-bridge, more accurately representing the saturated propanediyl moiety.

However, we found that the methylene-bridged Rh/M (M = Ru, Os) combinations tend to generate rearranged products with cumulenes, often generating bridging $\kappa^1:\eta^3$ trimethylenemethane fragments or their substituted analogues instead of the targeted C₃-bridged species, that are κ^1 -bound from each end of the C₃ unit to a different metal. As described earlier in Chapter 2, the addition of cumulenes to methylene-bridged Ir/Ru complexes results in Ir-based metallacycles in which the resulting C₃-based hydrocarbyl fragment is chelating on Ir, presumably a result of the greater Ir–C bonds strengths. Subsequent reactions of these iridacycle products with additional cumulene resulted in two or more C–H bond activations within the added cumulene, reactivity that was also observed with [IrRu(CO)₄(dppm)₂]⁺, as described in Chapter 3. The current study focuses on the Ir/Os metal combination, having strong M–C bonds at both metal centres, which we anticipated might be conducive to retention of the bridging C₃ fragments.

In this chapter, we report the reactions of allene, methylallene, and 1,1-dimethylallene with [IrOs(CO)₃(μ -CH₂)(dppm)₂]⁺ in further attempts to generate models for propanediyl-bridged intermediates, and to compare the reactivity with that of the Rh/Ru, Rh/Os and Ir/Ru metal combinations. We hoped that by investigating this series of cumulenes using the Ir/Os metal combination we could gain more information regarding the roles of the different metals in C–C bond formation. We also sought to compare the reactivity of [IrOs(CO)₄(dppm)₂]⁺ to the analogous Ir/Ru system, anticipating that this study could yield additional information on the roles of the different metals in the unexpected multiple C–H bond activations observed with the Ir/Ru system.

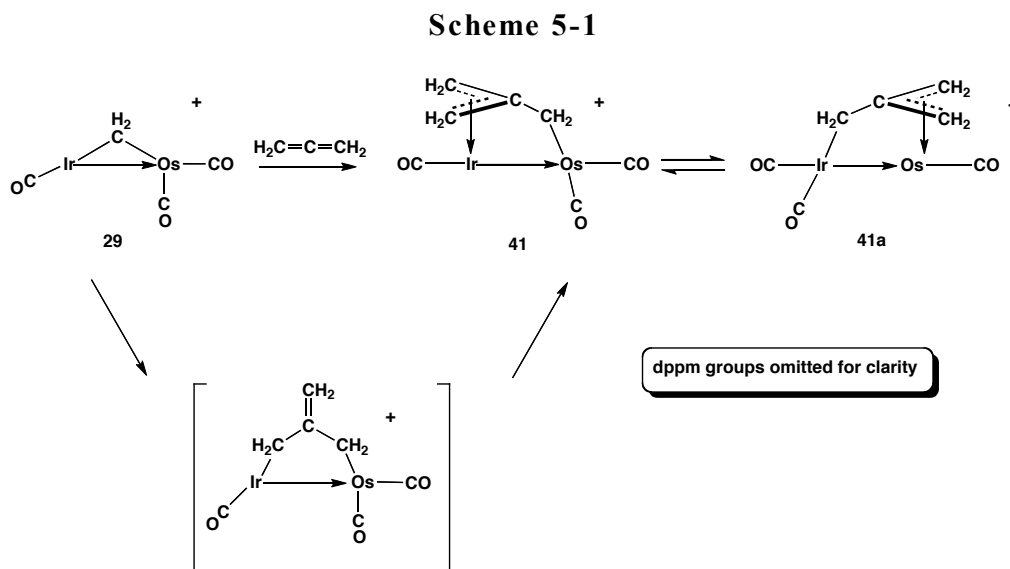
5.2 Results and Compound Characterization

5.2.1 Reactivity of [IrOs(CO)₃(μ -CH₂)(dppm)₂]⁺ with Cumulenes

5.2.1.1 Allene

The methylene-bridged tetracarbonyl complex [IrOs(CO)₄(μ -CH₂)(dppm)₂][BF₄] (**28-BF₄**) reacts over a 20 h period with propadiene (allene) to generate an equilibrium mix of two isomers of [IrOs(CO)₃(μ - η^3 : κ^1 -

$C(CH_2)_3(dppm)_2[BF_4]$ (**41/41a**), in an approximate 4:3 ratio (Scheme 5-1), accompanied by CO loss. If the same reaction is carried out using the methylene-bridged tricarbonyl analogue, $[IrOs(CO)_3(\mu-CH_2)(dppm)_2][BF_4]$ (**29-BF₄**), the identical two isomers are obtained within 10 h. In all subsequent reactions the methylene-bridged tricarbonyl (**29**) is used in order to take advantage of the shorter reaction times. The assignment of the spectroscopic data for compounds **41** and **41a** to the structures shown in Scheme 5-1 is based on NMR methods, and differentiating between the two compounds is challenging since neither metal displays coupling to the NMR active nuclei in the compounds (^{31}P , ^{13}C , 1H) and the chemical shifts for the respective nuclei bound to these metals are in approximately the same regions of the spectra.



Each isomer displays two resonances in the $^{31}P\{^1H\}$ NMR spectrum (shown in Figure 5-1), consistent with an AA'BB' spin system, in which the ends of the diphosphines bound to the different metals are inequivalent, (**41**: $\delta -9.5$, $\delta -27.2$; **41a**: $\delta -7.3$ and $\delta -19.2$). Assignment of the observed NMR resonances to **41/41a** is accomplished by NMR experiments involving heteronuclear decoupling (^{31}P , ^{13}C , 1H), and on literature precedent with analogous mononuclear Ir and Os complexes, as explained in what follows. The two downfield signals represent the ^{31}P nuclei bound to the metal with the κ^1 -bound methylene in both

isomers, while the upfield signals represent the ^{31}P nuclei of the metal with the η^3 -allyl-type interaction. In the ^1H NMR spectrum the CH_2 protons of the dpmm ligands appear at δ 5.04 and δ 4.06 (**41**) and δ 5.62 and δ 4.94 (**41a**), with an average mutual two-bond coupling of 15.5 Hz. The protons from the η^3 -allyl-type interaction appear at δ 2.72 and δ 1.94 in **41**, and δ 3.55 and δ 1.29 in **41a**. These data are consistent with known allyl complexes of complexes of Os^5 and Ir^6 in which the Ir-bound allyl group protons resonate at lower field than those on the

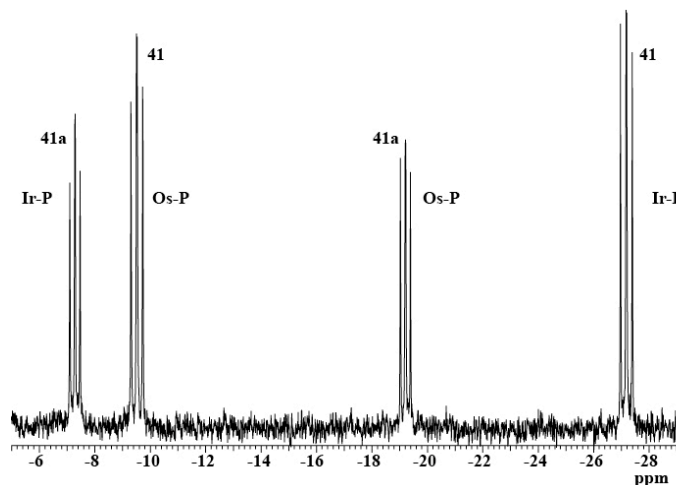


Figure 5-1. $^{31}\text{P}\{^1\text{H}\}$ NMR spectrum of **41/41a** in CD_2Cl_2 .

Os-bound group. Interestingly, the CH_2 protons of the κ^1 -bound methylene group appear at very different chemical shifts in **41** (δ 1.74, $^3J_{\text{HP}(\delta-9.5)} = 10.7$ Hz) and **41a** (δ 4.35 $^3J_{\text{HP}(\delta-7.3)} = 4.8$ Hz), which aid in the identification of each isomer, on the basis that Os-bound CH_2 protons have been shown to appear downfield of Ir-bound CH_2 protons in similar complexes.^{1g} Proton spin-saturation-transfer experiments also support the presence of the equilibrium as proposed above, in which irradiating the CH_2 proton resonance at δ 1.74 in **41** results in a decrease in intensity of the CH_2 proton resonance at δ 4.35, and vice versa. In a $^{13}\text{CH}_2$ -enriched sample of **41/41a**, the $^{13}\text{C}\{^1\text{H}\}$ NMR spectrum has one broad signal for the labeled carbon of the κ^1 -methylene in *both* isomers, however, scrambling of the $^*\text{CH}_2$ label is also observed over the other two equivalent methylene groups of the trimethylenemethane, the signal for which appears at δ 64.4, consistent with

the exchange process suggested above. ^{13}C NMR experiments with selective ^1H and ^{31}P decoupling confirm that the metal with the η^3 -allyl-type interaction has one carbonyl bound to it, while the other metal has two, consistent with the changing hapticity of the trimethylenemethane ligand with respect to the two metals being accompanied by migration of a carbonyl from metal to metal. In this way, each metal maintains an $18e^-$ configuration.

An X-ray structure determination of **41/41a**, in which the tetrafluoroborate has been exchanged with triflate, is shown, for the complex cation in Figure 5-2, and confirms the $\mu\text{-}\eta^3\text{:}\kappa^1$ trimethylenemethane moiety and

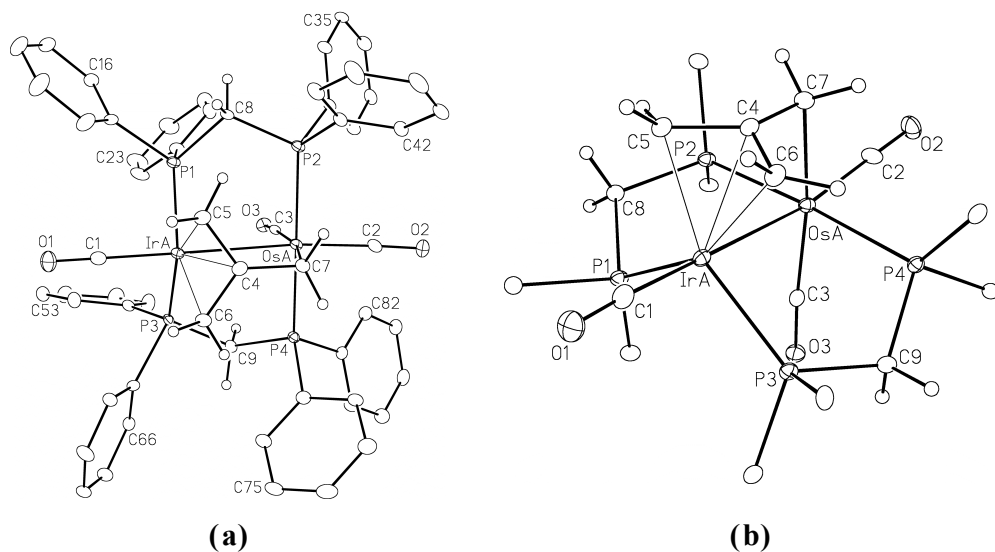


Figure 5-2. (a) Perspective view of the complex cation of $[\text{IrOs}(\text{CO})_3(\mu\text{-}\eta^3\text{:}\kappa^1\text{-C}(\text{CH}_2)_3)(\text{dppm})_2][\text{CF}_3\text{SO}_3]$ (**41/41a**- CF_3SO_3). Thermal ellipsoids are shown at the 20 % probability level except for hydrogens, which are omitted for the phenyl groups but are shown arbitrarily small for the others. Note that the atoms Ir(A) and Os(A) are refined as a combination of 50 % Ir and 50 % Os, so the alternate conformation (**41a**), comprised of Ir(B) and Os(B), is equally abundant. (b) Alternate view of the cation of **41/41a**- CF_3SO_3 with only the ipso carbons of the phenyl rings shown.

the carbonyl arrangement suggested above. Differentiating the two metals using crystallographic methods is difficult, owing to their similar X-ray scattering amplitudes, and refining this structure with both possibilities of metal assignments, does not suggest a preferred isomer. However, refinement is marginally better when each metal site is refined as 50 % Ir and 50 % Os, suggesting a disordered mix of isomers. Dissolving the crystals used for X-ray analysis showed the presence of both isomers in the same 4:3 ratio. Furthermore, as noted, both metals have saturated $18e^-$ configurations in both isomers so the metals cannot be distinguished on the basis of their electronic preferences.

The Ir–Os separation of 2.9162(4) Å, is somewhat shorter than the intraligand P–P distances of *ca.* 3.09 Å, suggesting a metal–metal bonding interaction resulting in compression along the axis of the metals. However, the nature of the metal–metal bond and the corresponding metal oxidation states are uncertain. In the formulations shown in Scheme 5-1, an Ir(I)/Os(II) formulation is accompanied by a dative Ir→Os bond, although an alternate formulation has an Ir(II)/Os(I) formulation and a conventional Ir–Os bond. We favour the former description since it corresponds to the favoured oxidation states of the metals. Compounds **41** and **41a** differ in the binding of the trimethylenemethane moiety and the carbonyl ligands. In **41** the trimethylenemethane unit is bound in a κ^1 manner to Os while η^3 -bound to Ir, while in **41a** it has the opposite arrangement. In both cases, the metal centre with the κ^1 -bound ligand has two CO ligands bound to it while the metal with the η^3 -bound ligand has only one.

The geometry about the monocarbonyl end, Ir(A)/Os(B), is a slightly distorted trigonal bipyramid while the dicarbonyl end, (Os(A)/Ir(B)) is a distorted octahedron. Within the trimethylenemethane moiety, the C(4)–C(7) bond length (1.456(9) Å) is shorter than expected for a single bond, while the C(4)–C(5) and C(4)–C(6) bond lengths (1.437(8) Å and 1.449(8) Å respectively) are intermediate between double and single bonds, as expected for an η^3 -allyl group.⁷ These bond lengths are consistent with the reported bond lengths for other metal-bound trimethylenemethane units.⁸ The C(6)–C(4)–C(5) angle of 124.1(6)° is as

expected for an sp^2 hybridized carbon. The bridging diphosphines have a cis arrangement at the metal bound to the η^3 -allylic fragment ($P(1)-Ir(A)-P(3) = 112.69(5)^\circ$) and a trans arrangement at the other ($P(2)-Os(A)-P(4) = 174.91(5)^\circ$; see Figure 5-2(b)), as seen in a number of such compounds.^{1c,6b}

Table 5-1. Selected Bond Lengths and Angles for Compound 41/41a-CF₃SO₃

(a) Distance (Å)

atom 1	atom 2	distance	atom 1	atom 2	distance
Ir(A)	Os(A)	2.9162(4)	Os(A)	C(7)	2.202(6)
Ir(A)	C(4)	2.278(6)	C(4)	C(5)	1.437(8)
Ir(A)	C(5)	2.233(6)	C(4)	C(6)	1.449(8)
Ir(A)	C(6)	2.219(6)	C(4)	C(7)	1.456(9)

(b) Angles (deg)

atom 1	atom 2	atom 3	angle	atom 1	atom 2	atom 3	angle
C(6)	C(4)	C(5)	124.1(6)	Os(A)	Ir(A)	C(6)	86.2(2)
Os(A)	C(7)	C(4)	99.6(4)	P(1)	Ir(A)	P(3)	112.69(5)
Os(A)	Ir(A)	C(4)	64.8(2)	Ir(A)	Os(A)	C(7)	77.1(2)
Os(A)	Ir(A)	C(5)	85.4(2)	P(2)	Os(A)	P(4)	174.91(5)

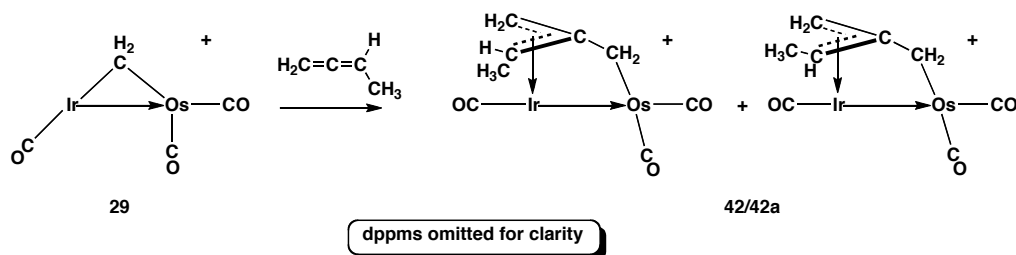
Attempts to observe intermediates in the formation of **41/41a** by the addition of allene to a CH_2Cl_2 solution of **29-BF₄** at $-78^\circ C$ resulted in the observation of several compounds at this temperature, for which the peaks in the $^{31}P\{^1H\}$ NMR spectrum were broad and overlapping, preventing their characterization. Upon warming to $+10^\circ C$, the formation of **41/41a** is observed in small amounts (*ca.* 10 %) along with the aforementioned unidentified species, and warming to ambient temperature results in complete conversion to **41/41a** within 10 h.

5.2.1.2 Methylallene

Compound **29** also reacts with 1,2-butadiene (methylallene) over a 10 h period, generating two isomers of $[IrOs(CO)_3(\mu-\eta^3:\kappa^1-C(CH_3)(CH_2)_2)-(dppm)_2][CF_3SO_3]$ (**42/42a**) in a 1:1 ratio, as shown in Scheme 5-2. In this case

isomers **42** and **42a** have the same orientation of the hydrocarbyl fragment and positions of the CO ligands, and differ only in the orientation of the methyl group of the η^3 -allyl-type moiety, being either *syn* or *anti* to the Os-bound CH₂ group.

Scheme 5-2



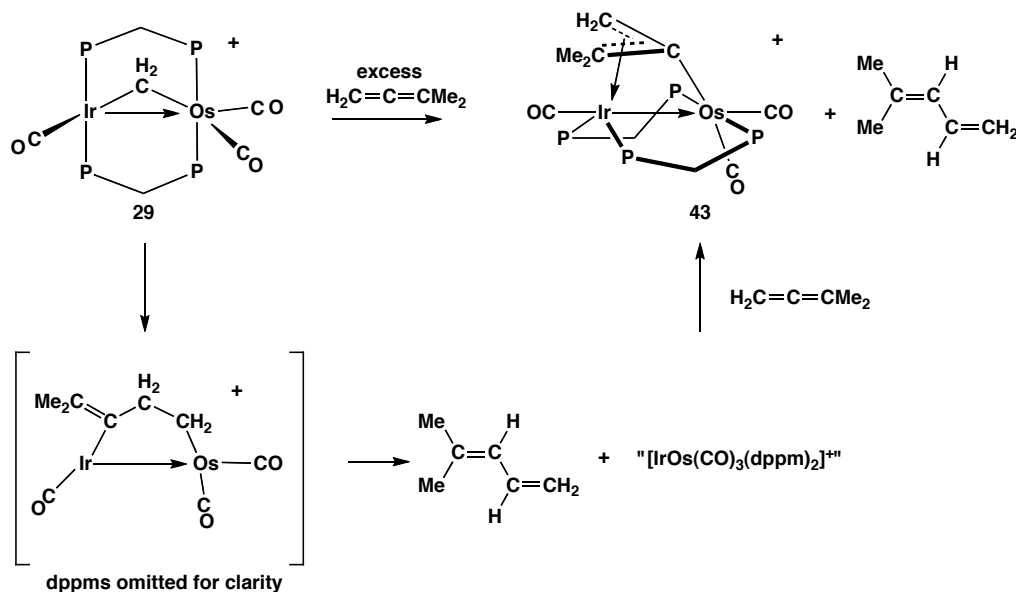
The $^{31}\text{P}\{^1\text{H}\}$ NMR spectrum of compounds **42** and **42a** contains 8 resonances, representing the four chemically inequivalent ^{31}P nuclei for both isomers. These resonances are often overlapping, making the differentiation of **42** and **42a** difficult. The ^1H NMR spectrum for **42/42a** consists of eight resonances for the dppm CH₂ protons and three signals for the four CH₂ protons of the η^3 -allyl moiety of both isomers (δ 5.20, δ 3.79, δ 2.90) in a 1:1:2 ratio, the last being an overlapping resonance for the two olefinic *anti* protons of the two isomers. The methyl groups of the two isomers appear at δ 1.60 and δ 1.10 and their adjacent protons at δ 3.12 and δ 4.69, respectively, while there are two overlapping signals for the four protons for the Os-bound CH₂ protons at δ 1.84 and δ 1.80. The chemical shift of these CH₂ protons supports the orientation of the η^3 -allyl-type moiety, as shown in Scheme 5-2; the signal for these protons would be expected near δ 4, for the reverse orientation.¹⁸ Previous work on 1-methyl-substituted allyl groups bound to rhodium⁹ reports *syn* protons adjacent to methyl groups appearing between δ 4.06 and δ 5.19 and *anti* protons adjacent to methyl groups appearing upfield between δ 3.25 and δ 3.65. This information suggests that the methyl resonance at δ 1.60 corresponds to the methyl group being *syn*, and the resonance at δ 1.10 corresponds to the *anti* isomer with respect to the κ^1 -CH₂ group. The $^{13}\text{C}\{^1\text{H}\}$ NMR spectrum displays five CO resonances (δ 185.4, δ 177.9, δ 177.0, δ 171.0, and δ 162.1) in a 2:1:1:1:1 ratio, consistent

with each isomer having three carbonyls; however, the overlap in the $^{31}\text{P}\{^1\text{H}\}$ NMR spectrum prevents the use of selective ^{31}P -decoupling experiments to accurately assign the carbonyls to a specific isomer or metal. A sample of compounds **42/42a**, prepared from $^{13}\text{CH}_2$ -enriched **29** displays only one signal at $\delta -9.5$ in the $^{13}\text{C}\{^1\text{H}\}$ NMR spectrum, consistent with this group remaining on Os.

5.2.1.3 1,1-Dimethylallene

The methylene-bridged compound, **29**, also reacts with excess 1,1-dimethylallene at ambient temperature over an 8 h period to form a $\mu\text{-}\eta^3\text{:}\kappa^1$ adduct, $[\text{IrOs}(\text{CO})_3(\mu\text{-}\eta^3\text{:}\kappa^1\text{-CH}_2\text{CCMe}_2)(\text{dppm})_2][\text{CF}_3\text{SO}_3]$ (**43**), as shown in Scheme 5-3. The $^{31}\text{P}\{^1\text{H}\}$ NMR spectrum of **43** displays four resonances characteristic of an ABCD spin system in which all four ^{31}P nuclei are chemically inequivalent (see Figure 5-3 for labelling). The two-bond $\text{P}_\text{A}\text{-P}_\text{C}$ coupling constant is 254.9 Hz,

Scheme 5-3



typical for ^{31}P nuclei in a mutually trans arrangement while the smaller $\text{P}_\text{B}\text{-P}_\text{D}$ coupling constant of 23.7 Hz suggests a cis arrangement. Intraligand two-bond $\text{P}_\text{A}\text{-P}_\text{B}$ coupling ($^2J_{\text{PP}} = 64.6$ Hz) and $\text{P}_\text{C}\text{-P}_\text{D}$ coupling ($^2J_{\text{PP}} = 53.1$ Hz) is also observed, as well as three-bond $\text{P}_\text{A}\text{-P}_\text{D}$ coupling ($^3J_{\text{PP}} = 14.0$ Hz) and $\text{P}_\text{B}\text{-P}_\text{C}$ coupling ($^3J_{\text{PP}} = 7.6$ Hz). A simulation of the $^{31}\text{P}\{^1\text{H}\}$ NMR spectrum with the

coupling constants observed confirms the labeling scheme proposed (Figure 5-3). The ^1H NMR spectrum is as expected for the formulation shown, with four

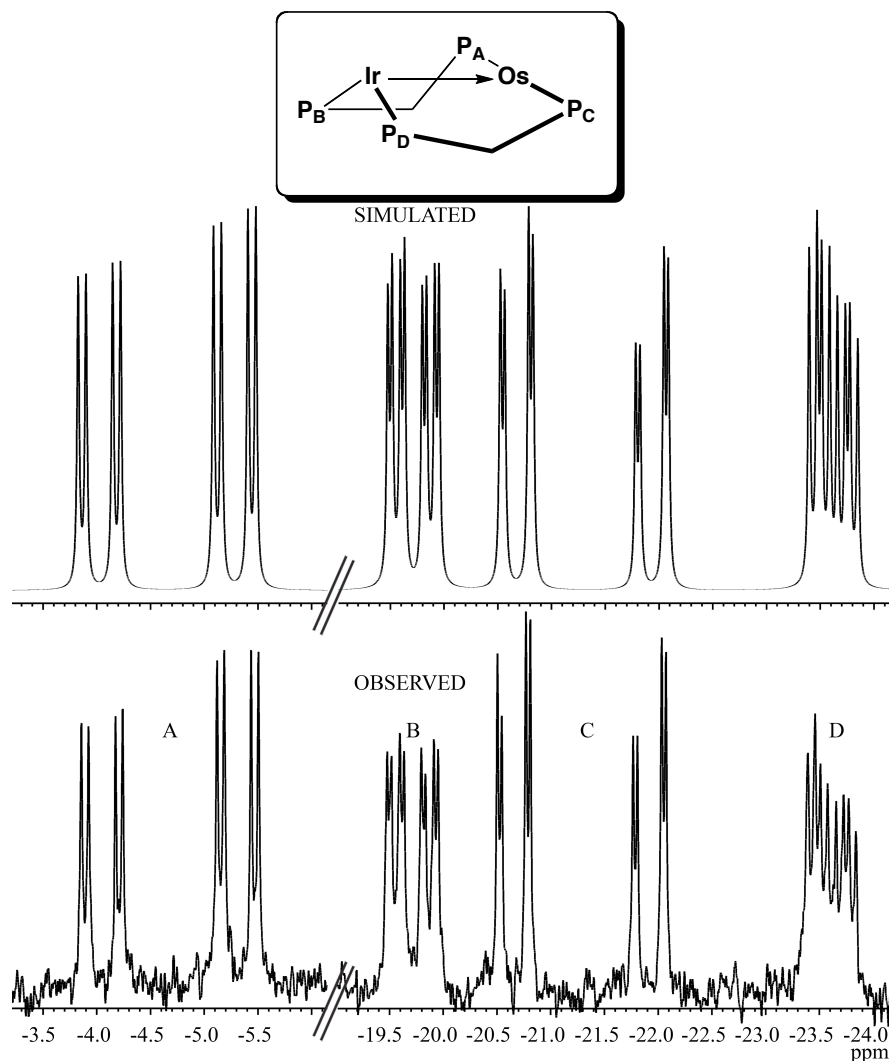


Figure 5-3. $^{31}\text{P}\{^1\text{H}\}$ NMR spectrum of **43** in CD_2Cl_2

signals for the dppm CH_2 protons (δ 4.70, δ 4.65, δ 3.81 and δ 3.24), two signals for the methyl groups (δ 1.68 and δ 1.63), and two signals for the two CH_2 protons of the η^3 -allyl group (δ 3.97 (*syn*), δ 2.17 (*anti*)). The chemical shifts of the allylic protons are indicative of an η^3 -allyl-type interaction with Ir, in which the allylic protons have shown to resonate downfield to those of Os η^3 -allylic protons (*ca.* δ 2 and δ 1, for *syn* and *anti*, respectively).⁵⁻⁶ The $^{13}\text{C}\{^1\text{H}\}$ NMR spectrum displays three resonances for the three carbonyls (δ 186.9, δ 178.0, δ

173.9). A crystal structure determination of an analogous complex generated from allene (*vide infra*) has the η^3 -allyl interaction at Ir and has similar allylic proton shifts in the ^1H NMR spectrum, also supporting the orientation of **43** as shown in Scheme 5-3.

Surprisingly, this product contains the dimethylallene moiety *without* the original metal-bridged “CH₂” group of compound **29**. A clue regarding the fate of this “CH₂” group is the presence of 4-methyl-1,3-pentadiene, the additional product of this reaction, which has resulted from coupling of the cumulene with the methylene group of **29**, accompanied by a 1,2-hydrogen shift, as has previously been reported.^{1c,1h} The diene compound was characterized by ^1H NMR spectroscopy. In the reaction of a $^{13}\text{CH}_2$ -enriched sample of **29** with dimethylallene, the terminal CH₂ group in this pentadiene product appears at δ 115.1. We propose that the formation of 4-methyl-1,3-pentadiene results from a sequence of cumulene insertion, β -hydride elimination, and reductive elimination steps, much as proposed earlier for the elimination of 1,3-butadiene in the Ir/Ru system, as discussed in Chapter 2.

The reaction of compound **29** with 1,1-difluoroallene yielded several unidentified products, even when carried out at low temperature. This result is slightly puzzling, as this substrate reacted cleanly with the analogous methylene-bridged Ir/Ru complex,^{1h} inserting into the Ir-CH₂ bond to generate an Ir-chelate, similar to the alkylcumulenes, although over time, alkyl migration to a carbonyl group generated an acyl compound.

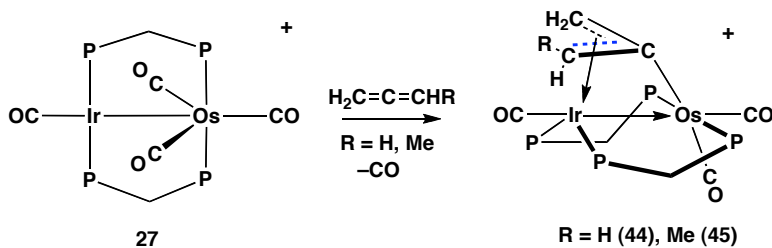
5.2.2 Reactivity of $[\text{IrOs}(\text{CO})_4(\text{dppm})_2][\text{BF}_4]$ with Cumulenes

The proposal above that the $\mu\text{-}\eta^3\text{:}\kappa^1\text{-1,1}$ -dimethylallene adduct resulted from cumulene attack on the tricarbonyl species, $[\text{IrOs}(\text{CO})_3(\text{dppm})_2]^+$, suggested that such species could be generated for the other cumulenes by CO loss from $[\text{IrOs}(\text{CO})_4(\text{dppm})_2]^+$ (**27**). The highly reactive tricarbonyl, $[\text{IrOs}(\text{CO})_3(\text{dppm})_2]^+$, is unstable and decomposes immediately in solution, therefore investigations focused on the reactions of $[\text{IrOs}(\text{CO})_4(\text{dppm})_2]^+$ (**27**) with cumulenes.

5.2.2.1 Allene and Methylallene

The tetracarbonyl complex $[\text{IrOs}(\text{CO})_4(\text{dppm})_2][\text{BF}_4]$ (**27-BF₄**) reacts with allene and methylallene, at ambient temperature over 4 h to generate the corresponding tricarbonyl $\mu\text{-}\eta^3\text{:}\kappa^1\text{-cumulene}$ adducts $[\text{IrOs}(\text{CO})_3(\mu\text{-}\eta^3\text{:}\kappa^1\text{-CH}_2\text{CCH}_2)(\text{dppm})_2][\text{BF}_4]$ (**44**), and $[\text{IrOs}(\text{CO})_3(\mu\text{-}\eta^3\text{:}\kappa^1\text{-CH}_2\text{CCHCH}_3)(\text{dppm})_2][\text{BF}_4]$ (**45**), respectively, in which the cumulene is bound κ^1 to one metal by the central carbon, and η^3 to the adjacent metal, as shown in Scheme 5-4. If a carbonyl is removed from $[\text{IrOs}(\text{CO})_4(\text{dppm})_2][\text{BF}_4]$ (**27-BF₄**) using TMNO, in the presence of allene or methylallene, the same products are formed immediately.

Scheme 5-4



The $^{31}\text{P}\{^1\text{H}\}$ NMR spectrum of compound **44** displays two resonances at $\delta -7.4$ and $\delta -19.3$ consistent with the chemical inequivalence of the Ir- and Os-bound ends of the diphosphines, while **45** displays three resonances at $\delta -7.3$, $\delta -16.8$, and $\delta -19.9$, in a 2:1:1 ratio, with the higher intensity signal resulting from coincidental overlap of the resonances of two of the four inequivalent ^{31}P nuclei. As noted earlier, the $^{31}\text{P}\text{-}^{31}\text{P}$ coupling constants are again consistent with a *cis/trans* arrangement of diphosphines at the different metals. The ^1H NMR spectrum of **44** displays two resonances for the dppm CH_2 protons at $\delta 5.61$ and $\delta 4.96$ ($^2J_{\text{HH}} = 15.1$ Hz) and the resonances for the allene protons appear at $\delta 4.35$ and $\delta 3.55$. The ^1H NMR parameters for the *syn* ($\delta 4.35$) and *anti* ($\delta 3.55$) protons are similar to that observed in a diiridium complex for which a crystal structure confirming this binding mode was obtained.^{6b} The ^1H NMR spectrum of **45** has four dppm CH_2 proton signals ($\delta 5.64$, $\delta 5.57$, $\delta 5.05$, and $\delta 4.84$), two signals for the *syn* and *anti* CH_2 protons of the allene ($\delta 5.20$ and $\delta 3.79$, respectively), one

signal for the proton adjacent to the methyl group (δ 4.61) and one signal for the methyl protons (δ 1.09), with the latter two showing mutual three-bond coupling of 6.1 Hz. These data suggest that the methyl group is in an *anti* position on the allylic portion of the ligand,^{1c,6b,9} and the chemical shifts of the olefinic CH₂ protons of the allene suggest an η^3 -Ir binding mode.⁶ The ¹³C{¹H} spectrum of a ¹³CO-enriched sample of **44** confirms the loss of a carbonyl ligand with only three signals observed (δ 185.9, δ 178.0, and δ 171.7), with the two downfield signals coupling to the set of ³¹P nuclei at δ -7.4, and the upfield signal coupling to the other set of ³¹P nuclei at δ -19.3. In a ¹³CO-enriched sample of **45**, the carbonyl resonances appear at δ 185.9, δ 178.3 and δ 171.5; here the two downfield carbonyls show coupling to the ³¹P nuclei at δ -7.3, while the upfield carbonyl couples to the ³¹P nuclei at δ -16.0 and δ -19.9.

An X-ray structure determination of **44** verifies the geometry proposed above, in which the hydrocarbyl fragment is bound κ^1 to Os and η^3 to Ir. The complex cation of compound **44** is shown in Figure 5-4. Within the bridging

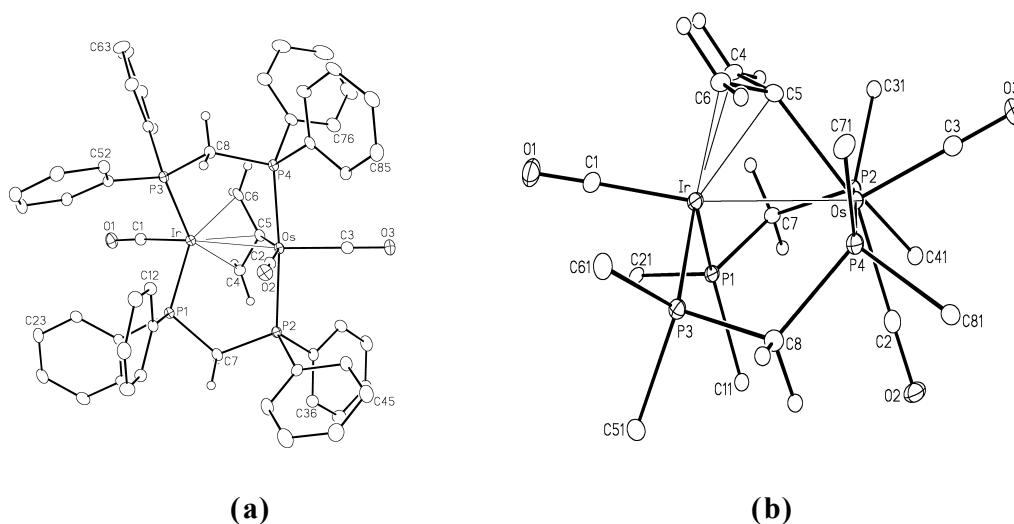


Figure 5-4. (a) Perspective view of the complex cation of $[\text{IrOs}(\text{CO})_3(\mu\text{-}\eta^3\text{:}\kappa^1\text{-H}_2\text{CCCH}_2)(\text{dppm})_2][\text{BF}_4]$ (**44**). Thermal ellipsoids are as in Figure 5-2. (b) Alternate view of the cation of **44** with only the ipso carbons of the phenyl rings shown.

allene group the C(4)–C(5) and C(5)–C(6) bond lengths (1.431(6) Å and 1.430(6) Å respectively) and C(4)–C(5)–C(6) angle of 106.7(4)° are typical of an η^3 -bound allyl.^{6b,7,10} Selected bond lengths and angles are presented in Table 5-2. Although not common, similar bridging allene coordination has been reported.^{6b,11} The allyl fragment is essentially equidistant from both metal centres (Ir–C(5) = 2.115(4) Å, Os–C(5) = 2.120(4) Å), and the Ir–Os separation of 2.8407(2) Å indicates compression along the Ir–Os axis compared to the intraligand P–P separations of *ca.* 3.07 Å. The P(1)–Ir–P(3) angle of 111.80(4)° is acute, being bent away from the η^3 -allyl moiety in a *cis* arrangement while the almost linear P(2)–Os–P(4) angle (170.34(4)°), indicates a *trans* arrangement at the Os, as illustrated in Figure 5-4(b).

Table 5-2. Selected Bond Lengths and Angles for Compound 44

(a) Distance (Å)

atom 1	atom 2	distance	atom 1	atom 2	distance
Ir	Os	2.8407(2)	Os	C(2)	1.919(4)
Ir	C(1)	1.897(4)	Os	C(3)	1.873(4)
Ir	C(4)	2.230(4)	Os	C(5)	2.120(4)
Ir	C(5)	2.115(4)	C(4)	C(5)	1.431(6)
Ir	C(6)	2.218(4)	C(5)	C(6)	1.430(6)

(b) Angles (deg)

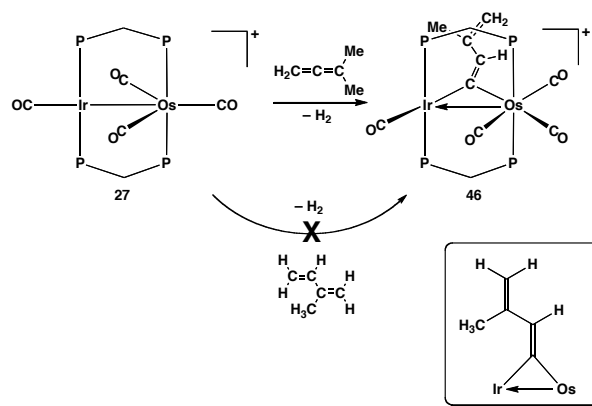
atom 1	atom 2	atom 3	angle	atom 1	atom 2	atom 3	angle
C(4)	C(5)	C(6)	106.7(4)	Os	Ir	C(6)	74.9(1)
Os	C(5)	C(4)	119.6(3)	P(1)	Ir	P(3)	111.80(4)
Os	C(5)	C(6)	121.5(3)	Ir	Os	C(5)	47.8(1)
Os	Ir	C(4)	74.0(1)	P(2)	Os	P(4)	170.34(4)
Os	Ir	C(5)	47.9(1)				

5.2.2.2 1,1-Dimethylallene

Compound **27** also reacts with excess 1,1-dimethylallene at ambient temperature over 12 h, in this case, giving a very different product, [IrOs(CO)₄(μ -

$\text{C}=\text{C}(\text{H})\text{C}(\text{CH}_3)=\text{CH}_2(\text{dppm})_2][\text{CF}_3\text{SO}_3]$ (**46**), having a bridging 3-methyl-1,3-butadienyliene fragment, as shown in Scheme 5-5, resulting from the activation

Scheme 5-5



of three C–H bonds – the two geminal C–H bonds of the cumulene, and one C–H bond of a methyl group, with the concomitant evolution of H_2 . This reactivity is reminiscent of that observed in the related Ir/Ru system (see Chapter 3).

The $^{31}\text{P}\{^1\text{H}\}$ NMR spectrum of **46** displays two signals, at $\delta -5.2$ and $\delta -9.2$, ruling out the formation of a $\mu-\eta^3:\kappa^1$ binding mode, as observed for the other alkylcumulenes, which is expected to give rise to four different ^{31}P environments. Four signals for the vinylvinylidene fragment appear in the ^1H NMR spectrum: the methyl group is observed at $\delta 0.41$, the lone proton on the β -carbon resonates at $\delta 8.01$, and the two geminal protons can be observed at $\delta 4.69$ and $\delta 4.46$. The data obtained from the $^{13}\text{C}\{^1\text{H}\}$ NMR spectrum support the carbonyl arrangement shown in Scheme 5-5 in which three carbonyls ($\delta 194.9$, $\delta 175.5$, $\delta 171.8$) are bound to one metal (Os) and one carbonyl ($\delta 179.9$) is bound to the other (Ir). Although the most downfield chemical shift is suggestive of a semi-bridging interaction, there is no resolvable coupling observed between it and the Ir-bound ^{31}P nuclei. This carbonyl arrangement is not surprising, given the decreased tendency for third-row metals to support bridging carbonyls.¹² Two of the Os-bound carbonyls show mutual two-bond coupling of 26.2 Hz, indicative of a trans arrangement, as shown in Scheme 5-5.

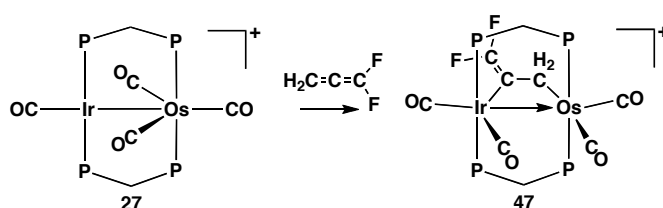
Compound **46** can be viewed as resulting from the geminal activation of both C–H bonds at the unsubstituted end of 2-methyl-1,3-butadiene, with the accompanying loss of H₂; however attempts to generate **46** by reaction of **27** with this substrate does not occur in the presence of 100 equiv of the substrate over several days, even when carried out at slightly elevated temperatures. The Ir/Ru analogue also did not react with this substrate.¹³

If the reaction of **27** with 1,1-dimethylallene is attempted in the presence of the decarbonylating agent, TMNO, the resultant product immediately obtained is [IrOs(CO)₃(μ-η³:κ¹-CH₂CCMe₂)(dppm)₂][CF₃SO₃] (**43**), the same product observed earlier in the reaction of the methylene-bridged complex, **29**, with excess 1,1-dimethylallene.

5.2.2.3 1,1-Difluoroallene

Compound **27** also reacts with 1,1-difluoroallene within 1 h at ambient temperature to form the adduct, [IrOs(CO)₄(μ-κ¹:κ¹-F₂C=C=CH₂)(dppm)₂][CF₃SO₃] (**47**) in which the fluoroallene bridges both metals (Scheme 5-6). The ³¹P{¹H} NMR spectrum displays the expected

Scheme 5-6



two resonances, at δ –12.0 and δ –19.5. In the ¹H NMR spectrum, the dppm CH₂ protons appear at δ 4.79 and δ 4.46 while the CH₂ protons of the cumulene ligand appear as a triplet at δ 1.55, coupling to the ³¹P nuclei at δ –12.0 (³J_{HP} = 11.8 Hz). The observation of one allene CH₂ resonance is consistent with binding through this end of the cumulene, as is typically observed.^{6b,13-14} The upfield chemical shift of the CH₂ protons also suggests that they are adjacent to Os and not Ir,^{1g} the latter of which characteristically resonate downfield at *ca.* δ 4. Binding of the 1,1-difluoroallene through the “C=CH₂” end is confirmed in the ¹⁹F NMR spectrum

by the pair of resonances at δ -74.3 and δ -92.2 for the two chemically inequivalent fluorines with mutual two-bond coupling of 60.4 Hz, which is typical for such an arrangement.^{6b,15} A ^{13}C -enriched sample of **47** displays four resonances in the $^{13}\text{C}\{^1\text{H}\}$ NMR spectrum at δ 183.4, 180.2, 177.5, and 154.2, and selective ^{31}P -decoupling experiments determine that two carbonyls are bound terminally to each metal.

An X-ray structure determination of **47** confirms the proposed connectivity in which the protons of the difluoroallene ligand are adjacent to the Os, as shown in Figure 5-5. Within the bridging fluoroallene unit, the C(5)–C(6) bond length of 1.511(4) Å is typical of a single bond between an sp^2 and sp^3 carbon.⁷ The C(5)–C(7) bond length (1.298(4) Å) is short for a double bond between two sp^2 carbons,⁷ however the electron withdrawing ability of the fluorines may account for the contraction of this bond. The geometry at each metal is a distorted octahedron with two terminal carbonyl ligands.

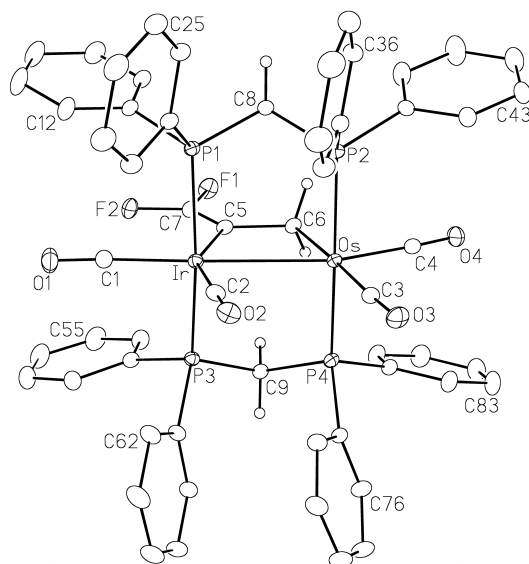


Figure 5-5. Perspective view of the complex cation of $[\text{IrOs}(\text{CO})_4(\mu\text{-}\kappa^1:\kappa^1\text{-F}_2\text{C}=\text{C}=\text{CH}_2)(\text{dppm})_2][\text{CF}_3\text{SO}_3]$ (**47**). Thermal ellipsoids are as shown in Figure 5-2.

Table 5-3. Selected Bond Lengths and Angles for Compound 47

(a) Distance (Å)

atom 1	atom 2	distance	atom 1	atom 2	distance
Ir	Os	2.9095(2)	Os	C(4)	1.887(3)
Ir	C(1)	1.931(3)	Os	C(6)	2.219(3)
Ir	C(2)	1.902(3)	C(5)	C(6)	1.511(4)
Ir	C(5)	2.111(3)	C(5)	C(7)	1.298(4)
Os	C(3)	1.921(3)	F(1)	C(7)	1.346(3)

(b) Angles (deg)

atom 1	atom 2	atom 3	angle	atom 1	atom 2	atom 3	angle
C(6)	C(5)	C(7)	121.5(3)	Os	Ir	C(5)	71.48(8)
Ir	C(5)	C(6)	112.1(2)	P(1)	Ir	P(3)	164.70(2)
Ir	C(5)	C(7)	126.4(2)	Ir	Os	C(4)	156.84(9)
F(1)	C(7)	F(2)	106.6(2)	Ir	Os	C(6)	70.77(7)
Os	Ir	C(1)	173.24(9)	P(2)	Os	P(4)	174.23(2)

Rearrangement of the bridging fluoroallene to a $\mu\text{-}\eta^3\text{:}\kappa^1$ hydrocarbyl fragment, as was observed with allene and methylallene, is never observed, with the fluoroallene moiety remaining intact upon heating to 40 °C for 8 h, after which time, decomposition occurred. The η^3 -allyl binding mode has only been reported for 1,1-difluoroallene in two multimetallic systems.^{14,16}

5.3 Discussion

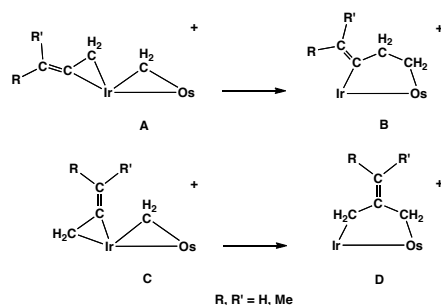
The reactions of the methylene-bridged compound $[\text{IrOs}(\text{CO})_3(\mu\text{-CH}_2)(\text{dppm})_2]^+$ (**29**) and the tetracarbonyl complex $[\text{IrOs}(\text{CO})_4(\text{dppm})_2]^+$ (**27**) with cumulenes as described in this chapter, display a surprising diversity in comparison to the related reactions of the other group 8/group 9 metal combinations (Rh/Ru and Rh/Os,^{1c} and Ir/Ru^{1h,13}). Although the Rh-based systems displayed many differences in reactivity compared to the Ir/Ru system, the current Ir/Os system compounds studied demonstrate essentially all of the diverse reactions observed in the previous three metal combinations.

5.3.1 Reactivity of $[\text{IrOs}(\text{CO})_3(\mu\text{-CH}_2)(\text{dppm})_2]^+$ with Cumulenes.

As was discussed in Chapter 4, $[\text{IrOs}(\text{CO})_4(\mu\text{-CH}_2)(\text{dppm})_2]^+$ (**28**) has a different structure than the analogous species involving the Rh/Ru, Rh/Os, and Ir/Ru combinations of metals,^{1g} in that all carbonyls are terminal, being symmetrically distributed – two on each metal. In contrast, all the other metal combinations have two terminal carbonyls on the group 8 metal, one bridging, and the fourth on the group 9 metal. The bridging carbonyl in these latter systems provides incipient unsaturation at the group 9 metal centre, by moving to the terminal position on the group 8 metal upon the introduction of nucleophiles and unsaturated substrates at the other metal. Without this incipient unsaturation in $[\text{IrOs}(\text{CO})_4(\mu\text{-CH}_2)(\text{dppm})_2]^+$ (**28**), the reactions with unsaturated substrates take much longer to complete, therefore we investigated the reactivity of cumulenes with the tricarbonyl analogue, $[\text{IrOs}(\text{CO})_3(\mu\text{-CH}_2)(\text{dppm})_2]^+$ (**29**), as a comparison to the other metal systems.

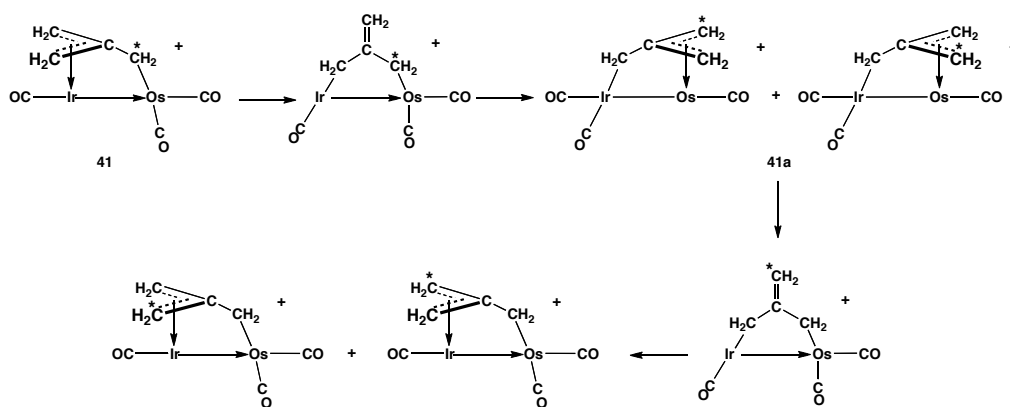
As part of our strategy to generate bridging C_3 hydrocarbonyl fragments we anticipated that the insertion of the cumulene substrate into the Ir–C bond could occur in one of two ways, as shown in Scheme 5-7. We propose that cumulene insertion into the Ir– CH_2 bond occurs to generate either structure **B** or **D**, depending on the cumulene orientation upon coordination at one metal. Neither insertion product **B** nor **D** is observed in this study, although structure **B** was observed in one study involving the Rh/Os metal combination.^{1c} In spite of our failure to observe these species, the rearranged products provide insight into the initial coordination mode and insertion pathways.

Scheme 5-7



Reaction of the methylene-bridged tricarbonyl, $[\text{IrOs}(\text{CO})_3(\mu\text{-CH}_2)(\text{dppm})_2]^+$ (**29**) with allene and methylallene results in the formation of the $\mu\text{-}\eta^3\text{:}\kappa^1$ complexes, $[\text{IrOs}(\text{CO})_3(\mu\text{-}\eta^3\text{:}\kappa^1\text{-C}(\text{CH}_2)_3)(\text{dppm})_2][\text{BF}_4]$ (**41/41a**), and $[\text{IrOs}(\text{CO})_3(\mu\text{-}\eta^3\text{:}\kappa^1\text{-C}(\text{CHCH}_3)(\text{CH}_2)_2)(\text{dppm})_2][\text{CF}_3\text{SO}_3]$ (**42/42a**), respectively. The generation of trimethylenemethane complexes (as in **41/41a**) has been documented in mononuclear^{8a-c,8e,17} and binuclear systems in which the the $\mu\text{-}\eta^3\text{-}\kappa^1$ binding mode has been observed and characterized.^{1c,4a,8d,18} Transformation of insertion product **D** to the $\mu\text{-}\eta^3\text{:}\kappa^1$ binding mode is hardly surprising, representing the transformation of a κ^1 -allylic moiety (relative to both metal centres), to an η^3 -allyl bridging mode at one end of the trimethylenemethane unit. The greater stability of the η^3 -allylic binding mode is well documented.¹⁹ The equilibrium between isomers **41** and **41a** is unusual, in which the $\eta^3\text{:}\kappa^1$ hapticity of the trimethylenemethane group alternates from metal to metal accompanied by migration of a carbonyl from one metal to the other, such that the metal that is κ^1 -bound to the hydrocarbyl fragment has the additional carbonyl, as shown in Scheme 5-1. The rearrangement of the trimethylenemethane moiety has been confirmed by labelling studies in which the $^{13}\text{CH}_2$ group of the $^{13}\text{CH}_2$ -labelled precursor **29** becomes incorporated into the other two methylene positions upon allene insertion. This scrambling process can be rationalized by a series of $\eta^3\text{:}\kappa^1$ to $\kappa^1\text{:}\kappa^1$ to $\eta^3\text{:}\kappa^1$ transformations as shown in Scheme 5-8 (showing only part of the scrambling process).

Scheme 5-8



Unlike the isomers **41** and **41a**, the isomers, $[\text{IrOs}(\text{CO})_3(\mu\text{-}\eta^3:\kappa^1\text{-C}(\text{CHCH}_3)(\text{CH}_2)_2)(\text{dppm})_2][\text{CF}_3\text{SO}_3]$ (**42/42a**), resulting from methylallene addition to **29**, are static, displaying only the coordination analogous to **41** in which η^3 -binding of the trimethylenemethane type unit is bound to Ir. As a consequence, no $^{13}\text{CH}_2$ scrambling is observed in this case, as this label remains κ^1 -bound to Os. The isomerization in this case results from *syn/anti* positioning of the methyl substituent on the allylic portion of the ligand.

The failure of **42/42a** to reverse hapticity from metal-to-metal as observed for **41/41a** is somewhat puzzling, since the introduction of a single methyl substituent would not appear to introduce unusual steric demands. However, it may be that the hapticity exchange, combined with carbonyl migration from metal-to-metal *and* the concomitant realignment of the diphosphines from mutually *cis* to mutually *trans*, is inhibited by the additional substituent on the trimethylenemethane ligand.

The generation of a $\mu\text{-}\eta^3:\kappa^1$ -trimethylenemethane fragment was also observed upon reaction of allene with the methylene-bridged Rh/Ru and Rh/Os analogues. However, in these systems facile carbonyl loss occurred from Rh generating a coordinatively unsaturated “(η^3 -allyl)RhP₂-type” fragment. The failure of this system to undergo the κ^1/η^3 isomerization observed for **41** and **41a** can be rationalized on the basis that the $\kappa^1:\kappa^1$ intermediate, analogous to that shown in Scheme 5-8, introduces additional coordinative unsaturation to an already unsaturated system, which is probably unfavourable.

The reactivity observed between $[\text{IrOs}(\text{CO})_3(\mu\text{-CH}_2)(\text{dppm})_2]^+$ (**29**) and allene is markedly different from that observed for the related Ir/Ru complex, $[\text{IrRu}(\text{CO})_4(\mu\text{-CH}_2)(\text{dppm})_2]^+$ (**1**), which reacts to generate 1,3-butadiene through allene-methylene coupling.^{1h} The loss of this diene fragment suggests that coordination of the cumulene and subsequent insertion into the Ir-CH₂ bond occurs via structures similar to **A** and **B** (Scheme 5-7), instead of through intermediates **C** and **D**, possibly attributable to a more crowded environment in the Ir/Ru complexes due to retention of a fourth carbonyl ligand. The β -

hydrogens present in this binding mode provide a route to the common decomposition pathway for propanediyl species,³ through β -H elimination, to yield 1,3-butadiene. The greater steric crowding in $[\text{IrRu}(\text{CO})_4(\mu\text{-CH}_2)(\text{dppm})_2]^+$ (**1**) is again evident in its reaction with methylallene, which again inserts via intermediates **A** and **B**, although in this case, the hydrocarbyl fragment migrates to the chelating position on Ir, instead of undergoing the 1,2-hydrogen shift.

The reaction of $[\text{IrOs}(\text{CO})_3(\mu\text{-CH}_2)(\text{dppm})_2]^+$ (**29**) with 1,1-dimethylallene appears to proceed much as it does in the Rh/Os system,^{1c} in which the dimethylallene couples with the methylene group (structures **A** and **B**, Scheme 5-7) and is lost as 4-methyl-1,3-pentadiene, presumably through the aforementioned β -H elimination and reductive elimination steps. In the current study, the “ $\text{IrOs}(\text{CO})_3^+$ ” fragment remaining after elimination of the pentadiene immediately reacts with any excess 1,1-dimethylallene to generate a $\mu\text{-}\eta^3\text{:}\kappa^1$ complex, $[\text{IrOs}(\text{CO})_3(\mu\text{-}\eta^3\text{:}\kappa^1\text{-CH}_2\text{CCMe}_2)(\text{dppm})_2][\text{CF}_3\text{SO}_3]$ (**43**). In contrast, the same reaction with $[\text{IrRu}(\text{CO})_4(\mu\text{-CH}_2)(\text{dppm})_2]^+$ (**1**) again favours the formation of an Ir-chelate.^{1h} In this case, the steric crowding at the metals due to the retention of a fourth carbonyl (unlike the tricarbonyl Ir/Os and Rh/Os species) is not conducive to the flexibility required for β -H elimination, and presumably deactivates the system to insertion into the β -C–H bond, favouring instead other pathways.

In all reactions of $[\text{IrRu}(\text{CO})_4(\mu\text{-CH}_2)(\text{dppm})_2]^+$ (**1**) with cumulenes, subsequent C–H bond activations upon incorporation of a second cumulene are observed, in which up to three C–H bonds can be activated.^{1h} No evidence of C–H activation with $[\text{IrOs}(\text{CO})_3(\mu\text{-CH}_2)(\text{dppm})_2]^+$ (**29**) is observed. Multiple C–H bond activations of cumulenes were also observed with $[\text{IrRu}(\text{CO})_4(\text{dppm})_2]^+$ (**13**),¹³ as discussed in Chapter 3, so we sought to gain information on how these multiple activations occurred using the Ir/Os metal combination.

5.3.2 Reactivity of $[\text{IrOs}(\text{CO})_4(\text{dppm})_2]^+$ with Cumulenes.

The addition of allene and methylallene to the tetracarbonyl complex $[\text{IrOs}(\text{CO})_4(\text{dppm})_2]^+$ (**27**) results in the formation of the cumulene-bridged complexes, $[\text{IrOs}(\text{CO})_3(\mu\text{-}\eta^3\text{:}\kappa^1\text{-C}(\text{CH}_2)_2)(\text{dppm})_2][\text{BF}_4]$ (**44**) and $[\text{IrOs}(\text{CO})_3(\mu\text{-}\eta^3\text{:}\kappa^1\text{-C}(\text{CH}_2)(\text{CHCH}_3))(\text{dppm})_2][\text{BF}_4]$ (**45**), respectively, analogous to **43**, yielding the $\eta^3\text{:}\kappa^1$ complexes with the loss of a carbonyl ligand. This coordination mode of allene and methylallene has been documented in related Ir₂ complexes,^{6b,20} and other multimetallic systems.¹¹ We assume that cumulene coordination on Ir leads to migration to the bridging position between both metals, such that the central carbon of the cumulene is bound to Os. Conversion of this κ^1 -allylic moiety on Ir to an η^3 -mode at this metal yields the observed $\eta^3\text{:}\kappa^1$ coordination mode.

This reactivity with allene and methylallene observed with Ir/Os is completely different than that observed in the with the analogous $[\text{IrRu}(\text{CO})_4(\text{dppm})_2]^+$ (**13**), in which two geminal C–H bond activations occur to generate the corresponding vinylidene-bridged complexes $[\text{IrRu}(\text{CO})_4(\mu\text{-C=CHR})(\text{dppm})_2]^+$ (R = CH₃ (**14**), C₂H₅ (**15**)), respectively, as described in Chapter 2. We assume that the strong M–C bonds in the Ir/Os species favours retention of the bridging hydrocarbyl unit and does not allow the activation of C–H bonds. Although the site of primary reactivity in these complexes is the group 9 metal for both combinations, the influence of the adjacent group 8 metal is again clearly displayed.

It is only when $[\text{IrOs}(\text{CO})_4(\text{dppm})_2]^+$ (**27**) is reacted with 1,1-dimethylallene that similarities between the Ir/Os and Ir/Ru systems are seen. In both cases, a triple C–H activation product is observed; two geminal C–H bonds as well as one methyl C–H bond are activated with concomitant loss of H₂. It is interesting that the C–H activating behavior of Ir/Os is only seen with the disubstituted cumulene. The influence of steric crowding in dictating the reactivity of the cumulenes is clearly seen in the differing reactivities of $[\text{IrOs}(\text{CO})_4(\text{dppm})_2]^+$ (**27**) and “[$\text{IrOs}(\text{CO})_3(\text{dppm})_2$]⁺” (generated *in situ* as

shown in Scheme 5-3) with 1,1-dimethylallene. While the tetracarbonyl complex results in C–H activation, the tricarbonyl complex yields the $\eta^3:\kappa^1$ -adduct, much as observed for allene and methylallene. Attempts to activate the C–H bonds of monoolefins and 1,3-butadiene with $[\text{IrOs}(\text{CO})_4(\text{dppm})_2]^+$ (**27**) were unsuccessful, although the formation of a double orthometallated Ir/Os species was observed (see Appendix I). This suggests that the triple C–H activation product generated with Ir/Os proceeds by a mechanism similar to the Ir/Ru system, as discussed in Chapter 3, where C–H activation is followed by hydrogen migrations through an alkynyl hydride intermediate, to generate the vinylvinylidene-bridged product.

Interestingly, the 1,1-difluorallene adduct of $[\text{IrOs}(\text{CO})_4(\text{dppm})_2]^+$ (**27**), namely $[\text{IrOs}(\text{CO})_4(\mu-\kappa^1:\kappa^1\text{-F}_2\text{C}=\text{C}=\text{CH}_2)(\text{dppm})_2][\text{CF}_3\text{SO}_3]$ (**47**), displays the $\mu-\kappa^1:\kappa^1$ -binding mode as proposed above, except that the binding is reversed, with the central carbon of the cumulene bound to Ir instead of to Os. In this case, however, rearrangement to the $\mu-\eta^3:\kappa^1$ -mode is not observed and the $18e^-/18e^-$ count is maintained by retention of all four carbonyls. Presumably, the failure of this complex to transform into the $\mu-\eta^3:\kappa^1$ -binding mode, is related to the poor donor ability of the η^3 -allyl moiety having electronegative fluorines attached, and its consequent inability to displace a carbonyl. In all cases,^{6b,13} when the fluoro cumulene bridges the metals, no C–H activation is observed, suggesting that either the $\mu-\kappa^1-\kappa^1$ arrangement is not conducive to C–H activation, or the electronegative fluorine substituents cause the distal C–H bonds to be strengthened,²¹ making them more resistant to cleavage. This is the only ligand investigated in this chapter to react similarly with three different metal combinations.

5.4 Conclusions

Our attempts to obtain better models for propanediyl species (when compared to the Rh/Os and Rh/Ru combinations) did not proceed as anticipated in this study, with the dominant theme of the reactivity being the formation of $\mu-\eta^3:\kappa^1$ binding modes – both for the products of coupling with the $\mu\text{-CH}_2$ group and for the cumulene adducts themselves. In the case of the coupling products,

this is apparently the result of the lower steric demands of the tricarbonyl precursor leading to intermediate **D**, which as a κ^1 -allyl group, readily rearranges to the η^3 -binding mode. In the most bulky cumulene studied, 1,1-dimethylallene, the alternate intermediate **B** apparently results, but is unstable to β -H elimination and subsequent liberation of 4-methyl-1,3-pentadiene occurs. Here the tendency of the third-row metals for β -H elimination is evident. The surprising difference in reactivity of the Ir/Os compared to that of Ir/Ru, wherein the latter system displayed facile multiple C–H bond activations, while the former favoured the $\eta^3:\kappa^1$ binding, is puzzling, but presumably is related to the stronger binding of the cumulene to Os (than to Ru), hence the stronger tendency of these groups to bridge the metals, where cleavage of the terminal C–H bonds of the cumulene is not favourable.

5.5 Experimental Section

5.5.1 General Comments

All solvents were dried using appropriate desiccants (given in Appendix II), distilled before use, and stored under a nitrogen atmosphere. Reactions were performed under an argon atmosphere using standard Schlenk techniques unless otherwise noted. Diazomethane was generated from Diazald,TM which was purchased from Aldrich, as was the ¹³C-enriched Diazald. ¹³C-enriched *N*-Methyl-*N*-nitroso-*p*-toluenesulfonamide was also prepared by using a modified version of the procedure for synthesizing the ¹⁴C-enriched radio-labeled analogue.²² The trimethylamine *N*-oxide dihydrate was also purchased from Aldrich and was dried according to the literature procedure,²³ and the ¹³CO was purchased from Cambridge Isotopes. The methylene-bridged complex $[\text{IrOs}(\text{CO})_3(\mu\text{-CH}_2)(\text{dppm})_2]^+$ (**29**) and the tetracarbonyl complex $[\text{IrOs}(\text{CO})_4(\text{dppm})_2]^+$ (**27**) were prepared according to published procedure.^{1g}

The 1,2-butadiene (methylallene) was purchased from Organic Technologies, allene from Matrix Scientific, 1,1-dimethylallene, 1,3-butadiene, and propylene from Aldrich, ethylene from Matheson, and isoprene (2-methyl-1,3-butadiene) from Alfa Aesar. 1,1-Difluoroallene was prepared using a

modification of the published procedures,^{6b,24} in which a solution of 100 μL of 2-bromo-3,3,3-trifluoro-1-propene (purchased from Aldrich) in 3 mL of diethyl ether was cooled to $-90\text{ }^{\circ}\text{C}$ in an acetone/liquid N_2 bath. To this was added dropwise 385 μL of a 2.5 M solution of *n*-butyllithium in hexanes (purchased from Aldrich), followed by stirring of the solution at this temperature for 30 min. The $-90\text{ }^{\circ}\text{C}$ bath was replaced by an acetonitrile/ $\text{CO}_{2(\text{s})}$ bath (ca. $-40\text{ }^{\circ}\text{C}$) and the solution was stirred for 15 min. The solution was then slowly warmed over 15 min to $-20\text{ }^{\circ}\text{C}$, resulting in the evolution of 1,1-difluoroallene gas.

The ^1H and $^{31}\text{P}\{^1\text{H}\}$ NMR spectra were recorded on a Varian Inova 400 spectrometer operating at 399.9 and 161.8 MHz, respectively. All low-temperature spectra and the heteronuclear decoupling experiments ($^{13}\text{C}\{^1\text{H}\}$ and $^{13}\text{C}\{^1\text{H}, ^{31}\text{P}\}$) were recorded on a Varian Unity spectrometer operating at 161.9 MHz for ^{13}C , 202.3 MHz for ^{31}P , and 499.8 MHz for ^1H . Mass spectrometry was performed on a Micromass ZabSpec TOF spectrometer by the mass spectrometry facility of this department, and elemental analyses were also carried out in the departmental facility.

5.5.2 Preparation of Compounds

Spectroscopic data for the compounds are presented in Table 5-4.

- (a) **$[\text{IrOs}(\text{CO})_3(\mu\text{-}\eta^3\text{:}\kappa^1\text{-C}(\text{CH}_2)_3)(\text{dppm})_2][\text{BF}_4]$ (41/41a).** Under an argon atmosphere, allene was passed through a stirred red solution of **29-BF₄** (42 mg, 0.031 mmol) in 10 mL of CH_2Cl_2 for 1 min at a rate of approximately 0.1 mL/s, resulting in an immediate colour change of the solution to yellow. The solution was left to stir under an allene atmosphere for 10 h after which time 30 mL of diethyl ether and 10 mL of pentane were added to a yellow/orange solution to precipitate a light yellow solid. This solid was recrystallized from CH_2Cl_2 /diethyl ether, washed with 2 x 5 mL of diethyl ether, and dried in vacuo (85 % yield). HRMS: m/z calcd for $\text{C}_{58}\text{H}_{50}\text{IrO}_3\text{OsP}_4$ (M^+), 1291.1949; found, 1291.1941 (M^+). Anal.

Table S-4. Spectroscopic Data for the Compounds

Compounds	NMR ^a		
	$\delta(^1\text{P}\{\text{H}\})^b$	$\delta(\text{H})^{c,d}$	$\delta(^{13}\text{C}\{\text{H}\})^{c,d}$
[$\text{I}(\text{O})\text{S}(\text{CO})_3(\mu-\eta^3-\kappa^1-\text{C}(\text{CH}_2)_3)(\text{dppm})_2$]- [BF_4] (41)	-9.5 (m, 2P), -27.2 (m, 2P)	5.04 (dm, 2H, $^2J_{\text{HH}} = 15.7$ Hz), 4.46 (dm, 2H, $^2J_{\text{HH}} = 15.7$ Hz), 2.72 (b, 2H), 1.94 (d, 2H, $^3J_{\text{HP}} = 2.1$ Hz), 1.74 (t, 2H, $^3J_{\text{HP}} = 10.7$ Hz)	186.4 (dt, 1C, $^2J_{\text{CP}} = 9.1$ Hz, $^2J_{\text{CC}} = 9.1$ Hz), 176.5 (t, 1C, $^2J_{\text{CP}} = 8.1$ Hz), 161.2 (m, 1C, $^2J_{\text{CP}} = 9.7$ Hz), 64.4 (m, 2C), -9.5 (bm, 1C)
[$\text{I}(\text{O})\text{S}(\text{CO})_3(\mu-\eta^3-\kappa^1-\text{C}(\text{CH}_2)_3)(\text{dppm})_2$]- [BF_4] (41a)	-7.3 (m, 2P), -19.2 (m, 2P)	5.62 (dm, 2H, $^2J_{\text{HH}} = 15.2$ Hz), 4.94 (dm, 2H, $^2J_{\text{HH}} = 15.2$ Hz), 4.35 (t, 2H, $^3J_{\text{HP}} = 4.8$ Hz), 3.55 (b, 2H), 1.29 (bd, 2H, $^3J_{\text{HP}} = 3.9$ Hz)	185.5 (t, 1C, $^2J_{\text{CP}} = 9.6$ Hz, $^2J_{\text{CC}} = 9.1$ Hz), 177.5 (t, 1C, $^2J_{\text{CP}} = 9.1$ Hz), 171.3 (m, 1C, $^2J_{\text{CP}} = 7.1$ Hz), -9.5 (bm, 1C)
[$\text{I}(\text{O})\text{S}(\text{CO})_3(\mu-\eta^3-\kappa^1-\text{C}(\text{CHCH}_3)(\text{CH}_2)_2)$]- (dppm) ₂] [CF_3SO_3] (42/42a)	-6.8 (om, 3P), -17.2 (om, 2P), -19.8 (ddd, 1P, $^2J_{\text{PP}} = 49.5$ Hz, $^2J_{\text{PP}} = 20.8$ Hz, $^3J_{\text{PP}} = 11.7$ Hz), -28.4 (ddd, 1P, $^2J_{\text{PP}} = 68.6$ Hz, $^2J_{\text{PP}} = 11.9$ Hz, $^3J_{\text{PP}} = 6.3$ Hz), -29.6 (ddd, 1P, $^2J_{\text{PP}} = 72.1$ Hz, $^2J_{\text{PP}} = 18.9$ Hz, $^3J_{\text{PP}} = 5.6$ Hz)	5.99 (dm, 1H, $^2J_{\text{HH}} = 15.2$ Hz), 5.64 (dm, 1H, $^2J_{\text{HH}} = 15.5$ Hz), 5.60 (dm, 1H, $^2J_{\text{HH}} = 15.2$ Hz), 5.20 (bs, 1H), 5.16 (dm, 1H, $^2J_{\text{HH}} = 15.5$ Hz), 5.03 (dm, 1H, $^2J_{\text{HH}} = 15.0$ Hz), 4.82 (dm, 1H, $^2J_{\text{HH}} = 15.0$ Hz), 4.69 (q, 1H, $^3J_{\text{HH}} = 6.0$ Hz), 4.65 (dm, 1H, $^2J_{\text{HH}} = 15.4$ Hz), 4.12 (dm, 1H, $^2J_{\text{HH}} = 15.4$ Hz), 3.79 (bs, 1H), 3.12 (q, 1H, $^3J_{\text{HH}} = 6.4$ Hz), 2.90 (o, 2H), 1.84 (o, 2H), 1.80 (o, 2H), 1.60 (dd, 3H, $^3J_{\text{HH}} = 6.4$ Hz, $^3J_{\text{HP}} = 7.0$ Hz), 1.10 (dd, 3H, $^3J_{\text{HH}} = 6.0$ Hz, $^3J_{\text{HP}} = 6.4$ Hz)	185.4 (om, 2C), 177.9 (t, 1C, $^2J_{\text{CP}} = 8.0$ Hz), 177.0 (t, 1C, $^2J_{\text{CP}} = 7.1$ Hz), 171.0 (t, 1C, $^2J_{\text{CP}} = 5.4$ Hz), 162.1 (t, 1C, $^2J_{\text{CP}} = 4.6$ Hz), -9.5 (om, 2C)

Table S-4. Spectroscopic Data for the Compounds (Continued)

Compounds	NMR ^a		
	$\delta(^1\text{P}\{\text{H}\})^b$	$\delta(\text{H})^{c,d}$	$\delta(^{13}\text{C}\{\text{H}\})^{c,d}$
[$\text{I}(\text{O})\text{S}(\text{CO})_3(\mu-\eta^3:\kappa^1\text{-CH}_2\text{CCMe}_2)$ - (dppm) ₂][CF_3SO_3](43)	-4.7 (ddd, 1P, ² J _{pp} = 254.9 Hz, ² J _{pp} = 64.6 Hz, ³ J _{pp} = 14.0 Hz), -19.7 (ddd, 1P, ² J _{pp} = 64.6 Hz, ² J _{pp} = 23.7 Hz, ³ J _{pp} = 7.6 Hz), -21.3 (ddd, 1P, ² J _{pp} = 254.9 Hz, ² J _{pp} = 53.1 Hz, ³ J _{pp} = 7.6 Hz), -23.6 (ddd, 1P, ² J _{pp} = 53.1 Hz, ² J _{pp} = 23.7 Hz, ³ J _{pp} = 14.0 Hz)	4.70 (dm, 1H, ² J _{HH} = 14.8 Hz), 4.65 (dm, 1H, ² J _{HH} = 14.2 Hz), 3.97 (bs, 1H), 3.81 (dm, 1H, ² J _{HH} = 14.8 Hz), 3.24 (dm, 1H, ² J _{HH} = 14.2 Hz), 2.17 (d, 1H, ³ J _{HP} = 5.8 Hz), 1.68 (bs, 3H), 1.63 (bs, 3H)	186.9 (dd, 1C, ² J _{CP} = 6.5 Hz, ² J _{CP} = 6.2 Hz), 178.0 (dd, 1C, ² J _{CP} = 121.8 Hz, ² J _{CP} = 9.7 Hz), 173.9 (dd, 1C, ² J _{CP} = 7.9 Hz, ² J _{CP} = 6.8 Hz), -9.1 (m, 1C)
[$\text{I}(\text{O})\text{S}(\text{CO})_3(\mu-\eta^3:\kappa^1\text{-CH}_2\text{CCH}_2)$ - (dppm) ₂][BF_4](44)	-7.4 (m, 2P), -19.3 (m, 2P)	5.61 (dm, 2H, ² J _{HH} = 15.1 Hz), 4.96 (dm, 2H, ² J _{HH} = 15.1 Hz), 4.35 (dm, 2H, ³ J _{HP} = 4.9), 3.55 (bm, 2H)	185.9 (t, 1C, ² J _{CP} = 9.1 Hz), 178.0 (t, 1C, ² J _{CP} = 6.9 Hz), 171.7 (t, 1C, ² J _{CP} = 5.0 Hz)
[$\text{I}(\text{O})\text{S}(\text{CO})_3(\mu-\eta^3:\kappa^1\text{-CH}_2\text{CCHCH}_3)$ - (dppm) ₂][BF_4](45)	-7.3 (om, 2P), -16.8 (ddd, 1P, ² J _{pp} = 48.0 Hz, ² J _{pp} = 25.3, ³ J _{pp} = 12.4 Hz), -19.9 (ddd, 1P, ² J _{pp} = 51.3 Hz, ² J _{pp} = 19.7 Hz, ³ J _{pp} = 12.4 Hz)	5.64 (dm, 1H, ² J _{HH} = 15.1 Hz), 5.57 (dm, 1H, ² J _{HH} = 15.1 Hz), 5.20 (td, 1H, ⁴ J _{HP} = 7.0 Hz, ² J _{HH} = 2.5 Hz), 5.05 (dm, 1H, ² J _{HH} = 15.1 Hz), 4.84 (dm, 1H, ² J _{HH} = 15.1 Hz), 4.61 (bq, 1H, ³ J _{HH} = 6.1 Hz), 3.79 (td, 1H, ⁴ J _{HP} = 5.3 Hz, ² J _{HH} = 2.5 Hz), 1.09 (dm, 3H, ³ J _{HH} = 6.1 Hz)	185.9 (t, 1C, ² J _{CP} = 8.9 Hz), 178.3 (t, 1C, ² J _{CP} = 8.6 Hz), 171.5 (m, 1C, ² J _{CP} = 5.4 Hz)
[$\text{I}(\text{O})\text{S}(\text{CO})_4(\mu\text{-C}=\text{C}(\text{H})\text{C}(\text{CH}_3)=\text{CH}_2)$ - (dppm) ₂][CF_3SO_3](46)	-5.2 (m, 2P), -9.2 (m, 2P)	8.01 (bs, 1H), 4.69 (bs, 1H), 4.46 (bs, 1H), 4.00 (dm, 2H, ² J _{HH} = 12.5 Hz), 2.91 (dm, 2H, ² J _{HH} = 12.5 Hz), 0.41 (bs, 3H)	194.9 (dt, 1C, ² J _{CC} = 26.2 Hz, ² J _{CP} = 7.2 Hz), 179.9 (t, 1C, ² J _{CP} = 11.1 Hz), 175.5 (t, 1C, ² J _{CP} = 7.1 Hz), 171.8 (dt, 1C, ² J _{CC} = 26.2 Hz, ² J _{CP} = 7.1 Hz)

Table S-4. Spectroscopic Data for the Compounds (Continued)

Compounds	NMR ^a		
	$\delta(^{31}\text{P}\{\text{H}\})^b$	$\delta(\text{H})^{c,d}$	$\delta(^{13}\text{C}\{\text{H}\})^{c,d}$
[HO δ (CO) δ (<i>l</i> - κ -F δ -C=C=CH δ)- (dppm) δ][CF δ SO δ] (47)	-12.0 (m, 2P), -19.5 (m, 2P)	4.79 (dm, 2H, $^2J_{\text{HH}} = 14.8$ Hz), 4.46 (dm, 2H, $^2J_{\text{HH}} = 14.8$ Hz), 1.55 (br, 2H, $^2J_{\text{HP}} = 11.8$ Hz)	183.4 (t, 1C, $^2J_{\text{CP}} = 5.7$ Hz), 180.2 (dt, 1C, $^4J_{\text{CF}} = 7.9$ Hz, $^2J_{\text{CP}} = 6.4$ Hz), 177.5 (t, 1C, $^2J_{\text{CP}} = 9.5$ Hz), 154.2 (td, 1C, $^2J_{\text{CP}} = 7.2$ Hz, $^4J_{\text{CF}} = 4.4$ Hz)

^a NMR abbreviations: s = singlet, d = doublet, t = triplet, q = quartet, m = multiplet, b = broad, o = overlapping. NMR data at 27 °C in CD δ Cl δ unless otherwise indicated. ^b ^{31}P chemical shifts referenced to external 85% H δ PO δ . ^c ^1H and ^{13}C chemical shifts referenced to TMS. ^d Chemical shifts for phenyl hydrogens and carbons not given.

Calcd for C₅₈F₃H₅₀IrO₆OsP₄S (**41/41a-CF₃SO₃**): C, 48.43; H, 3.50.
Found: C, 48.14; H, 3.61.

- (b) **[IrOs(CO)₃(μ-η³:κ¹-C(CH₃)(CH₂)₂)(dppm)₂][CF₃SO₃]**
(42/42a). Under an argon atmosphere, 1,2-butadiene (methylallene) was passed through a stirred red solution of **29** (33 mg, 0.024 mmol) in 10 mL of CH₂Cl₂ for 1 min at a rate of approximately 0.1 mL/s, resulting in an immediate colour change of the solution yellow. The solution was left to stir under a methylallene atmosphere for 10 h, after which time 30 mL of diethyl ether and 10 mL of pentane were added to a yellow/orange solution to precipitate a light yellow solid. This solid was recrystallized from CH₂Cl₂/diethylether, washed with 2 x 5 mL of diethyl ether, and dried in vacuo (83 % yield). HRMS: *m/z* calcd for C₅₉H₅₂IrO₃OsP₄ (M⁺), 1215.1493; found, 1215.1534 (M⁺). Anal. Calcd for C₅₉F₃H₅₂IrO₆OsP₄S: C, 48.79; H, 3.61. Found: C, 48.58; H, 3.96.

- (c) **[IrOs(CO)₃(μ-η³:κ¹-CH₂CCMe₂)(dppm)₂][CF₃SO₃]** **(43)**.
Compound **29** (47 mg, 0.034 mmol) was dissolved in 10 mL of CH₂Cl₂ to afford a red solution to which was added 1,1-dimethylallene (1.2 equiv, 0.042 mmol, 4.1 μL). The solution turned light yellow immediately and then darkened to a yellow-orange colour within 5 min. The solution was left to stir under an argon atmosphere for 8 h, after which time 30 mL of diethyl ether and 10 mL of pentane were added to the orange solution to precipitate a light orange solid. This solid was recrystallized from CH₂Cl₂/diethyl ether, washed with 2 x 5 mL of diethyl ether, and dried in vacuo (86 % yield). HRMS: *m/z* calcd for C₅₈H₅₂IrO₃OsP₄ (M⁺), 1305.2105; found, 1305.2085 (M⁺). Anal. Calcd for C₅₉F₃H₅₂IrO₆OsP₄S (**43**•**0.61** CH₂Cl₂): C, 47.60; H, 3.57. Found: C, 47.31; H, 3.70. ¹H NMR spectroscopy in CDCl₃ confirmed the presence of dichloromethane of crystallization. The gas formed from the reaction was condensed into another NMR tube and characterized by ¹H NMR. ¹H NMR data for 4-methyl-1,3-pentadiene (+27 °C in CD₂Cl₂): 1.77 (b, 6H), 4.94 (dd, 1H,

$^3J_{\text{HH}} = 9.9$ Hz, $^2J_{\text{HH}} = 1.9$ Hz), 5.09 (dd, 1H, $^3J_{\text{HH}} = 16.5$ Hz, $^2J_{\text{HH}} = 1.9$ Hz), 5.92 (m, 1H), 6.44 (dd, 1H, $^3J_{\text{HH}} = 16.5$ Hz, $^3J_{\text{HH}} = 9.9$ Hz)

- (d) **[IrOs(CO)₃(μ - η^3 : κ^1 -CH₂CCH₂)(dppm)₂][BF₄] (44).** Under an argon atmosphere, allene was passed through a stirred yellow/orange solution of compound **27-BF₄** (39 mg, 0.029 mmol) in 10 mL of CH₂Cl₂ for 1 min at a rate of approximately 0.1 mL/s. The solution was left to stir under an allene atmosphere for 4 h at ambient temperature, during which time the solution lightened to yellow. After stirring, the solution volume was reduced to 3 mL and to this was added 30 mL of diethyl ether to precipitate a yellow solid that was washed with 2 x 5 mL of diethyl ether and dried in vacuo (88% yield). HRMS: *m/z* calcd for C₅₆H₄₈IrO₃OsP₄ (M⁺), 1277.1792; found, 1277.1770 (M⁺). Anal. Calcd for BC₅₆F₄H₄₈IrO₃OsP₄: C, 49.38; H, 3.55. Found: C, 48.98; H, 3.64.
- (e) **[IrOs(CO)₃(μ - η^3 : κ^1 -CH₂CCHCH₃)(dppm)₂][BF₄] (45).** Under an argon atmosphere, methylallene gas was passed through a stirring yellow/orange solution of compound **27-BF₄** (33 mg, 0.024 mmol) in 5 mL of CH₂Cl₂ for 1 min at a rate of approximately 0.1 mL/s. The solution was left to stir under a methylallene atmosphere for 4 h at ambient temperature, during which time the solution lightened to yellow. After stirring, the solution volume was reduced to 2 mL and to this was added 30 mL of diethyl ether to precipitate a yellow solid that was washed with 2 x 5 mL of diethyl ether and dried in vacuo (85 % yield). HRMS: *m/z* calcd for C₅₇H₅₀IrO₃OsP₄ (M⁺), 1291.1949; found, 1291.1929 (M⁺). Anal. Calcd for BC₅₇F₄H₅₀IrO₃OsP₄: C, 49.75; H, 3.66. Found: C, 49.52; H, 3.74.
- (f) **[IrOs(CO)₄(μ -C=C(H)C(CH₃)=CH₂)(dppm)₂][CF₃SO₃] (46).** Compound **27** (39 mg, 0.028 mmol) was dissolved in 5 mL of CH₂Cl₂ to afford a yellow/orange solution to which was added 1,1-dimethylallene (10 equiv, 0.29 mmol, 28.4 μ L) by microsyringe. The solution was left to stir at ambient temperature for 12 h, after which time the solution had

lightened to yellow. The solvent volume was reduced to 3 mL and 30 mL of diethyl ether was added to precipitate a light yellow solid that was washed with 2 x 5 mL of diethyl ether, and dried in vacuo (82 % yield). HRMS: m/z calcd for $C_{59}H_{50}IrO_4OsP_4$ (M^+), 1331.1898; found, 1331.1883 (M^+). Anal. Calcd for $BC_{59}F_4H_{50}IrO_4OsP_4$: C, 50.04; H, 3.56. Found: C, 50.02; H, 3.67.

(g) $[IrOs(CO)_4(\mu-\kappa^1:\kappa^1-CF_2=C=CH_2)(dppm)_2][CF_3SO_3]$ (47).

Compound **27** (35 mg, 0.025 mmol) was dissolved in 0.7 mL of CD_2Cl_2 in an NMR tube fitted with a J. Young valve to afford an orange/yellow solution. The solution was cooled to -78 °C and the headspace was evacuated and replaced with 1,1-difluoroallene, generated as described above. The NMR tube was warmed over 30 min to ambient temperature and left to react at ambient temperature for 1 h, after which time 20 mL of diethyl ether and 5 mL of pentane were added to the yellow solution to precipitate a light yellow solid. This solid was recrystallized from CH_2Cl_2 /diethyl ether, washed with 2 x 5 mL of diethyl ether, and dried in vacuo (90 % yield). ^{19}F NMR of **47** ($+27$ °C in CD_2Cl_2): δ -74.3 (bd, 1F, $^2J_{FF} = 60.4$ Hz), δ -92.2 (bd, 1F, $^2J_{FF} = 60.4$ Hz). HRMS: m/z calcd for $C_{57}F_2H_{46}IrO_4OsP_4$ (M^+), 1341.1553; found, 1341.1560 (M^+). Anal. Calcd for $C_{58}F_5H_{46}IrO_7OsP_4S$: C, 46.80; H, 3.12. Found: C, 46.82; H, 3.22.

(h) Reaction of $[IrOs(CO)_4(dppm)_2][CF_3SO_3]$ (27) with 2-methyl-1,3-butadiene. To a stirring yellow/orange solution of **27** (24 mg, 0.018 mmol) was added 2-methyl-1,3-butadiene (100 equiv, 0.18 mmol, 180 μ L) by microsyringe. The solution was left to react at ambient temperature for one week and after this time the $^{31}P\{^1H\}$ NMR spectrum revealed compound **27** as the only phosphorus-containing product. Slightly elevated temperatures did not result in a reaction.

5.5.3 X-ray Structure Determinations

5.5.3.1 General

Crystals were grown via layered-solvent slow diffusion using the following solvent systems: CH₂Cl₂/pentane (**41**), acetonitrile/Et₂O (**44**), CH₂Cl₂/Et₂O (**47**). Data were collected using a Bruker APEX II CCD detector/D8 diffractometer²⁵ (**41**, **44**) or with a Bruker APEX II CCD detector/PLATFORM diffractometer²⁵ (**47**); all data were collected using Mo K α radiation ($\lambda = 0.71073$ Å) and with the crystals cooled to -100 °C. The data were corrected for absorption via a multi-scan method (**41**) or through Gaussian integration from indexing of the crystal faces (**44**, **47**). Structures were solved using Patterson search/structure expansion (*DIRDIF-2008*²⁶) (**41**, **47**) or direct methods (*SHELXS-97*²⁷), and least-squares refinements were completed using the program *SHELXL-97*.²⁷ Hydrogen atoms attached to carbons were assigned positions based on the sp² or sp³ hybridization geometries of their attached carbons, and were given thermal parameters 20 % greater than those of their parent atoms. See Appendix III.4 for a listing of crystallographic experimental data for all structures in this chapter.

5.5.3.2 Special Refinement Conditions

(i) **41**: The metal atom positions were each refined as a combination of 50 % Ir and 50% Os sharing the same site. The Cl–C distances (d(Cl(1S)–C(1S)), d(Cl(2S)–C(1S))) within the disordered solvent CH₂Cl₂ molecule were restrained to be 1.75(1) Å during refinement.

(ii) **47**: The Cl–C distances within the minor (30 %) component of the disordered solvent CH₂Cl₂ molecule were restrained during refinement: d(Cl(3S)–C(2S)) = d(Cl(4S)–C(2S)) = 1.75(1) Å.

(iii) For each of the complexes in which the metals have dissimilar coordination environments, the final models were tested by switching the identities of the metal atom centres (Ir for Os and vice versa) and refining these to completion. In each case, the final indices became subtly but noticeably worse for

the “reversed-metals” models (**44**: from $R_1 = 0.0289$, $wR_2 = 0.0619$ to $R_1 = 0.0293$, $wR_2 = 0.0639$; **47**: from $R_1 = 0.0204$, $wR_2 = 0.0564$ to $R_1 = 0.0207$, $wR_2 = 0.0577$).

5.6 References

- (a) Trepanier, S. J.; Sterenberg, B. T.; McDonald, R.; Cowie, M. *J. Am. Chem. Soc.* **1999**, *121*, 2613. (b) Trepanier, S. J.; Dennett, J. N. L.; Sterenberg, B. T.; McDonald, R.; Cowie, M. *J. Am. Chem. Soc.* **2004**, *126*, 8046. (c) Chokshi, A.; Rowsell, B. D.; Trepanier, S. J.; Ferguson, M. J.; Cowie, M. *Organometallics* **2004**, *23*, 4759. (d) Rowsell, B. D.; Trepanier, S. J.; Lam, R.; McDonald, R.; Cowie, M. *Organometallics* **2002**, *21*, 3228. (e) Rowsell, B. D.; McDonald, R.; Ferguson, M. J.; Cowie, M. *Organometallics* **2003**, *22*, 2944. (f) Dell'Anna, M. M.; Trepanier, S. J.; McDonald, R.; Cowie, M. *Organometallics* **2001**, *20*, 88. (g) MacDougall, T. J.; Llamazares, A.; Kuhnert, O.; Ferguson, M. J.; McDonald, R.; Cowie, M. *Organometallics* **2011**, *30*, 952. (h) MacDougall, T. J.; Trepanier, S. J.; Dutton, J. L.; Ferguson, M. J.; McDonald, R.; Cowie, M. *Organometallics* **2011**, *30*, 5882.
- (a) Theopold, K. H.; Bergman, R. G. *J. Am. Chem. Soc.* **1980**, *102*, 5694. (b) Howard, T. R.; Lee, J. B.; Grubbs, R. H. *J. Am. Chem. Soc.* **1980**, *102*, 6876. (c) Lee, J. B.; Gajola, G. J.; Schaefer, W. P.; Howard, T. R.; Ikariya, T.; Straus, D. A.; Grubbs, R. H. *J. Am. Chem. Soc.* **1981**, *103*, 7358. (d) Motyl, K. M.; Norton, J. R.; Schauer, C. K.; Anderson, O. P. *J. Am. Chem. Soc.* **1982**, *104*, 7325.
- (a) Kao, S. C.; Thiel, C. H.; Pettit, R. *Organometallics* **1983**, *2*, 914. (b) Sumner, C. E.; Riley, P. E.; Davis, R. E.; Pettit, R. *J. Am. Chem. Soc.* **1980**, *102*, 1752. (c) Theopold, K. H.; Bergman, R. G. *J. Am. Chem. Soc.* **1981**, *103*, 2489.

4. (a) Knox, S. A. R. *J. Cluster Sci.* **1992**, *3*, 385. (b) Sumner, C. E.; Collier, J. A.; Pettit, R. *Organometallics* **1982**, *1*, 1350. (c) Colborn, R. E.; Davies, D. L.; Dyke, A. F.; Knox, S. A. R.; Mead, K. A.; Orpen, A. G. *J. Chem. Soc. Dalton Trans.* **1989**, 1799. (d) Wigginton, J. R.; Chokshi, A.; Graham, T. W.; McDonald, R.; Ferguson, M. J.; Cowie, M. *Organometallics* **2005**, *24*, 6398.
5. (a) Mui, H. D.; Brumaghim, J. L.; Gross, C. L.; Girolami, G. S. *Organometallics* **1999**, *18*, 3264. (b) Esteruelas, M. A.; Gonzáles, A. I.; López, A. M.; Oliván, M.; Oñate, E. *Organometallics* **2006**, *25*, 693.
6. (a) Madrahimov, S. T.; Markovic, D.; Hartwig, J. F. *J. Am. Chem. Soc.* **2009**, *131*, 7228. (b) Ristic-Petrovic, D.; Anderson, D. J.; Torkelson, J. R.; Ferguson, M. J.; McDonald, R.; Cowie, M. *Organometallics* **2005**, *24*, 3711.
7. (a) Allen, F. H.; Kennard, O.; Watson, D. G.; Brammer, L.; Orpen, A. G.; Taylor, R. *J. Chem. Soc., Perkin Trans. 2* **1987**, S1. (b) $r_c(\text{sp}^3) = 0.77 \text{ \AA}$; $r_c(\text{sp}^2) = 0.74 \text{ \AA}$.
8. (a) Fryzuk, M. D.; Joshi, K.; Rettig, S. J. *Organometallics* **1991**, *10*, 1642. (b) Herberich, G. E.; Spaniol, T. P. *J. Chem. Soc. Chem. Commun.* **1991**, 1457. (c) Herberich, G. E.; Spaniol, T. P. *J. Chem. Soc. Dalton Trans.* **1993**, 2471. (d) Fildes, M. J.; Knox, S. A. R.; Orpen, A. G.; Turner, M. L.; Yates, M. I. *J. Chem. Soc., Chem. Commun.* **1989**, 1680. (e) Donaldson, W. A.; Cushnie, C. D.; Guo, S.; Kramer, M. J.; Bennett, D. W. *Transition Met. Chem.* **1997**, *22*, 592.
9. Fryzuk, M. D. *Inorg. Chem.* **1982**, *21*, 2134.
10. Hay, C. M.; Horton, A. D.; Mays, M. J.; Raithby, P. R. *Polyhedron* **1988**, *7*, 987.
11. (a) Ben-Shoshan, R.; Pettit, R. *Chem. Commun. (London)* **1968**, 247. (b) Davis, R. E. *Chem. Commun. (London)* **1968**, 248. (c) Kühn, A.; Burschka, C.; Werner, H. *Organometallics* **1982**, *1*, 496. (d) Arce, A. J.; De Sanctis, Y.; Deeming, A. J.; Hardcastle, K. I.; Lee, R. *J. Organomet. Chem.* **1991**, *406*, 209. (e) Chetcuti, M. J.; Fanwick, P. E.; McDonald, S.

- R.; Rath, N. N. *Organometallics* **1991**, *10*, 1551. (f) Chacon, S. T.; Chisholm, M. H.; Folting, K.; Huffman, J. C.; Hampden-Smith, M. J. *Organometallics* **1991**, *10*, 3722. (g) Seyferth, D.; Anderson, L. L.; Davis, W. B.; Cowie, M. *Organometallics* **1992**, *11*, 3736. (h) Chisholm, M. H.; Folting, K.; Lynn, M. A.; Streib, W. E.; Tiedtke, D. B. *Angew. Chem. Int. Ed. Engl.* **1997**, *36*, 52. (i) Chisholm, M. H.; Streib, W. E.; Tiedtke, D. B.; Wu, D.-D. *Chem. Eur. J.* **1998**, *4*, 1470.
12. Elschenbroich, C. In *Organometallics*; 3rd ed.; Wiley-VCH: Weinheim, Germany, 2006, p 360.
 13. MacDougall, T. J.; Samant, R. G.; Trepanier, S. J.; Ferguson, M. J.; McDonald, R.; Cowie, M. *Accepted to Organometallics*, **2012**.
 14. (a) Lentz, D.; Willemsen, S. *Organometallics* **1999**, *18*, 3962. (b) Lentz, D.; Nickelt, N.; Willemsen, S. *Chem. Eur. J.* **2002**, *8*, 1205. (c) Lentz, D. *J. Fluorine Chem.* **2004**, *125*, 853.
 15. Slaney, M. E.; Anderson, D. J.; Ferguson, M. J.; McDonald, R.; Cowie, M. *J. Am. Chem. Soc.* **2010**, *132*, 16544.
 16. Lentz, D.; Willemsen, S. *Angew. Chem. Int. Ed.* **2001**, *40*, 2087.
 17. (a) Jones, M. D.; Kemmitt, R. D. W. *Adv. Organomet. Chem* **1987**, *27*, 279. (b) Moore, T.; Kiely, C.; Reeves, P. C. *J. Organomet. Chem.* **2001**, *620*, 308. (c) Ward, J. S.; Pettit, R. *Chem. Commun.* **1970**, 1419.
 18. (a) Chetcuti, M. J.; Fanwick, P. E.; Grant, B. E. *Organometallics* **1991**, *10*, 3003. (b) Whitesides, T. H.; Slaven, R. W. *J. Organomet. Chem.* **1974**, *67*, 99.
 19. Hartwig, J. F.; Pouy, M. J. In *Organotransition Metal Chemistry*; Hartwig, J. F., Ed.; University Science Books: Sausalito, 2010, p 104.
 20. Torkelson, J. R.; McDonald, R.; Cowie, M. *J. Am. Chem. Soc.* **1998**, *120*, 4047.
 21. Bent, H. A. *Chem. Rev.* **1961**, *61*, 275.
 22. Rhee, S. W.; Ryan, K. J.; Tracy, M.; Kelson, A. B.; Clizbe, L. A.; Chang, M.-H.; Park, J. S.; Roh, J.-K.; Kong, J.-Y.; Yang, J. G.; Kim, W.-B.; Ok, K.-D. *J. Labelled Compd. Radiopharm.* **1997**, *39*, 773.

23. Soderquist, J. A.; Anderson, C. L. *Tetrahedron Lett.* **1986**, 27, 3961.
24. Drakesmith, F. G.; Stewart, O. J.; Tarrant, P. *J. Org. Chem.* **1968**, 33, 280.
25. Programs for diffractometer operation, unit cell indexing, data collection, data reduction and absorption correction were those supplied by Bruker. Absorption corrections were applied using programs of the SHELXTL system (Bruker, 2008).
26. Beurskens, P. T.; Beurskens, G.; de Gelder, R.; Garcia-Granda, S.; Israel, R.; Gould, R. O.; Smits, J. M. M. *The DIRDIF-99 program system*; Crystallography Laboratory, University of Nijmegen, The Netherlands, 1999.
27. Sheldrick, G. M. *Acta Crystallogr.* **2008**, A64, 112.

Chapter 6: Conclusions and Final Remarks

6.1 Foundations for Thesis Goals

The surface cluster analogy by E. L. Muetterties,¹ suggested that metal clusters, having adjacent metal centres, could be effective models for the reactions of substrates on a metal surface. However, the inherent insolubility and the complexity of multiple metal centres present in clusters made it difficult to obtain detailed mechanistic information about the transformations studied. For these reasons the smaller and easier to study bimetallic complexes – the simplest compounds with adjacent metals – have been widely used to obtain information regarding the roles of adjacent metals in substrate transformations.

One of the ongoing interests in the Cowie group is the Fischer-Tropsch (FT) process in which syngas ($\text{CO} + \text{H}_2$) is converted to linear hydrocarbons over a late-metal catalyst. Although the mechanism for carbon-carbon chain growth in this system remains poorly understood, there is general agreement on the importance of surface bound methylene-groups (presumably bridging pairs of adjacent metals on the surface) in the process.² Most of the recent proposals for chain growth have been inspired by studies involving well characterized transition-metal complexes, particularly those involving methylene-bridged binuclear complexes.^{2f,3} Owing to our group's additional interest in heterobimetallic complexes, containing pairs of *different* metals, and the recent interest in the use of FT catalysts incorporating combinations of group 8 and 9 metals,^{3k-m,4} we became interested in the use of well-defined mixed-metal complexes, bridged by a methylene group, in order to elucidate the roles of the different metals in chemistry involving this C_1 fragment. The Rh/Os combination was particularly successful in demonstrating reactivity that was reminiscent of FT chemistry, showing temperature-dependent coupling of methylene groups by $[\text{RhOs}(\text{CO})_4(\text{dppm})_2][\text{CF}_3\text{SO}_3]$ to yield either C_1 and C_3 , or C_4 fragments bound to the metals (see Scheme 1-18).^{3l,m} Labelling studies (^{13}C and ^2H) suggested the sequential insertion of methylene groups into the Rh-C bond of bridging

hydrocarbyl fragments, with the reaction pathways diverging to either C₁ and C₃, or C₄ fragments after the formation of the C₃-bridged fragment.

Species containing the C₃-bridged hydrocarbyl fragment in this system were not observed so studies involving the coupling of unsaturated C₂ units (olefins, alkynes) and a bridging methylene group were initiated both with this system,^{3i,5} and with different metal combinations.^{4h,5a,6} Although the Rh/Os and Rh/Ru systems were heavily studied, the analogous Ir/Ru system had received little attention at the time this work was initiated and the Ir/Os system had not been studied. We proposed that a full understanding of the roles of the different metals could not be gained without information from each of the metal combinations.

6.2 Ir/Ru Complexes

The methylene-bridged complex, $[\text{IrRu}(\text{CO})_4(\mu\text{-CH}_2)(\text{dppm})_2]^+$ (**1**),^{4h} unfortunately, *did not* display methylene coupling as observed in the analogous Rh/Os system, presumably owing to the stronger Ir–C bonds. In order to model FT chemistry and C₃-bridged fragments, we utilized other unsaturated substrates capable of insertion into the Ir–CH₂ bond to generate these bridged fragments, as discussed in Chapter 2. Cumulenes appeared to be good substrates for this modelling, as they had the potential of inserting into the Ir–CH₂ bond such that the unsaturation remained *exo* to the C₃-bridge, more accurately representing the proposed propanediyl-bridged (C₃-) intermediate in the Rh/Os example. In our studies of the methylene-bridged Ir/Ru complex, we observed that the addition of allene resulted in the generation of free 1,3-butadiene and $[\text{IrRu}(\text{CO})_4(\text{dppm})_2]^+$ (**13**), clearly a result of coupling of allene with the methylene group, followed by elimination of the C₃-bridged species via a series of β -H elimination and reductive elimination steps,⁷ a common decomposition route for propanediyl-bridged species.^{3j,8} The alkylcumulenes, methylallene and 1,1-dimethylallene, did give rise to isolable C₃-containing complexes; however, the hydrocarbyl groups resulting from insertion had moved out of the bridging position between both metals and was instead chelating at Ir, suggesting that modeling C₃-bridged

species, at least using cumulenes, would be difficult with this system owing to the obvious disparity in the Ir–C and Ru–C bond strengths,⁹ and presumably also a consequence of the strain involved in these C₃-bridged targets, that favour the 4-membered metallacycle instead.

Interestingly, these Ir-chelated complexes of 1,1-dimethylallene react further with a second equiv of cumulene, giving rise to unexpected multiple C–H bond activations, involving at least the two geminal C–H bonds and, in some cases, the accompanying activation of a methyl C–H bond. These activations could be achieved by using different combinations of cumulene substrates to generate a variety of complexes that ultimately contained an Ir-bound κ^1 -alkenyl fragment (from the first equiv of cumulene), and a bridging alkynyl group κ^1 -bound to Ir and η^2 -bound to Ru (from the second equiv of cumulene).

The Ir/Ru metal combination was not an effective model system for FT-type chemistry, as the C–H bond activation products (albeit products of *multiple* C–H bonds) were often observed. Although this unexpected C–H bond activation was not the original goal of this study, the geminal C–H bond activation of olefins, as observed in the activation of cumulenes discussed above, is a rare process.¹⁰ Of the few examples reported, only one system is monometallic,^{10c} which suggests that a pair of adjacent metals is important in this transformation. The demonstration that the Ir/Ru metal combination resulted in facile C–H bond activation of geminal pairs of C–H bonds in cumulenes, led us to investigate the related complex [IrRu(CO)₄(dppm)₂]⁺ (**13**), in which the absence of a bridging methylene group eliminates the possibility of insertion chemistry involving the first equiv of the cumulene. As anticipated, geminal C–H activation of allene, methylallene, and 1,1-dimethylallene was readily achieved using this complex.¹¹ However, the activation of monoolefins or conjugated olefins did not occur, possibly attributable to necessary precoordination of these substrates prior to activation, that was never observed with the Ir/Ru metal coordination. The activation of a single C–H bond in ethylene or propylene could be effected, upon removal of a carbonyl but these vinyl hydride products did not undergo

subsequent activation of a second C–H bond, leading us to suggest that the geminal activation did not involve the sequential C–H activation of the first C–H bond at one metal followed by activation of the second at the adjacent metal. The reversible conversion of the final vinylidene-bridged products into alkynyl hydride species by carbonyl removal or addition, respectively, suggested instead that the observed conversions of cumulenes into vinylidene-bridged species occurred by a sequence of carbonyl loss, activation of the first C–H bond, the (unobserved) 1,3-hydrogen shift to generate the alkynyl hydride, followed by the observed conversion, upon carbonyl addition, to give the vinylidene-bridged products. These geminal activations are in contrast to those observed in related Ir₂^{10a,12} systems, in which a number of α -olefins react to give the vinylidene-bridged hydrides, presumably by a sequential pair of C–H bond activation steps.

6.3 Ir/Os Complexes

In parallel with the above C–H activation reactions, we returned to the insertion chemistry of the bridging methylene group, reasoning that implementing a group 8 metal capable of forming stronger M–C bonds with the substrate could prevent the chelate formation observed with the Ir/Ru system, and promote retention of the hydrocarbyl bridge. It was with this logic that we chose to investigate the Ir/Os combination of two third-row metals, which was relatively unexplored in our group.

As was the case for the Ir/Ru system, the methylene-bridged complex, [IrOs(CO)₄(μ -CH₂)(dppm)₂]⁺ (**28**),¹³ *did not* react with diazomethane, so no subsequent incorporation of methylene groups was observed. Although no methylene coupling was observed, the Ir/Os combination better resembled FT-type chemistry, as is evident with the insertion chemistry described below. Initially, in Chapter 4, we investigated the coupling of symmetric alkynes (HFB and DMAD) with the μ -CH₂ group of [IrOs(CO)₃(μ -CH₂)(dppm)₂]⁺ (**29**) resulting in alkyne insertion into the Ir–CH₂ bond to generate C₃-bridged hydrocarbyl fragments, much as observed for the other metal combinations. Depending on the alkyne added to generate the C₃-bridge (HFB or DMAD), the addition of excess

diazomethane generated either a C₄-bridged hydrocarbyl fragment susceptible to methylene loss (HFB), or facile formation of a C–O bond between the newly introduced methylene group and a carbonyl oxygen from the original alkyne (DMAD). The C₄-bridged product from HFB was not isolable, and a methylene group was lost at ambient temperature to generate ethylene, and restore the stronger Ir–C(sp²) bond (compared to Ir–C(sp³)). Our second strategy to generate C₄-bridged fragments by double methylene insertion into the Ir–C bond of alkyne-bridged species, succeeded in generating a C₃-bridged isomer having an “Ir–CH₂–HFB–Os” core but did not react with a second equiv of diazomethane.

The C–C bond formation involving the Ir/Os metal combination with cumulenes, is discussed in Chapter 5, in which we set out first to generate products resembling the propanediyl-bridged complexes of Rh/Os, and second to compare this system with the related Ir/Ru systems. Reaction of allene and methylallene with [IrOs(CO)₃(μ-CH₂)(dppm)₂]⁺ (**29**), led to reactivity paralleling the Rh-based systems, in which cumulene insertion into the Ir–CH₂ bond was followed by rearrangement of the hydrocarbyl fragment to a μ-η³:κ¹-trimethylenemethane moiety. In the case of allene insertion, the observation of an equilibrium mix of two isomers, in which the hapticity of the trimethylenemethane moiety reversibly changes from metal to metal (η³ to κ¹), accompanied by CO migration to the metal having the κ¹-bound CH₂ group, suggests an exchange process that appears to be the first example of such a rearrangement in trimethylenemethane complexes.

The addition of 1,1-dimethylallene to **29** resulted in coupling of the cumulene with the μ-CH₂ group and loss of the resultant organic fragment (4-methyl-1,3-pentadiene), which suggested a β-H elimination, reductive elimination mechanism, as previously observed in similar complexes,^{5a} and in Chapter 2. The resulting “[IrOs(CO)₃(dppm)₂]⁺” fragment reacted with excess substrate to generate a dimethylallene adduct κ¹-bound to Os by the central carbon, generating a metallaallyl moiety which is η³-bound to Ir. Similar complexes could also be

generated by the addition of allene and methylallene to $[\text{IrOs}(\text{CO})_4(\text{dppm})_2]^+$ (**27**), by loss of a carbonyl ligand.

Surprisingly however, the reaction of dimethylallene with the tetracarbonyl species (**27**) generated a very different product than noted above for the tricarbonyl analogue, in which the activation of three C–H bonds (the pair of geminal C–H bonds and one of the methyl C–H bonds) was observed, with the retention of all CO ligands. This reactivity was very reminiscent of that described in Chapters 2 and 3 for the Ir/Ru system, and in fact represents one of the few cases for which the reactivity of the Ir/Ru and Ir/Os systems was similar. The different reactivities of the cumulenes studied is presumably owing to the initial coordination of the substrate, which appears to be influenced by sterics. The strong M–C bonds in the Ir/Os system is evident in the stronger tendency for the cumulenes to bridge the metals (if sterically favoured) where cleavage of the terminal C–H bonds of the cumulene is not favourable.

This geminal activation observed with Ir/Os led us to attempt the activation of C–H bonds in monoolefins and conjugated dienes with $[\text{IrOs}(\text{CO})_4(\text{dppm})_2]^+$ (**27**); however, these attempts were unsuccessful. The propensity for double C–H activation *was* observed upon leaving **27** for several days in solution in which double orthometallation accompanied by H_2 loss occurs, as described in Appendix I.

6.4 Roles of Adjacent Metals

An important goal of this work was to attempt to elucidate the roles of the adjacent metals in the transformations of small molecules. By changing the group 9 metal from Rh to Ir, we generated systems with stronger M–C bonds at this metal, which was illustrated immediately by the inability for additional diazomethane-generated CH_2 units to insert into the strong Ir– CH_2 bonds of both systems studied. In addition, for reactions requiring CO loss the stronger Ir–CO bonds resulted in less labile Ir/Ru and Ir/Os systems. The Rh–C bond strengths in the Rh/Os system appeared to be crucial for the sequential addition of methylene

groups, with the weaker Rh–C bonds being sufficiently weak to facilitate CH₂ insertion into the existing Rh–CH₂ bond, while also allowing facile migration of CO from Rh to Os. By replacing Rh by Ir, methylene insertion into the stronger Ir–CH₂ bond was no longer favoured, and instead the propensity for low-valent Ir to undergo the oxidative addition of C–H bonds often dominated the reactivity of the complex. In spite of the stronger Ir–CH₂ bond, insertion of alkynes and cumulenes occurred readily, as described above.

Interestingly, in spite of the fact that the majority of the chemistry appears to occur at the group 9 metal, changing the group 8 metal (Ir/Ru to Ir/Os) usually resulted in very different reactivity. The multiple C–H bond activations of cumulenes occurred widely with the Ir/Ru metal combination, but was only observed in one anomalous case (1,1-dimethylallene) in the Ir/Os system. This is presumably related to the stronger binding of the cumulene to Os (than to Ru), hence the stronger tendency of these groups to bridge the metals, where cleavage of the terminal C–H bonds of the cumulene is not favourable.

6.5 Future Work and Closing Remarks

From all of the research involving the Rh/Os and Ir/M (M = Ru, Os) complexes, it was obvious that the metal combinations comprised of a second- and third-row metal resulted in the most active systems for small molecule transformations across two *different* metals. Although the methylene-bridged Rh/Os, Rh/Ru, and Ir/Os systems could be used to isolate C₃-bridged FT-type hydrocarbyl intermediates, the Rh/Os combination still represents the best model system for this process, owing to its ability to couple of to four methylene groups. We certainly have examined a number of methylene-bridged metal combinations, which have yielded valuable information about the roles of the different metals in small molecule transformations. The applicability of these complexes as bimetallic model FT catalysts, however, is diminished by the realization that these metals are not used industrially because of their cost compared to the commonly used iron and cobalt catalysts.¹⁴ Nonetheless, we were able to demonstrate the facile C–C bond formation with bridging methylene units, both with other

methylene groups and other unsaturated substrates. As is often seen in chain growth mechanisms, we also observed C–H bond activation as a competing process for C–C bond formation.

Ideally this study could be expanded to include other dppm-bridged metal combinations, such as Rh/Fe and Co/Ru to more accurately model the commercial C–C bond forming processes using FT chemistry. The Rh/Fe complex, $[\text{RhFe}(\text{CO})_4(\mu\text{-CH}_2)(\text{dppm})_2]^+$ has been synthesized in the Cowie group,¹⁵ however, its reactivity has not been explored. Both Rh and Fe have been shown to be active for the formation of oxygenates in FT chemistry, so complexes involving this metal combination may provide a good model for the formation of such species. The dppm ligand binds well to the softer, late metals described in this dissertation; however, its increased lability with the lighter metals, such as Co and Fe, was demonstrated in the bimetallic compound, $[\text{RhCo}(\text{CO})_3(\text{dppm})_2]$, which reversibly undergoes fragmentation into the two mononuclear ions, $[\text{Rh}(\text{CO})(\text{dppm})_2]^+$ and $\text{Co}(\text{CO})_4^-$, under an atmosphere of CO.¹⁶ Exploring these combinations could provide us with more accurate FT models than the combinations discussed in this dissertation, however we could also attempt to expand the scope of our current study by changing the diphosphine ligand.

The Ir/M (M = Ru, Os) systems would be interesting to investigate with a smaller, more basic diphosphine, such as depm (*bis*(diethylphosphino)methane), which has been shown to be an effective ancillary ligand useful in Ir₂ chemistry for the activation of C–F and C–H bonds.^{12,17} This could allow us to further exploit C–H bond activation reactions of these systems both by providing additional electron density, and by decreasing the steric demands of the diphosphine ligands. This more basic environment could also help promote the cleavage of H₂ at the metal centres, and the reductive elimination of the “FT-type” organic products, which was not observed in the analogous dppm-bridged Ir/M (M = Ru, Os) complexes.

Elucidating the roles of adjacent metal centres in the transformation of small molecules has proven to be a difficult task. Nonetheless, it has always been

our contention that a variety of *different* combinations of metals with *different* substrates represents a necessary approach to fully understanding the roles of the different metals. What has become clear is that although the metals directly involved in the reactivity obviously play an important role, the adjacent metals also play a pivotal role, although being involved more indirectly in substrate reactivity.

6.6 References

1. (a) Muetterties, E. L. *Science* **1977**, *196*, 839. (b) Muetterties, E. L. *Angew. Chem. Int. Ed.* **1978**, *17*, 545. (c) Muetterties, E. L.; Rhodin, T. N.; Band, E.; Brucker, C. F.; Pretzer, W. R. *Chem. Rev.* **1979**, *79*, 91.
2. (a) Fischer, F.; Tropsch, H. *Brennst. Chem.* **1926**, *7*, 97. (b) Fischer, F.; Tropsch, H. *Chem. Ber.* **1926**, *59*, 830. (c) Brady, R. C.; Pettit, R. *J. Am. Chem. Soc.* **1980**, *102*, 6181. (d) Brady, R. C.; Pettit, R. *J. Am. Chem. Soc.* **1981**, *103*, 1287. (e) Biloen, P.; Sachtler, W. M. H. *Adv. Catal.* **1981**, *30*, 165. (f) Maitlis, P. M.; Long, H. C.; Quyoum, R.; Turner, M. L.; Wang, Z.-Q. *Chem. Commun.* **1996**, *1*. (g) Long, H. C.; Turner, M. L.; Fornasiero, P.; Kaspar, J.; Graziani, M.; Maitlis, P. M. *J. Catal.* **1997**, *167*, 172. (h) Dry, M. E. *Appl. Catal. A* **1996**, *138*, 319.
3. (a) Saez, I. M.; Andrews, D. G.; Maitlis, P. M. *Polyhedron* **1988**, *7*, 827. (b) Isobe, K.; Andrews, D. G.; Mann, B. E.; Maitlis, P. M. *J. Chem. Soc. Chem. Commun.* **1981**, 809. (c) Maitlis, P. M.; Ma, F.; Martinez, J.; Byers, P. K.; Saez, I.; Sunley, G. J. *Adv. Chem. Ser.* **1992**, *230*, 565. (d) Maitlis, P. M. *J. Organomet. Chem.* **1995**, *500*, 239. (e) Isobe, K.; Vázquez de Miguel, A.; Bailey, P. M.; Okeya, S.; Maitlis, P. M. *J. Chem. Soc. Dalton Trans.* **1983**, 1441. (f) Maitlis, P. M.; Quyoum, R.; Long, H. C.; Turner, M. L. *Appl. Catal. A* **1999**, *186*, 363. (g) Martinez, J. M.; Adams, H.; Bailey, N. A.; Maitlis, P. M. *J. Chem. Soc. Chem. Commun.* **1989**, 286. (h) Martinez, J.; Gill, J. B.; Adams, H.; Bailey, N. A.; Saez, I. M.; Sunley, G. J.; Maitlis, P. M. *J. Organomet. Chem.* **1990**, *394*, 583. (i)

- Sumner, C. E.; Collier, J. A.; Pettit, R. *Organometallics* **1982**, *1*, 1350. (j) Sumner, C. E., Jr.; Riley, P. E.; Davis, R. E.; Pettit, R. *J. Am. Chem. Soc.* **1980**, *102*, 1752. (k) Rowsell, B. D.; Trepanier, S. J.; Lam, R.; McDonald, R.; Cowie, M. *Organometallics* **2002**, *21*, 3228. (l) Trepanier, S. J.; Dennett, J. N. L.; Sterenberg, B. T.; McDonald, R.; Cowie, M. *J. Am. Chem. Soc.* **2004**, *126*, 8046. (m) Trepanier, S. J.; Sterenberg, B. T.; McDonald, R.; Cowie, M. *J. Am. Chem. Soc.* **1999**, *121*, 2613.
4. (a) da Silva, A. C.; Piotrowski, H.; Mayer, P.; Polborn, K.; Severin, K. *Eur. J. Inorg. Chem.* **2001**, 685. (b) Sinfelt, J. H. *Bimetallic Catalysts: Discoveries, Concepts, and Applications*; Wiley: New York, 1983. (c) Alexeev, O. S.; Gates, B. C. *Ind. Eng. Chem. Res.* **2003**, *42*, 1571. (d) Iglesia, E.; Soled, S. L.; Fiato, R. A.; Via, G. H. *J. Catal.* **1993**, *143*, 345. (e) Huang, L.; Xu, Y. *Catal. Lett.* **2000**, *69*, 145. (f) Dombek, B. D. *Organometallics* **1985**, *4*, 1707. (g) Trepanier, S. J.; McDonald, R.; Cowie, M. *Organometallics* **2003**, *22*, 2638. (h) Dell'Anna, M. M.; Trepanier, S. J.; McDonald, R.; Cowie, M. *Organometallics* **2001**, *20*, 88. (i) Torkelson, J. R.; McDonald, R.; Cowie, M. *J. Am. Chem. Soc.* **1998**, *120*, 4047.
5. (a) Chokshi, A.; Rowsell, B. D.; Trepanier, S. J.; Ferguson, M. J.; Cowie, M. *Organometallics* **2004**, *23*, 4759. (b) Wigginton, J. R.; Chokshi, A.; Graham, T. W.; McDonald, R.; Ferguson, M. J.; Cowie, M. *Organometallics* **2005**, *24*, 6398.
6. Rowsell, B. D.; McDonald, R.; Ferguson, M. J.; Cowie, M. *Organometallics* **2003**, *22*, 2944.
7. MacDougall, T. J.; Trepanier, S. J.; Dutton, J. L.; Ferguson, M. J.; McDonald, R.; Cowie, M. *Organometallics* **2011**, *30*, 5882.
8. (a) Theopold, K. H.; Bergman, R. G. *J. Am. Chem. Soc.* **1981**, *103*, 2489. (b) Kao, S. C.; Thiel, C. H.; Pettit, R. *Organometallics* **1983**, *2*, 914.
9. (a) Armentrout, P. B. In *Bonding Energetics in Organometallic Compounds*; Marks, T. J., Ed.; American Chemical Society: Washington, DC, 1990, p 18. (b) Ziegler, T.; Tschinke, V. In *Bonding Energetics in*

- Organometallic Compounds*; Marks, T. J., Ed.; American Chemical Society: Washington, DC, 1990, p 279.
10. (a) Ristic-Petrovic, D.; Torkelson, J. R.; Hilts, R. W.; McDonald, R.; Cowie, M. *Organometallics* **2000**, *19*, 4432. (b) Suzuki, H.; Omori, H.; Hwan Lee, D.; Yoshida, Y.; Fukushima, M.; Tanaka, M.; Moro-oka, Y. *Organometallics* **1994**, *13*, 1129. (c) Bell, T. W.; Haddleton, D. M.; McCamley, A.; Partridge, M. G.; Perutz, R., N.; Willner, H. *J. Am. Chem. Soc.* **1990**, *112*, 9212. (d) Boncella, J. M.; Green, M. L. H. *J. Organomet. Chem.* **1987**, *325*, 217. (e) Deeming, A. J.; Underhill, M. *J. Organomet. Chem.* **1972**, *42*, C60. (f) Boncella, J. M.; Green, M. L. H.; O'Hare, D. *J. Chem. Soc., Chem. Commun.* **1986**, 618. (g) Deeming, A., J.; Underhill, M. *J. C. S. Chem. Comm.* **1973**, 277. (h) Deeming, A., J.; Underhill, M. *J. C. S. Dalton* **1974**, 1415. (i) Deeming, A., J.; Hasso, S.; Underhill, M.; Canty, A. J.; Johnson, B. F. G.; Jackson, W. G.; Lewis, J.; Matheson, T. W. *J. C. S. Chem. Comm.* **1974**, 807.
 11. MacDougall, T. J.; Samant, R. G.; Trepanier, S. J.; Ferguson, M. J.; McDonald, R.; Cowie, M. *Accepted for publication, Organometallics, January 18, 2012.*
 12. Slaney, M. E.; Anderson, D. J.; Ferguson, M. J. D.; McDonald, R.; Cowie, M. *Accepted for publication in Organometallics, January 16, 2012.*
 13. MacDougall, T. J.; Llamazares, A.; Kuhnert, O.; Ferguson, M. J.; McDonald, R.; Cowie, M. *Organometallics* **2011**, *30*, 952.
 14. Tullo, A. H. *Chem. Eng. News* **2003**, *81*, 18.
 15. Lo, J.; Cowie, M. *Unpublished Results.*
 16. (a) Antonelli, D. M.; Cowie, M. *Organometallics* **1990**, *9*, 1818. (b) Elliot, D. J.; Holah, D. G.; Hughes, A. N.; Vittal, J. J.; Puddephatt, R. J. *Organometallics* **1993**, *12*, 1225.
 17. Slaney, M. E.; Ferguson, M. J.; McDonald, R.; Cowie, M. *Accepted for publication in Organometallics, January 11, 2012.*

Appendices

Appendix I

Attempted C–H Bond Activation of Monoolefins with $[\text{IrOs}(\text{CO})_4(\text{dppm})_2]^+$

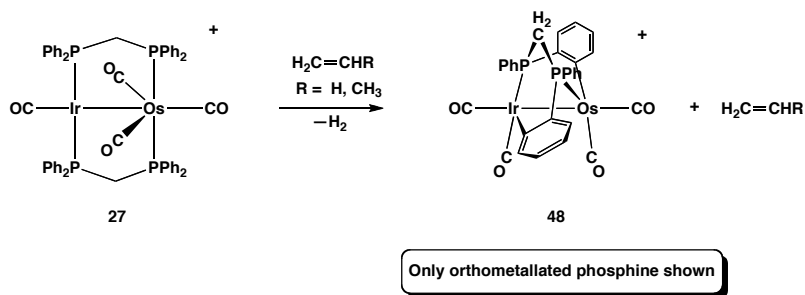
Introduction

Following up on the attempts to effect the C–H bond activation of monoolefins with Ir/Ru, we sought to investigate the applicability of the Ir/Os metal combination in such transformations. The Ir/Ru system, as discussed in Chapter 3, failed to activate the C–H bonds of ethylene and propylene unless a carbonyl ligand was removed, in which case the activation of a single C–H bond to generate a vinyl hydride product was observed at $-20\text{ }^\circ\text{C}$, presumably activating at the Ir centre. However, the activation of the second geminal C–H bond, did not occur upon warming the solution to ambient temperature. The Ir/Os combination, containing two third-row metals, appeared to be a system capable of this double activation.

Results and Discussion

The addition of ethylene and propylene to **27** results in the formation of a new compound, $[\text{IrOs}(\text{CO})_4(\mu^2-\eta^4\text{-(o-C}_6\text{H}_4)\text{PhPCH}_2\text{PPh(o-C}_6\text{H}_4)\text{(dppm))}]$ - $[\text{CF}_3\text{SO}_3]$ (**48**), together with H_2 loss, in 10% yield within 24 h, but requiring 10 d for completion at ambient temperature, as shown in Scheme I-1. Compound **48**

Scheme I-1



is the double orthometallation product – a result of the activation of two ortho C–H bonds, one at each metal, of two different phenyl rings of the same dpmm ligand.

The $^{31}\text{P}\{^1\text{H}\}$ NMR spectrum of **48** displays four resonances at δ –8.7, δ –22.8, δ –33.2, and δ –38.2, as shown in Figure I-1. The two downfield signals display mutual trans coupling of 242.0 Hz and the two upfield signals display a weaker cis coupling of 16.5 Hz. The ^1H NMR spectrum displays the protons for the dpmm methylene protons at δ 5.69, δ 4.93, δ 4.07, and δ 2.44, and the aryl protons in the usual region. Differentiating between the protons on the orthometallated phenyl rings and the protons of the other phenyl rings is not possible due to the overlap of peaks in the phenyl region. The $^{13}\text{C}\{^1\text{H}\}$ NMR spectrum of a ^{13}CO -enriched sample of **48** displays four carbonyl resonances; the pair at δ 184.4 and δ 172.6 are bound to one metal while those at δ 177.4 and δ 158.8 are bound to the other.

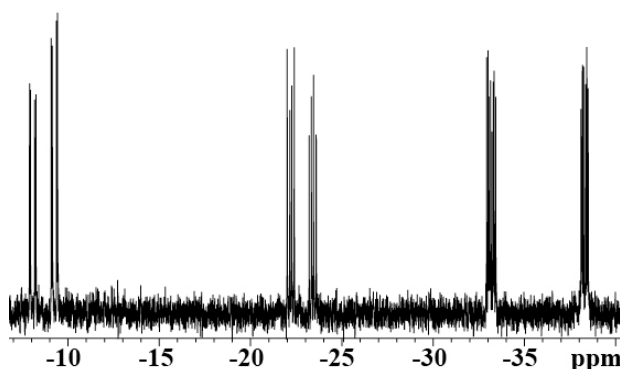


Figure I-1. $^{31}\text{P}\{^1\text{H}\}$ NMR spectrum of **48** in CD_2Cl_2

The X-Ray structure determination of $[\text{IrOs}(\text{CO})_4(\mu^2-\eta^4-(o\text{-C}_6\text{H}_4)\text{PhPCH}_2\text{PPh}(o\text{-C}_6\text{H}_4)(\text{dpmm}))][\text{CF}_3\text{SO}_3]$ (**48**), as shown for the complexation in Figure I-2, clearly establishes the double orthometallation in which one phenyl ring has orthometallated onto Ir, and another from the same dpmm ligand has orthometallated onto the Os. The coordination environment around each metal is similar in that each contains two carbonyl ligands as well as the orthometallated ligand. However, the arrangement of the dpmm ligands is

different at each metal, as the ends of the diphosphines are in a trans arrangement at Os and in a cis arrangement at Ir. Selected bond lengths and angles are given in Table I-1. Both metal centres are bound to one ^{31}P atom from a typical dppm

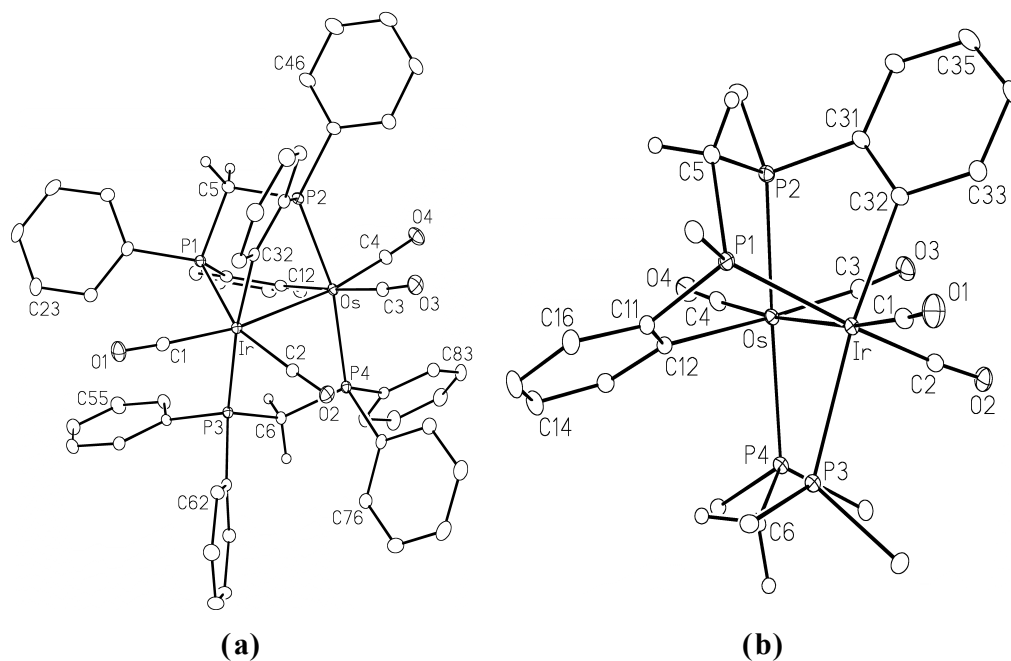


Figure I-2. (a) Perspective view of the complex cation of $[\text{IrOs}(\text{CO})_4-(\mu^2-\eta^4-(o\text{-C}_6\text{H}_4)\text{PhPCH}_2\text{PPh}(o\text{-C}_6\text{H}_4)(\text{dppm}))][\text{CF}_3\text{SO}_3]$ (**48**). Thermal ellipsoids are shown at the 20 % probability level except for hydrogens, which are shown artificially small. (b) Alternate view of the cation of **48** with only the ipso carbons shown for the non-metallated phenyl rings.

ligand and one ^{31}P atom that contains a phenyl ring orthometallated on the adjacent metal. The orthometallation causes significant twisting around the metal–metal axis, as is obvious by the torsion angles relating the dppm ligands being *ca.* 37° , the largest deviation from planarity in all of the Ir/Os compounds studied in this thesis. The geometry at both metals is a slightly distorted octahedron; at the Ir center, the two ^{31}P nuclei bound to Ir occupy cis positions ($\text{P}(1)\text{--Ir--P}(3) = 96.19(3)^\circ$), while those bound to Os occupy the more typical trans arrangement, although $\text{P}(2)\text{--Os--P}(4)$ is slightly acute at $166.30(3)^\circ$, as shown

better in Figure I-2(b), with the distortion owing to the strain imposed by the orthometallation.

Table I-1. Selected Bond Lengths and Angles for Compound 48

(a) Distance (Å)

atom 1	atom 2	distance	atom 1	atom 2	distance
Ir	Os	2.8932(2)	Ir	P(3)	2.3904(8)
Ir	C(1)	1.959(4)	Os	P(2)	2.3466(8)
Ir	C(2)	1.912(3)	Os	P(4)	2.3877(8)
Ir	C(32)	2.149(3)	Os	C(3)	1.924(3)
Ir	C(32)	2.149(3)	Os	C(4)	1.874(3)
Ir	P(1)	2.3506(8)	Os	C(12)	2.189(3)

(b) Angles (deg)

atom 1	atom 2	atom 3	angle	atom 1	atom 2	atom 3	angle
Os	Ir	P(1)	77.39(2)	Ir	Os	P(2)	78.04(2)
Os	Ir	P(3)	91.56(2)	Ir	Os	P(4)	89.17(2)
Os	Ir	C(1)	171.81(9)	Ir	Os	C(4)	171.84(11)
Os	Ir	C(32)	87.70(9)	Ir	Os	C(12)	88.63(9)
P(1)	Ir	P(3)	96.19(3)	P(2)	Os	P(4)	166.30(3)

The orthometallation itself is not extremely surprising as this reaction occurs when the heterobimetallic complex is being prepared from its monometallic precursors.¹ The orthometallation of dppm ligands has been reported for other multimetallic complexes, often requiring heating or refluxing conditions.² Although the orthometallation observed was initially with the addition of olefins, the same orthometallation occurs spontaneously in solution over 10 d, or by refluxing **27** in THF for 72 h.

Conclusions

Although the Ir/Os centre contains low-valent Ir capable of C–H bond activation, the activation of monoolefins does not occur with this system. However, the potential for this system to undergo double C–H bond activation is

seen in the product obtained in which two ortho C–H bonds from the dppm phenyl rings are activated to generate two strong M–C bonds (one on Ir and one on Os) with the concomitant loss of H₂. Thus, this metal combination favours intramolecular C–H bond activation to the intermolecular activation of monoolefins, in contrast to the Ir/Ru system. This system displays the tendency for oxidative addition to occur at both Os⁰ and Ir^I metal centres.

Experimental

All solvents were dried using appropriate desiccants (given in Appendix II), distilled before use, and stored under a nitrogen atmosphere. The tetracarbonyl complex [IrOs(CO)₄(dppm)₂]⁺ (**27**) was prepared according to published procedure.³ The propylene was purchased from Aldrich and the ethylene from Matheson. The ¹H and ³¹P{¹H} NMR spectra were recorded on a Varian Inova 400 spectrometer operating at 399.9 and 161.8 MHz, respectively. All low-temperature spectra and the heteronuclear decoupling experiments (¹³C{¹H} and ¹³C{¹H,³¹P}) were recorded on a Varian Unity spectrometer operating at 161.9 MHz for ¹³C, 202.3 MHz for ³¹P, and 499.8 MHz for ¹H. Mass spectrometry was performed on a Micromass ZabSpec TOF spectrometer by the mass spectrometry facility of this department, and elemental analyses were also carried out in the departmental facility.

(a) [IrOs(CO)₄(μ²-η⁴-(*o*-C₆H₄)PhPCH₂PPh(*o*-C₆H₄)(dppm))][CF₃SO₃]
(**48**). Compound **27** (25 mg, 0.018 mmol) was dissolved in 0.7 mL of CD₂Cl₂ in an NMR tube fitted with a J. Young valve. The NMR tube was cooled to –78 °C and the argon headspace was evacuated and replaced by 5 mL of ethylene. The NMR tube was warmed to ambient temperature and after 24 h the appearance of **48** was confirmed in the ³¹P{¹H} NMR spectrum. After 10 days, compound **48** was the only phosphorus-containing product, which could be precipitated as a yellow solid by the addition of 20 mL of diethyl ether and 5 mL of pentane. The solid was recrystallized with CH₂Cl₂/diethyl ether, washed with 2 x 5 mL of diethyl ether, and dried in vacuo (86% yield). HRMS: *m/z* calcd for C₅₄H₄₂IrO₄OsP₄ (M⁺), 1263.1267; found, 1263.1272 (M⁺). Anal. Calcd for

C₅₅F₃H₄₂IrO₇OsP₄S: C, 46.84; H, 3.00. Found: C, 47.00; H, 3.40. ³¹P NMR data (+27 °C in CD₂Cl₂): δ -8.7 (ddd, 1P, ²J_{PP} = 242.0 Hz, ²J_{PP} = 57.8 Hz, ³J_{PP} = 12.0 Hz), δ -22.8 (ddd, 1P, ²J_{PP} = 242.0 Hz, ²J_{PP} = 50.4 Hz, ³J_{PP} = 27.0 Hz), δ -33.2 (ddd, 1P, ²J_{PP} = 57.8 Hz, ²J_{PP} = 16.5 Hz, ³J_{PP} = 27.0 Hz), δ -38.2 (ddd, 1P, ²J_{PP} = 50.4 Hz, ²J_{PP} = 16.5 Hz, ³J_{PP} = 12.0 Hz). ¹H NMR data (+27 °C in CD₂Cl₂): δ 5.70 (dm, 1H, ²J_{HH} = 14.8 Hz), δ 4.94 (dm, 1H, ²J_{HH} = 12.7 Hz), δ 4.09 (dm, 1H, ²J_{HH} = 14.8 Hz), δ 2.45 (dm, 1H, ²J_{HH} = 12.7 Hz). ¹³C NMR data (+27 °C in CD₂Cl₂): δ 184.4 (t, 1C, ²J_{CP} = 7.0 Hz), δ 177.4 (t, 1C, ²J_{CP} = 8.2 Hz), δ 172.6 (t, 1C, ²J_{CP} = 7.5 Hz), δ 158.8 (t, 1C, ²J_{CP} = 6.2 Hz).

X-Ray Structure Determination

(a) General. Crystals were grown via layered-solvent slow diffusion using CH₂Cl₂/Et₂O. Data were collected using a Bruker APEX II CCD detector/D8 diffractometer⁴ and all data were collected using Mo K α radiation ($\lambda = 0.71073 \text{ \AA}$) and with the crystal cooled to -100 °C. The data were corrected for absorption through Gaussian integration from indexing of the crystal faces. Structures were solved using Patterson search/structure expansion (*DIRDIF-2008*)⁵, and least-squares refinements were completed using the program *SHELXL-97*.⁶ Hydrogen atoms attached to carbons were assigned positions based on the sp² or sp³ hybridization geometries of their attached carbons, and were given thermal parameters 20 % greater than those of their parent atoms. See Appendix III.5 for a listing of crystallographic experimental data for compound **48**. **(b) Special Refinement Conditions:** Distances within the minor (25 %) conformer of one of the disordered solvent CH₂Cl₂ molecules were fixed during refinement: d(Cl(3S)-C(2S)) = d(Cl(4S)-C(2S)) = 1.75(1) Å; d(Cl(3S)⋯Cl(4S)) = 2.86(1) Å.

References

1. Hilts, R. W.; Franchuk, R. A.; Cowie, M. *Organometallics* **1991**, *10*, 1297.
2. (a) Mizra, H. A.; Vittal, J. J.; Puddephatt, R. J. *Can. J. Chem.* **1995**, *73*, 903. (b) Kabir, S. E.; Johns, C. A.; Malik, K. M. A.; Mottalib, M. A.; Rosenberg, E. *J. Organomet. Chem.* **2001**, *625*, 112. (c) Hassan, M. R.; Hogarth, G.; Hossain, G. M. G.; Kabir, S. E.; Raha, A. K.; Saha, M. S.; Tocher, D. A. *Organometallics* **2007**, *26*, 6473. (d) Teets, T. S.; Cook, T. R.; McCarthy, B. D.; Nocera, D. G. *Inorg. Chem.* **2011**, *50*, 5223.
3. MacDougall, T. J.; Llamazares, A.; Kuhnert, O.; Ferguson, M. J.; McDonald, R.; Cowie, M. *Organometallics* **2011**, *30*, 952.
4. Programs for diffractometer operation, unit cell indexing, data collection, data reduction and absorption correction were those supplied by Bruker. Absorption corrections were applied using programs of the SHELXTL system (Bruker, 2008).
5. Beurskens, P. T.; Beurskens, G.; de Gelder, R.; Garcia-Granda, S.; Israel, R.; Gould, R. O.; Smits, J. M. M. *The DIRDIF-99 program system*; Crystallography Laboratory, University of Nijmegen, The Netherlands, 1999.
6. Sheldrick, G. M. *Acta Crystallogr.* **2008**, *A64*, 112.

Appendix II Drying Agents/Indicators for Solvents

Solvent	Drying Agent	Indicator
acetonitrile	calcium hydride (CaH)	N/A
benzene	sodium metal (Na)	benzophenone
dichloromethane	phosphorus pentoxide (P ₂ O ₅)	N/A
diethyl ether	sodium metal (Na)	benzophenone
methanol	magnesium sulphate (MgSO ₄)	N/A
<i>n</i> -pentane	sodium metal (Na)	N/A
tetrahydrofuran	sodium metal (Na)	benzophenone

Appendix III Crystallographic Experimental Details

AIII.1 Crystallographic Details for Chapter 2 Compounds

Table III.1-1 Crystallographic Details for 4·Et₂O and 5·Et₂O		
	4·Et₂O	5·Et₂O
<i>A. Crystal Data</i>		
formula	C ₆₅ H ₆₇ BF ₄ IrNO ₄ P ₄ Ru	C ₆₄ H ₆₅ BF ₄ IrNO ₄ P ₄ Ru
formula weight	1430.16	1416.13
crystal dimensions (mm)	0.26 x 0.14 x 0.09	0.54 x 0.30 x 0.22
crystal system	triclinic	triclinic
space group	<i>P</i> $\bar{1}$ (No. 2)	<i>P</i> $\bar{1}$ (No. 2)
unit cell parameters ^a		
<i>a</i> (Å)	12.6752(7)	12.6893(11)
<i>b</i> (Å)	15.0112(9)	14.9289(13)
<i>c</i> (Å)	19.2987(11)	19.3173(16)
α (deg)	67.2482(9)	67.1788(12)
β (deg)	84.5581(10)	84.9075(14)
γ (deg)	68.1660(9)	68.7623(12)
<i>V</i> (Å ³)	3138.2(3)	3138.2(5)
<i>Z</i>	2	2
ρ calcd (g cm ⁻³)	1.514	1.499
μ (mm ⁻¹)	2.519	4.519
<i>B. Data Collection and Refinement Conditions</i>		
diffractometer	Bruker PLATFORM/SMART 1000 CCD ^b	
radiation (λ [Å])	graphite-monochromated Mo K α (0.71073)	
temperature (°C)	-80	
scan type	ω scans (0.3°) (25 s exposures)	ω scans (0.3°) (20 s exposures)
$2\theta_{\max}$ (deg)	52.78	52.86
total data collected	24341 ($-15 \leq h \leq 15, -18 \leq k \leq 18, -24 \leq l \leq 24$)	24242 ($-15 \leq h \leq 15, -18 \leq k \leq 18, -24 \leq l \leq 24$)
independent reflections	12757 ($R_{int} = 0.0292$)	12822 ($R_{int} = 0.0210$)
number of observed reflections (NO)	10937 [$F_o^2 \geq 2\sigma(F_o^2)$]	11625 [$F_o^2 \geq 2\sigma(F_o^2)$]
range of transmission factors	0.8050–0.5604	0.6073–0.3433
data/restraints/parameters	12757/25 ^c /712	12822 /0/712
goodness-of-fit (S) ^d [all data]	1.045 [$F_o^2 \geq -3\sigma(F_o^2)$]	1.050 [$F_o^2 \geq -3\sigma(F_o^2)$]
final <i>R</i> indices ^e		
R_1 [$F_o^2 \geq 2\sigma(F_o^2)$]	0.0331	0.0339
wR_2 [$F_o^2 \geq -3\sigma(F_o^2)$]	0.0856	0.0931
largest diff peak and hole (e Å ⁻³)	1.640 and -1.007	1.440 and -1.035

^a Obtained from least-squares refinement of 6516 reflections with $4.56^\circ < 2\theta < 52.64^\circ$ (**4·Et₂O**) or 6869 reflections with $4.90^\circ < 2\theta < 52.84^\circ$ (**5·Et₂O**).

^b Programs for diffractometer operation, data collection, data reduction and absorption correction were those supplied by Bruker.

^c The B–F and F \cdots F distances within the disordered BF₄ ion were restrained to be 1.35(1) and 2.20(1) Å, respectively. The geometry about C7B in the minor part of the disordered 2-methylpen-2-ene-3,5-diyl fragment had the following distance restraints during refinement: C7B–C8B and C7B–C9B, 1.50(1) Å; C8B \cdots C9B, 2.60(1) Å; C6B–C8B and C6B–C9B, 2.45(1) Å.

^d $S = [\sum w(F_o^2 - F_c^2)^2 / (n - p)]^{1/2}$ (n = number of data; p = number of parameters varied; $w = [\sigma^2(F_o^2) + (0.0472P)^2]^{-1}$ (**4·Et₂O**) or $w = [\sigma^2(F_o^2) + (0.0529P)^2 + 3.4151P]^{-1}$ (**5·Et₂O**) where $P = [\text{Max}(F_o^2, 0) + 2F_c^2]/3$).

^e $R_1 = \sum ||F_o| - |F_c|| / \sum |F_o|$; $wR_2 = [\sum w(F_o^2 - F_c^2)^2 / \sum w(F_o^4)]^{1/2}$.

Table III.1-2 Crystallographic Details for 8-CF₃SO₃·1.5CH₂Cl₂ and 10·2CH₂Cl₂		
	8-CF₃SO₃·1.5CH₂Cl₂	10·2CH₂Cl₂
<i>A. Crystal Data</i>		
formula	C _{66.5} H ₆₃ Cl ₃ F ₃ IrO ₆ P ₄ RuS	C ₆₄ H ₆₂ BCl ₄ F ₄ IrO ₃ P ₄ Ru
formula weight	1570.73	1524.90
crystal dimensions (mm)	0.69 x 0.59 x 0.46	0.45 x 0.31 x 0.31
crystal system	triclinic	triclinic
space group	<i>P</i> $\bar{1}$ (No. 2)	<i>P</i> $\bar{1}$ (No. 2)
unit cell parameters ^a		
<i>a</i> (Å)	12.5683(8)	12.4286(6)
<i>b</i> (Å)	12.8768(8)	15.0216(7)
<i>c</i> (Å)	20.1977(13)	18.6676(8)
α (deg)	99.4872(9)	95.2809(5)
β (deg)	90.1385(9)	100.1560(5)
γ (deg)	94.0337(9)	112.2561(5)
<i>V</i> (Å ³)	3215.8(4)	3126.4(2)
<i>Z</i>	2	2
ρ calcd (g cm ⁻³)	1.622	1.620
μ (mm ⁻¹)	2.618	2.698
<i>B. Data Collection and Refinement Conditions</i>		
diffractometer	Bruker PLATFORM/SMART 1000 CCD ^b	
radiation (λ [Å])	graphite-monochromated Mo K α (0.71073)	
temperature (°C)	-80	-100
scan type	ω scans (0.3°) (15 s exposures)	ω scans (0.3°) (20 s exposures)
$2\theta_{\max}$ (deg)	52.76	55.12
total data collected	25718 ($-15 \leq h \leq 15$, $-15 \leq k \leq 15$, $-25 \leq l \leq 25$)	28261 ($-16 \leq h \leq 16$, $-19 \leq k \leq 19$, $-24 \leq l \leq 24$)
independ reflns (<i>R</i> _{int})	13107 (<i>R</i> _{int} = 0.0155)	14387 (<i>R</i> _{int} = 0.0127)
number of observed reflections (NO)	12141 [$F_o^2 \geq 2\sigma(F_o^2)$]	13492 [$F_o^2 \geq 2\sigma(F_o^2)$]
range of transmission factors	0.3788–0.2652	0.4923–0.3738
data/restraints/parameters	13107/2 ^c /986	14387 0/742
goodness-of-fit (S) ^d	1.049 [$F_o^2 \geq -3\sigma(F_o^2)$]	1.047 [$F_o^2 \geq -3\sigma(F_o^2)$]
final <i>R</i> indices ^e		
<i>R</i> ₁ [$F_o^2 \geq 2s(F_o^2)$]	0.0227	0.0345
<i>wR</i> ₂ [$F_o^2 \geq -3s(F_o^2)$]	0.0611	0.0964
largest diff peak and hole (e Å ⁻³)	1.618 and -0.652	2.520 and -1.668

^a Obtained from least-squares refinement of 7275 reflections with $4.74^\circ < 2\theta < 52.74^\circ$ (**8-CF₃SO₃·1.5CH₂Cl₂**) or 9841 reflections with $4.70^\circ < 2\theta < 55.12^\circ$ (**10·2CH₂Cl₂**).

^b Programs for diffractometer operation, data collection, data reduction and absorption correction were those supplied by Bruker.

^c An idealized geometry was imposed upon the μ -2-methylbut-1-en-3-ynyl ligand by constraining the disordered parts of the ligand to planarity (ie. Requiring the sets of atoms [C11A, C12A, C13A, C14A] and [C11B, C12B, C13B, C14B] to each form a tetrahedron with a volume of no more than 0.002 Å³

^d $S = [\sum w(F_o^2 - F_c^2)^2 / (n - p)]^{1/2}$ (*n* = number of data; *p* = number of parameters varied; $w = [\sigma^2(F_o^2) + (0.0354P)^2 + 1.7780P]^{-1}$ (**8-CF₃SO₃·1.5CH₂Cl₂**) or $w = [\sigma^2(F_o^2) + (0.0485P)^2 + 9.0044P]^{-1}$ (**10·2CH₂Cl₂**) where $P = [\text{Max}(F_o^2, 0) + 2F_c^2]^{1/3}$).

^e $R_1 = \sum ||F_o| - |F_c|| / \sum |F_o|$; $wR_2 = [\sum w(F_o^2 - F_c^2)^2 / \sum w(F_o^4)]^{1/2}$.

AIII.2 Crystallographic Details for Chapter 3 Compounds

Table III.2-1 Crystallographic Details for 14-CF ₃ SO ₃ ·0.5CH ₂ Cl ₂ ·Et ₂ O and 16-CF ₃ SO ₃ ·3.5THF		
	14-CF ₃ SO ₃ ·0.5CH ₂ Cl ₂ ·Et ₂ O	16-CF ₃ SO ₃ ·3.5THF
A. Crystal Data		
formula	C62.5H59ClF3IrO8P4RuS	C ₇₄ H ₇₈ F ₃ IrO _{10.5} P ₄ RuS
formula weight	1461.23	1641.57
crystal dimensions (mm)	0.32 x 0.24 x 0.15	0.44 x 0.43 x 0.29
crystal system	monoclinic	orthorhombic
space group	C2/c (No. 15)	Pnma (No. 62)
unit cell parameters ^a		
a (Å)	34.714(3)	18.5564(13)
b (Å)	17.3092(14)	15.2146(10)
c (Å)	20.5712(17)	24.4022(16)
α (deg)		
β (deg)	96.598(2)	
γ (deg)		
V (Å ³)	12278.8(18)	6889.4(8)
Z	8	4
ρ _{calcd} (g cm ⁻³)	1.601	1.583
μ (mm ⁻¹)	2.656	2.340
B. Data Collection and Refinement Conditions		
diffractometer	Bruker PLATFORM/SMART 1000 CCD ^b	Bruker D8/APEX II CCD ^b
radiation (λ [Å])	graphite-monochromated Mo Kα (0.71073)	
temperature (°C)	-80	-100
scan type	ω scans (0.3°) (20 s exposures)	ω scans (0.3°) (20 s exposures)
2θ _{max} (deg)	52.78	55.08
total data collected	46539 (-43 ≤ h ≤ 43, -21 ≤ k ≤ 21, -25 ≤ l ≤ 25)	58677 (-24 ≤ h ≤ 24, -19 ≤ k ≤ 19, -31 ≤ l ≤ 31)
independent reflections	12566 (R _{int} = 0.0531)	8238 (R _{int} = 0.0273)
number of observed reflections (NO)	8816 [F _o ² ≥ 2σ(F _o ²)]	7294 [F _o ² ≥ 2σ(F _o ²)]
range of transmission factors	0.6915–0.4837	0.5462–0.4237
data/restraints/parameters	12566/19 ^c /704	8239/0/505
goodness-of-fit (S) ^d	1.003 [F _o ² ≥ -3σ(F _o ²)]	1.131 [all data]
final R indices ^e		
R ₁ [F _o ² ≥ 2σ(F _o ²)]	0.0416	0.0608
wR ₂ [F _o ² ≥ -3σ(F _o ²)]	0.1103	0.1379
largest diff peak and hole (e Å ⁻³)	1.849 and -1.137	2.007 and -3.122

^a Obtained from least-squares refinement of 5502 reflections with 4.87° < 2θ < 52.49° (14-CF₃SO₃·0.5CH₂Cl₂·Et₂O) or 9605 reflections with 4.80° < 2θ < 55.06° (16-CF₃SO₃·3.5THF).

^b Programs for diffractometer operation, data collection, data reduction and absorption correction were those supplied by Bruker.

^c The minor orientation of the disordered triflate was restrained to have the same geometry as that of the major orientation during refinement by use of the SHELXL SAME instruction.

^d S = [Σw(F_o² - F_c²)/(n - p)]^{1/2} (n = number of data; p = number of parameters varied; w = [σ²(F_o²) + (0.0645P)²]⁻¹ (14-CF₃SO₃·0.5CH₂Cl₂·Et₂O) or w = [σ²(F_o²) + (0.0338P)² + 42.5779sP]⁻¹ (16-CF₃SO₃·3.5THF) where P = [Max(F_o², 0) + 2F_c²]/3).

^e R₁ = Σ||F_o| - |F_c|| / Σ|F_o|; wR₂ = [Σw(F_o² - F_c²)² / Σw(F_o⁴)]^{1/2}.

Table III.2-2 Crystallographic Details for 21-CF₃SO₃·0.5CH₂Cl₂	
21-CF₃SO₃·0.5CH₂Cl₂	
A. Crystal Data	
formula	C _{57.5} H ₄₇ ClF ₃ IrO ₇ P ₄ RuS
formula weight	1391.61
crystal dimensions (mm)	0.38 x 0.38 x 0.11
crystal system	monoclinic
space group	<i>I</i> 2/a (an alternate setting of <i>C</i> 2/c [No. 15])
unit cell parameters ^a	
a (Å)	17.5797(11)
b (Å)	23.6325(15)
c (Å)	26.4280(17)
α (deg)	
β (deg)	95.2753
γ (deg)	
V (Å ³)	10933.1(12)
Z	8
ρ _{calcd} (g cm ⁻³)	1.691
μ (mm ⁻¹)	2.975
B. Data Collection and Refinement Conditions	
diffractometer	Bruker PLATFORM/SMART 1000 CCD ^b
radiation (λ [Å])	graphite-monochromated Mo Kα (0.71073)
temperature (°C)	-80
scan type	ω scans (0.3°) (20 s exposures)
2θ _{max} (deg)	54.90
total data collected	45746 (-22 ≤ h ≤ 22, -30 ≤ k ≤ 30, -34 ≤ l ≤ 34)
independent reflections	12470 (<i>R</i> _{int} = 0.0308)
number of observed reflections (NO)	10108 [<i>F</i> _o ² ≥ 2σ(<i>F</i> _o ²)]
range of transmission factors	0.7355–0.3977
data/restraints/parameters	12470/29 ^c /737
goodness-of-fit (S) ^d	1.122 [<i>F</i> _o ² ≥ -3σ(<i>F</i> _o ²)]
final <i>R</i> indices ^e	
<i>R</i> ₁ [<i>F</i> _o ² ≥ 2σ(<i>F</i> _o ²)]	0.0303
<i>wR</i> ₂ [<i>F</i> _o ² ≥ -3σ(<i>F</i> _o ²)]	0.0911
largest diff peak and hole (e Å ⁻³)	1.478 and -0.864

^a Obtained from least-squares refinement of 7473 reflections with 4.36° < 2θ < 54.86°.

^b Programs for diffractometer operation, data collection, data reduction and absorption correction were those supplied by Bruker.

^c The triflate ion was determined to be disordered over two different sites. At one of these (at approximate crystal coordinates [0.38, 0.46, 0.52]) the triflate ion was defined with two sets of equally-abundant (25% occupancy) positions ({S(2A), F(94A), F(95A), F(96A), O(94A), O(95A), O(96A), C(92A)} and {S(2B), F(94B), F(95B), F(96B), O(94B), O(95B), O(96B), C(92B)}). Distances within these sets of atoms were restrained during refinement: d(S–O) = 1.45 (1) Å; d(S–C) = 1.80(1) Å; d(F–C) = 1.35 (1) Å; d(F···F) = 2.20(1) Å; d(O···O) = 2.37 (1) Å. At the same site is located a solvent dichloromethane molecules (refined with an occupancy factor of 50%) to which the following restraints were applied: d(Cl–C) = 1.80(1) Å; d(Cl···Cl) = 2.95(1) Å. The atoms at the other triflate ion site [0.76, 0.42, 0.0], located near the crystallographic twofold rotational axis [3/4, *y*, 0] were refined with an occupancy factor of 50% and with no geometric restraints applied.

^d $S = [\sum w(F_o^2 - F_c^2)^2 / (n - p)]^{1/2}$ (*n* = number of data; *p* = number of parameters varied; $w = [\sigma^2(F_o^2) + (0.0505P)^2 + 12.4433P]^{-1}$ where $P = [\text{Max}(F_o^2, 0) + 2F_c^2]/3$).

^e $R_1 = \sum ||F_o| - |F_c|| / \sum |F_o|$; $wR_2 = [\sum w(F_o^2 - F_c^2)^2 / \sum w(F_o^4)]^{1/2}$.

AIII.3 Crystallographic Details for Chapter 4 Compounds

Table III.3-1 Crystallographic Experimental Details for 28·3.5CH₃CN and 32·1.5CH₂Cl₂		
	28·3.5CH₃CN	32·1.5CH₂Cl₂
A. Crystal Data		
formula	C ₆₃ H _{56.5} F ₃ IrN _{3.5} O ₇ OsP ₄ S	C _{60.5} H ₄₉ Cl ₃ F ₉ IrO ₆ OsP ₄ S
formula weight	1569.96	1687.69
crystal dimensions (mm)	0.48 x 0.38 x 0.31	0.48 x 0.25 x 0.10
crystal system	triclinic	monoclinic
space group	<i>P</i> $\bar{1}$ (No. 2)	P2 ₁ / <i>n</i> (an alternate setting of P2 ₁ / <i>c</i> [No. 14])
unit cell parameters ^a		
a (Å)	11.2757(4)	12.4449(9)
b (Å)	13.0139(4)	19.1398(14)
c (Å)	21.2552(7)	25.8758(19)
α (deg)	91.0983(3)	
β (deg)	99.1756(3)	97.6740(10)
γ (deg)	91.4100(3)	
V (Å ³)	3077.32(18)	6108.2(8)
Z	2	4
ρ _{calcd} (g cm ⁻³)	1.694	1.835
μ (mm ⁻¹)	4.425	4.603
B. Data Collection and Refinement Conditions		
diffractometer	Bruker D8/APEX II CCD ^b	
radiation (λ [Å])	graphite-monochromated Mo Kα (0.71073)	
temperature (°C)	-100	-100
scan type	ω scans (0.3°) (10 s exposures)	ω scans (0.3°) (20 s exposures)
2θ _{max} (deg)	55.00	55.02
total data collected	27615 (-14 ≤ h ≤ 14, -16 ≤ k ≤ 16, -27 ≤ l ≤ 27)	52376 (-16 ≤ h ≤ 16, -24 ≤ k ≤ 24, -33 ≤ l ≤ 33)
independent reflections	14048 (R _{int} = 0.0104)	13998 (R _{int} = 0.0249)
number of observed reflections (NO)	13394 [F _o ² ≥ 2σ(F _o ²)]	12854 [F _o ² ≥ 2σ(F _o ²)]
range of transmission factors	0.3408–0.2233	0.6299–0.2074
data/restraints/parameters	14048/0/751	13998/12°/808
goodness-of-fit (S) ^d	1.067 [all data]	1.056 [F _o ² ≥ -3σ(F _o ²)]
final R indices ^e		
R ₁ [F _o ² ≥ 2σ(F _o ²)]	0.0176	0.0262
wR ₂ [F _o ² ≥ -3σ(F _o ²)]	0.0452	0.0674
largest diff peak and hole (e Å ⁻³)	0.804 and -0.658	2.583 and -1.039

^a Obtained from least-squares refinement of 9802 reflections with 4.40° < 2θ < 55.00° (**28·3.5CH₃CN**) or 9860 reflections with 4.54° < 2θ < 55.02° (**32·1.5CH₂Cl₂**).

^b Programs for diffractometer operation, data collection, data reduction and absorption correction were those supplied by Bruker.

^c The Cl–C and Cl···Cl distances of the disordered solvent dichloromethane molecules were restrained to be 1.80(1) and 2.80(1) Å, respectively.

^d S = [Σw(F_o² - F_c²)/(n - p)]^{1/2} (n = number of data; p = number of parameters varied; w = [σ²(F_o²) + (0.0203P)² + 3.2425P]⁻¹ (**28·3.5CH₃CN**) or w = [σ²(F_o²) + (0.0328P)² + 13.5179P]⁻¹ (**32·1.5CH₂Cl₂**) where P = [Max(F_o², 0) + 2F_c²]/3).

^e R₁ = Σ||F_o| - |F_c|| / Σ|F_o|; wR₂ = [Σw(F_o² - F_c²)² / Σw(F_o⁴)]^{1/2}.

Table III.3-2 Crystallographic Details for 33-BF₄ and 37-BF₄·2CH₂Cl₂		
	33-BF₄	37-BF₄·2CH₂Cl₂
<i>A. Crystal Data</i>		
formula	C ₆₁ H ₅₄ BF ₄ IrO ₇ OsP ₄	C ₆₁ H ₅₄ BCl ₄ F ₄ IrO ₇ OsP ₄
formula weight	1492.13	1633.93
crystal dimensions (mm)	0.65 x 0.17 x 0.12	0.61 x 0.26 x 0.14
crystal system	triclinic	triclinic
space group	<i>P</i> $\bar{1}$ (No. 2)	<i>P</i> $\bar{1}$ (No. 2)
unit cell parameters ^a		
<i>a</i> (Å)	11.3495(7)	11.5146(14)
<i>b</i> (Å)	13.8540(9)	14.703(2)
<i>c</i> (Å)	19.5589(12)	19.180(3)
α (deg)	97.5953(7)	87.307(13)
β (deg)	90.3465(7)	76.756(13)
γ (deg)	111.6572(7)	84.880(10)
<i>V</i> (Å ³)	2828.2(3)	3147.0(8)
<i>Z</i>	2	2
ρ_{calcd} (g cm ⁻³)	1.752	1.724
μ (mm ⁻¹)	4.774	4.463
<i>B. Data Collection and Refinement Conditions</i>		
diffractometer	Bruker D8/APEX II CCD ^b	Enraf-Nonius CAD4 ^b
radiation (λ [Å])	graphite-monochromated Mo K α (0.71073)	
temperature (°C)	-100	-50
scan type	ω scans (0.3°) (20 s exposures)	θ -2 θ scans ([0.8 + 0.34tan θ])
2 θ_{max} (deg)	55.08	49.92
total data collected	24859 (-14 $\leq h \leq 14$, -17 $\leq k \leq 17$, -25 $\leq l \leq 25$)	11386 (-13 $\leq h \leq 13$, -17 $\leq k \leq 17$, 0 $\leq l \leq 22$)
independ reflns (<i>R</i> _{int})	12821 (<i>R</i> _{int} = 0.0146)	11013 (<i>R</i> _{int} = 0.0439)
number of observed reflections (NO)	11661 [<i>F</i> _o ² $\geq 2\sigma(F_o^2)$]	8501 [<i>F</i> _o ² $\geq 2\sigma(F_o^2)$]
range of transmission factors	0.6074–0.1446	0.5738–0.1716
data/restraints ^c /parameters	12821/20/706	11013 /25 ^d /731
goodness-of-fit (<i>S</i>) ^e	1.038 [<i>F</i> _o ² $\geq -3\sigma(F_o^2)$]	1.047 [<i>F</i> _o ² $\geq -3\sigma(F_o^2)$]
final <i>R</i> indices ^e		
<i>R</i> ₁ [<i>F</i> _o ² $\geq 2s(F_o^2)$]	0.0299	0.0458
<i>wR</i> ₂ [<i>F</i> _o ² $\geq -3s(F_o^2)$]	0.0792	0.1489
largest diff peak and hole (e Å ⁻³)	6.753 and -1.860	2.732 and -2.065

^a Obtained from least-squares refinement of 9814 reflections with 4.40° < 2 θ < 55.08° (**33-BF₄**) or 24 reflections with 20.38° < 2 θ < 23.92° (**37-BF₄·2CH₂Cl₂**).

^b Programs for diffractometer operation and data collection were those supplied by Enraf-Nonius. The data were reduced using the program *XCAD4* (Harms, K.; Wocadlo, S. University of Marburg, 1995). Absorption corrections were applied using programs of the *SHELXTL* system (Bruker, 2008).

^c F–B distances were constrained to be equal (within 0.03 Å) during refinement as were the F···F distances of F–B–F angles.

^d Cl–C distances were constrained to be equal (within 0.03 Å) during refinement as were the Cl···Cl distances of Cl–C–Cl angles.

^e $S = [\sum w(F_o^2 - F_c^2)^2 / (n - p)]^{1/2}$ (*n* = number of data; *p* = number of parameters varied; $w = [\sigma^2(F_o^2) + (0.0382P)^2 + 10.1474P]^{-1}$ (**33-BF₄**) or $w = [\sigma^2(F_o^2) + (0.1052P)^2 + 2.9618P]^{-1}$ (**37-BF₄·2CH₂Cl₂**) where $P = [\text{Max}(F_o^2, 0) + 2F_c^2]^{1/3}$).

AIII.4 Crystallographic Details for Chapter 5 Compounds

Table III.4-1 Crystallographic Details for 41·2CH ₂ Cl ₂ and 44·0.5Et ₂ O		
	41·2CH ₂ Cl ₂	44·0.5Et ₂ O
<i>A. Crystal Data</i>		
formula	C ₆₀ H ₅₄ Cl ₄ F ₃ IrO ₆ OsP ₄ S	C ₅₈ H ₅₃ BF ₄ IrO _{3.50} OsP ₄
formula weight	1608.17	1399.09
crystal dimensions (mm)	0.75 x 0.16 x 0.05	0.22 x 0.13 x 0.07
crystal system	triclinic	triclinic
space group	<i>P</i> $\bar{1}$ (No. 2)	<i>P</i> $\bar{1}$ (No. 2)
unit cell parameters ^a		
<i>a</i> (Å)	11.4554(10)	12.7514(5)
<i>b</i> (Å)	12.7418(11)	13.2551(5)
<i>c</i> (Å)	23.037(2)	17.0522(7)
α (deg)	98.8679(12)	79.0395(5)
β (deg)	96.8074(12)	78.3979(4)
γ (deg)	112.3778(11)	68.9294(4)
<i>V</i> (Å ³)	3013.8(5)	2612.54(18)
<i>Z</i>	2	2
ρ_{calcd} (g cm ⁻³)	1.772	1.779
μ (mm ⁻¹)	4.689	5.157
<i>B. Data Collection and Refinement Conditions</i>		
diffractometer	Bruker PLATFORM/APEX II CCD ^b	Bruker D8/APEX II CCD ^b
radiation (λ [Å])	graphite-monochromated Mo K α (0.71073)	
temperature (°C)	-100	-100
scan type	ω scans (0.3°) (15 s exposures)	ω scans (0.3°) (20 s exposures)
$2\theta_{\text{max}}$ (deg)	55.16	55.16
total data collected	26054 ($-14 \leq h \leq 14$, $-16 \leq k \leq 16$, $-29 \leq l \leq 29$)	23300 ($-16 \leq h \leq 16$, $-17 \leq k \leq 17$, $-22 \leq l \leq 22$)
independ reflns (R_{int})	13777 ($R_{\text{int}} = 0.0451$)	11938 ($R_{\text{int}} = 0.0336$)
number of observed reflections (NO)	10820 [$F_o^2 \geq 2\sigma(F_o^2)$]	9358 [$F_o^2 \geq 2\sigma(F_o^2)$]
range of transmission factors	0.8062–0.1259	0.7173–0.3966
data/restraints/parameters	13777/2 ^c /743	11938/0/651
goodness-of-fit (S) ^d	1.048 [all data]	1.007 [all data]
final <i>R</i> indices ^e		
R_1 [$F_o^2 \geq 2s(F_o^2)$]	0.0452	0.0289
wR_2 [$F_o^2 \geq -3s(F_o^2)$]	0.0971	0.0619
largest diff peak and hole (e Å ⁻³)	2.819 and -2.442	0.800 and -0.996

^a Obtained from least-squares refinement of 9962 reflections with $4.32^\circ < 2\theta < 55.02^\circ$ (41·2CH₂Cl₂) or 9849 reflections with $4.38^\circ < 2\theta < 52.00^\circ$ (44·0.5Et₂O).

^b Programs for diffractometer operation, data collection, data reduction, and absorption correction were those supplied by Bruker.

^c The Cl–C distances (d(Cl(1S)–C(1S), d(Cl(2S)–C(1S))) within the disordered solvent CH₂Cl₂ molecule were restrained to be 1.75(1) Å.

^d $S = [\sum w(F_o^2 - F_c^2)^2 / (n - p)]^{1/2}$ (n = number of data; p = number of parameters varied; $w = [\sigma^2(F_o^2) + (0.0163P)^2 + 19.8901P]^{-1}$ (41·2CH₂Cl₂) or $w = [\sigma^2(F_o^2) + (0.0189P)^2 + 2.7555P]^{-1}$ (44·0.5Et₂O) where $P = [\text{Max}(F_o^2, 0) + 2F_c^2]^{1/3}$).

Table III.4-2 Crystallographic Details for 47·CH₂Cl₂	
47·CH₂Cl₂	
<i>A. Crystal Data</i>	
formula	C ₅₉ H ₄₈ Cl ₂ F ₅ IrO ₇ OsP ₄ S
formula weight	1573.21
crystal dimensions (mm)	0.40 x 0.35 x 0.22
crystal system	monoclinic
space group	<i>P2₁/n</i> (an alternate setting of <i>P2₁/c</i> [No. 14])
unit cell parameters ^a	
<i>a</i> (Å)	16.6500(5)
<i>b</i> (Å)	18.0975(6)
<i>c</i> (Å)	19.5586(6)
<i>α</i> (deg)	
<i>β</i> (deg)	90.0824(4)
<i>γ</i> (deg)	
<i>V</i> (Å ³)	5893.5(3)
<i>Z</i>	4
<i>ρ</i> _{calcd} (g cm ⁻³)	1.773
<i>μ</i> (mm ⁻¹)	4.712
<i>B. Data Collection and Refinement Conditions</i>	
diffractometer	Bruker PLATFORM/APEX II CCD ^b
radiation (λ [Å])	graphite-monochromated Mo Kα (0.71073)
temperature (°C)	-100
scan type	ω scans (0.3°) (15 s exposures)
2θ _{max} (deg)	55.10
total data collected	52294 (-21 ≤ <i>h</i> ≤ 21, -23 ≤ <i>k</i> ≤ 23, -25 ≤ <i>l</i> ≤ 25)
independ reflns (<i>R</i> _{int})	13586 (<i>R</i> _{int} = 0.0195)
number of observed reflections (NO)	12373 [<i>F</i> _o ² ≥ 2σ(<i>F</i> _o ²)]
range of transmission factors	0.4251–0.2538
data/restraints/parameters	13586/2 ^c /727
goodness-of-fit (<i>S</i>) ^d	1.041 [all data]
final <i>R</i> indices ^e	
<i>R</i> ₁ [<i>F</i> _o ² ≥ 2s(<i>F</i> _o ²)]	0.0204
<i>wR</i> ₂ [<i>F</i> _o ² ≥ 3s(<i>F</i> _o ²)]	0.0564
largest diff peak and hole (e Å ⁻³)	1.601 and -1.171

^a Obtained from least-squares refinement of 9987 reflections with 4.50° < 2θ < 46.24°.

^b Programs for diffractometer operation, data collection, data reduction, and absorption correction were those supplied by Bruker.

^c The Cl–C distances within the minor (30 %) component of the disordered CH₂Cl₂ molecule were restrained during refinement: d(Cl(3S)–C(2S)) = d(Cl(4S)–C(2S)) = 1.75(1) Å.

^d $S = [\sum w(F_o^2 - F_c^2)^2 / (n - p)]^{1/2}$ (*n* = number of data; *p* = number of parameters varied; $w = [\sigma^2(F_o^2) + (0.0278P)^2 + 8.1187P]^{-1}$ where $P = [\text{Max}(F_o^2, 0) + 2F_c^2]^{1/5}$).

^e $R_1 = \sum | |F_o| - |F_c| | / \sum |F_o|$; $wR_2 = [\sum w(F_o^2 - F_c^2)^2 / \sum w(F_o^4)]^{1/2}$.

AIII.5 Crystallographic Details for Appendix I

Table III.5-1 Crystallographic Details for 48·1.5CH ₂ Cl ₂	
48·1.5CH ₂ Cl ₂	
A. Crystal Data	
formula	C _{56.5} H ₅₅ Cl ₃ F ₃ IrO ₇ OsP ₄ S
formula weight	1537.61
crystal dimensions (mm)	0.29 x 0.16 x 0.08
crystal system	monoclinic
space group	<i>P</i> 2 ₁ / <i>n</i> (an alternate setting of <i>P</i> 2 ₁ / <i>c</i> [No. 14])
unit cell parameters ^a	
a (Å)	11.2276(5)
b (Å)	30.8259(13)
c (Å)	16.2456(7)
α (deg)	
β (deg)	94.9072(5)
γ (deg)	
V (Å ³)	5602.0(4)
Z	4
ρ _{calcd} (g cm ⁻³)	1.823
μ (mm ⁻¹)	4.996
B. Data Collection and Refinement Conditions	
diffractometer	Bruker D8/APEX II CCD ^b
radiation (λ [Å])	graphite-monochromated Mo Kα (0.71073)
temperature (°C)	-100
scan type	ω scans (0.3°) (20 s exposures)
2θ _{max} (deg)	52.86
total data collected	44532 (-14 ≤ <i>h</i> ≤ 14, -38 ≤ <i>k</i> ≤ 38, -20 ≤ <i>l</i> ≤ 20)
independent reflections	11509 (<i>R</i> _{int} = 0.0365)
number of observed reflections (NO)	9947 [<i>F</i> _o ² ≥ 2σ(<i>F</i> _o ²)]
range of transmission factors	0.6907–0.3213
data/restraints/parameters	11509 /3 ^c /713
goodness-of-fit (S) ^d	1.022 [all data]
final <i>R</i> indices ^e	
<i>R</i> ₁ [<i>F</i> _o ² ≥ 2σ(<i>F</i> _o ²)]	0.0227
<i>wR</i> ₂ [<i>F</i> _o ² ≥ 3σ(<i>F</i> _o ²)]	0.0521
largest diff peak and hole (e Å ⁻³)	1.478 and -0.864

^a Obtained from least-squares refinement of 9877 reflections with 4.50° < 2θ < 52.84°

^b Programs for diffractometer operation, data collection, data reduction, and absorption correction were those supplied by Bruker.

^c Distances within the minor (25 %) conformer of one of the disordered solvent CH₂Cl₂ molecules were fixed during refinement: d(Cl(3S)–C(2S)) = d(Cl(4S)–C(2S)) = 1.75(1) Å; d(Cl(3S)···Cl(4S)) = 2.86(1) Å.

^d S = [Σ*w*(*F*_o² – *F*_c²)/(*n* – *p*)]^{1/2} (*n* = number of data; *p* = number of parameters varied; *w* = [σ²(*F*_o²) + (0.0214*P*)² + 6.4964*P*]⁻¹ where *P* = [Max(*F*_o², 0) + 2*F*_c²]/3).

^e *R*₁ = Σ||*F*_o| – |*F*_c|| / Σ|*F*_o|; *wR*₂ = [Σ*w*(*F*_o² – *F*_c²)/Σ*w*(*F*_o⁴)]^{1/2}.

Appendix IV Crystallographic Data

The crystallographic information files (CIFs), structure reports and checkCIF reports for all of the structure discussed in Chapters 2-5 and Appendix II can be obtained free of charge by contacting either Dr. Robert McDonald or Dr. Michael Ferguson at the address listed below and quoting the internal reference number(s) for the appropriate compound(s), provided in chart form below:

X-Ray Crystallography Laboratory (Chemistry East Room E3-13)

Department of Chemistry, University of Alberta

11227 Saskatchewan Drive

Edmonton, AB, Canada, T6G 2G2

Tel.: 1-780-492-2485

Fax.: 1-780-492-8231

Email: bob.mcdonald@ualberta.ca

michael.ferguson@ualberta.ca

Table IV.1 Chapter 2 Crystallographic Reference Numbers

Compound Number	Internal Reference Number
4	COW0412
5	COW0415
8-CF ₃ SO ₃	COW0514
10	COW1122

Table IV.2 Chapter 3 Crystallographic Reference Numbers

Compound Number	Internal Reference Number
14-CF ₃ SO ₃	COW0323
16-CF ₃ SO ₃	COW1034
21-CF ₃ SO ₃	COW0816

Table IV.3 Chapter 4 Crystallographic Reference Numbers

Compound Number	Internal Reference Number
28	COW1030
32	COW0827
33-BF ₄	COW0832
37-BF ₄	COW9521

Table IV.4 Chapter 5 Crystallographic Reference Numbers

Compound Number	Internal Reference Number
41	COW1124
44	COW1145
47	COW1144

Table IV.5 Appendix I Crystallographic Reference Numbers

Compound Number	Internal Reference Number
48	COW0848

Appendix V Coauthor Contributions

AV.1 Chapters 1 and 6

Martin Cowie assisted with all revising and editing.

AV.2 Chapter 2

Steven Trepanier first prepared and characterized the Ir-chelate complexes, $[\text{IrRu}(\text{CO})_4(\kappa^1:\kappa^1\text{-Me}_2\text{C}=\text{CCH}_2\text{CH}_2)(\text{dppm})_2]^+$ (**2**) and $[\text{IrRu}(\text{CO})_4(\kappa^1:\kappa^1\text{-MeCH}=\text{CCH}_2\text{CH}_2)(\text{dppm})_2]^+$ (**3**), and obtained crystal structures of the carbonyl substituted products $[\text{IrRu}(\text{CO})_3(\text{NCCH}_3)(\kappa^1:\kappa^1\text{-Me}_2\text{C}=\text{CCH}_2\text{CH}_2)(\text{dppm})_2]^+$ (**4**) and $[\text{IrRu}(\text{CO})_3(\text{NCCH}_3)(\kappa^1:\kappa^1\text{-MeCH}=\text{CCH}_2\text{CH}_2)(\text{dppm})_2]^+$ (**5**). Jason Dutton obtained a crystal of the triple C–H activation product, $[\text{IrRu}(\text{CO})_3(\kappa^1\text{-C}(\text{CH}_2\text{CH}_3)=\text{C}(\text{CH}_3)_2)(\mu\text{-}\kappa^1:\eta^2\text{-C}\equiv\text{CC}(\text{CH}_3)=\text{CH}_2)(\text{dppm})_2]^+$ (**8**), and Jason and Steven initiated the studies into the triple activation products. Michael J. Ferguson and Robert McDonald completed all crystal structure determinations and Martin Cowie assisted with supervising the project, editing and revising.

AV.3 Chapter 3

Steven Trepanier and Rahul Samant initiated the studies of $[\text{IrRu}(\text{CO})_4(\text{dppm})_2]^+$ (**13**) with unsaturated substrates; Steve obtained a crystal of $[\text{IrRu}(\text{CO})_4(\mu\text{-C}=\text{C}(\text{H})\text{CH}_3)(\text{dppm})_2]^+$ (**14**) while Rahul obtained a crystal of $[\text{IrRu}(\text{CO})_4(\mu\text{-C}=\text{CH}_2)(\text{dppm})_2]^+$ (**21**). Michael J. Ferguson and Robert McDonald completed all crystal structure determinations and Martin Cowie assisted with supervising the project, editing and revising.

AV.4 Chapter 4

Angela Llamazares and Oliver Kuhnert initiated studies of the $[\text{IrOs}(\text{CO})_4(\text{dppm})_2]^+$ (**27**) with alkynes, and Angela obtained a crystal of $[\text{IrOs}(\text{CO})_3(\mu\text{-}\kappa^1:\kappa^1\text{-C}(\text{CO}_2\text{Me})=\text{CCO}_2\text{Me})(\text{dppm})_2]^+$ (**37**). Michael J. Ferguson and Robert McDonald completed all crystal structure determinations and Martin Cowie assisted with supervising the project, editing and revising.

AV.5 Chapter 5

Michael J. Ferguson and Robert McDonald completed all crystal structure determinations and Martin Cowie assisted with supervising the project, editing and revising.